19

Beyond the Bucket: Development of a Global Gradient-Based Groundwater Modeling Software – Its Evaluation and Integration into a Global Hydrological Model

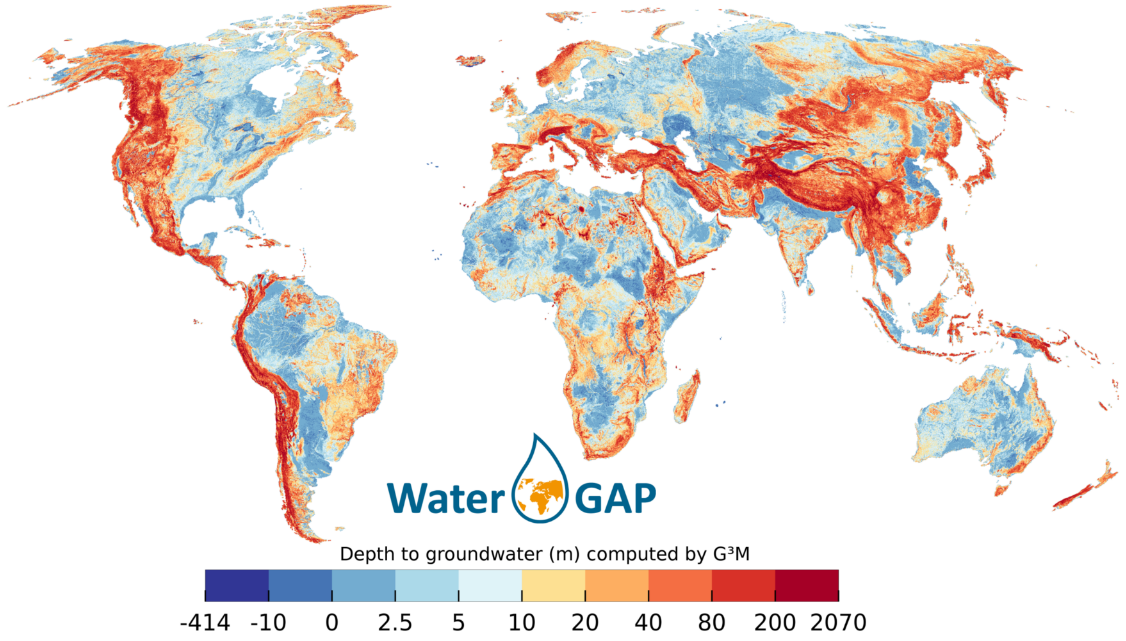

Robert REINECKE

2020

Frankfurt Hydrology Paper

GOETHE UNIVERSITÄT
FRANKFURT AM MAIN

Frankfurt Hydrology Papers:

01 A Digital Global Map of Irrigated Areas - An Update for Asia

02 Global-Scale Modeling of Nitrogen Balances at the Soil Surface

03 Global-Scale Estimation of Diffuse Groundwater Recharge

04 A Digital Global Map of Artificially Drained Agricultural Areas

05 Irrigation in Africa, Europe and Latin America -
Update of the Digital Global Map of Irrigation Areas to Version 4

06 Global data set of monthly growing areas of 26 irrigated crops

07 The Global Crop Water Model (GCWM):
Documentation and first results for irrigated crops

08 Towards mapping the extent of irrigation in the last century:
time series of irrigated area per country

09 Global estimation of monthly irrigated and rainfed crop areas
on a 5 arc-minute grid

10 Entwicklung der transdisziplinären Methode „Akteursbasierte Modellierung“
und ihre Anwendung im Problemfeld der mobilen, organischen Fremdstoffe

11 Expert-based Bayesian Network modeling for environmental management

12 Anthropogenic river flow alterations and their impacts on freshwater ecosystems in China

13 Design, implementation and evaluation of a participatory strategy development – A regional case study in the problem field of renewable electricity generation

14 Global-scale modelling and quantification of indicators for assessing transboundary aquifers. A contribution to the GEF Transboundary Waters Assessment Programme (TWAP)

15 Evaluating alternative water sources and their use for small-holder agriculture from a systemic perspective. A focus on water reuse and rainwater harvesting in Namibia

16 Evaluation, modification and application of a global hydrological model

17 Modeling Water Storage Dynamics in Large Floodplains and Wetlands

18 Global irrigation in the 20th century:
Extension of the WaterGAP Global Irrigation Model (GIM)
with the spatially explicit Historical Irrigation Data set (HID)

19 Beyond the Bucket: Development of a Global Gradient-Based Groundwater Modeling Software – Its Evaluation and Integration into a Global Hydrological Model

Institute of Physical Geography, Goethe University Frankfurt
Altenhöferallee 1, 60438 Frankfurt, Germany

Please cite as:

Reinecke, R. (2020): Beyond the Bucket: Development of a Global Gradient-Based Groundwater Modeling Software – Its Evaluation and Integration into a Global Hydrological Model. *Frankfurt Hydrology Paper 19*, Institute of Physical Geography, Goethe University Frankfurt, Frankfurt am Main, Germany. URN: urn:nbn:de:hebis:30:3-531419

DISSERTATION
ZUR ERLANGUNG DES DOKTORGRADES
DER NATURWISSENSCHAFTEN

Beyond the Bucket: Development of a Global Gradient-Based Groundwater Modeling Software – Its Evaluation and Integration into a Global Hydrological Model

Von linearen Speichermodellen zu gradientenbasierter Grundwassermodellierung: Die Entwicklung eines globalen Grundwassermodells und seine Integration in ein globales hydrologisches Modell

von:
Robert REINECKE M.Sc.
aus Mainz

*vorgelegt beim Fachbereich 11 Geowissenschaften / Geographie
der Johann Wolfgang Goethe-Universität
in Frankfurt am Main*

Frankfurt 2020

vom Fachbereich 11 Geowissenschaften / Geographie der Johann Wolfgang Goethe - Universität als Dissertation angenommen.

Dekan: Prof. Dr. Georg Rümpker

Gutachter: Prof. Dr. Petra Döll, Prof. Dr. Laura Foglia, Prof. Dr. Thorsten Wagener

Datum der Disputation: 20.12.2019

“To young men contemplating a voyage I would say go. The tales of rough usage are for the most part exaggerations, as also are the tales of sea danger. To face the elements is, to be sure, no light matter when the sea is in its grandest mood. You must then know the sea, and know that you know it, and not forget that it was made to be sailed over.”

Joshua Slocum

GOETHE-UNIVERSITY FRANKFURT

Abstract

Beyond the Bucket: Development of a Global Gradient-Based Groundwater Modeling Software –
Its Evaluation and Integration into a Global Hydrological Model

by Robert REINECKE M.Sc.

Groundwater is the largest source of accessible freshwater with its dynamics having significantly changed due to human withdrawals, and being projected to continue to as a result of climate change. The pumping of groundwater has led to lowered water tables, decreased base flow, and depletion.

Global hydrological models (GHMs) are used to simulate the global freshwater cycle, assessing impacts of changes in climate and human freshwater use. Currently, groundwater is commonly represented by a bucket-like linear storage component in these models. Bucket models, however, cannot provide information on the location of the groundwater table. Due to this limitation, they can only simulate groundwater discharge to surface water bodies but not recharge from surface water to groundwater and calculate no lateral and vertical groundwater flow whatsoever among grid cells. For instance this may lead to an underestimation of groundwater resources in semiarid areas, where groundwater is often replenished by surface water. In order to overcome these limitations it is necessary to replace the linear groundwater model in GHMs with a hydraulic head gradient-based groundwater flow model.

This thesis presents the newly developed global groundwater model G^{3}M and its coupling to the GHM WaterGAP spanning over 70,000 lines of newly developed code. Development and validation of the modeling software are discussed along with numerical challenges. Based on the newly developed software, a global natural equilibrium groundwater model is presented showing better agreements with observations than previous models. Groundwater discharge to rivers is found to be the most dominant flow component globally, compared to flows to other surface water bodies and lateral flows. Furthermore, first global maps of the distribution of gaining and losing surface water bodies are displayed.

For the purpose of determining the uncertainty in model outcomes a sensitivity study is conducted with an innovative approach through applying a global sensitivity analysis for a computationally complex model. First global maps of spatially distributed parameter sensitivities are presented. The results at hand indicate that globally simulated hydraulic heads are equally sensitive to hydraulic conductivity, groundwater recharge and surface water body elevation, even though parameter sensitivities do vary regionally.

A high resolution model of New Zealand is developed to further understand the involved uncertainties connected to the spatial resolution of the global model. This thesis finds that a new understanding is necessary how these models can be evaluated and that a simple increase in spatial resolution is not improving the model performance when compared to observations.

Alongside the assessment of the natural equilibrium, the concept of a fully coupled transient model as integrated storage component replacing the former model in the hydrological model WaterGAP is discussed. First results reveal that the model shows reasonable response to seasonal variability although it contains persistent head trends leading to global overestimates of water table depth due to an incomplete coupling. Nonetheless, WaterGAP-G^{3}M is already able to show plausible long term storage trends for areas that are known to be affected by groundwater depletion. In comparison with two established regional models in the Central Valley the coupled model shows a highly promising simulation of storage declines.

Acknowledgements

Firstly, I would like to express my sincere gratitude to my advisors Prof. Dr. Petra Döll and Prof. Dr. Laura Foglia for the continuous support throughout my Ph.D and related research, for their patience, motivation, and immense knowledge. Their guidance helped me build my research skills, supported me in difficult stages of this endeavour, and in writing challenging research papers. I could not have hoped for better advisors and mentors.

I would also like to thank the Friedrich Ebert Foundation for their support throughout this fellowship. Without them this thesis would not have been possible to even start with and I would not have met so many wonderful and talented people during this journey.

My sincerest thanks also go to Prof. Dr. Laura Foglia and Prof. Dr. Steffen Mehl, who provided me with an opportunity to join them in California, and who gave valuable feedback and motivation throughout this research. Without their precious support it would not have been possible to conduct this project.

Gratitude goes to my fellow colleagues for the stimulating discussions, the sleepless nights we were working together towards deadlines, and for all the fun we had over the last five years. Notably, I would like to thank Tim Trautmann for his friendship, his support, and for reviewing this thesis. And I would like to thank Alexander Wachholz for his curiosity and coffee recommendations that carried me throughout the final phase. I also would like to thank my friends in the following institutions: UC Davis, California and TU Darmstadt, Germany. I am particularly grateful to Prof. Dr. Jonathan D. Hermann who enlightened me on the topics of global sensitivity analysis.

Finally, I would like to thank my family for supporting me spiritually throughout this PhD endeavour and my life in general, and Nora Staab for her continuous support and love that helped me to finish this thesis.

Contents

Dedicated to my mother and father for their love and never-ending support in all my endeavours.

Chapter 1

Introduction

Our Planet Earth is covered mainly by water which gained it the well-known name 'blue planet'. It is the source of all life which has developed over millions of years. For us humans it provides as pivotal source of drinking water as well as for growing crops. Nowadays it is the basis for versatile industrial processes. Over the course of the last century, global population has quadrupled and altered terrestrial water fluxes with lasting impact (Wada et al., 2017). Humans have continuously threatened this unique resource by altering surface waters, pumping groundwater and changing precipitation patterns due to anthropogenic climate change. Discussions about climate change impacts revolve around how and where the planets' water is affected, e.g. if and how much the water level of the oceans continues to rise and whether particular regions have to deal on the one hand with extreme floods and on the other hand with droughts (Global Risk Network, 2018; Masson-Delmotte et al., 2018).

Groundwater is a central source of fresh water with an estimated volume of 22.6 million km^3 in the upper 2 km of the continental crust compared to 100.000 km^3 stored in surface water (Gleeson et al., 2016). It is a reliable source throughout the year, even in times of drought, making it indispensable for agriculture in arid and semi-arid regions. Furthermore, groundwater can sustain flow in streams even in times of little precipitation through continuous baseflow, and is thus an essential source of water for freshwater biota in rivers, lakes, and wetlands. Groundwater flows happen on multiple temporal scales and can take thousands of years to reach a stream or well, or sometimes even only a couple of days, depending on the local geological configuration.

Groundwater is the source of estimated 40% of all human water abstractions (Döll et al., 2014). Regions with frequent drought events and/or pronounced agricultural industry often use groundwater as additional water source for irrigation. Extensive groundwater abstraction for a prolonged time that exceeds the natural groundwater recharge can lead to overexploitation or even groundwater depletion (Wada et al., 2010; Taylor et al., 2013). This groundwater depletion can cause (1) drying up of wells, (2) reduction of water in streams and lakes, (3) deterioration of water quality, (4) increased pumping costs, and (5) even land subsidence. On a global scale the rising groundwater use for irrigation has led to lowered groundwater tables and depletion (Scanlon et al., 2012; Gleeson et al., 2012; Döll et al., 2014) and contributes a considerable amount to sea level rise (Wada et al., 2010; Konikow, 2011; Wang et al., 2018). Additionally, model results suggest that climate change may have a considerable impact on groundwater fluxes as they could equilibriate to these new climate conditions on human time scales (Cuthbert et al., 2019).

The importance of groundwater resources for food security and freshwater ecosystems necessitates improvement of our understanding of the groundwater system. Depleted aquifers are a persistent threat to ecosystems as well as humans that force legislators to take unprecedented actions. For example, following the massive droughts in recent history, California decided to implement the Sustainable Groundwater Management Act, enforcing the development of groundwater sustainability plans for all overdrafted basins in the state (Kearns et al., 2018). International programs like the UNESCO's programm on International Shared Aquifer Resources Management (ISARM)[1] and the ongoing Transboundary Waters Assessment Program (TWAP)[2] show that in a globalized world this understanding needs not only to be local but global.

A globally connected water cycle, in which trade and consumption affect remote water resources, requires to manage water over large domains and to understand the involved processes which has launched the development of global hydrological models (GHMs). An increasing availability of large-scale datasets, e.g. through satellite observations, enables this development further. GHMs simulate the global continental water cycle by calculating flows between multiple storage compartments like canopy, snow and soil along with routed river flow.

A central part of the global hydrological cycle, that is not yet well represented in GHMs, is groundwater. Most current GHMs (Sood and Smakhtin, 2015) simulate groundwater by using a bucket-like linear storage. Linear storage models, however, (1) can only simulate groundwater discharge to surface water bodies but not recharge from surface water to groundwater, (2) provide no information on the location of the groundwater table, and (3) assume that there is no groundwater flow among grid cells. This may lead to an underestimation of groundwater resources in semi-arid areas, where groundwater is often replenished by surface water, or to an underestimation of evapotranspiration where the groundwater table is close to the land surface. In order to overcome these limitations, it is necessary to replace the linear storage model in GHMs with a hydraulic head gradient-based groundwater flow model. In general, the importance of including sub-scale processes into the spatially coarse large-scale models has been highlighted by e.g. Bierkens et al. (2015) and Fan et al. (2019).

It is the goal of this thesis to improve the groundwater representation in the state-of-the-art GHM WaterGAP (Alcamo et al., 2003; Döll et al., 2003, 2012, 2014; Müller Schmied et al., 2014) by implementing and integrating a global gradient-based groundwater model that replaces the old linear storage component. To this end, a new groundwater modeling framework is developed from scratch that allows to build regional as well as global groundwater models. This code is developed with the goal of building an efficient global model that can be closely integrated within the GHM WaterGAP while at the same time providing a stable and tested framework that can also be used by the scientific community. Based on this framework the **g**lobal **g**radient-based **g**roundwater **m**odel named G^{3}M is developed and evaluated.

The evaluation firstly focuses on an uncoupled global steady-state (natural equilibrium) model that is used to further explore the parameter uncertainties of the model especially regarding the available global datasets, parameterization and evaluation, and numerical stability. Furthermore, the impact of spatial resolution on model performance is investigated based on a high resolution model of New Zealand. New Zealand is selected due to its clear ocean boundary condition, smaller runtimes compared to the global model, and focus on a local perspective of the global results.

[1] `http://isarm.org` (last accessed 1. January 2019)

[2] `http://www.geftwap.org` (last accessed 1. January 2019)

Finally, the full coupling of the model is discussed and first results of global simulations from 1901 until 2013 are shown. The following section, provides an overview of the current state of research in global groundwater modeling and the challenges in building a global groundwater model. Research questions are developed along four leading questions, one for each main chapter of the thesis. An outline of the structure of the dissertation is provided with an overview of scientific publications and contributions of the author.

1.1 Global groundwater models

Groundwater models covering more than a thousand square kilometers are rare and have mainly been developed for highly impacted and data-rich regions such as the Central Valley (Faunt et al., 2016). On the continental scale Fan et al. (2007) and Miguez-Macho et al. (2007) linked a two-dimensional gradient-based groundwater model to a land surface model on a spatial resolution of 1.25 km. A computationally very expensive integrated simulation of dynamic surface water, soil, and groundwater flow employing Richards' equation for variably saturated flow was achieved at a spatial resolution of 1 km for the continental US (Maxwell et al., 2015) and Europe (Keune et al., 2016) with the ParFlow model.

A first simulation of the steady-state groundwater table for the whole globe at the high resolution of 30″ (arc-seconds) was presented by Fan et al. (2013) and compared to an extensive compilation of observed hydraulic heads. However, interactions with surface water bodies were not included and only simulated through the discard of groundwater above the land surface. The first global gradient-based groundwater model that was coupled to a GHM was developed by de Graaf et al. (2015, 2017), based on the groundwater modeling software MODFLOW and coupled to the GHM PCR-GLOBWB (van Beek et al., 2011). Groundwater recharge, river-groundwater interactions, and capillary rise drive the coupling between the two models. However, in order to achieve plausible discharge performance in mountainous springs, they found it necessary to increase drainage from groundwater beyond the drainage driven by the hydraulic head difference between groundwater and rivers. Moreover, the simulated hydraulic heads systematically underestimate observations. The calibrated specific yield of over 30% (de Graaf et al., 2017), which is unreasonably high, also shows that further research is necessary to model groundwater on a global scale.

1.2 Challenges and scope of this thesis

This thesis presents a new global groundwater model, its development, and its evaluation. Building a global groundwater model is a challenging task that is hindered by the following factors: (1) The availability of data for parameterization of the model, e.g. hydrogeological data, as well as for validation of the model performance through observations e.g. global datasets of well observations. (2) The numerical challenges of solving a complex system of equations on a spatial scale that has not been well understood yet by the scientific community. (3) Solving this problem in an amount of time that enables to investigation of the model uncertainties through e.g. sensitivity analysis. (4) The integration of the model into a GHM which is running on a different spatial resolution and is putting additional stress on the numerical solution through non-linearities that emerge due to the coupled processes.

This thesis advances science by presenting a computationally efficient novel groundwater simulation software that is used to build a global gradient-based groundwater model. The developed model is furthermore integrated into an existing state-of-the-art GHM. The development and software architecture of the model are explained together with an evaluation of a natural equilibrium version that is also used to investigate the model uncertainties in great detail. Moreover, first results of a fully coupled transient model are presented and discussed. The research questions driving this thesis are presented in the following.

1.3 Research questions

Research questions (RQs) are split into four overarching main questions corresponding to four chapters of this thesis. Their discussion follows in chapter 7 (Synthesis). The first RQ focuses on the model software implementation, the second on the exploration of global groundwater processes, the third on the uncertainties of global groundwater modeling, and the last RQ on the transient and fully coupled simulation of groundwater. The reader finds each of the questions expressed in detail along numerous smaller questions and background explanations below.

RQ 1: Which kind of software architecture is necessary for a complex scientific model intended to simulate groundwater on a global scale as efficiently as possible providing the capability to be coupled to an existing GHM?

RQ 1.1: What is a possible software architecture that enables to build global groundwater models that can efficiently be coupled to GHMs?
Multiple software platforms exist to build local- to regional-scale groundwater models. Neither of these software packages has been designed for the purpose of building a global scale model nor for the efficient coupling to an existing hydrology model. It has to be investigated whether the effort of building a new modeling platform is necessary and how this new software needs to be designed to fulfill the aforementioned requirements.

RQ 1.2: What means are necessary to ensure high quality in a complex scientific software?
The required software for this research is complex and its code was developed by only one researcher. However, research and industry experience showed that peer review of software can be even more effective than testing (Garousi, 2010). Nevertheless, the emerging model results need to be sound and the software at hand properly tested. What can be learned from existing software and what design principles lead to a high software quality that also allows to flexibly adapt it to new regiments during the research?

RQ 1.3: What kind of equations and numerical approaches are best to solve the groundwater equation on the spatial scale of GHMs?
Established groundwater models exist only for local to regional scales and it is unknown what equations are needed to represent the involved processes efficiently on the global scale. Furthermore, existing numerical solvers may need to be modified to still produce reliable results at coarse spatial scales.

RQ 2: Is it possible to simulate groundwater on a global scale with a gradient-based approach and what do global groundwater processes look like?

RQ 2.1: How large are lateral and vertical fluxes of groundwater and how do they compare to other flows?
Flows of groundwater can take millennia to recharge into surface water bodies or the ocean. Can a coarsely scaled global model replicate these different timescales? How do the lateral and vertical flows compare to groundwater recharge and the flows from and to surface water bodies and which one accounts the most for hydraulic head results?

RQ 2.2: Which surface water bodies lose water, which gain water, in what amounts, and how are they distributed?
In times of drought, groundwater provides important baseflow to streams and wetlands that helps to keep them from running dry (Stonestrom and Harrill, 2007). On the other hand, losing streams can sustain groundwater levels in regions without, or low, groundwater recharge. How are gaining and losing conditions distributed world-wide?

RQ 2.3: How should we treat groundwater in mountainous regions?
No deep groundwater observations are available for mountainous regions. Flows of groundwater can only be indirectly observed through changes in streamflow or through tracer studies providing information on groundwater age e.g. (Tague and Grant, 2009; Manning and Caine, 2007; Goode, 1996). Others investigated purged alpine aquifers (Hood et al., 2006) but, at the present time, no information is available on deep aquifers below mountains. Should we assume an impermeable bedrock at a certain elevation or should we entirely exclude them from the simulation? How should the anisothropy be changed globally as vertical conductivity can increase through fractures?

RQ 2.4: How much groundwater leaves through the ocean boundary?
While the majority of freshwater ends up in the ocean via streams and/or through evapotranspiration and precipitation, it is unknown how large the direct flows of groundwater to the ocean boundary are.

RQ 2.5: How well does the developed groundwater model represent world-wide observations in steady-state conditions?
The first model version is a steady-state model to investigate what model components influence the results the most and to provide a starting point for the transient model. Comparisons to long-time mean groundwater observations can provide a first performance measurement of the model and hint what processes might contribute to long-time over- or under-estimates of the observations.

RQ 3: What uncertainties are inherent to global groundwater modeling and can we quantify them?

RQ 3.1: What parameters have the most impact on the model results and how are uncertainties distributed?

For a valid evaluation and future improvement of the model it is necessary to explore the involved uncertainties. Moreover, as the model contains non-linear processes (the interactions with surface water bodies) in every computational cell, it is important to explore what parameters, input data, spatial and temporal resolution lead to a numerically stable result.

RQ 3.2: How does the spatial resolution of the model affect the results?
The GHM is running on 0.5° and the groundwater model on 5′ (arc-minute). Can the results be improved when running on finer spatial resolutions e.g. 30″ (arc-seconds)? How is the model runtime affected? How can we parameterize and evaluate high resolution models on the global scale in the absence of global datasets?

RQ 4: How can a global gradient-based groundwater model be integrated within an existing GHM?

RQ 4.1: How can the newly developed model be integrated into the existing model WaterGAP? How can the different spatial and temporal resolutions be integrated?
The hydrological model WaterGAP currently runs on a spatial resolution of 0.5°. Assuming that an appropriate representation of groundwater processes requires a higher spatial resolution the developed groundwater model, that is integrated into the GHM, runs on a spatial resolution of 5′. Future models may even run on higher resolutions. This entails a challenge in coupling both models, because flows of surface water to groundwater need to be scaled correctly between the two models. In addition to the spatial resolution, the temporal resolution may be different as well, e.g. to assure numerical convergence. Again this can have major effects on the behavior of the coupled models.

RQ 4.2: How does the complexity of the integrated model affect the model runtime?
The simulation of a gradient-based groundwater flow is numerically challenging and thus needs more computational resources than a simple linear groundwater storage model.

RQ 4.3: Does the non-linearity, introduced through the coupling, affect the numerical stability of the groundwater model? What temporal resolution is necessary to provide stable results?
In a fully coupled model the calculations of the GHM affect the surface water head in the groundwater model. These changes can lead to switches from gaining to losing conditions for the surface water bodies. Because of the non-linear nature of that switch, this can can pose a challenge to the numerical solver. Both models run on different spatial and possibly temporal scales. How the two models need to be coupled to provide stable results requires further investigation.

RQ 4.4: Is the fully coupled groundwater model able to represent groundwater seasonality compared to observations and other large scale groundwater models? How is groundwater affected by global seasonal changes?
Seasonal accuracy of the groundwater levels can show if the temporal variability of the involved processes is correctly represented. Even if the observed water table

depth differs by multiple meters, due to the coarse spatial resolution of the model, the seasonal response may still be acceptable.

RQ 4.5: How much has the groundwater storage changed within the last century?
Groundwater depletion has been reported for multiple aquifers (Scanlon et al., 2012). Unfortunately, for many aquifers of the world no observations are available. Can we (1) replicate the storage decline in known aquifers and (2) how is the groundwater storage changing world-wide in unmonitored aquifers?

RQ 4.6: How do gaining and losing conditions of surface water bodies change over time in a fully coupled groundwater model?
Depending on the difference between the groundwater table and the surface water bodies, water flows to or from the aquifer. How is this process changing with seasons and over the last century on a global scale?

RQ 4.7: How do the outputs of WaterGAP differ from the integrated groundwater model compared to the former model with a linear storage model?
The integration of a gradient-based groundwater model is a complex challenge affected by the scale and the available data. It needs to be investigated if this actually improves the results of GHMs or even increases the uncertainty in model results compared to the former linear storage model.

1.4 Outline of the thesis

The main chapters of this thesis is outlined as follows. Chapter 2 (RQ 1) describes the implementation of the modeling framework that was developed to build the global groundwater model. It provides insight on the software architecture, the internal solver, and the evaluation process of the newly developed software. The global groundwater model itself is described in Chapter 3 (RQ 2) and results based on a steady-state version of the model are presented. Following this, the parameter uncertainties of the steady-state model are then further investigated in chapter 4 (RQ 3). A discussion of the impact of spatial resolution on global groundwater modeling results in chapter 5 (RQ 3) and the transient coupling to the GHM is presented in chapter 6 (RQ 4). Chapter 7 finally summarizes the answers to the posed RQs and draws conclusions.

1.5 Authors' contributions

Chapters 3, 4, and 5 have been submitted or were already published in various scientific journals (Table 1.1). All publications contain contributions of other authors as listed in the following.

Contribution paper 1 (chapter 3): Robert Reinecke (RR) led the development of the software, formal analysis, methodology, visualization, and writing of the original draft and revisions after peer-review. Laura Foglia (LF) and Petra Döll (PD) supported conceptualization. LF and Steffen Mehl (SM) made suggestions regarding analysis and specifically supported the numerical solver development. TT (Tim

Trautmann) and DC (Denise Cáceres) made suggestions regarding analysis, structure, and wording of the text and design of figures. PD supervised the work of RR together with LF and made suggestions regarding analysis, structure, and wording of the text and design of tables and figures.

Contribution paper 2 (chapter 4): RR led conceptualization, formal analysis, methodology, software, visualization, and writing of the original draft. Jonathan D. Herman (JH), LF, SM, TT supported review and editing as well as the development of the methodology. Alexander Wachholz (AW) supported visualization and writing of the original draft. PD supervised the work of RR and made suggestions regarding analysis, structure, and wording of the text and design of tables and figures.

Contribution paper 3 (chapter 5): RR led conceptualization, formal analysis, methodology, software development, visualization, and writing of the original draft. AW build the 30″ datasets, ran the models, led the initial analysis, and did initial visualization. AW supported visualization and writing of the original draft. LF, SM, Christoph Niemann (CN) supported review and editing. PD supervised the work of RR and made suggestions regarding analysis, structure, and wording of the text and design of tables and figures.

TABLE 1.1: Overview of publications presented in this thesis. Names of the authors are abbreviated analogous to the preceding text.

RQ #	Chapter #	Authors	Title	Journal	Publication status	Citation
2	3	RR[1], LF[3], SM[5], TT[1], DC[1], PD[1,2]	*Challenges in developing a global gradient-based groundwater model (G^3M v1.0) for the integration into a global hydrological model*	Geoscientific Model Development	Published 18. June 2019	Reinecke et al. (2019a)
3	4	RR[1], LF[3], SM[5], JH[4], AW[1], TT[1], PD[1,2]	*Spatially distributed sensitivity of simulated global groundwater heads and flows to hydraulic conductivity, groundwater recharge and surface water body parameterization*	Hydrology and Earth System Science	Published 14. Nov 2019	Reinecke et al. (2019b)
3	5	RR[1], AW[6], SM[5], LF[3], CN[1], PD[1,2]	*Importance of spatial resolution in global groundwater modeling*	Groundwater (Special issue: MODFLOW and More 2019)	Accepted 03. March 2020	DOI: 10.1002/GWAT.12996

[1] Institute of Physical Geography, Goethe University Frankfurt, Frankfurt am Main, Germany
[2] Senckenberg Leibniz Biodiversity and Climate Research Centre Frankfurt (SBiK-F), Frankfurt am Main, Germany
[3] Department of Land, Air and Water Resources, University of California, Davis, USA
[4] Department of Civil & Environmental Engineering, University of California, Davis, USA
[5] Department of Civil Engineering, California State University, Chico, USA
[6] Department of Aquatic Ecosystem Analysis, Helmholtz Centre for Environmental Research, Magdeburg, Germany

Chapter 2

Software development and evaluation

The global groundwater model G^{3}M was implemented based on a new modeling framework that was created from the ground up. This chapter examines the development, testing and evaluation of the framework and what design decisions influenced the code structure. G^{3}M refers to the global groundwater model implementation and G^{3}M-f refers to the underlying core framework that supports the implementation of the model. The development of the framework was guided by the following requirements:

- The software needs to be able to solve the groundwater flow equation with a conjugate gradient-based approach. The implementation should be similar to the established model framework MODFLOW (Harbaugh, 2005).
- The results need to be at least of the same quality as with MODFLOW. To enable this, the framework should be able to support small artificial test models and regional models as well that can be compared to existing MODFLOW projects.
- Other than MODFLOW G^{3}M-f should be build with the purpose of being a platform for a global groundwater model and to be coupled eventually to an existing GHM.
- The software needs to be as efficient as possible to keep runtimes of the global model as low as possible to enable e.g. sensitivity analysis that requires hundreds or thousands of model runs.
- Requirements can quickly change during scientific software projects. G^{3}M-f needs to be of a modular design that allows continuous changes to the software to promptly integrate new ideas and equations.

The remainder of the chapter first provides general information about the model framework and its purpose. Section 2.1 describes the interfaces of the framework and how information is passed from and to the implemented model. The chosen code structure is discussed along with the resulting modules in 2.2 followed by the internally used numerical solver in section 2.3. In 2.4 the development process is summarized, followed by the applied test models in section 2.4.1 and a summary of possible improvements in computational performance in 2.5. An extended documentation of the model code can be found in appendix C. The applied design pattern and design principles are explained in detail in appendix B.

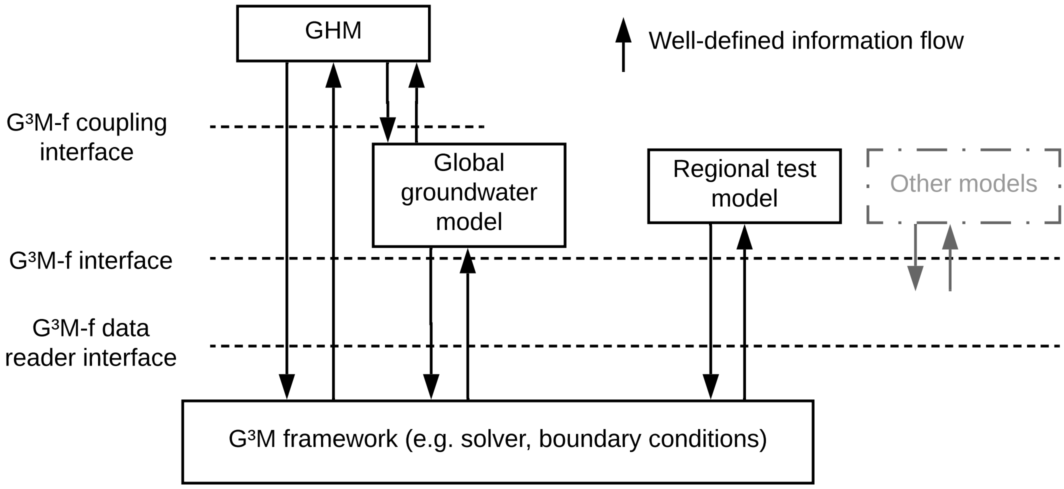
GHM
Well-defined information flow
G³M-f coupling interface
Global groundwater model
Regional test model
Other models
G³M-f interface
G³M-f data reader interface
G³M framework (e.g. solver, boundary conditions)

FIGURE 2.1: Multiple models can be build by using G^{3}M-f. All models need to comply with the G^{3}M-f interface that controls information flow from the framework to the model.

2.1 Model framework G^{3}M-f

The framework was written in C++14 and consists of over 6,000 (70,000 for the global model) lines of code. Internally the frameworks utilized the OpenSource library Eigen3[1] for linear algebra and the sparse matrix operations (see section 2.3). The development of the equations was guided by the MODFLOW documentation (Harbaugh, 2005).

The general idea of a software framework is to provide generic functionality which can selectively be changed by additional user-written code. It is a reusable software environment that provides a standard way to build applications. In fact, the framework dictates an overall program flow while the user is still able to extend, but not modify, the existing code with specific functionality. For the presented framework it means that information is always exchanged through a well-defined interface (Fig. 2.1) in a certain manner. This information flow may consist of the result of the current numerical solution (e.g. simulated hydraulic heads, flows between surface water and groundwater) or what kind of data should be read by the framework to obtain that solution (e.g. hydraulic conductivity). The framework provides an additional coupling interface to integrate groundwater models with GHMs in a guided way. Therefore, G^{3}M-f can be used to build regional as well as global groundwater models and provides interfaces to either run them independently or couple them to existing models. The capability to run regional models as well, is a side product of the flexibility of the framework and allows the implementation of test models of well studied regions, with reduced runtime requirements compared to the global model, or artificial test models or in general as benefit for the community to use the software for multiple purposes.

2.1.1 The interfaces

The fully coupled global groundwater model integrated into the GHM WaterGAP requires the implementation of three interfaces (Fig. 2.1): (1) the groundwater model interface (G^{3}M-f interface) which controls the model setup, (2) the model coupling

[1] `http://eigen.tuxfamily.org` (last accessed 8. July 2019)

interface and (3) the data reader interface. Through the implementation of the interfaces the user is guided to use existing functionality from the framework. For example the data reader interface provides functionality in reading specific data formats like CSV (comma-separated values) that are processed in a way that the framework can use them internally. The user is only left with selecting which files should be read in in which order but is still able to implement his own methods if he or she needs to.

The model interface requires to implement methods to (1) load the settings from a configuration file e.g. a standard path to the file, (2) setup the simulation by using the configuration and loading additional input data, (3) run a certain number of simulation steps with a given time step (e.g. daily, monthly), and initialize a coupling interface if needed.

The coupling interface requires the user to implement how specific model data (from the model it is coupled to) such as groundwater recharge is updated in the coupling process. Data is passed through the interface in a uniform container chosen by the user.

The data reader interface provides functionality to read in data (e.g. from NetCDF (Network Common Data Form) files) in a specific way to be useful to the model framework. It guides the user in implementing his own methods to read in his or her available data.

2.2 Code structure and modules

The software at hand is complex. In its core its needs to solve a challenging numerical problem that needs to be constrained in a specific way to be solvable. Additionally, large data need to be read in efficiently that may also change over the usage of the software e.g. when new climate forcings are available or the data format has changed. Ideally solving the equation and reading in the necessary data should be completed as computationally efficient as possible. Additionally, due to its nature as research software, requirements change along the development phase. This requires the software to be highly adaptable, extensible and maintainable (Kang et al., 1999) (see also appendix B). An established method to achieve this for complex software projects is object-oriented programming. Readers are referred to e.g. Meyer (1988); Gamma et al. (1995); Padhy et al. (2018) for a more in depth discussion. The core idea is that humans are used to interact with objects and their properties and how these objects interact with each other for example that a car has a certain speed and is capable of transporting a number of passengers that have certain properties themselves like weight. Representing software components in this way enables us to use natural language to talk about their relationships and encapsulate specific functionalities in these components. For example in case of the presented modeling software each model cell is an object that may contain a river object that encapsulates the functionality of computing its own conductance.

G^{3}M-f was written in an object oriented design and implemented using established design patterns (Gamma et al., 1995) wherever possible. Design patterns are established software engineering solutions for reoccurring software challenges (see appendix B). Figure 2.2 shows all major components that are part of the modeling framework and how the framework is used by the two models discussed in this thesis: the fully coupled model with WaterGAP and the standalone steady-state model. Each major component of the software is represented as an object e.g. the *simulation* itself, and the *equation* that can be solved (Fig. 2.2). Objects like the *simulation* have properties e.g. each *simulation* contains a representation of the groundwater *equation*. Further, the objects contain methods to modify other objects or themselves in a certain way e.g. the *simulation* has a *simulate()* method that will eventually call the *solve()* method of the *equation* object. The following provides an overview of the framework components shown in Fig. 2.2. A full description of the classes and methods can be found in appendix C.

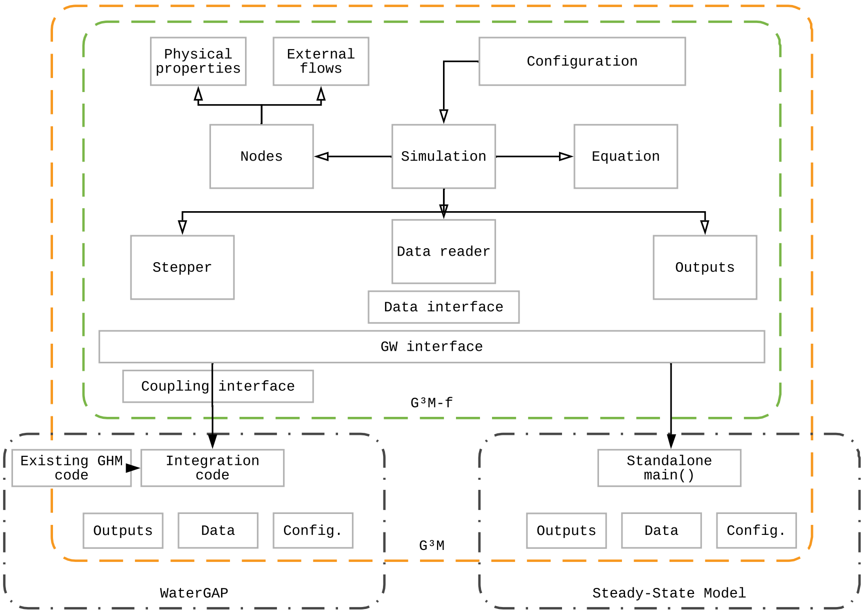

FIGURE 2.2: Overview of the components involved in building a standalone, steady-state, or fully coupled global groundwater model. Green depicts the boundary of the model framework, orange the boundary of the global model G^{3}M, and black the boundary of additional code of the two models. The boxes Outputs, Data, and Config. represent the components: outputs that are written, data that needs to be read in, and the configuration of the model.

Physical properties are characteristics of each computation cell (called *Node* in the framework). For example its size, hydraulic conductivity, and its neighbouring nodes.

External flows is a generic term for all flows that can be added to a node except for the lateral and vertical flows for neighboring nodes. Hence, e.g. a river or groundwater recharge are expressed as external flows with specific characteristics.

The Configuration holds all user defined configurations e.g. data paths, convergence criterions, and other options that can be configured before starting a simulation. It is supplied as JSON (JavaScript Object Notation) file (appendix C).

Nodes are the central building block of the framework and represent the computational unit that is a certain spatial unit of the real world that the model shall express.

Each node has physical properties and may contain a number of external flows and is connected to neighboring nodes. It is furthermore able to compute lateral and vertical transmissivities to and from its neighbors.

The Simulation contains all nodes and is responsible to fill the nodes with information from the configuration and user supplied data. As well, it sets up the equation object.

The Equation is responsible for compiling the information from all nodes into a groundwater flow equation that can be solved. The equation as well sets up the conjugate gradient solver and can be asked to solve itself.

The Stepper controls the temporal dimension of the solution process. It is implemented as an iterator that allows to loop (just as in a classical *for-loop*) over the timesteps and solve the equation accordingly for each.

The Data reader contains methods to read data of different formats into the simulation.

Outputs are written by multiple objects that are flexible enough to write out data in different formats e.g. CSV or NetCDF. The main purpose is to decouple the code that writes out data from the code that performes computational tasks.

2.3 Numerical Approach

The internal solver needs to solve the groundwater flow equation discussed in chapter 3, which is explained in more detail in appendix A. Essentially this requires to solve an equation of the form $\boldsymbol{A} \times \boldsymbol{x} = \boldsymbol{b}$, where $\boldsymbol{A}$ is a matrix that contains the conductance derived for every flux of every computational cell with a size n^2 where n is the number of cells, $\boldsymbol{x}$ is a vector of hydraulic heads that is unknown and needs to be calculated for this timestep, and $\boldsymbol{b}$ the flux in or out of the computational cell. To be as memory efficient as possible the sparsity of $\boldsymbol{A}$ is used

$$\boldsymbol{A} = \begin{pmatrix} c_1 & & & & \\ & c_2 & & & \\ & & \ddots & & \\ & & & c_{n-1} & \\ & & & & c_n \end{pmatrix} \tag{2.1}$$

where c represents multiple matrix entries for each flux of the computational cell from 1 to n (for each side of the cell and the pertaining fluxes e.g. from/to surface water bodies, see Eq. A.9 for details). Because all other entries of the matrix are zero we can efficiently compress the matrix in memory by only storing non-zero values.

The equation is then solved in two nested loops (Picard Iteration) explained in detail in chapter 3. Before actually solving the equation, using a conjugate gradient approach, the matrix is optimized with a preconditioner. A preconditioner modifies a given problem by pivoting the matrix (e.g. using Cholesky decomposition (Fang and O'Leary, 2008)) into a form that is more suitable to be solved numerically. The preconditioner used in G^{3}M-f is currently based on the incomplete LUT (incomplete lower–upper factorization with dual-threshold strategy) (Saad, 1994) solver of the Eigen3 library. Preconditioning the matrix before solving the equation can improve the convergence time of the solver significantly. Writing preconditioners is a very challenging task and the reader is referred to the Eigen3 documentation for details. The following will focus on explaining the used conjugate gradient solver which is a modified version of the one provided by the Eigen3 library. The conjugate gradient algorithm is shown in Alg. 1 and separated into three parts: parameters, initialization, and main loop. In the first part the parameters and their explanations are introduced. The second part is the initialization of primarily internal variables like the initial residuals based on an initial guess that can be supplied by the user (for G^{3}M this is the solution of Fan et al. (2013)). If the initial solution is already precise (inside a margin of error that is specified by the user) the solver returns without any computation. Next, the threshold for the actual numerical step is computed. Different metrics can be used to measure the goodness of the solution step. The original solver used the $||.||_2$ norm also known as Euclidean norm. After discussing with MODFLOW expert Steffen Mehl (personal communication, 2017) this was changed into the infinity norm $||.||_\infty$ representing the maximum flow budget change per inner iteration. If the computed threshold is smaller than the user supplied maximum error no computation is necessary. Before starting the main loop the algorithm is computing the inital search direction p based on a steepest descent method using the preconditioner. Steepest descent is an extension of Laplace's method for approximating an integral. The main idea is to roughly decend towards a saddle point in the complex plane (Debye, 1909). For the global groundwater model G^{3}M, later presented in this thesis, this first solution step is already supplying a guess close to the final solution. Thus, the residuals during the further numerical approximation can be very small as the solution is not changing as much. The conjugate gradient algorithm then proceeds further along the gradients to find a better solution until the user supplied convergence criterion is met or the maximum number of iterations are exceeded. A full and vivid description and explanation of the conjugate gradient method can be found in Shewchuk et al. (1994).

2.3.1 Automated SI unit checks

A model, like the one considered in this thesis, is a simplified representation of physical processes that we express in the form of equations. When writing down the equations and discussing them inside the scientific community we take care that the units used are consistent. The same is true for any figure shown in a scientific publication. Without a given unit it is unclear what the shown number might represent. Unfortunately, this is not the case for model code. Depending on the programming language different types of numbers like `double` or `int` are available, representing floating point numbers or integers respectively. The problem is that while translating the equation from a piece of paper or a researchers mind to code, information about the used units is lost. It is impossible, other than by looking at the code, to confirm that the output of an implemented method actually returns a specific unit. But even if the developer of that method is sure that based on a number of inputs it produces the right result, there is no way to verify that the method is not called with the wrong units. This can easily happen if another researcher is modifying the code later and misinterprets the documentation or makes wrong assumptions due to a missing documentation. We assume in the following that the raw input that is read

Algorithm 1 The conjugate gradient algorithm

```
procedure CONJUGATE_GRADIENT
Parameters:
    $resError \leftarrow$ Convergence criterion: residual norm
    $maxItter \leftarrow$ Convergence criterion: max. iterations
    $i \leftarrow$ Number of iterations: 0
    $rhs \leftarrow$ The right hand side: vector $b$
    $mat \leftarrow$ The matrix $A$
    $x \leftarrow$ The hydraulic head solution
Initialization:
    $residual \leftarrow rhs - mat \times x$
    $rhsNorm \leftarrow ||rhs||_\infty$
    if $rhsNorm == 0$ then
        $x \leftarrow 0$
        $i \leftarrow 0$
        return;
    $threshold \leftarrow rhsNorm * resError^2$
    $residualNorm \leftarrow ||residual||_\infty$
    if $residualNorm < threshold$ then
        $i \leftarrow 0$
        $Total\ residual\ error \leftarrow \sqrt{residualNorm/rhsNorm}$
        return;
    $p \leftarrow preconditioner(residual,mat)$
    $abs \leftarrow residual \cdot p$
Loop:
    while $i < maxItter$ do
        $tmp \leftarrow mat \times p$
        $\alpha \leftarrow abs/(p \cdot tmp)$
        $x \leftarrow x + \alpha \times p$
        $residual \leftarrow residual - \alpha \times tmp$
        $residualNorm \leftarrow ||residual||_\infty$
        if residualNorm < threshold then
            break;
        $z \leftarrow preconditioner(residual,mat)$
        $abs_{i+1} \leftarrow residual \cdot z$
        $\beta \leftarrow abs_{i+1}/abs_i$
        $p \leftarrow z + beta \times p$
        $i \leftarrow i + 1$
```

into the model code from stored data is in the correct units. The proposed approach does not help if the units are already read in incorrectly.

The Gaukler-Mannings equation (chosen here as a well known and simple example equation) (Gauckler, 1867) computes the average velocity of a liquid flowing in a conduit that does not completely enclose the liquid. Written as code the signature of the method[2] may look like this in C++: `double calc_manning(double n, double r, double s)` where n is the Gaukler-Manning coefficient, r the hydraulic radius and s the slope of the hydraulic grade line. Based on the parameters the implementation, no matter what it actually looks like, will compute an output that is a `double`. If the assumed output unit is ms^{-1} and the method is called with a hydraulic radius in km, or even completely wrong in m^2, the output will still be a `double`. C++ has no default mechanism to catch that error and the output will be wrong. It can be close

[2] A method signature defines the inputs and outputs for a subroutine. Depending on the programming language their type and order can be defined as well.

to impossible to track such errors for a developer or user.

The developed model framework G^{3}M-f implements a lot of complex equations that can be the source of such errors. Additionally, the code was developed to be able to be used in different temporal and spatial resolutions. To alleviate the issue of wrong unit conversions due to the use of floating point numbers the code implements type checking based on SI (Système international (d'unités)) units. To this end G^{3}M-f uses the library *libboost*[3]. It provides a framework that allows to force the compiler to check if units used in the code match and otherwise refuses the compilation. To implement this boost uses the already existing type system of C++ that results in code that is as fast as if only floating point numbers were used. As an example the signature of the Gaukler-Mannings equation with the use of SI units in C++ looks like this: `quantity<MeterPerTime> calc_manning(quantity<TimePerMeterThird > n, quantity<Meter> r, quantity<MeterPerMeter> s)`. Now when compiling the code each parameter is checked whether it exactly fits the description of the methods signature. Errors like the example mentioned in the latter are impossible; again assuming that the initial inputs supplied by the user are correct and that no other programming errors were made. If the implementation of the equation is wrong e.g. `return s/r*n` it would not compile either because the return value would not be of meter per time as defined in the method signature. Additionally, all time units are checked for consistency as well and can be changed to a specific value like day or month if required. Wherever possible this method is used in G^{3}M-f to ensure the correctness of the implementation.

2.4 Development Process

The modelling framework was developed in an iterative process of implementation, testing and refactoring[4]. The implementation of the equations was guided by the documentation of MODFLOW 2005 (Harbaugh, 2005) (see appendix A). For each code unit (not to be confused with the units of the latter section), e.g. a method computing the harmonic mean, a unit test was written and automatically executed on every build. Unit testing is a software testing method that strives to construct tests for units of source code to automatically examine whether that unit behaves as intended. Thus, during the complete development cycle the integrity of the smallest units was always kept consistent with the initial concept. The automated tests ensured that even with many code changes the intended behaviour was still intact. This is pivotal in a complex development process that to this day (June 2019, based on git reports) constitutes over 200 million single code changes. As the code was developed by a single person[5] the process shown in Fig. 2.3 was implemented to still assure a high software quality. With the initial architecture (the architecture was revised three times and resulted in two complete rewrites of the code) first test cases were implemented e.g. testing that the solver would correctly stop the solving process if invalid numbers were produced. After writing the tests the actual code was implemented and adapted until it met the test requirements or the test needed to be revised because of a conceptual error. After the implementation of the architecture (finally resulting in G^{3}M-f) test models described in the next section were built and

[3] https://www.boost.org (last accessed 9. July 2019)

[4] Refactoring refers to the process of changing existing code without changing its external behaviour. The goal is to improve the readability and/or reduce code complexity.

[5] Research and industry experience has shown that peer review of software can be even more effective than testing (Garousi, 2010).

checked for consistency with what observations and or experts believed to be a valid solution.

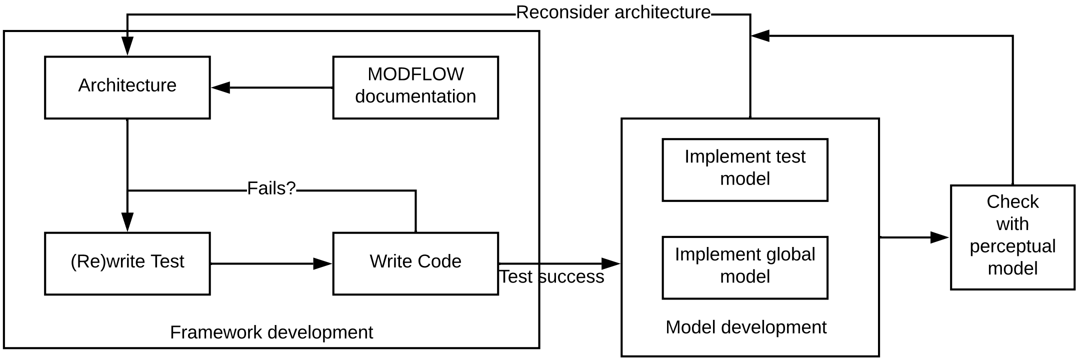

FIGURE 2.3: Overview of the development process of G^{3}M. Perceptual model refers to what model an expert has of the reality that then can be compared to the actual model behaviour (Beven, 2012).

2.4.1 Additional evaluation

Automated tests cannot verify if the model is behaving in a way that is expected. Hence, multiple smaller test models were built.

A simple groundwater model

Because the developed software was built using the documentation of the well established modeling software MODFLOW (Harbaugh, 2005) a simple test model was built in MODFLOW and in G^{3}M-f. Additionally, the model results were compared to an analytical solution of the software Matlab and the transient implementation verified together with one of the MODFLOW developers. The simple model consists of a grid of 10 by 10 cells (1 m by 1 m) with an equal conductivity of 0.8 m day^{-1} (Fig. 2.4), a river in the center (3 m river head elevation and 2 m bottom elevation with a high conductance of 480 m^{2}day^{-1}), and an area of 10 m^2 with applied groundwater recharge of 0.002 m^{3}day^{-1}. A now-flow boundary surrounds the model. The initial head was set to 5 m everywhere. The model additionally represents a slope from 9 m to 0 m surface elevation according to the column numbers. The second layer has the same hydraulic conductivity. Both layers are 10 m thick. Both software frameworks MODFLOW and G^{3}M-f are able to solve this problem in under a second. The model was used to test steady-state as well as transient conditions and is now part of the testing framework that is enclosed in the modeling framework - both for testing purposes and for new users to understand the modeling software. A steady-state model computes an equilibrium state in which the storage component of the groundwater equation is zero (see also chapter 3).

Regional and continental models

After the simple test model provided satisfying results multiple regional test-areas were selected, a model built for that selected area, and compared to available predevelopment (before extensive pumping) observations. The model inputs and the settings are more thoroughly described in chapter 3. This section is intended to show

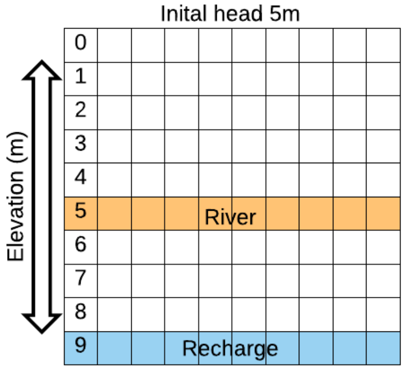

FIGURE 2.4: A simple two layer groundwater model (second layer not shown).

which models have been built to validate the software and were part of the development cycle. It is not intended to fully discuss the model configuration, results and/or inputs. The spatial boundary condition for all models, if no ocean boundary is present, is the 5′ average of the 30″ simulated hydraulic head by Fan et al. (2013).

For a first evaluation the equilibrium is assumed to be close to the pre-development (pre-pumping) state of the aquifer. For the analysis two well known aquifers in the US were selected with available pre-development observations: the High Plains aquifer and the Central Valley aquifer. Additionally, using the Central Valley as study region has the advantage of two existing large scale groundwater models, CVHM (Faunt et al., 2016) and C2VSim (Brush et al., 2013), which are also further used in chapter 6 to evaluate the fully coupled model. Both are the most affected aquifers by pumping in the US (Scanlon et al., 2012; Konikow, 2013).

To evaluate the model behavior, on an even larger scale, without using to much computation time, a model of North America was created. This continental scale model helped especially in optimizing the overall behaviour of the model in respect to the estimation of a realistic water table depth.

2.4.2 Results

The simple steady-state model

The results of the steady-state solution of the simple model are shown in Fig. 2.5. A clear gradient is visible from the zone of applied recharge on the right towards the river in column 5 that ultimately drains all the water close to its river head. The heads left of the river equilibriate to the same elevation of 3.06 m, 6 cm above the river head elevation. This keeps the river in a gaining condition that is able to drain the incoming recharge.

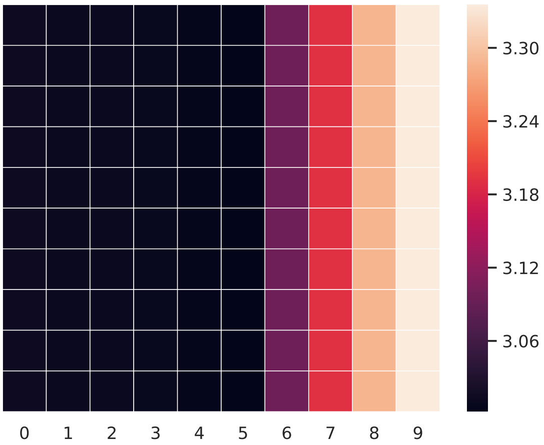

FIGURE 2.5: Resulting hydraulic heads (m) for the simple example model. The applied recharge column is to the right (Turned by 90° compared to Fig. 2.4).

The High Plains Aquifer and the Central Valley

The High Plains aquifer simulation is compared to pre-development observations from the Groundwater Availability Model (GAM)[6]. The simulated depth to groundwater in this early version of G^{3}M (Fig 2.6) showed a relatively good estimate for an uncalibrated model of the depth to groundwater for lower elevation but overestimates in mountainous regions (Rocky Mountains) possibly due to perched aquifers that are not represented in the model. A similar pattern is visible for the Central Valley. Again the pre-development states (initial head of the two models) were compared to the simulated heads of the steady-state G^{3}M (Fig. 2.7). Before pumping increased in the 1960s (Faunt et al., 2016) in Central Valley the South and North contained large groundwater-fed wetlands that can be seen in both the CVHM and C2VSim assumed pre-development depth to groundwater. G^{3}M computes a similar pattern of shallow groundwater in the steady-state. Initial experiments with

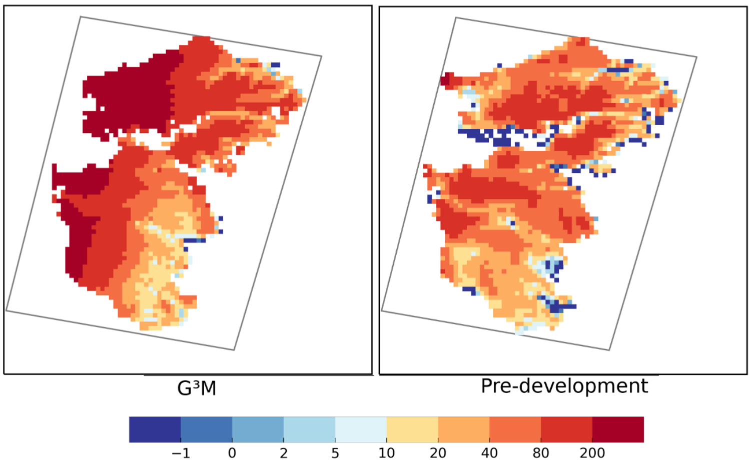

FIGURE 2.6: Steady-state depth to groundwater (m) compared to pre-development observations of the High-Plains aquifer. The G^{3}M output is based on an early model version.

[6] https://www.twdb.texas.gov/groundwater/models/gam/hpas/hpas.asp (last accessed 9. July 2019)

a surface water body elevation at the average of a 30″ (arc-second) DEM showed widespread overestimates of depth to groundwater due to the systemic underestimation of the hydraulic conductivity by the used dataset (see chapter 3), compared to what both established models assume. First experiments increased that conductivity to drain the additional water that G^{3}M was computing. This led to a deeper water table in the valley but also very deep groundwater in the Sierra Nevada. After multiple experiments the surface water body elevation was found to be a key factor and was set to the P_{30} of the 30″ DEM. Additionally, multiple experiments were conducted to verify the computed conductance of the surface water bodies and the applied recharge patterns (not shown).

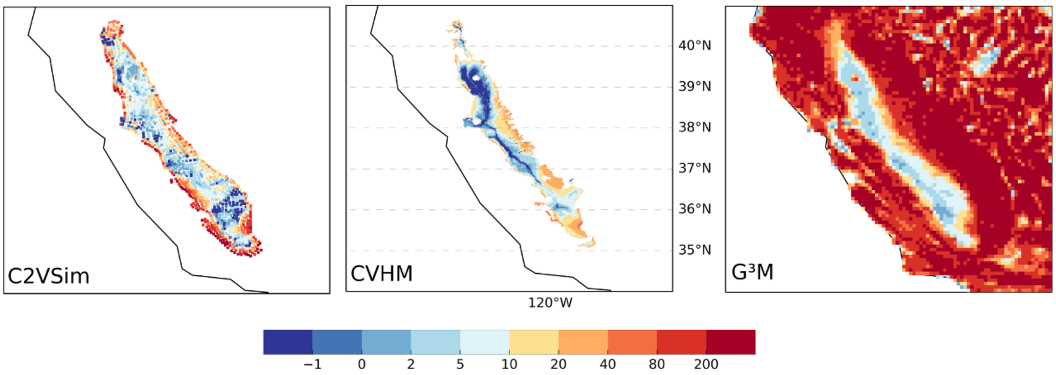

FIGURE 2.7: Comparison of depth to groundwater (m) of three different models. CVHM and C2VSim depth to groundwater is based on the head that is assumed in the established models as initial predevelopment head. The G^{3}M head is a steady-state solution.

North America

To evaluate the model behavior, on an even larger scale, without using too much computation time, a model of North America was created. The model confirmed that the P_{30} was the best estimate for the surface water body elevation until a better approximation could be found. To assess the impact of water abstractions on the model behavior, net abstraction from groundwater was integrated into the North America model at an early stage (Fig. 2.8 a). Because the abstraction is not stopped in the steady-state model if the groundwater level drops below a certain boundary, depletion is heavily over pronounced in the results (Fig. 2.8 b). Nevertheless, it shows that the model correctly reacts to changes in recharge patterns in areas e.g. like the High-Plains aquifer.

2.5 Computational performance and possible runtime improvements

G^{3}M-f is developed to be as computationally efficient as possible. Nevertheless, multiple possible performance improvements remain and are highlighted in the following. To guide future development they are annotated with the complexity ↺ of that improvement and the possible speedup ↑.

- Results from the inner iterations are updated by copying the resulting hydraulic head to each node. A more efficient way would be a reference in each

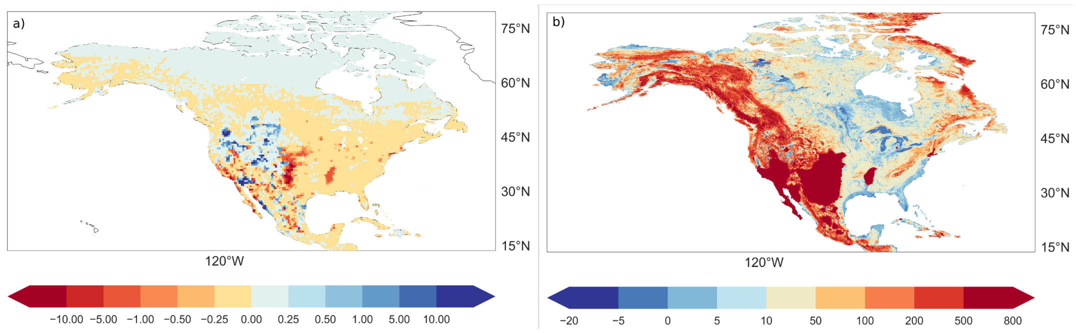

FIGURE 2.8: Impact of net-abstraction from groundwater on a steady-state model. a) shows the difference in groundwater recharge with human impact (recharge minus net abstraction from groundwater) to natural recharge in percent. Groundwater recharge and net abstraction from groundwater are yearly averages of WaterGAP 2.2.c from 1901-2013.
b) shows how a steady-state simulation is affected when net abstraction from groundwater is taken into account.

node to the part of the memory where the vector of the solver resides. This would also reduce the memory footprint. ↻ large, ↑ small to medium

- The preconditioner is currently not running in parallel. The use of a multigrid solver could speed up the solve process. ↻ large, ↑ large

- The solver and preconditioner can be further optimized to fit the matrix configuration. This could also allow larger stepsize e.g. month. ↻ large, ↑ large

- Domain-decomposition is the most promising optimization. All continents currently are computed together in one matrix system. Because some of them do not share a boundary condition e.g. America and Europe they can be computed at the same time. The solver already operates in parallel but this could especially improve the preconditioning. ↻ small, ↑ large

- If the global model needs to run on higher spatial resolution an adaptation to a message-passing based parallelization scheme for a cluster computer is necessary. It is advisable to replace the Eigen solver with a MPI compatible solver from an established library. The interfaces for such an implementation are already included in G^{3}M-f. ↻ very large, ↑ very large

Chapter 3

Challenges in developing a global gradient-based groundwater model (G^{3}M v1.0) for the integration into a global hydrological model

Geosci. Model Dev., 12, 2401–2418, 2019
https://doi.org/10.5194/gmd-12-2401-2019

Geoscientific Model Development
Open Access

Challenges in developing a global gradient-based groundwater model (G^{3}M v1.0) for the integration into a global hydrological model

Robert Reinecke[1], **Laura Foglia**[2], **Steffen Mehl**[3], **Tim Trautmann**[1], **Denise Cáceres**[1], and **Petra Döll**[1,4]

[1]Institute of Physical Geography, Goethe University Frankfurt, Frankfurt am Main, Germany
[2]Department of Land, Air and Water Resources, University of California, Davis, CA, USA
[3]Department of Civil Engineering, California State University, Chico, CA, USA
[4]Senckenberg Leibniz Biodiversity and Climate Research Centre Frankfurt (SBiK-F), Frankfurt am Main, Germany

Correspondence: Robert Reinecke (reinecke@em.uni-frankfurt.de)

Received: 2 May 2018 – Discussion started: 15 May 2018
Revised: 20 May 2019 – Accepted: 29 May 2019 – Published: 18 June 2019

Abstract. In global hydrological models, groundwater (GW) is typically represented by a bucket-like linear groundwater reservoir. Reservoir models, however, (1) can only simulate GW discharge to surface water (SW) bodies but not recharge from SW to GW, (2) provide no information on the location of the GW table, and (3) assume that there is no GW flow among grid cells. This may lead, for example, to an underestimation of groundwater resources in semiarid areas where GW is often replenished by SW or to an underestimation of evapotranspiration where the GW table is close to the land surface. To overcome these limitations, it is necessary to replace the reservoir model in global hydrological models with a hydraulic head gradient-based GW flow model.

We present G^{3}M, a new global gradient-based GW model with a spatial resolution of 5′ (arcminutes), which is to be integrated into the 0.5° WaterGAP Global Hydrology Model (WGHM). The newly developed model framework enables in-memory coupling to WGHM while keeping overall runtime relatively low, which allows sensitivity analyses, calibration, and data assimilation. This paper presents the G^{3}M concept and model design decisions that are specific to the large grid size required for a global-scale model. Model results under steady-state naturalized conditions, i.e., neglecting GW abstractions, are shown. Simulated hydraulic heads show better agreement to observations around the world compared to the model output of de Graaf et al. (2015). Locations of simulated SW recharge to GW are found, as is expected, in dry and mountainous regions but areal extent of SW recharge may be underestimated. Globally, GW discharge to rivers is by far the dominant flow component such that lateral GW flows only become a large fraction of total diffuse and focused recharge in the case of losing rivers, some mountainous areas, and some areas with very low GW recharge. A strong sensitivity of simulated hydraulic heads to the spatial resolution of the model and the related choice of the water table elevation of surface water bodies was found. We suggest to investigate how global-scale groundwater modeling at 5′ spatial resolution can benefit from more highly resolved land surface elevation data.

1 Introduction

Groundwater (GW) is the source of about 40 % of all human water abstractions (Döll et al., 2014) and is also an essential source of water for freshwater biota in rivers, lakes, and wetlands. GW strongly affects river flow regimes and supplies the majority of river water during ecologically and economically critical periods with little precipitation. GW storage and flow dynamics have been altered by human GW abstractions as well as climate change and will continue to change in the future (Taylor et al., 2012). Around the globe, GW abstractions have led to lowered water tables and, in some regions, even GW depletion (Döll et al., 2014; Scanlon et al., 2012; Wada et al., 2012; Konikow, 2011). This has resulted in reduced base flows to rivers and wetlands (with negative impacts on water quality and freshwater ecosystems), land

Published by Copernicus Publications on behalf of the European Geosciences Union.

subsidence, and increased pumping costs (Wada, 2016; Döll et al., 2014; Gleeson et al., 2012, 2016). The strategic importance of GW for global water and food security will probably intensify under climate change as more frequent and intense climate extremes increase variability in surface water (SW) flows (Taylor et al., 2012). International efforts have been made to promote sustainable GW management and knowledge exchange among countries, e.g., UNESCO's program on International Shared Aquifer Resources Management (ISARM) (http://isarm.org, last access: 1 June 2019) and the ongoing GW component of the Transboundary Waters Assessment Program (TWAP) (http://www.geftwap.org, last access: 1 June 2019). To support prioritization for investment among transboundary aquifers, as well as identification of strategies for sustainable GW management, information on current conditions and possible trends of the GW systems is required (UNESCO-IHP, IGRAC, WWAP, 2012). In a globalized world, an improved understanding of GW systems and their interactions with SW and soil is needed not only at the local and regional scale but also at the global scale.

To assess GW at the global scale, global hydrological models (GHMs) are used (e.g. Wada et al., 2012; Wada, 2016; Döll et al., 2012, 2014). In particular, they serve to quantify GW recharge (Döll and Fiedler, 2008). Like typical hydrological models at any scale, GHMs simulate GW dynamics by a linear reservoir model. In such a model, the temporal change of GW storage in each grid cell is computed from the balance of prescribed inflows and an outflow that is a linear function of GW storage. Linear reservoir models can only simulate GW discharge to SW bodies but not a reversal of this flow, even though losing streams may provide focused GW recharge that allows the aquifer to support ecosystems alongside the GW flow path (Stonestrom et al., 2007) as well as human GW abstractions. Losing streams typically occur in semiarid and arid regions but also seasonally in humid regions. In addition, such linear reservoir models provide no information on the location of the GW table and assume that GW flow among grid cells is negligible. To simulate the dynamics of water flow between SW bodies and GW in both directions as well as the effect of capillary rise on evapotranspiration, it is necessary to compute lateral GW flows among grid cells as a function of hydraulic head gradients and thus the dynamic location of the GW table. To achieve an improved understanding of GW systems at the global scale, and in particular of the interactions of GW with SW and soil, it is therefore necessary to replace the linear GW reservoir model in GHMs by a hydraulic gradient-based GW flow model.

Large-scale gradient-based GW flow models are still rare and mainly available for data-rich regions, e.g., Death Valley (Belcher and Sweetkind, 2010) and the Central Valley (Belcher and Sweetkind, 2010; Faunt, 2009; Dogrul et al., 2016) in the USA, but also for large fossil groundwater bodies in arid regions (e.g., the Nubian Aquifer System in northern Africa; Gossel et al., 2004). However, they are in most cases not integrated within hydrological models that quantify GW recharge based on climate data and provide information on the condition of SW (e.g., streamflow and storage). For North America, Fan et al. (2007) and Miguez-Macho et al. (2007) linked a land surface model with a two-dimensional gradient-based GW model and computed, with a daily time step, GW flow, water table elevation, GW–SW interaction, and capillary rise, using a spatial resolution of 1.25 km. One challenge was the determination of the river conductance that affects the degree of GW–SW interaction. A computationally very expensive integrated simulation of dynamic SW, soil, and GW flow using Richards' equation for variably saturated flow was achieved at a spatial resolution of 1 km for the continental US by applying the ParFlow model (Maxwell et al., 2015). In both studies, GW abstractions were not taken into account.

A first simulation of the steady-state GW table for the whole globe at the very high resolution of 30″ (arcseconds) was presented by Fan et al. (2013) and compared to an extensive compilation of observed hydraulic heads. However, there was no head-based interactions with SW; GW above the land surface was simply discarded. Global GW flow modeling is strongly hampered by poor data availability, including the geometry of aquifers and aquitards as well as parameters like hydraulic conductivity (de Graaf et al., 2017), and by computational restrictions on spatial resolution leading to conceptual problems, e.g., regarding SW–GW interactions (Morel-Seytoux et al., 2017). Recently, some GW flow models that are in principle applicable for the global scale were developed but were applied only regionally in data-rich regions (Rhine basin: Sutanudjaja et al., 2011; France: Vergnes et al., 2012, 2014). The first global gradient-based GW model that was run for both steady-state (de Graaf et al., 2015) and transient conditions (de Graaf et al., 2017) was driven by GW recharge and SW data of the GHM PCR-GLOBWB (van Beek et al., 2011). However, to achieve plausible discharge performance, they found it necessary to increase drainage from GW to rivers beyond the drainage driven by the hydraulic head difference between GW and river. This additional drainage, which accounts for about 50 % of global GW flow into SW, is simulated as a function of GW storage above the floodplain.

In this study, we present the Global Gradient-based Groundwater Model (G^{3}M), which is to be integrated into the GHM WaterGAP 2 to improve estimation of flows between SW and GW (affecting both streamflow and groundwater recharge and thus water availability for humans and ecosystems) and implement capillary rise (affecting evapotranspiration). Table 1 provides a comparative summary of G^{3}M as well as the global groundwater models by Fan et al. (2013), de Graaf et al. (2015, 2017), and the continental-scale model ParFlow (Maxwell et al., 2015).

The objective of this paper is to learn from a steady-state model, a well-established first step in groundwater model development, to (1) understand the basic model behavior by limiting model complexity and degrees of freedom and thus

Table 1. Comparison of global- and continental-scale groundwater models. DEM is digital elevation model. n/a means not applicable.

Aspect	G^{3}M	de Graaf et al. (2015, 2017)	Fan et al. (2013)	ParFlow
Extent	global	global	global	continental USA
Resolution	$5'$	$6'$	$30''$	1 km
Software	G^{3}M-f	MODFLOW	unnamed	ParFlow
Computational expense	medium	medium	high	very high
Flow representation	3-D saturated	3-D saturated	2-D saturated	3-D saturated or unsaturated
Timescale	steady-state or (transient)	steady-state or transient	steady-state	steady-state or transient
Vertical layers	2	2	1	5
Full coupling possible	yes	yes	yes	yes (already coupled)
In-memory coupling	yes	no	n/a	yes
Constant saturated thickness	yes	yes	no	no
Impermeable bottom	no	no	no	yes
Surface water body location	in every cell	in almost every cell	no surface water	created during simulation
Surface water body elevation	P_{30} of $30''$ DEM	avg. of $30''$ DEM	n/a (outflow if WTD < 0.25 m)	n/a
Deviation from observations	large	very large	medium	medium

(2) providing insights into dominant processes and uncovering potential model-inherent characteristics difficult to observe in a fully coupled transient model. A transient model might obfuscate model-inherent trends due to the slow-changing nature of groundwater processes e.g., trends towards large overestimation or underestimation due to wrong parameterization. A fully coupled model furthermore adds complexity and uncertainty to the model outcome. The presented steady-state model is furthermore used to (3) investigate parameter sensitivity and sensitivity to spatial resolution. In addition, the steady-state solution can be used as (4) an initial condition for future fully coupled transient runs.

The model concept and equations as well as applied data and parameter values are presented in Sect. 2. In Sect. 3, we show steady-state results of G^{3}M driven by WGHM data. Simulated hydraulic heads are compared to observations world-wide and to the output of existing large-scale GW models (Table 1). Furthermore, sensitivity to parameters and grid size is shown for the example of New Zealand. Finally, the implications of modeling decisions and grid size are discussed (Sect. 4) and conclusions are drawn (Sect. 5).

2 Model description

2.1 G^{3}M model concept

Although G^{3}M is based on principles of the well-known GW flow modeling software MODFLOW (Harbaugh, 2005), G^{3}M differs in its parameterization from traditional local and regional GW models. These models are generally based on rather detailed information on hydrogeology (including aquifer geometry and properties such as hydraulic conductivity derived from pumping tests), topography, pumping wells, location, and shape of SW bodies as well as on observations of hydraulic head in GW and SW. Local observations guide the developer in constructing the model such that local conditions and processes can be properly represented. The lateral extent of individual grid cells of such GW flow models is generally smaller or similar to the depth of the aquifer(s) and the size of the SW bodies that interact with the GW. The global GW flow model G^{3}M, however, covers all continents of the Earth except Greenland and Antarctica. At this scale, information listed above is poor or non-existing, and the lateral extent of grid cells needs to be relatively large due to computational (and data) constraints. We selected a grid cell size of $5'$ by $5'$ (approx. 9 km by 9 km at the Equator) as this size fits well to WaterGAP and is smaller than the suggested $6'$ of Krakauer et al. (2014). WaterGAP 3 (Eisner, 2016) has the same cell size, and 36 such cells fit into one 0.5° WaterGAP 2 cell. Global climate data are only available for 0.5° grid cells. The land mask of G^{3}M, i.e., location and size of $5'$ grid cells, is that of WaterGAP 3 and encompasses 2.2 million $5'$ grid cells on each layer.

Due to the lack of the spatial distribution of hydrogeological properties, we chose to use, in the current version of G^{3}M, two GW layers with a vertical size of 100 m each (Fig. 1). We performed a sensitivity analysis that confirmed the findings of others (de Graaf et al., 2015) that the aquifer thickness has a relatively small impact on the model results. Therefore, selecting a uniform thickness of 100 m (motivated by the assumed depth of validity of the lithology data) (Fig. 1) worldwide for the first layer and also for the second layer is expected to lead to less uncertainties as compared to hydraulic conductivities and the surface water table elevation.

G^{3}M focuses on a plausible simulation of water flows between GW and SW, and we deemed it suitable to have an upper GW layer that interacts with SW and soil (the soil layer

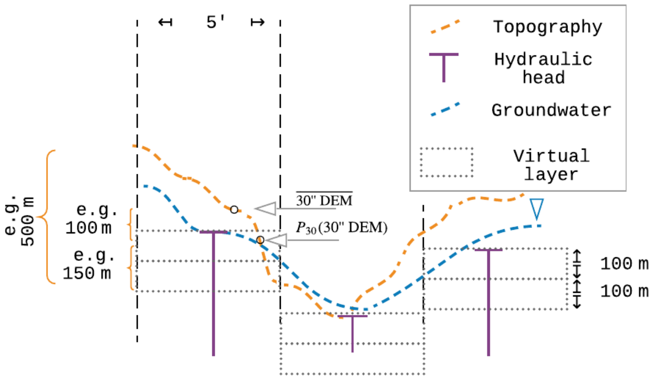

Figure 1. Schematic of G^{3}M's spatial structure with 5′ grid cells, hydraulic head per cell, and the conceptual virtual layers (virtual because at this stage only confined conditions are computed). The underlying variability in the topography changes the perception of simulated depth to groundwater depending on what metrics are used to represent it on a coarser resolution. Layers in G^{3}M are of a conceptual nature and describe the saturated flow between locations of head laterally and vertically. The P_{30} is used in the presented steady-state model as SW elevation instead of an average or minimum per grid cell.

of WaterGAP is described in detail in Sect. S1 in the Supplement) and a lower one in which GW may flow laterally without such interactions. As land surface elevation within each 5′ grid cell, with an area of approximately 80 km^2, may vary by more than 200 m (Fig. S4.1), neighboring cells in G^{3}M may not be adjacent anymore (Fig. 1), in contrast to (regional) GW models with smaller grid cells. This makes G^{3}M a rather conceptual model in which water exchange between groundwater cells is driven by hydraulic head gradients but flow can no longer be conceptualized as occurring through continuous pore space. In addition, due to the coarse spatial scale and the possible large variations in land surface elevations within each grid cell, the upper model layers should not be considered to be aligned with an average land surface elevation. The model layers can be rather thought to be vertically aligned with the elevation of the surface water body table, as this prescribed elevation is, together with the sea level, the only elevation included in the groundwater flow equation (Eq. 1).

The simulation of aquifers that contain dry cells and/or cells that oscillate between wet and dry states poses great challenges to solving Eq. (1) (Niswonger et al., 2011). G^{3}M-f (the framework code used to implement G^{3}M) implements the traditional wetting approach from Harbaugh (2005) as well as the approach proposed by Niswonger et al. (2011) along with the proposed damping scheme. Both approaches have proven to be insufficient to simulate head-based transmissivities (unconfined conditions) on the global scale. Large mountainous areas would be excluded if unconfined conditions are assumed from the beginning of the solution step, as the head is often far below the deepest model layer, resulting in a no-flow condition and imposing convergence issues to the matrix solver. We choose to simulate both layers with a specific saturated thickness even though the upper layer can be expected to decrease in water level and thus in transmissivity (hydraulic conductivity times saturated depth). The large uncertainties regarding hydraulic conductivities (possibly an order of magnitude), further justifies using the computationally more efficient assumption of specified saturated thickness. This approach is consistent with findings that this is accurate for large, complex groundwater models (Sheets et al., 2015). Furthermore, it is consistent with recent presented large-scale studies, e.g., for the Rhine–Meuse basin of Sutanudjaja et al. (2011) (using one confined layer), the Death Valley Regional Flow Model (Belcher, 2004; Faunt et al., 2011), and the global groundwater model of de Graaf et al. (2017) (two layers and partially unconfined conditions are simulated by parametrization of the model input and not by a head-dependant transmissivity).

Three-dimensional groundwater flow is described by a partial differential equation (approximated in the model implementation by using the finite differences method, Sect. 2.4)

$$\frac{\mathrm{dGWS}}{\mathrm{d}t} = \left(\frac{\partial}{\partial x}\left(K_x\frac{\partial h}{\partial x}\right) + \frac{\partial}{\partial y}\left(K_y\frac{\partial h}{\partial y}\right) + \frac{\partial}{\partial z}\left(K_z\frac{\partial h}{\partial z}\right) + W\right)\Delta x\Delta y\Delta z = S_\mathrm{s}\frac{\partial h}{\partial t}\Delta x\Delta y\Delta z, \qquad (1)$$

where $K_{x,y,z}$ is the hydraulic conductivity $[LT^{-1}]$ along the x, y, and z axes between the cells (harmonic mean of grid cell conductivity values); S_s the specific storage $[L^{-1}]$; $\Delta x\Delta y\Delta z$ $[L^3]$ the volume of the cell; and h the hydraulic head $[L]$. In- and out-flows in the groundwater are accounted for as

$$W\Delta x\Delta y\Delta z = R_\mathrm{g} + Q_\mathrm{swb} - \mathrm{NA_g} - Q_\mathrm{cr} + Q_\mathrm{ocean}, \qquad (2)$$

where Q_swb is flow between the SW bodies (rivers, lakes, reservoirs, and wetlands) and GW $[L^3T^{-1}]$; Q_cr is capillary rise, i.e., the flow from GW to the soil; and Q_ocean is the flow between ocean and GW $[L^3T^{-1}]$, representing the boundary condition. In the case of Q_swb and Q_ocean, a positive value represents a flow into the groundwater.

Q_swb in Eq. (3) replaces k_g GWS and $R_\mathrm{g\_swb}$ in the linear storage equation of WaterGAP (Eq. S1), such that losing conditions of all types of SW bodies can be simulated dynamically. It is calculated as a function of the difference between the elevation of the water table in the SW bodies h_swb $[L]$ and h_aq as

$$Q_\mathrm{swb} = \begin{cases} c_\mathrm{swb}\left(h_\mathrm{swb} - h_\mathrm{aq}\right) & h_\mathrm{aq} > B_\mathrm{swb}, \\ c_\mathrm{swb}\left(h_\mathrm{swb} - B_\mathrm{swb}\right) & h_\mathrm{aq} \leq B_\mathrm{swb}, \end{cases} \qquad (3)$$

where c_swb is the conductance $[L^2T^{-1}]$ of the SW body bed (river, lake, reservoir, or wetland) and B_swb the SW body bottom elevation $[L]$.

Conductance of SW bodies is often a calibration parameter in traditional GW models (Morel-Seytoux et al., 2017). Following Harbaugh (2005), it can be estimated by

$$c_{\text{swb}} = \frac{K\,L\,W}{h_{\text{swb}} - B_{\text{swb}}}, \tag{4}$$

where K is hydraulic conductivity, L is length and W is width of the SW body per grid cell. For lakes (including reservoirs) and wetlands, c_{swb} is estimated based on hydraulic conductivity of the aquifer K_{aq} and SW body area (Table 2). For gaining rivers, conductance is quantified individually for each grid cell following an approach proposed by Miguez-Macho et al. (2007). The value of river conductance c_{riv}, according to Miguez-Macho et al. (2007), in a GW flow model needs to be set to such values so that, for steady-state conditions, the river is the sink for all the inflow to the grid cell (GW recharge and inflow from neighboring cells) that is not transported laterally to neighboring cells such that

$$c_{\text{riv}} = \frac{R_{\text{g}} + Q_{\text{eq}_{\text{lateral}}}}{h_{\text{eq}} - h_{\text{riv}}} \quad h_{\text{aq}} > h_{\text{riv}}. \tag{5}$$

For G^{3}M, we computed the equilibrium head h_{eq} as the 5$'$ average of the 30$''$ steady-state heads calculated by Fan et al. (2013). Using WGHM, diffuse GW recharge lateral equilibrium flow, $Q_{\text{eq}_{\text{lateral}}}$ $[L^3T^{-1}]$, is the net lateral inflow into the cell computed based on the h_{eq} distribution as well as G^{3}M K_{aq} and cell thickness (Table 2). Elevation of the river water table, h_{riv} $[L]$, is provided by WGHM. Using a fully dynamic approach, i.e., utilizing the hydraulic head and lateral flows from the current iteration to recalculate c_{riv} in each iteration towards the steady-state solution, has proven to be too unstable due to its nonlinearity affecting convergence. We limit c_{riv} to a maximum of 10^7 m^2 d^{-1}; this would be approximately the value for a 10 km long and 1 km wide river with a head difference between GW and river of 1 m and hydraulic conductivity of the river bed of 10^{-5} m s^{-1}.

If the river recharges the GW (losing river), Eq. (5) cannot be used as the Fan et al. (2013) high-resolution equilibrium model only models groundwater outflows but not inflows from SW bodies. If h_{aq} drops below h_{riv}, Eq. (4) is used to compute c_{riv}, with K equal to K_{aq}.

The flux across the model domain boundary Q_{ocean} is modeled as a head-dependent flow based on a static head boundary.

$$Q_{\text{ocean}} = c_{\text{ocean}}\left(h_{\text{ocean}} - h_{\text{aq}}\right), \tag{6}$$

where h_{ocean} is the elevation of the ocean water table $[L]$, h_{aq} the hydraulic head in the aquifer $[L]$, and c_{ocean} the conductance of the boundary condition $[L^2T^{-1}]$ (Table 2). We assume that the density difference to sea water is negligible at this scale. Q_{cr} is not yet implemented in G^{3}M.

2.2 The steady-state uncoupled model version

In the first implementation stage, G^{3}M was developed as a steady-state (right-hand side of Eq. 1 is zero) stand-alone model that represents naturalized conditions (i.e., without taking into account human water use) during 1901–2013. Input data and parameters used are listed in Table 2 and described below.

Gleeson et al. (2014) provided a global subsurface permeability dataset from which K_{aq} was computed. The dataset was derived by relating permeabilities from a large number of local to regional GW models to the type of hydrolithological units (e.g., “unconsolidated” or “crystalline”). The geometric mean permeability values of nine hydrolithological units were mapped to the high-resolution global lithology map GLiM (Hartmann and Moosdorf, 2012). In continuous permafrost areas, a very low permeability value was assumed by Gleeson et al. (2014). The estimated values represent the shallow surface on the scale of 100 m depth. The unique dataset has three inherent problems when used as input for a GW model. (1) At this scale, important heterogeneities such as discrete fractures or connected zones of high hydraulic conductivity controlling the GW flow are not visible. (2) Jurisdictional boundaries due to different data sources in the global lithological map lead to artifacts. (3) The differentiation between coarse- and fine-grained unconsolidated deposits is only available in some regions resulting in 10^{-4} m s^{-1} as hydraulic conductivity for coarse-grained unconsolidated deposits. If the distinction is not available, a rather low value of 10^{-6} m s^{-1} is set for unconsolidated porous media (Fig. S4.3). The original data were gridded to 5$'$ by using an area-weighted average and used as hydraulic conductivity of the upper model layer. For the second layer, hydraulic conductivity of the first layer is reduced assuming that conductivity decreases exponentially with depth. Based on the e-folding factor f used by Fan et al. (2013) (a calibrated parameter based on terrain slope), conductivity of the lower layer is calculated by multiplying the upper layer value by $\exp(-50m\,f^{-1})^{-1}$ (Fan et al., 2007).

Mean annual GW recharge computed by WaterGAP 2.2c for the period 1901–2013 is used as input (Fig. S4.4), while no net abstraction from GW was taken into account. It would not be meaningful to try to derive a steady-state solution under existing net groundwater abstractions that in some regions cause GW depletion with continuously dropping water tables. The 0.5° data of WaterGAP were equally distributed to the pertaining cells. Regarding the ocean boundary condition, h_{ocean} is set to 0 m and c_{ocean} to 10 m^2 d^{-1} (Table 2), reflecting a global average conductance based on hydraulic conductivity and lateral surface area.

It is assumed that there is exchange of water between GW and one river stretch in each 5$'$ grid cell, and additionally where lakes and wetlands exist according to WaterGAP 3, which provides, for each grid cell, the area of “local” and “global” lakes and wetlands. In WaterGAP, local SW bodies are only recharged by runoff produced within the grid cell, while global SW bodies also obtain inflow from the upstream cell. In an uncoupled model, it is difficult to prescribe the, in reality temporal variable, area of lakes and wetlands that

Table 2. Model parameter values, input data sources, and other information about the steady-state simulation.

Parameter	Symbol	Units	Description	Eq. no.
Land mask	–	–	location and area of 2 161 074 cells at $5'$ resolution based on WaterGAP 3 (Eisner, 2016)	–
GW recharge	R_g	L^3T^{-1}	mean annual diffuse GW recharge 1901–2013 of WaterGAP 2.2c (Müller Schmied et al., 2014) forced with EWEMBI (Lange, 2016), spatial resolution 0.5° (Fig. S4.4)	2, 5, S1
Hydraulic conductivity	K_aq	LT^{-1}	derived from Gleeson et al. (2014) (Fig. S4.3)	1, 3
Hydraulic head	$h_{(\mathrm{aq})}$	L	head of the aquifer in a computational cell, initial estimate based on $5'$ average of $30''$ head by Fan et al. (2013)	1, 6, 5
Ocean boundary conductivity	c_ocean	L^2T^{-1}	$10\,\mathrm{m}^2\,\mathrm{d}^{-1}$	2, 6
Ocean boundary head	h_ocean	L	global mean sea level of 0 m	6
SW head	h_swb	L	30th quantile (P_{30}) of $30''$ land surface elevation by Fan et al. (2013) per $5'$ grid cell	3
SW bottom elevation	B_swb	L	2 m (wetlands), 10 m (local lakes), 100 m (global lakes) below P_{30}	4
Area of global and local lakes and global and local wetlands	WL	L^2	per $5'$ grid cell, based on WaterGAP 3 (Eisner, 2016),	4
Length of the river	L	L	per $5'$ grid cell, based on WaterGAP 3 (Eisner, 2016)	4
Width of the river	W	L	per $5'$ grid cell, based on WaterGAP 3 (Eisner, 2016)	4
River head	h_riv	L	h_swb	4, 5
River bottom elevation	B_riv	L	$h_\mathrm{riv} - 0.349 \times Q_\mathrm{bankfull}^{0.341}$ (Allen et al., 1994)	5
Equilibrium hydraulic head	h_eq	L	steady-state hydraulic head by Fan et al. (2013) (averaged to $5'$ from original spatial resolution of $30''$)	5
Layers	–	–	two confined, 100 m thick each	–
Land surface elevation	–	L	$5'$ average of $30''$ digital elevation map by Fan et al. (2013) (Fig. S4.2)	–
E-folding factor	–	–	applied only to lower layer for 150 m depth, based on area-weighted average by Fan et al. (2013)	–
Time step	t	T	daily time step	–
Head convergence criterion (outer loop)	–	L	max head change globally $<$ 10 m in three consecutive iterations	–
Residual convergence criterion (inner loop)	–	–	$\|\|$ conjugate gradient residuals $\|\|_\mathrm{inf} < 10^{-100}$ in $\mathrm{m}^3\,\mathrm{d}^{-1}$	
Maximum number of inner iterations	–	–	maximum 50 inner iterations between outer Picard iterations (Naff and Banta, 2008)	–

affect the flow exchange between SW body and GW. Maps generally show the maximum spatial extent of SW bodies. This maximum extent is seldom reached, in particular in the case of wetlands in dry areas. For global wetlands (wetlands greater than one $5'$ cell), it is therefore assumed in this model version that only 80 % of their maximum extent is reached. In the transient model SW body areas change over time. A further difficulty in an uncoupled model run is that the water table elevation of SW bodies does not react to the GW–SW exchange flows Q_swb and that water supply from SW is not limited by availability. A losing river may in reality dry out and therefore cease to lose any more water. For rivers, B_swb is set to $h_\mathrm{riv} - 0.349 \times Q_\mathrm{bankfull}^{0.341}$ (Allen et al., 1994), where Q_bankfull is the bank-full river discharge in the $5'$ grid cell

(Verzano et al., 2012). Globally constant values are used for B_{swb} for wetlands, local lakes, and global lakes (Table 2).

For the steady-state model, all SW bodies in a grid cell are assumed to have the same head, i.e., $h_{\mathrm{riv}} = h_{\mathrm{swb}}$. We found that for both gaining and losing conditions, Q_{swb} and thus computed hydraulic heads are highly sensitive to h_{swb}. The overall best agreement with the hydraulic head observations by Fan et al. (2013) was achieved if h_{swb} (Eqs. 3, 4, and 5) was set to the 30th percentile (P_{30}) of the 30′′ land surface elevation values by Fan et al. (2013) per 5′ cell, e.g., the 30′′ elevation that is exceeded by 70 % of the one-hundred 30′′ elevation values within one 5′ cell. To decrease convergence time, we used h_{eq} derived from the high-resolution steady-state hydraulic head distribution by Fan et al. (2013) as initial guess of h_{aq}. In each outer iteration (Sect. 2.4) gaining and losing conditions may change depending on the current head solution.

2.3 Integration into WGHM

We intend to integrate G^{3}M into WaterGAP 2, i.e., the 0.5° version of WaterGAP (for details see Sect. S1), to keep computation time low enough for performing sensitivity analyses and ensemble-based data assimilation and calibration, instead of integrating it into WaterGAP 3 (Eisner, 2016), which has the same spatial resolution as G^{3}M. However, data from WaterGAP 3 were used to set up G^{3}M. Location and area of the 5′ grid cells of G^{3}M are the same as in the land mask of WaterGAP 3. In addition, the percentage of the 5′ grid cell area that is covered by lakes (including reservoirs) and by wetlands, based on Lehner and Döll (2004), is taken from WaterGAP 3, as well as the length and width of the main river within each 5′ grid cell as (Table 2).

2.4 Model implementation

G^{3}M is implemented using a newly developed open-source model framework G^{3}M-f (Reinecke, 2018a). The main motivation to develop a new model framework is the efficient in-memory coupling to the GHM and flexible adaptation to the specific requirements of global-scale modeling. Written in C++14, the framework allows the implementation of global and regional groundwater models alike while providing an extensible purely object-oriented model environment. It is primarily targeted as an extension to WaterGAP but allows for an in-memory coupling to any GHM or can be used as a stand-alone groundwater model. It provides a unit-tested (Dustin, 2006) environment offering different modules that can couple in-memory results to a different model or write out data flows to different file formats. G^{3}M-f has the following advantages over using an established GW modeling software such as MODFLOW. G^{3}M-f enables an improved coupling capability. Unlike MODFLOW, it provides a clear development interface to the programmer coupling a model to G^{3}M-f. It can be easily compiled as a library and provides a clearly separated logic between computation and data read-in or write-out). It is written in the same language as the target GHM enabling a straight-forward in-memory access to arrays without the need to write data to disk, required when coupling with MODFLOW (a very computationally expensive operation even if that disk is a RAM-disk). Even though it is possible to call FORTRAN functions from C++, it is very complicated to pass file pointers properly, as the I/O implementation of both languages differs substantially and it is widely considered bad practice to handle I/O in two different languages at once. As MODFLOW was never designed to be coupled or integrated to or into other models, it is not possible to separate the I/O logic fully from the computational logic without substantial code changes that are hard to test. To this end, G^{3}M-f provides a highly modularized framework that is written with extensibility as design goal while implementing all required groundwater mechanisms.

Equation (1) is reformulated as finite-difference equation and solved using a conjugate gradient approach and an incomplete LUT (incomplete lower–upper factorization with dual-threshold strategy) preconditioner (Saad, 1994). In order to keep the memory footprint low, the conjugate gradient method makes use of the sparse matrix. Furthermore, it solves the equations in parallel (preconditioner currently nonparallel). As internal numerical library, G^{3}M uses Eigen3 (http://eigen.tuxfamily.org, last access: 1 June 2019). G^{3}M can compute the presented steady-state solution (with the right-hand side of Eq. 1 being zero and the heads by Fan et al., 2013, as initial guess, Tables 1, 2) on a commodity computer with four computational cores and a standard solid-state drive in about 30 min while occupying 6 GB of RAM.

Similar to MODFLOW, G^{3}M-f solves Eq. (1) in two nested loops using a Picard iteration (Mehl, 2006): (1) the outer iteration checks the head and residual convergence criterion (if the maximum head change between iterations is below a given value in three consecutive iterations and/or the norm of the residual vector of the conjugate gradient (Harbaugh, 2005; Niswonger et al., 2011) is below a given value). It adjusts head-dependant values, for example, from gaining to losing conditions and updates the system of linear equations if flows are no longer head dependent. (2) The inner loop primarily consists of the conjugate gradient solver, which runs for a number of iterations defined by the user or until the residual convergence criterion is reached (Table 2), solving the current system of linear equations.

Because switching between Eqs. (4) and (5), which occurs if, for example, h_{aq} drops below h_{riv} from one iteration to the next, causes an abrupt change of c_{riv} inducing a nonlinearity that affects convergence, we introduced an $\epsilon = 1$ m interval around h_{riv} and interpolate c_{riv} between Eqs. (4) and (5) by a cubic hermite spline polynomial over that interval. This allows for a smoother transition between both states, reducing the changes in the solution if a river is in a gaining condition in one iteration and in a losing condition in the next or vice versa.

Different from Vergnes et al. (2014), G^{3}M's computations are not based on spherical coordinates directly but on an irregular grid of quadratic cells of different size depending on the latitude. Cell sizes are provided by WaterGAP3 and are derived from their spherical coordinates maintaining their correct area and center location. The model code will be adapted in the future to account for the different lengths in x and y directions per cell correctly.

3 Results

3.1 Global hydraulic head and water table depth distribution under natural steady-state conditions

As expected, the computed global distribution of steady-state hydraulic head (in the upper model layer) under natural conditions (Fig. 2a) largely follows the land surface elevation (Fig. S4.2), albeit with a lower range and locally different ratios between the hydraulic head and land surface gradients (Fig. S4.6). Water table depth (WTD), i.e., the distance between the groundwater table and the land surface, can be computed by subtracting the hydraulic head computed by G^{3}M for the upper layer of each 5′ grid cell from the arithmetic mean of the land surface elevations of the one-hundred 30″ grid cells within each 5′ cells (Fig. S4.2). The global map of steady-state WTD (Fig. 2b) clearly resembles the map of differences between surface elevation and P_{30} , the assumed water level of SW bodies h_{swb}, shown in Fig. S4.1, which indicates that simulated WTD is strongly governed by the assumed water level in SW bodies.

Deep GW, i.e., a large WTD, occurs mainly in mountainous regions (Fig. 2b). These high values of WTD are mainly a reflection of the steep relief in these areas as quantified either by the differences in mean land surface elevations between neighboring grid cells (Fig. S4.7) or the difference between mean land surface elevation and P_{30}, the 30th percentile of the 30″ land surface elevations (Fig. S4.1). When computed hydraulic head is subtracted not from average land surface elevation but from P_{30} (the assumed water table elevation of SW bodies), the resulting map shows that the groundwater table is mostly above P_{30}, in both flat and steep terrain (Fig. 2c). Thus, high WTD values at the 5′ resolution do not indicate deep unsaturated zones and losing rivers but just high land surface elevation variations within a grid cell. In steep terrain, 5′ water tables are higher above water level in the surface water bodies than in flat terrain (Fig. 2c). Deep GW tables that are not only far below the mean land surface elevation but also below the water table of surface water bodies are simulated to occur in some (steep or flat) desert areas with very low GW recharge. Negative WTD only occurs in places were the P_{30} is above the mean surface elevation, e.g., parts of the Netherlands (Fig. 2b). Fewer than 10 cells experience WTD less than −10 m, which is very likely due to a not fully converged head solution.

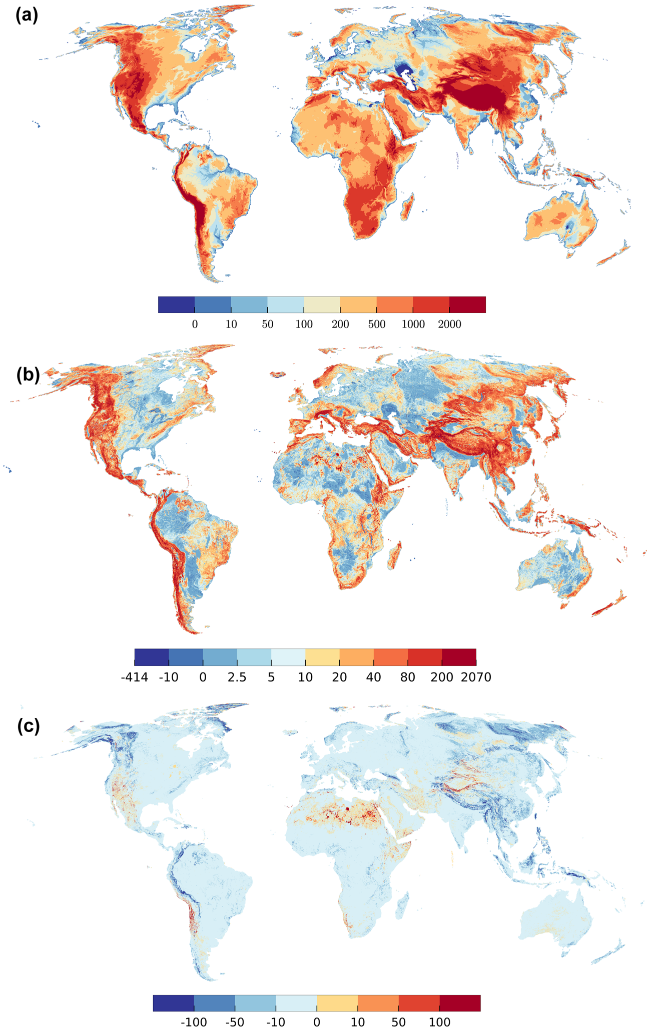

Figure 2. (a) Simulated steady-state hydraulic head of groundwater above sea level (meters). Maximum value 6375 m, minimum −414 m (extremes included in dark blue and dark red). **(b)** Water table depth (meters). **(c)** Difference between 30th percentile of the 30″ land surface elevation per 5′ grid cell (chosen elevation for surface water bodies h_{swb}) and simulated groundwater head (meters). Maximum value 1723 m, minimum value −1340 m (extremes included in dark blue and dark red).

In 2.1 % of all cells, GW head is simulated to be above the average land surface elevation by more than 1 m in 0.3 % and by more than 100 m in 0.004 % of the cells. The shallow water table in large parts of the Sahara is caused by losing rivers (and some wetlands) that cannot run dry in the model, causing an overestimation of the GW table (Sect. 2.2). Please note that the computed steady-state WTD certainly underestimates the steady WTD in GW depletion areas such as the High Plains Aquifer and the Central Valley in the USA (Sect. S2), northwestern India, the North China Plain, and parts of Saudi Arabia and Iran (Döll et al., 2014) as ground-

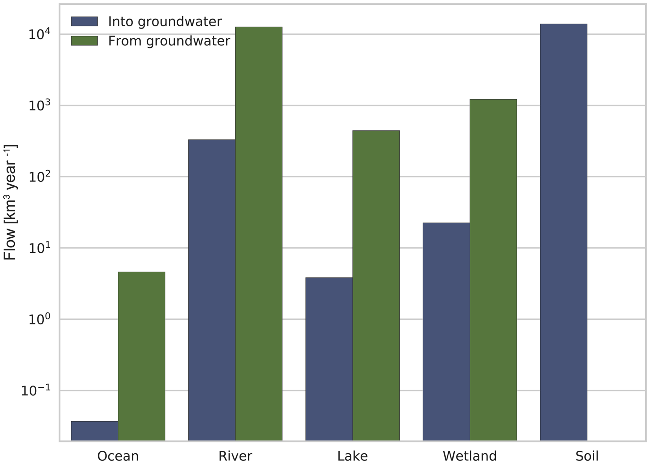

Figure 3. Global sums of flows from different compartments into or from GW at steady state. Flows into the GW are denoted by the color blue, flows out of the GW into the different compartments by green. The compartment soil is the diffuse GW recharge from soil calculated by WaterGAP.

water withdrawals are not taken into account in the presented steady-state simulation of G^{3}M.

3.2 Global water budget

Inflows to and outflows from GW of all G^{3}M grid cells were aggregated according to the compartments ocean, river, lake, wetland, and diffuse GW recharge from soil (Fig. 3). The difference between the global sum of inflows and outflows is less than 10^{-6} %. This small volume balance error indicates the correctness of the numerical solution.

Total diffuse GW recharge, model input from WaterGAP, from soil is 10^4 km^3 yr^{-1} and approximately equal to the simulated flow of GW to rivers (Fig. 3). Rivers are the ubiquitous drainage component of the model, followed by wetlands, lakes, and the ocean boundary. According to G^{3}M, the amount of river water that recharges GW is more than 1 order of magnitude smaller than GW flow to rivers (Fig. 3). Possibly, flow from SW bodies to GW is overestimated, as outflow from SW is not limited by water availability in the SW, and depending on the hydraulic conductivity, Eqs. (4) and (5) can lead to rather large flows. Inflow from the ocean, which is more than 2 orders of magnitude smaller than outflow to ocean, occurs in regions where $h_{\mathrm{swb}} = P_{30}$ is below h_{ocean}, e.g., the Netherlands. Globally, lakes and wetlands are computed to receive up to 10^3 km^3 yr^{-1} of water from GW, and lose 1–2 orders of magnitude less.

3.3 GW–SW interactions

Figure 4 plots the spatial distribution of simulated flows from and to lakes and wetlands (Fig. 4a) as well as from and to rivers (Fig. 4b). Parallel to the overall budget (Fig. 3), the map reveals the globally large, but locally strongly varying, influence of lakes and wetlands (Fig. 4a). Rivers with riparian wetlands such as the Amazon River receive comparably small amounts of GW as most of the GW is drained by the wetland (compare Fig. 4a and b). Similarly, areas dominated by wetlands and lakes (e.g., parts of Canada and Scandinavia) show less inflow for rivers (Fig. 4b). In G^{3}M, all SW bodies (rivers, lakes, and wetlands) in a grid cell either lose or gain water. Consistent with negative or positive differences between h_{swb} and h_{aq} (Fig. 2c), 93 % of all grid cells contain gaining rivers and only 7 % losing rivers. Gaining lakes and wetlands are found in 12 % and 11 % of the cells, respectively, whereas only 0.2 % contain a losing lake or wetland.

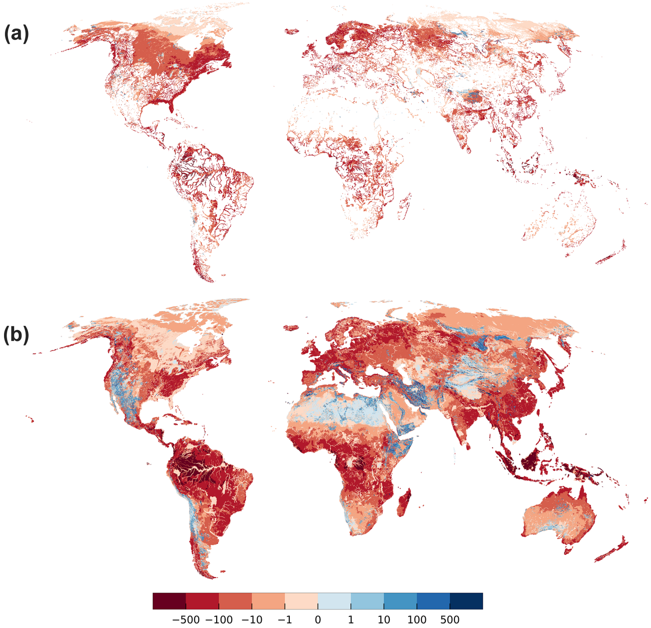

Figure 4. Flow Q_{swb} (mm yr^{-1}) from or to wetlands, lakes **(a)**, and losing or gaining streams **(b)** with respect to the 5′ grid cell area. Gaining surface water bodies are shown in red, surface water bodies recharging the aquifer in blue. Focused aquifer recharge occurs in arid regions, e.g., alongside the river Nile, and in mountainous regions where the average water table is well below the land surface elevation.

Gaining rivers, lakes, and wetlands with very high absolute Q_{swb} values over 500 mm yr^{-1} (averaged over the grid cell area of approximately 80 km^2) can be found in the Amazon and Congo basins as well in Bangladesh and Indonesia, where GW recharge in very high (Fig. S4.4). Values below 1 mm yr^{-1} occur in dry and permafrost areas where groundwater recharge is low.

Losing SW bodies are caused by a combination of low GW recharge from soil (Fig. S4.4) and steep mountainous terrain (Fig. S4.7). While the steep Himalayas receive enough GW recharge to have gaining SW bodies, this is not the case for the much dryer mountain ranges around the Taklamakan desert in central Asia or mountainous Iran where SW bodies are losing. In the Sahara, GW recharge is so low that SW bodies are losing even in relatively high terrain.

Rivers lose more than 100 mm yr^{-1} in Ethiopia and Somalia, west Asia, northern Russia, the Rocky Mountains, and the Andes, whereas lower values can be observed in Australia and in the Sahara. High values of outflow from wetlands and lakes are found in Tibet, the Andes, and northern Russia, and lower values in the Sahara and Kazakhstan. The river Nile in northern Republic of Sudan and Egypt is correctly simulated to be a losing river (Fig. 4b), being an allogenic river that is mainly sourced from the upstream humid areas, including the artificial Lake Nasser (Elsawwaf et al., 2014) (Fig. 4a). Furthermore, the following lakes and riparian wetlands are simulated to recharge GW: parts of the Congo River, Lake Victoria, the IJsselmeer, Lake Ladoga, the Aral Sea, parts of the Mekong Delta, the Great Lakes of North America. On the other hand, no losing stretches are simulated along the Niger River and its wetlands and almost none in the northeastern Brazil even though losing conditions are known to occur there (Costa et al., 2013; FAO, 1997). This is also true when the minimum elevation for SW bodies is assumed (compare Fig. S4.10) leading to the conclusion that the misrepresentation might be linked to an inadequate representation of the local geology.

Simulated flows between GW and SW depend on assumed conductances for both rivers and lakes or wetlands (Eqs. 3, 4, 5) shown in Fig. 5. Q_{swb} (Fig. 4) correlates positively with conductance. Conductance for gaining rivers correlates positively with GW recharge (Eq. 5 and Fig. S4.4). High river conductance values are reached in the tropical zone due to a high GW recharge but are capped at a plausible maximum value of 10^7 m^2 d^{-1} in the case of a river (Sect. 2.1) (Fig. 5b). Lakes and wetlands can have larger values of conductance due to their large areas, e.g., in Canada or Florida.

3.4 Lateral flows

Figure 6 shows lateral GW flow (between grid cells, summing up over all model layers) in percent of the sum of diffuse GW recharge from soil and GW recharge from SW bodies. The percentage of recharge that is transported through lateral flow to neighboring cells depends on five main factors: (1) hydraulic conductivity (Fig. S4.3), (2) diffuse GW recharge (Fig. S4.4), (3) losing or gaining SW bodies (Fig. 4), (4) their conductance (Fig. 5), and (5) the head gradients (Fig. 2a).

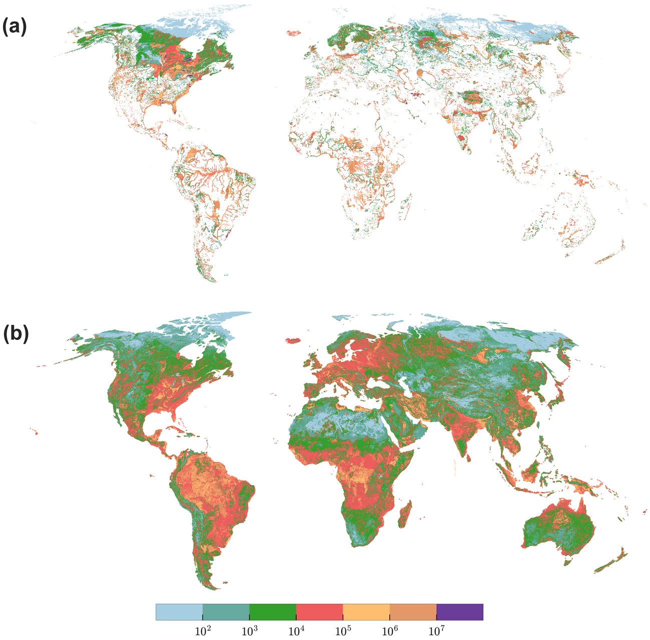

Figure 5. Conductance (m^2 d^{-1}) of lakes and wetlands **(a)** and rivers **(b)**. In regions close to the pole, conductance is in general lower due to the influence of the low aquifer conductivity (losing conditions), and relatively small GW recharge due to permafrost conditions (only applies for gaining conditions). Max conductance of wetlands is 10^8 m^2 d^{-1}.

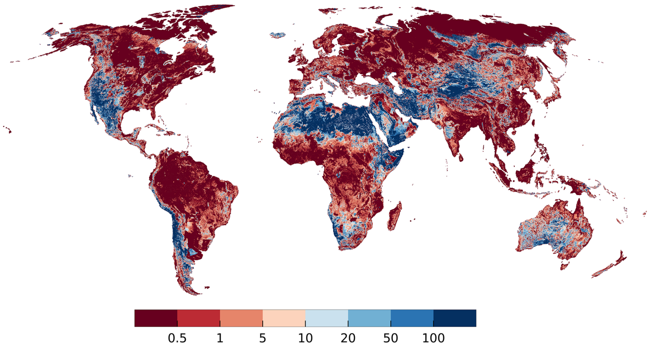

Figure 6. Percentage of GW recharge from soil and surface water inflow that is transferred to neighboring cells through lateral out flow (sum of both layers). Grid cells with zero total GW recharge are shown in white (a few cells in the Sahara and the Andes).

On large areas of the globe, where GW discharges to SW bodies, the lateral flow percentage is less than 0.5 % of the total GW recharge to the grid cell, as most of the GW recharge in a grid cell is simulated to leave the grid cell by discharge to SW bodies. For example, in the permafrost regions, the assumed very low hydraulic conductivity limits the outflow to neighboring cells of the occurring recharge, leading to these very low percent values. Such values also occur in regions with high SW conductances and rather low hydraulic conductivities, e.g., in the Amazon Basin. Values of more than 5 % occur where hydraulic conductivity is high even if the terrain in rather flat, such as in Denmark. Higher values may occur in the case of gaining SW bodies in dry areas like Australia or in the Taklamakan desert. They can also be observed in mountainous regions where large hydraulic gradients can develop. In mountains with gaining surface water bodies, lateral outflows may even exceed GW recharge of the cell. In grid cells where SW bodies recharge the GW, outflow tends to be a large percentage of total GW recharge as there is no outflow from GW other than in the lateral directions, and values often exceed 100 % (Fig. 6).

3.5 Comparison to groundwater well observations and the output of two higher-resolution models

Global observations of WTD were assembled by Fan et al. (2007, 2013). We selected only observations with known land surface elevation and removed observations where a comparison to local studies suggested a unit conversion error. This left a total of 1 070 402 WTD observations. An “observed head” per 5′ model cell was then calculated by first computing the hydraulic head of each observation by subtracting WTD from the 5′ average of the 30″ land surface elevation and then calculating the arithmetic mean of all observations within the 5′ model cell. This resulted in 78 664 grid cells with observations out of a total of 2.2 million G^{3}M top-layer grid cells. Multiple obstacles limit the comparability of observations to simulated values. (1) Observations were recorded at a certain moment in time influenced by seasonal effects and abstraction from GW, whereas the simulated heads represent a natural steady-state condition. (2) Observation locations are biased towards river valleys and productive aquifers. (3) Observations may be located in valleys with shallow local water tables too small to be captured by a coarse resolution of 5′.

Simulated steady-state hydraulic heads in the upper model layer are compared to observations in Fig. 7. Shallow GW is generally better represented by the model than deeper GW. Especially the water table in mountainous areas is underestimated, which may be related to observations in perched aquifers caused by low permeability layers (Fan et al., 2013) that are not represented in G^{3}M due to lacking information. Because the steady-state model cannot take into account the impact of GW abstraction, the computed WTD values are considerably smaller than currently observed values in GW depletion areas like the Central Valley in California (where once wetlands existed before excessive GW use depleted the aquifer) and the High Plains Aquifer in the American Midwest of the USA. Still, the elevation of the GW table in the nondepleted Rhine valley in Germany is overestimated, too. Overestimates in the Netherlands may partially be due to artificial draining. Figure 8a shows the hydraulic head comparison as a scatter plot. Overall, the simulation results tend to underestimate observed hydraulic head but much less than the steady-state model presented by de Graaf et al. (2015) (their Fig. 6).

To compare the performance of G^{3}M to the steady-state results of two high-resolution models by Fan et al. (2013) and ParFlow (Maxwell et al., 2015) (Table 1), heads in 30″ (Fan et al., 2013) and 1 km (ParFlow) grid cells were averaged to the G^{3}M 5′ grid cells. The comparison of 5′ observations to the 5′ average of ParFlow seems to be consistent with the 1 km model comparison in Maxwell et al. (2015) (their Fig. 5), even though overestimates or underestimates in the original resolution seem to be smoothed out by averaging to 5′ (not shown). The heads by Fan et al. (2013) fit better to observations than G^{3}M heads, with less underestimation (Fig. 8b) and a RMSE (root mean square error) of 26.0 m compared to the 32.4 m RMSE of G^{3}M. The comparison of G^{3}M heads to values by Fan et al. (2013) for all 5′ grid cells, which are also the initial heads of G^{3}M and the basis to compute river conductances, shows that heads computed with the G^{3}M are mostly much lower except in regions with a shallow GW (Fig. 8c); RMSE is 46.7 m. This cannot be attributed to the 100 times lower spatial resolution per se but to the selection of the 30th percentile of the 30″ as the SW drainage level. Outliers in the upper half of the scatter plot, with much larger G^{3}M heads than the initial values (Fan et al., 2013), are mainly occurring in steep mountainous areas like the Himalayas where the 5′ model is not representing smaller valleys with a lower head. For the continental US, the computationally expensive 1 km integrated hydrological model ParFlow (Maxwell et al., 2015) fits much better to observations than G^{3}M (Fig. 8d, e), with a RMSE of 14.3 m (ParFlow) compared to 34.2 m (G^{3}M). G^{3}M produces a generally lower water table (Fig. 8f), a main reason being that ParFlow assumes an impermeable bedrock at a depth of 100 m below the land surface elevation.

The global map of head comparison (Fig. 7) suggests that G^{3}M performs reasonably well in flat areas compared to mountainous regions. This is corroborated by Fig. 9, which shows the difference between observed and simulated hydraulic heads for five land surface elevation categories. It is evident that model performance deteriorates with increasing land surface elevation and positively correlates with variations in land surface elevation within each grid cell (Fig. S4.7).

Plotting hydraulic head instead of WTD has the disadvantage that the goodness of fit is dominated by the topography as the observed heads are calculated based on the surface elevation of the model. Well observations provide WTD and only sometimes contain complementary data specifying the elevation at which the measurements were taken. Even though hydraulic heads are a direct result of the model and are forcing lateral GW flows, WTD is more relevant for processes like capillary rise. For G^{3}M, there is almost no correlation between WTD observations and simulated values. To our knowledge, no publication on large-scale GW modeling has presented correlations of simulated with observed WTD.

3.6 Testing sensitivity of computed steady-state hydraulic heads to parameter values and spatial resolution

To limit the computational effort for assessing model sensitivity to both parameters and grid size, we selected New Zealand as a representative “small world” that includes a complex topography and the ocean as a clear boundary con-

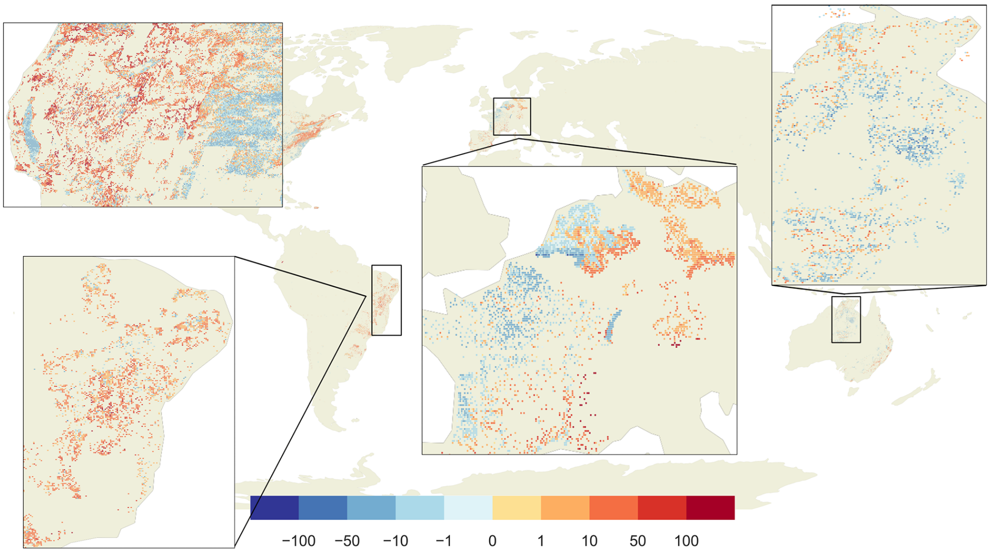

Figure 7. Differences between observed and simulated hydraulic head (metres). Red dots show areas where the model simulated deeper GW as observed, blue shallower GW. In the gray areas, no observations are available.

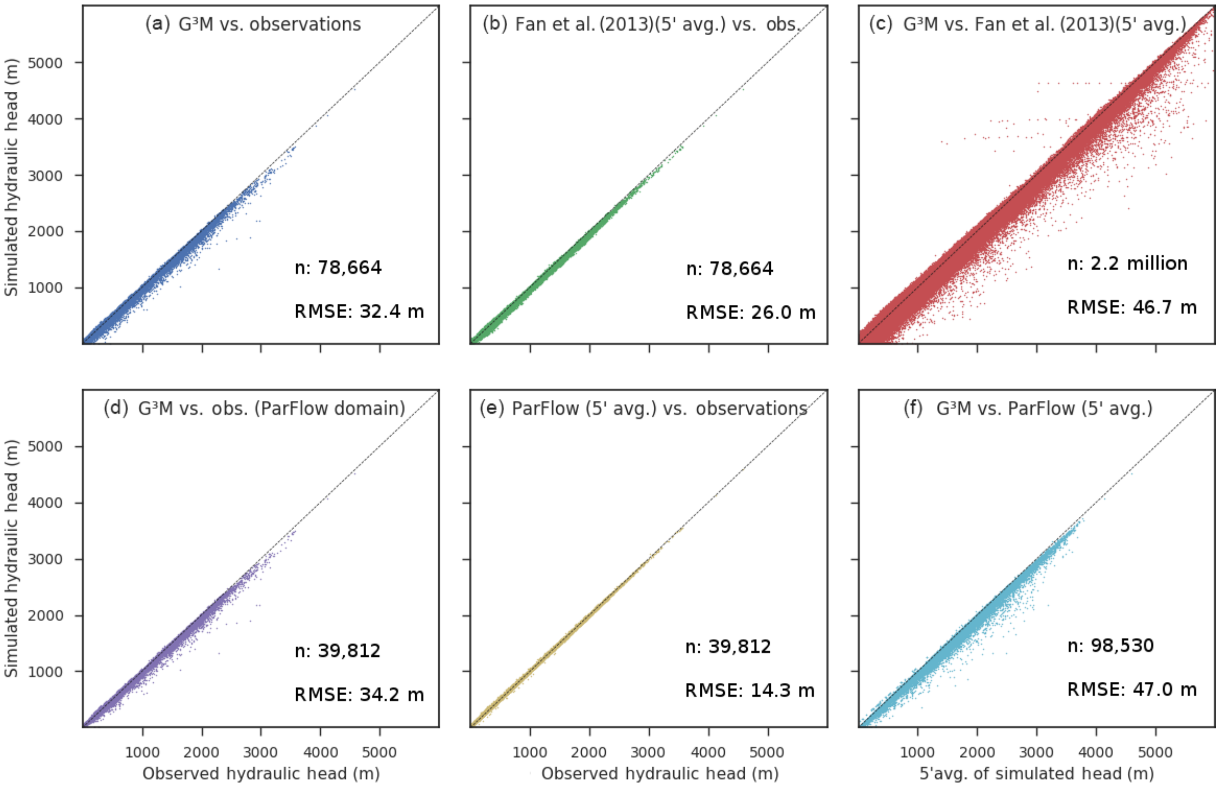

Figure 8. Scatter plots of simulated vs. observed hydraulic head and inter-model comparison of heads. The steady-state run of G^{3}M vs. observations **(a)**, the 5′ average of the equilibrium head by Fan et al. (2013) vs. observations **(b)**, and the avg. equilibrium vs. G^{3}M **(c)**. The steady-state run of G^{3}M vs. observations only for the ParFlow domain **(d)**, the 5′ average of the ParFlow average annual GW table (Maxwell et al., 2015) vs. observations **(e)**, and the steady-state run of G^{3}M vs. 5′ average of the ParFlow average annual GW table **(f)**.

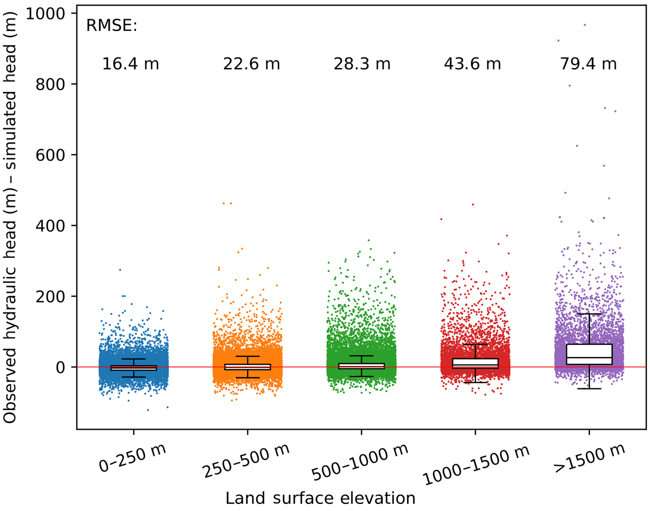

Figure 9. Observed minus simulated hydraulic head for different land surface elevation categories. The whiskers of the boxplots show the interquartile range.

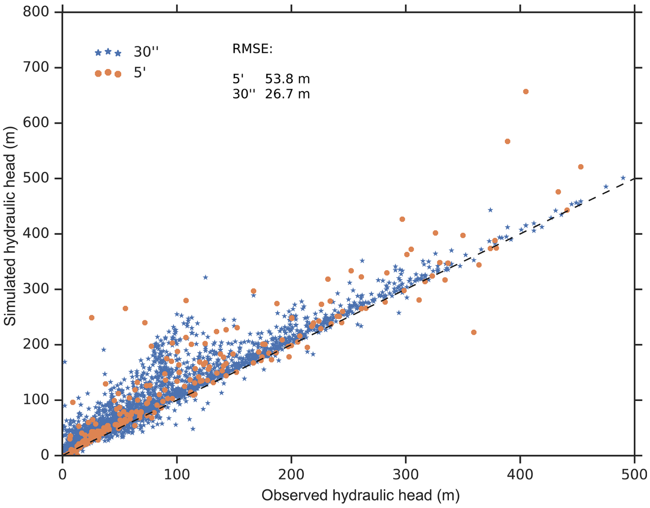

Figure 10. Low (5′) vs. high (30″) spatial resolution for the Canterbury region in New Zealand: comparison of observed vs. simulated hydraulic head for both resolutions. The observed head is the geometric mean per 5′ and 30″, respectively.

dition. All inputs and parameters are the same as in the global 5′ model.

3.6.1 Parameter sensitivity

To determine which parameters simulated hydraulic heads are most sensitive to, we used the established sensitivity tool UCODE 2005 (Hill and Tiedeman, 2007) to compute composite scaled sensitivity (CSS) values for seven model parameters (Sect. S3). CSS of h_{swb} is orders of magnitude larger than the CSS of the other parameters. This confirms our observations during model development when an appropriate value had to be found (Sect. 2.2). The second-most important parameter is K_{aq} and the third-most important R_{g}. CSS of the conductance of lakes is 1 order of magnitude less than CSS of R_{g} but as only few cells contain lakes, the CSS value that averages over all grid cells indicates a large sensitivity to c_{Lakes} for grid cells with lakes. Simulated hydraulic heads were found to be rather insensitive to changes in the conductance of rivers, wetlands, or ocean boundary.

3.6.2 Sensitivity to spatial resolution

The extremely high sensitivity of simulated hydraulic heads to the choice of h_{swb} (Sect. 3.6.1) and the better agreement of the continental models with a higher spatial resolution of approx. 30″ (the Fan et al., 2013, model and ParFlow, Sect. 3.5) motivated us to run G^{3}M for New Zealand with a spatial resolution of 30″ to understand the impact of spatial resolution on simulated hydraulic heads. The 30″ G^{3}M model uses the same input as the 5′ model except for the land surface elevation, h_{swb}, and the location of rivers. While the total lengths and widths of the rivers are equal in both models – a river is assumed to exist in all 5′ grid cells – the river is concentrated – in the 30″ model – to a few 30″ grid cells within each 5′ grid cell. The river cell locations at 30″ are determined based on 30″ HydroSHEDS (https://hydrosheds.org/, last access: 1 June 2019) information on flow accumulation. Starting with the 30″ cell with the highest number of upstream cells per 5′ cell, a river is added to this 30″ cell using the length and information of HydroSHEDS until the size of the river of the 5′ model is reached for all 30″ cells within a 5′ cell. The areal fraction of all other SW bodies from 5′ grid data is used for all 30″ grid cells within the 5′ grid cell. h_{swb} is set to the land surface elevation.

Figure 10 compares the performance of the two model versions. The comparison of simulated hydraulic head to observations for the Canterbury region (Westerhoff et al., 2018) shows that the overall performance of the 30″ model is better, with a smaller RMSE of 26.7 m as compared to a RMSE of 53.8 m in the case of the original spatial resolution of 5′. The 30″ model results in generally lower simulated hydraulic heads leading to a closer fit to the observed values. This is likely caused by the improved estimation of SW body elevation, which generally leads to lower estimates of h_{swb}. On the other hand, overestimates of observed hydraulic heads prevails in the 30″ model, even though h_{swb} was set to the land surface elevation, indicating that further investigation is necessary. The underestimates are likely due to large GW abstractions for irrigation in the particular region (Westerhoff et al., 2018).

4 Discussion

The objective of global gradient-based groundwater flow modeling with G^{3}M is to better simulate water exchange between SW and GW in the GHM WaterGAP, e.g., for an improved estimation of GW resources in dry regions of the globe that are augmented by focused recharge from SW bodies. We assume that the fully coupled model will lead to an improved WaterGAP performance during droughts with an increased drop in streamflow due to the now possible switch from gaining to losing conditions. It is presumable that a calibration of c_{swb} and c_{riv} is necessary to achieve a good discharge performance. The presented steady-state model is the first step in this direction. It helped to understand basic model behavior, e.g., the sensitivity to SW body elevation, and the necessary improvement of its parameterization, before moving to the more complex integrated transient model. The reduced runtime of the steady-state model in comparison to a fully integrated transient run supported the investigation of parameter sensitivity and sensitivity to spatial resolution. Additionally, the presented steady-state model can be used in future fully integrated transient runs as initial condition.

A major challenge for simulating GW–SW interactions (but also capillary rise) at the global scale is the large size of grid cells that is required due to computational constraints. Within the 5′ grid cells, land surface elevation at the scale of 30″ very often varies by more than 20 m, and often by 200 m and more (Fig. S4.1), while the vertical position of the cell and the hydraulic head are approximated in the model by just one value. The question is whether head-dependent flows between grid cells, between GW and SW, and from GW to soil (capillary rise) can be simulated successfully at the global scale, i.e., whether an improved quantification of these flows as compared to the simple linear reservoir model currently used in most GHMs can be achieved by this approach. This question cannot be answered before a dynamic coupling of G^{3}M with a global hydrological model has been achieved, but one may speculate that some innovative approach to take into account the elevation variations within the grid cells is needed.

It is difficult to the assess quality of the presented steady-state G^{3}M results. Model performance assessment is hindered by poor data availability and the coarse model resolution. (1) To our knowledge the data collection of depth to groundwater by Fan et al. (2013) is unique. However, they do not represent steady-state values. Apart from depth to groundwater observations, hardly any relevant data are available at the global scale. Especially the exchange between surface water and groundwater is difficult to measure even at the local scale. Therefore, we compared G^{3}M results with the results from other large-scale models. Comparison to the results of catchment-scale groundwater flow models is planned for transient runs that will be possible after integration into WaterGAP. (2) Scale differences make the comparison to point observations of depth to groundwater difficult. Often, observations are biased towards alluvial aquifers in valleys. The calculated hydraulic head of the grid cell may represent the average groundwater level per grid cell correctly but can be still far off the local observations of depth to groundwater. As the current model only represents an uncalibrated natural steady state, a comparison to observations only provides the first indicator where the model and the performance measurements need to be improved as we move to a fully transient model.

The presented development of the uncoupled steady-state global GW flow model enabled us to better understand how the spatial hydraulic head pattern relates to the fundamental drivers of topography, climate, and geology (Fan et al., 2007) and how the interaction to SW bodies governs the global head distribution. Simulated depth to groundwater is particularly affected by the assumed hydraulic head in SW bodies, the major GW drainage component in the model. As rivers represent a naturally occurring drainage at the lowest point in a given topography, one would assume that the minimum elevation 30″ land surface elevation per 5′ grid cell is a reasonable choice. Experiments have shown that this will induce a head distribution well below the average 5′ elevation that is much below observations by Fan et al. (2013). We also tested setting h_{swb} to the average elevation of all "blue" cells (with a WTD of less than 0.25 m) of the steady-state 30″ water table results by Fan et al. (2013) that indicate the locations where GW discharges to the surface or SW bodies. This leads to an overall underestimation of the observed hydraulic heads (Fig. S4.9) as the assumed SW elevation is too low. Furthermore, it leads to an increase in losing SW bodies (compare Fig. S4.10 with Fig. 4). However, it is difficult to judge whether this improves the simulation. More stretches of the Nile and its adjacent wetlands and also of the Niger wetlands and rivers in northeastern Brazil are losing in the case of lower h_{swb}, which appears to be reasonable. Additionally, choosing the average as SW elevation provides, on the on hand, a better fit to observations (Fig. S4.9 right) but leads to a worldwide flooding (Fig. S4.9) and a much longer convergence time due to an increased oscillation between gaining and losing conditions.

The problem is very likely one of scale. All three models (Fan et al., 2013; ParFlow, and G^{3}M 30″) (Table 1), even the simple one by Fan et al. (2013), fit better to observations than the 5′ model G^{3}M (Figs. 8, 10). In the case of high resolution, there are a number of grid cells at an elevation above the average 5′ land surface elevation, leading to higher hydraulic heads in parts of the 5′ area that drain towards the SW body in a lower 30″ grid cell. In the case of the low spatial resolution of 5′ in which h_{swb} is set to the elevation of the fine-resolution drainage cell, the 5′ hydraulic head is rather close to this (low) elevation (Fig. S4.8 center), resulting in an underestimation of hydraulic head and thus an overestimation of WTD. While it is plausible and necessary to assume that there is SW–GW interaction within each of the approximately 80 km^2 cells, this is not the case for the 2 orders of magnitude smaller 30″ grid cells. Thus, with high resolution, heads are not strongly controlled everywhere by the head in SW bodies. Selecting the 30th percentile of the 30″ land surface, elevation as h_{swb} was found – by trial-and-error – to lead to a hydraulic head distribution that fits reasonably well to observed head values. This avoids the situation when the simulated GW table drops too low while also avoiding the excessive flooding that occurs if h_{swb} is set to the average of $30''$ land surface elevations, i.e., the $5'$ land surface elevation (Fig. S4.9).

The constraint that the selected h_{swb} value puts on simulated hydraulic heads is also linked to the conductance of the SW bodies. A higher conductance will lead to aquifer heads closer to h_{swb}. If the hydraulic head drops below the bottom level of the SW body, the hydraulic gradient is assumed to become 1 and the SW body recharges the GW with a rate of K_{aq} per unit SW body area. In the case of a K_{aq} value of 10^{-5} m s^{-1}, the SW body would lose approximately 1 m of water each day. Further investigations are needed regarding the appropriate choice of SW body elevation and conductance. The simple conductance approach applied in G^{3}M could possibly be improved by the approach by Morel-Seytoux et al. (2017), who proposes an analytical, and physically based, estimate of the leakance coefficient for coarse-scale models based on river and aquifer properties.

De Graaf et al. (2015) set their SW head (h_{swb}) to the mean land surface elevation (Table 1) of the $6'$ grid cells minus river depth at bank-full conditions plus water depth at average river discharge as compared to P_{30} in the $5'$ G^{3}M. Together with the missing interaction between lakes and wetlands and a different approach to river conductance, this might be a reason for the additional drainage above the floodplain that was necessary to improve the discharge to rivers (Sutanudjaja et al., 2014). On the other hand, the additional drainage leads to drainage of water even if the hydraulic head is below the SW elevation, which might have led to the global underestimation of hydraulic heads. Thus, the difference in model heads seems to be closely related to the sensitivity to SW body elevation.

Due to the course spatial resolution and lack of data, G^{3}M does not capture the actual variability in topography, aquifer depth (Richey et al., 2015) or (vertical) heterogeneity of subsurface properties. The lack of information about the three-dimensional distribution of hydraulic conductivity is expected to negatively impact the quality of simulated GW flow. For example, the lateral conductivity and connectivity of groundwater along thousands of kilometers from the Rocky Mountains in the central USA to the coast as well as the vertical connectivity are likely to be overestimated by G^{3}M, as vertical faults and interspersed aquitards are not represented; this is expected to lead to an underestimation of hydraulic head in those mountainous areas.

5 Conclusions

We have presented the concept and first results of a new global gradient-based $5'$ GW flow model G^{3}M that is to be integrated into the 0.5° GHM WaterGAP. The uncoupled steady-state model has provided important insights into challenges of global GW flow modeling mainly related to the necessarily large grid cell sizes ($5'$ by $5'$). In addition, first global maps of SW–GW interactions were generated. Simulated heads were found to be strongly impacted by assumptions regarding the interaction with SW bodies, in particular the selected elevation of the SW table. We have demonstrated that simulated G^{3}M hydraulic heads fit better to observed heads when compared to the heads of the comparable steady-state GW model by de Graaf et al. (2015), without requiring additional drainage. Furthermore, we provided insights into how the choice of surface water body elevation h_{swb} affects model outcome. In a next step, approaches for utilizing high-resolution topographic data to improve the selection of h_{swb} will be investigated.

The presented results are the first step towards a fully coupled model in which SW heads are jointly computed, also taking into account the impact of SW and GW abstraction. Especially the interaction with SW bodies that can run dry will make the G^{3}M behavior more realistic. The fully coupled model will simulate transient behavior reflecting climate variability and change. Simulated hydraulic head dynamics will be compared to observed head time series as well as to the output of large-scale regional models, while total water storage variations will be compared to GRACE satellite data. However, it will be challenging to judge the dynamics of GW and the quality of simulated GW–SW interactions due to a scarcity of observations.

Code and data availability. The model-framework code is available at http://globalgroundwatermodel.org (last access: 1 June 2019) or at https://doi.org/10.5281/zenodo.1175540 (Reinecke, 2018b) with a description of how to compile and run a basic GW model. The code is available under the GNU General Public License 3. Model output is available at https://doi.org/10.5281/zenodo.1315471 (Reinecke, 2018c).

Supplement. The supplement related to this article is available online at: https://doi.org/10.5194/gmd-12-2401-2019-supplement.

Author contributions. RR led conceptualization, formal analysis, methodology, software, visualization, and writing of the original draft. LF and SM supported review and editing as well as the development of the methodology. TT and DC supported review. PD supervised the work of RR and made suggestions regarding analysis, structure, wording of the text, and design of tables and figures.

Competing interests. The authors declare that they have no conflict of interest.

Acknowledgements. We are very grateful to Ying Fan and Gonzalo Miguez-Macho for fruitful discussions and data provisioning. We thank the reviewers for their thoughtful comments that helped to improve the paper. Furthermore, we would like to thank Alexander Wachholz for contributing to the New Zealand figures and Rogier Westerhof for providing the observations for New Zealand.

Financial support. This research has been supported by the Friedrich Ebert foundation PhD fellowship.

Review statement. This paper was edited by Wolfgang Kurtz and reviewed by Edwin Sutanudjaja and four anonymous referees.

References

Allen, P. M., Arnold, J. C., and Byars, B. W.: Downstream channel geometry for use in planning-level models, J. Am. Water Resour. As., 30, 663–671, https://doi.org/10.1111/j.1752-1688.1994.tb03321.x, 1994.

Belcher, W. R. (Ed.): Death Valley Regional Ground-water Flow System, Nevada and California-Hydrogeologic Framework and Transient Ground-water Flow Model, U.S. Geological Survey Professional Paper, 408 pp., available at: https://pubs.usgs.gov/sir/2004/5205/ (last access: 1 June 2019), 2004.

Belcher, W. R. and Sweetkind, D. S.: Death Valley regional groundwater flow system, Nevada and California – Hydrogeologic framework and transient groundwater flow model, U.S. Geological Survey Professional Paper 1711, 398 pp., available at: https://pubs.usgs.gov/pp/1711/ (last access: 1 June 2019), 2010.

Costa, A. C., Foerster, S., de Araújo, J. C., and Bronstert, A.: Analysis of channel transmission losses in a dryland river reach in north-eastern Brazil using streamflow series, groundwater level series and multi-temporal satellite data, Hydrol. Process., 27, 1046–1060, https://doi.org/10.1002/hyp.9243, 2013.

de Graaf, I. E. M., Sutanudjaja, E. H., van Beek, L. P. H., and Bierkens, M. F. P.: A high-resolution global-scale groundwater model, Hydrol. Earth Syst. Sci., 19, 823–837, https://doi.org/10.5194/hess-19-823-2015, 2015.

de Graaf, I. E. M., van Beek, R. L. P. H., Gleeson, T., Moosdorf, N., Schmitz, O., Sutanudjaja, E. H., and Bierkens, M. F. P.: A global-scale two-layer transient groundwater model: Development and application to groundwater depletion, Adv. Water Resour., 102, 53–67, https://doi.org/10.1016/j.advwatres.2017.01.011, 2017.

Dogrul, E., Brush, C., and Kadir, T.: Groundwater Modeling in Support of Water Resources Management and Planning under Complex Climate, Regulatory, and Economic Stresses, Water, 8, 592, https://doi.org/10.3390/w8120592, 2016.

Döll, P. and Fiedler, K.: Global-scale modeling of groundwater recharge, Hydrol. Earth Syst. Sci., 12, 863–885, https://doi.org/10.5194/hess-12-863-2008, 2008.

Döll, P., Hoffmann-Dobrev, H., Portmann, F. T., Siebert, S., Eicker, A., Rodell, M., Strassberg, G., and Scanlon, B. R.: Impact of water withdrawals from groundwater and surface water on continental water storage variations, J. Geodyn., 59–60, 143–156, https://doi.org/10.1016/j.jog.2011.05.001, 2012.

Döll, P., Müller Schmied, H., Schuh, C., Portmann, F. T., and Eicker, A.: Global-scale assessment of groundwater depletion and related groundwater abstractions: Combining hydrological modeling with information from well observations and GRACE satellites, Water Resour. Res., 50, 5698–5720, https://doi.org/10.1002/2014WR015595, 2014.

Dustin, E.: Effective software testing: 50 specific ways to improve your testing, 5th printing, Addison-Wesley, Boston, Mass., USA, XV, 271 s., 2006.

Eisner, S.: Comprehensive evaluation of the WaterGAP3 model across climatic, physiographic, and anthropogenic gradients, University of Kassel, Kassel, Germany, 2016.

Elsawwaf, M., Feyen, J., Batelaan, O., and Bakr, M.: Groundwater-surface water interaction in Lake Nasser, Southern Egypt, Hydrol. Process., 28, 414–430, https://doi.org/10.1002/hyp.9563, 2014.

Fan, Y., Miguez-Macho, G., Weaver, C. P., Walko, R., and Robock, A.: Incorporating water table dynamics in climate modeling: 1. Water table observations and equilibrium water table simulations, J. Geophys. Res., 112, D10125, https://doi.org/10.1029/2006JD008111, 2007.

Fan, Y., Li, H., and Miguez-Macho, G.: Global patterns of groundwater table depth, Science, 339, 940–943, https://doi.org/10.1126/science.1229881, 2013.

FAO: Irrigation potential in Africa, available at: http://www.fao.org/docrep/w4347e/w4347e0i.htm (last access: 1 May 2018), 1997.

Faunt, C. C. (Ed.): Groundwater Availability of the Central Valley Aquifer, California, U.S. Geological Survey Professional Paper, 1766, 225 pp., available at: https://pubs.usgs.gov/pp/1766/ (last access: 1 June 2019), 2009.

Faunt, C. C., Provost, A. M., Hill, M. C., and Belcher, W. R.: Comment on "An unconfined groundwater model of the Death Valley Regional Flow System and a comparison to its confined predecessor" by R.W.H. Carroll, G.M. Pohll and R.L. Hershey [J. Hydrol. 373/3–4, pp. 316–328], J. Hydrol., 397, 306–309, https://doi.org/10.1016/j.jhydrol.2010.11.038, 2011.

Gleeson, T., Wada, Y., Bierkens, M. F. P., and van Beek, L. P. H.: Water balance of global aquifers revealed by groundwater footprint, Nature, 488, 197–200, https://doi.org/10.1038/nature11295, 2012.

Gleeson, T., Moosdorf, N., Hartmann, J., and van Beek, L. P. H.: A glimpse beneath earth's surface: GLobal HYdrogeology MaPS (GLHYMPS) of permeability and porosity, Geophys. Res. Lett., 41, 3891–3898, https://doi.org/10.1002/2014GL059856, 2014.

Gleeson, T., Befus, K. M., Jasechko, S., Luijendijk, E., and Cardenas, M. B.: The global volume and distribution of modern groundwater, Nat. Geosci., 9, 161–167, https://doi.org/10.1038/ngeo2590, 2016.

Gossel, W., Ebraheem, A. M., and Wycisk, P.: A very large scale GIS-based groundwater flow model for the Nubian sandstone aquifer in Eastern Sahara (Egypt, northern Sudan and eastern Libya), Hydrogeol. J., 12, 698–713, https://doi.org/10.1007/s10040-004-0379-4, 2004.

Harbaugh, A. W.: MODFLOW-2005, the US Geological Survey modular ground-water model: the ground-water flow process, US Department of the Interior, US Geological Survey, Reston, USA, 2005.

Hartmann, J. and Moosdorf, N.: The new global lithological map database GLiM: A representation of rock properties at the Earth surface, Geochem. Geophy. Geosy., 13, Q12004, https://doi.org/10.1029/2012GC004370, 2012.

Hill, M. C. and Tiedeman, C. R.: Effective groundwater model calibration: With analysis of data, sensitivities, predictions, and uncertainty, Wiley-Interscience, Hoboken, NJ, USA, 2007.

Konikow, L. F.: Contribution of global groundwater depletion since 1900 to sea-level rise, Geophys. Res. Lett, 38, L17401, https://doi.org/10.1029/2011GL048604, 2011.

Krakauer, N. Y., Li, H., and Fan, Y.: Groundwater flow across spatial scales: importance for climate modeling, Environ. Res. Lett., 9, 34003, https://doi.org/10.1088/1748-9326/9/3/034003, 2014.

Lange, S.: EartH2Observe, WFDEI and ERA-Interim data Merged and Bias-corrected for ISIMIP (EWEMBI), GFZ Data Services, https://doi.org/10.5880/pik.2016.004, 2016.

Lehner, B. and Döll, P.: Development and validation of a global database of lakes, reservoirs and wetlands, J. Hydrol., 296, 1–22, https://doi.org/10.1016/j.jhydrol.2004.03.028, 2004.

Maxwell, R. M., Condon, L. E., and Kollet, S. J.: A high-resolution simulation of groundwater and surface water over most of the continental US with the integrated hydrologic model ParFlow v3, Geosci. Model Dev., 8, 923–937, https://doi.org/10.5194/gmd-8-923-2015, 2015.

Mehl, S.: Use of Picard and Newton iteration for solving nonlinear ground water flow equations, Ground Water, 44, 583–594, https://doi.org/10.1111/j.1745-6584.2006.00207.x, 2006.

Miguez-Macho, G., Fan, Y., Weaver, C. P., Walko, R., and Robock, A.: Incorporating water table dynamics in climate modeling: 2. Formulation, validation, and soil moisture simulation, J. Geophys. Res., 112, D13108, https://doi.org/10.1029/2006JD008112, 2007.

Morel-Seytoux, H. J., Miller, C. D., Miracapillo, C., and Mehl, S.: River Seepage Conductance in Large-Scale Regional Studies, Ground Water, 55, 399–407, https://doi.org/10.1111/gwat.12491, 2017.

Müller Schmied, H., Eisner, S., Franz, D., Wattenbach, M., Portmann, F. T., Flörke, M., and Döll, P.: Sensitivity of simulated global-scale freshwater fluxes and storages to input data, hydrological model structure, human water use and calibration, Hydrol. Earth Syst. Sci., 18, 3511–3538, https://doi.org/10.5194/hess-18-3511-2014, 2014.

Naff, R. L. and Banta, E. R.: The US Geological Survey modular ground-water model-PCGN: a preconditioned conjugate gradient solver with improved nonlinear control, Geological Survey (US), 2008-1331, available at: https://pubs.er.usgs.gov/publication/ofr20081331 (last access: 1 June 2019), 2008.

Niswonger, R. G., Panday, S., and Ibaraki, M.: MODFLOW-NWT, a Newton formulation for MODFLOW-2005, US Geological Survey Techniques and Methods, 6-A37, https://doi.org/10.3133/tm6A37, 2011.

Reinecke, R.: G^{3}M-f a global gradient-based groundwater modelling framwork, JOSS, 3, 548, https://doi.org/10.21105/joss.00548, 2018a.

Reinecke, R.: G^{3}M framework, Zenodo, https://doi.org/10.5281/zenodo.1175540, 2018b.

Reinecke, R.: Model Output, Zenodo, https://doi.org/10.5281/zenodo.1315471, 2018c.

Richey, A. S., Thomas, B. F., Lo, M.-H., Famiglietti, J. S., Swenson, S., and Rodell, M.: Uncertainty in global groundwater storage estimates in a Total Groundwater Stress framework, Water Resour. Res, 51, 5198–5216, https://doi.org/10.1002/2015WR017351, 2015.

Saad, Y.: ILUT: A dual threshold incomplete LU factorization, Numer. Linear Algebr., 1, 387–402, https://doi.org/10.1002/nla.1680010405, 1994.

Scanlon, B. R., Faunt, C. C., Longuevergne, L., Reedy, R. C., Alley, W. M., McGuire, V. L., and McMahon, P. B.: Groundwater depletion and sustainability of irrigation in the US High Plains and Central Valley, P. Natl. Acad. Sci. USA, 109, 9320–9325, https://doi.org/10.1073/pnas.1200311109, 2012.

Sheets, R. A., Hill, M. C., Haitjema, H. M., Provost, A. M., and Masterson, J. P.: Simulation of water-table aquifers using specified saturated thickness, Ground Water, 53, 151–157, https://doi.org/10.1111/gwat.12164, 2015.

Stonestrom, D. A., Constantz, J., Ferre, T. P. A., and Leake, S. A.: Ground-water recharge in the arid and semiarid southwestern United States, U.S. Geological Survey Professional Paper 1703, 414 pp., available at: https://pubs.usgs.gov/pp/pp1703/ (last access: 1 June 2019), 2007.

Sutanudjaja, E. H., van Beek, L. P. H., de Jong, S. M., van Geer, F. C., and Bierkens, M. F. P.: Large-scale groundwater modeling using global datasets: a test case for the Rhine-Meuse basin, Hydrol. Earth Syst. Sci., 15, 2913–2935, https://doi.org/10.5194/hess-15-2913-2011, 2011.

Sutanudjaja, E. H., van Beek, L. P. H., de Jong, S. M., van Geer, F. C., and Bierkens, M. F. P.: Calibrating a large-extent high-resolution coupled groundwater-land surface model using soil moisture and discharge data, Water Resour. Res., 50, 687–705, https://doi.org/10.1002/2013WR013807, 2014.

Taylor, R. G., Scanlon, B., Döll, P., Rodell, M., van Beek, R., Wada, Y., Longuevergne, L., Leblanc, M., Famiglietti, J. S., Edmunds, M., Konikow, L., Green, T. R., Chen, J., Taniguchi, M., Bierkens, M. F. P., MacDonald, A., Fan, Y., Maxwell, R. M., Yechieli, Y., Gurdak, J. J., Allen, D. M., Shamsudduha, M., Hiscock, K., Yeh, P. J.-F., Holman, I., and Treidel, H.: Ground water and climate change, Nat. Clim. Change, 3, 322–329, https://doi.org/10.1038/nclimate1744, 2012.

UNESCO-IHP, IGRAC, WWAP: GEF-TWAP Methodology Transboundary Aquifers, available at: http://isarm.org/sites/default/files/resources/files/TWAP Methodology Groundwater Component (Revised Aug 2012).pdf (last access: 9 October 2017), 2012.

van Beek, L. P. H., Wada, Y., and Bierkens, M. F. P.: Global monthly water stress: 1. Water balance and water availability, Water Resour. Res., 47, W07517, https://doi.org/10.1029/2010WR009791, 2011.

Vergnes, J.-P., Decharme, B., Alkama, R., Martin, E., Habets, F., and Douville, H.: A Simple Groundwater Scheme for Hydrological and Climate Applications: Description and Offline Evaluation over France, J. Hydrometeorol., 13, 1149–1171, https://doi.org/10.1175/JHM-D-11-0149.1, 2012.

Vergnes, J.-P., Decharme, B., and Habets, F.: Introduction of groundwater capillary rises using subgrid spatial variability of topography into the ISBA land surface model, J. Geophys. Res.-Atmos., 119, 11065–11086, https://doi.org/10.1002/2014JD021573, 2014.

Verzano, K., Bärlund, I., Flörke, M., Lehner, B., Kynast, E., Voß, F., and Alcamo, J.: Modeling variable river flow velocity on continental scale: Current situation and climate change impacts in Europe, J. Hydrol., 424–425, 238–251, https://doi.org/10.1016/j.jhydrol.2012.01.005, 2012.

Wada, Y.: Modeling Groundwater Depletion at Regional and Global Scales: Present State and Future Prospects, Surv. Geophys., 37, 419–451, https://doi.org/10.1007/s10712-015-9347-x, 2016.

Wada, Y., van Beek, L. P. H., and Bierkens, M. F. P.: Nonsustainable groundwater sustaining irrigation: A global assessment, Water Resour. Res., 48, W00L06, https://doi.org/10.1029/2011WR010562, 2012.

Westerhoff, R., White, P., and Miguez-Macho, G.: Application of an improved global-scale groundwater model for water table estimation across New Zealand, Hydrol. Earth Syst. Sci., 22, 6449–6472, https://doi.org/10.5194/hess-22-6449-2018, 2018.

Supplement of Geosci. Model Dev., 12, 2401–2418, 2019
https://doi.org/10.5194/gmd-12-2401-2019-supplement

Geoscientific
Model Development
Open Access

Supplement of

Challenges in developing a global gradient-based groundwater model (G^3M v1.0) for the integration into a global hydrological model

Robert Reinecke et al.

Correspondence to: Robert Reinecke (reinecke@em.uni-frankfurt.de)

Supplement

1 Coupling to WGHM

With a spatial resolution of 0.5° by 0.5° (approximately 55 km by 55 km at the equator), the WaterGAP 2 model (Alcamo et al., 2003) computes human water use in five sectors and the resulting net abstractions from GW and SW for all land areas of the globe excluding Antarctica. These net abstractions are then taken from the respective water storages in the WaterGAP Global Hydrology Model (WGHM) (Müller Schmied et al., 2014; Döll et al., 2003; 2012; 2014). With daily time steps, WGHM simulates flows among the water storage compartments canopy, snow, soil, GW, lakes, man-made reservoirs, wetlands and rivers. As in other GHMs, the dynamic of GW storage (GWS) is represented in WGHM by a linear GW reservoir model, i.e.

$$\frac{dGWS}{dt} = R_g + R_{g\_swb} - NA_g - k_g\, GWS \tag{S1}$$

where R_g $[L^3T^{-1}]$ is diffuse GW recharge from soil, R_{g_swb} $[L^3T^{-1}]$ GW recharge from lakes, reservoirs and wetlands (only in arid and semiarid regions, with a global constant value per SW body area), NA_g $[L^3T^{-1}]$ net GW abstraction. The product $k_g\, GWS$ quantifies GW discharge to SW bodies as a function of GWS and the GW discharge coefficient k_g (Döll et al., 2014). G^{3}M is to replace this linear reservoir model in WGHM. Capillary rise is not included in the presented steady-state simulation, as simulation of capillary rise requires information of soil moisture that is only available when G^{3}M is fully integrated into WGHM.

G^{3}M will be integrated into WGHM by exchanging information on (1) R_{g_swb} and NA_g, (2) soil water content, (3) Q_{cr}, (4) h_{swb}, and (5) Q_{swb}. Figure S1.1 indicates the direction of the information flows. Water flows from the 0.5° cells of WGHM are distributed equally to all 5' G^{3}M grid cells inside a 0.5° cell. Flows transferred from the 5' cells of G^{3}M to WGHM are aggregated. GW recharge and net abstraction from GW together with SW tables are the main drivers of the GW model that will be provided dynamically by WGHM. GW-SW flow volumes computed by G^{3}M will be aggregated and added or subtracted from the SW body volumes in WGHM, and SW body heads will be recalculated. WGHM soil water content together with G^{3}M WTD will be used to calculate capillary rise and thus a change of soil water content. WaterGAP includes a one layer soil water storage compartment characterized by land cover specific rooting depth, maximum storage capacity and soil texture (Döll et al., 2014). The water content in the soil storage is increased by incoming precipitation and decreased by evapotranspiration and runoff generation (Döll et al., 2014). Capillary rise is not yet implemented in G^{3}M, and SW heads are currently based on land surface elevation.

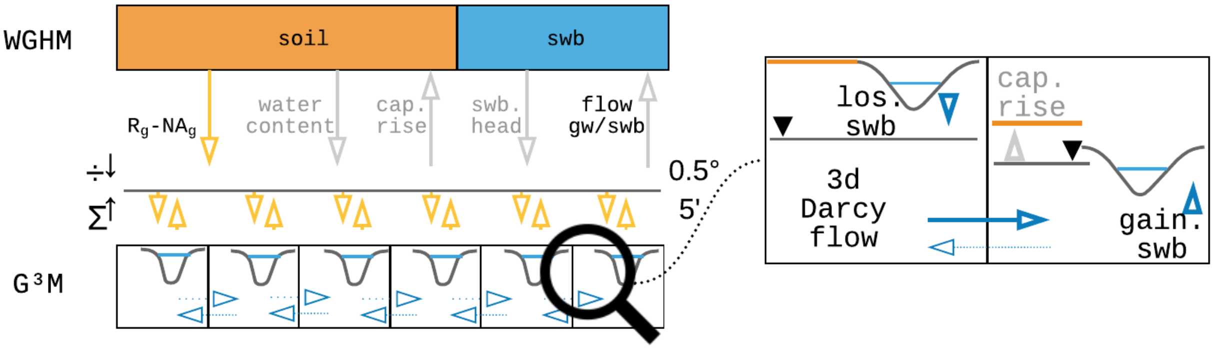

Figure S1.1 Conceptual view of the coupling between WGHM and G³M. WGHM provides calculated GW recharge (R_g) (Döll and Fiedler, 2008) and if the human impact is considered, net abstraction from GW (NA_g) (Döll et al., 2012). G^{3}M spreads this input equally to all 5' grid cells inside a 0.5° cell and calculates hydraulic head and interactions with SW bodies (swb) as well as capillary rise (cap. rise) at the 5' resolution. Grey arrows show information flow that is not yet implemented.

2 Case study Central Valley

To evaluate G^{3}M further, its results were analysed for to a well-studied region, the Central Valley in California, USA. The Central Valley is one of the most productive agricultural regions of the world and heavily relies on GW pumpage to meet irrigation demands (Faunt et al., 2016). GW pumping in the valley increased rapidly in the 1960s (Faunt, 2009). Figure S2.1 shows simulated WTD for the Central Valley, the coast and the neighboring Sierra Nevada mountainside as well as parts of the Great Basin. The WTD table represents natural conditions without any pumping and is rather small. It roughly resembles the WTD assumed in the Central Valley Hydrological Model (CVHM) as initial condition, representing a natural state (Faunt, 2009) (Fig. S2.1b). G³M correctly computes the shallow conditions with groundwater above the surface in the north, partially in the south of the valley and decreasing towards the Sierra Nevada. The difference in the extend of flooded area could be due to large wetlands areas still present in the early 60s which are not represented in this extent in the data used by G³M. Beyond the CVHM domain, WTD in mountainous regions is probably overestimated by G³M. The elevation of neighboring cells may differ up to a 1000 meter resulting in a large gradient (Fig. S4.5b and S4.5e).

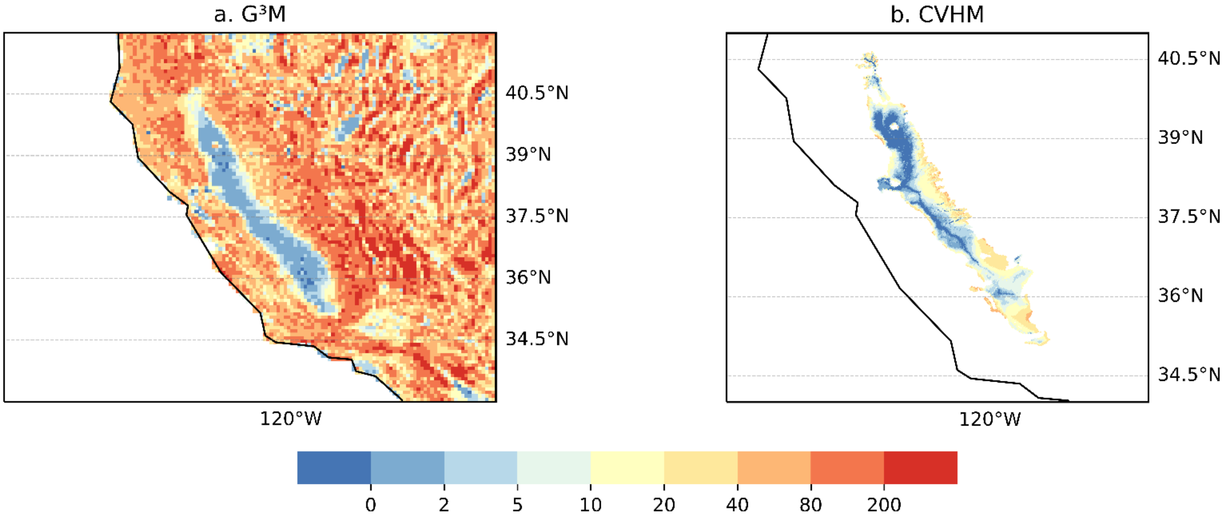

Figure S2.1 Plots of WTD [*m*] as calculated by G³M for the Central Valley and the Great Basin (a), and as used by CVHM as the natural state and starting condition (Faunt, 2009) (b).

3 Sensitivity Analysis

Sensitivities are calculated using forward differences (Poeter et al., 2014).

$$\frac{\Delta y_i{}'}{\Delta b_j} = \frac{y_i{}'(b_j + \Delta b_j - y_i{}'(b_j))}{\Delta bj_j} \tag{S2}$$

where $y_i{}'$ is the simulated hydraulic head at position i from ND number of cells and b_j the perturbed parameter, here a multiplier for grid specific values shown in Table S1, in a vector of all parameter b of length j. Based on these values the composite scaled sensitivity is computed as

$$CSS_j = \sqrt{\sum\nolimits_{i=1}^{ND} \frac{\Delta y_i{}'}{\Delta b_j} ND^{-1}} \tag{S3}$$

The result of the CSS is in units of meters. The higher the CSS, the more sensitive are the computed hydraulic heads to the parameter (Table S1).

Table S1 Ranges of parameter multipliers used in the local sensitivity analysis and their resulting composite scaled sensitivity values. The multiplier for the wetlands applies to global and local wetlands.

Parameter	$\boldsymbol{\Delta b}$	**Composite Scaled Sensitivity [m]**
h_{swb}	0.01	39132.1
K_{aq}	0.01	76.8
R_g	0.1	39.8
c_{Lakes}	0.1	3.2
$c_{Wetlands}$	0.1	0.014
c_{riv}	0.1	0.013
c_{ocean}	0.1	0.013

4 Additional Figures

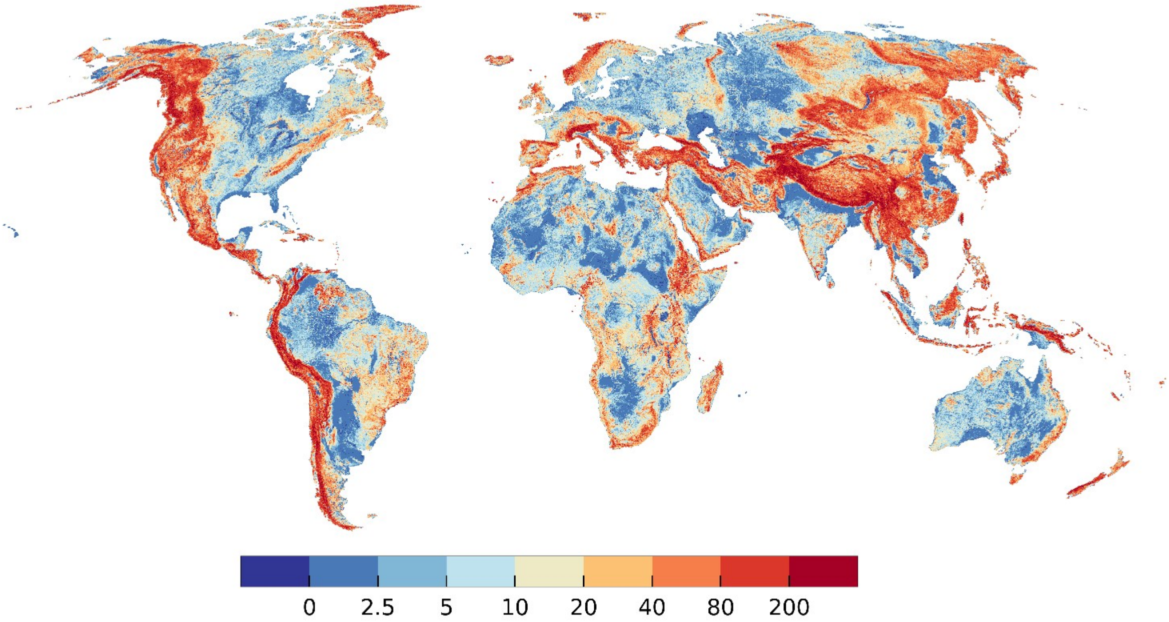

Figure S4.1 Difference [***m***] between 5' average of 30" land surface elevation and P30 elevation. Maximum value 1365 m**.**

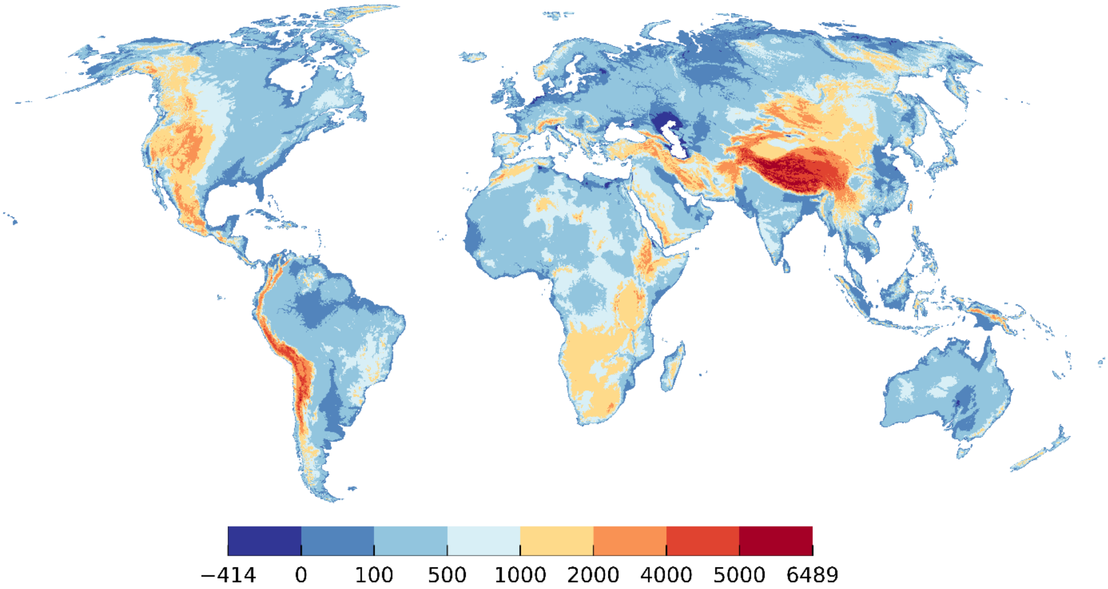

Figure S4.2 Land surface elevation [***m***] used in G³M: 5' average of 30" land surface elevation used in Fan et al. (2013).

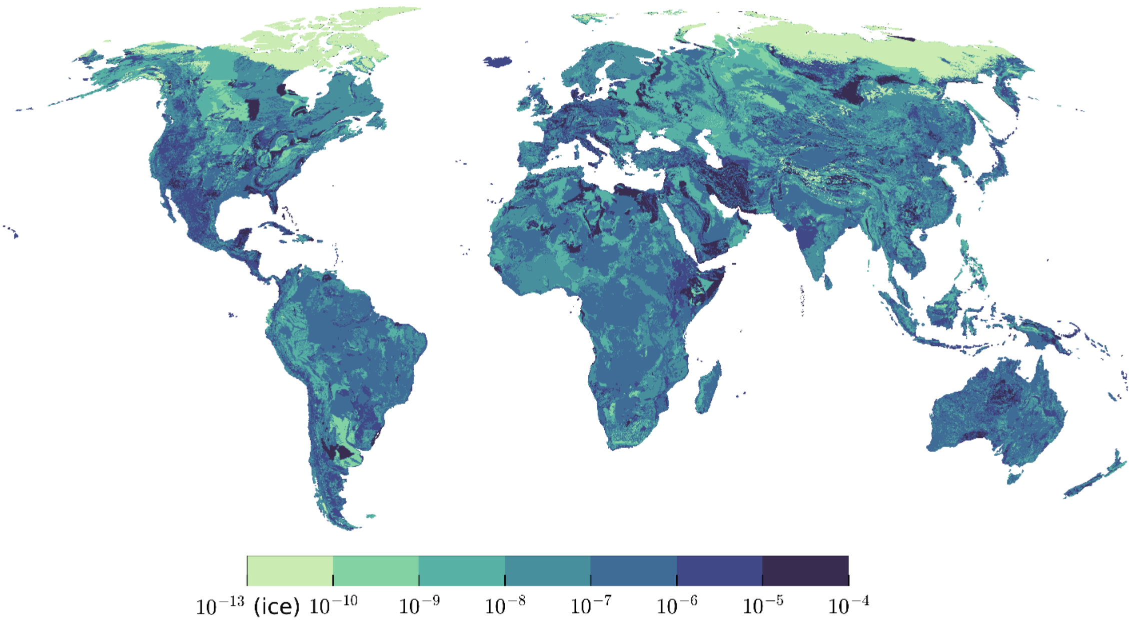

Figure S4.3 Hydraulic conductivity [$\boldsymbol{ms^{-1}}$] derived from Gleeson et al. (2014) by scaling it with the geometric mean to 5'. Very low values in the northern hemisphere are due to permafrost conditions.

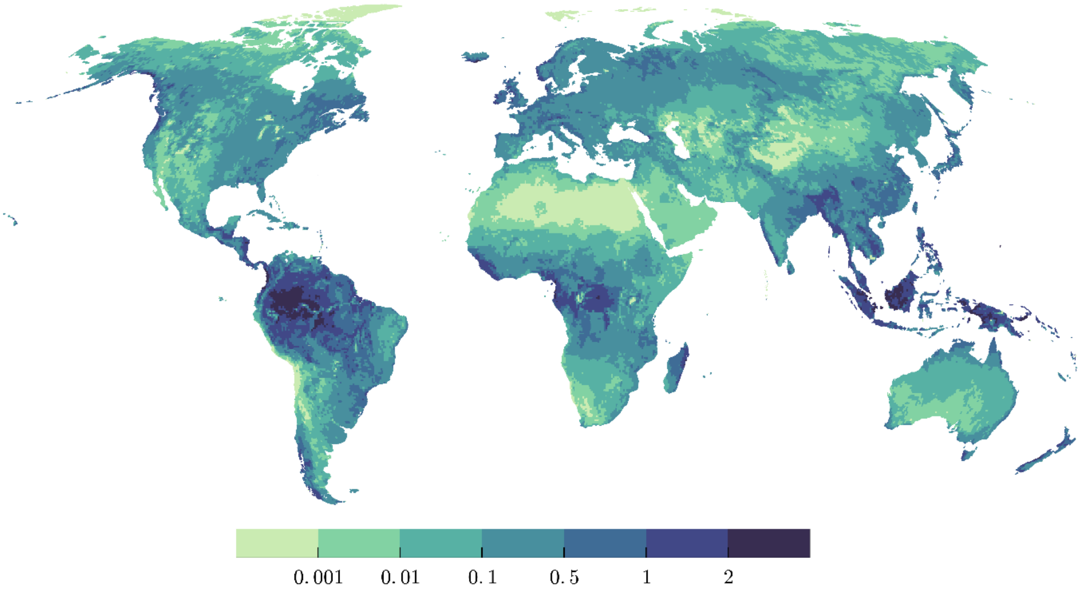

Figure S4.4 Mean annual groundwater recharge [$\boldsymbol{mm\ day^{-1}}$] between 1901-2013, from WaterGAP 2.2c.

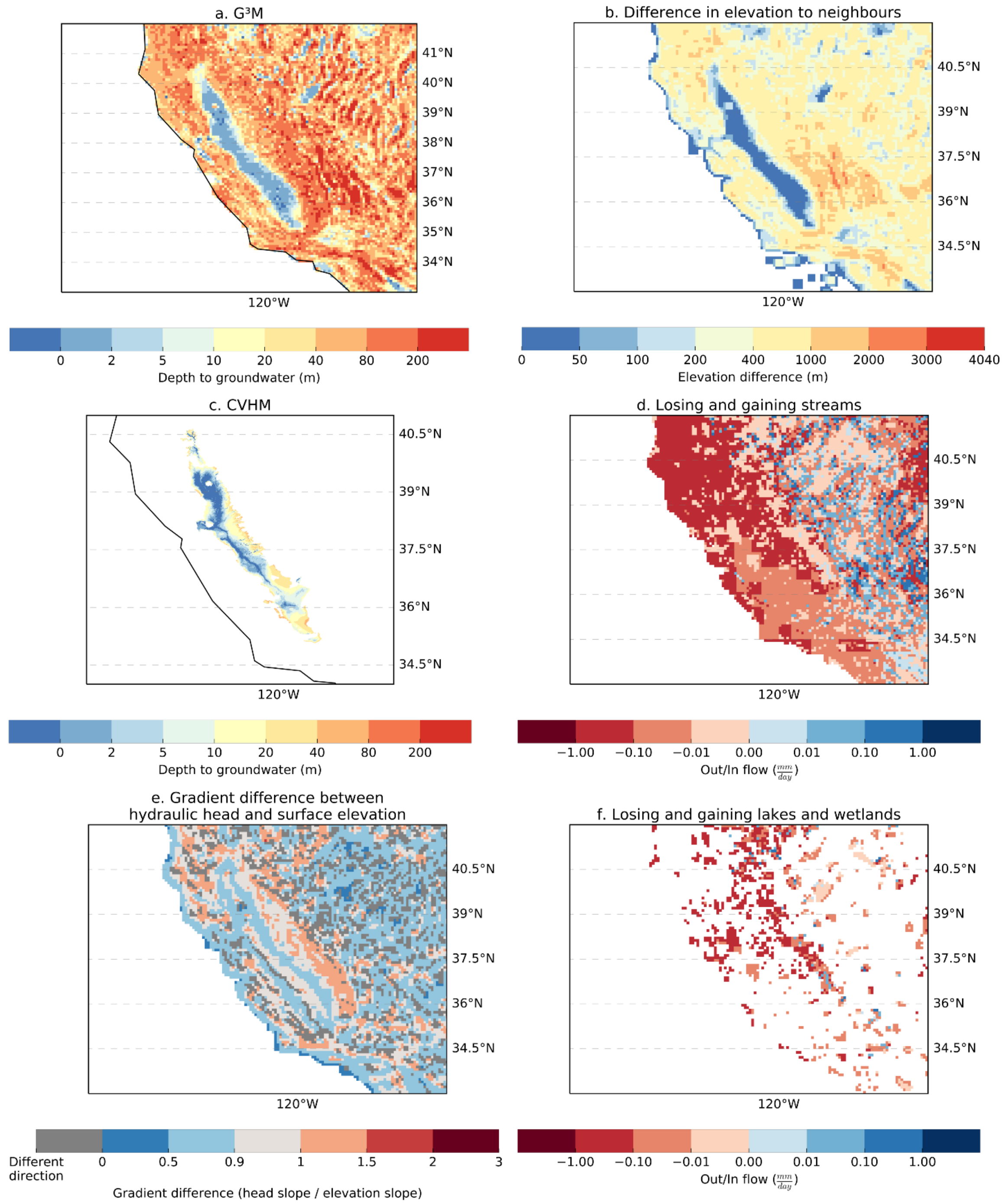

Figure S4.5 Plots of WTD as calculated by G³M (a), difference in surface elevation to neighbouring cells (b), WTD as used by the CVHM as the natural state and starting condition (Faunt, 2009) (c), losing and gaining streams as calculated by G³M (d), difference in gradient of hydraulic head and surface elevation (e), losing and gaining lakes and wetlands as calculated by G³M for the Central Valley and the Great Basin.

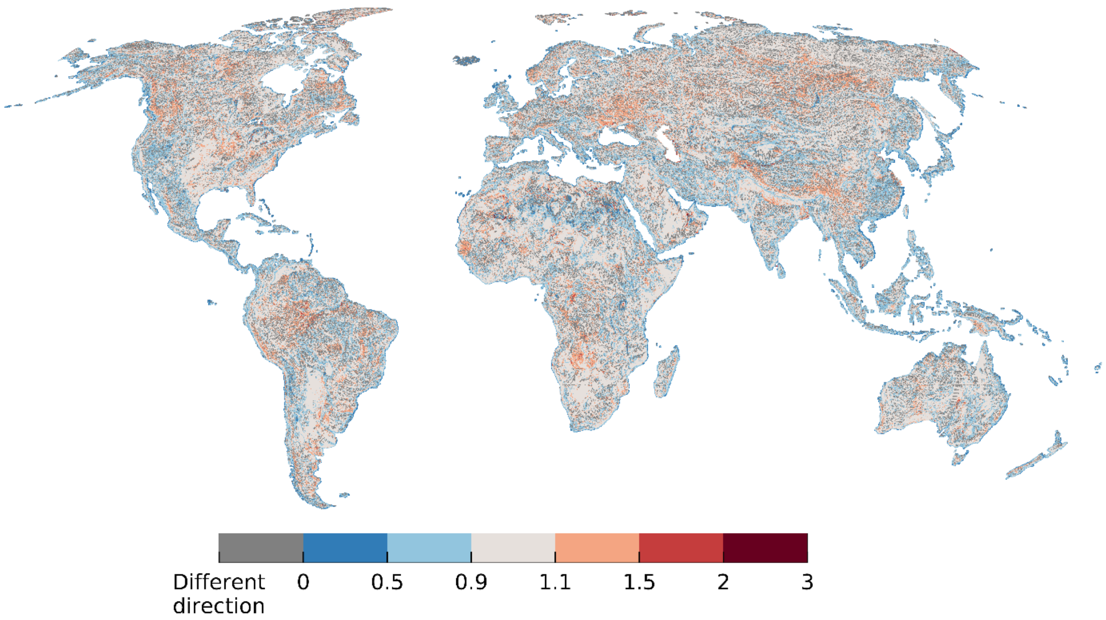

Figure S4.6 Ratio of hydraulic head gradient to 5' mean surface elevation gradient, only computed if the difference in direction of the gradient was smaller than 45°.

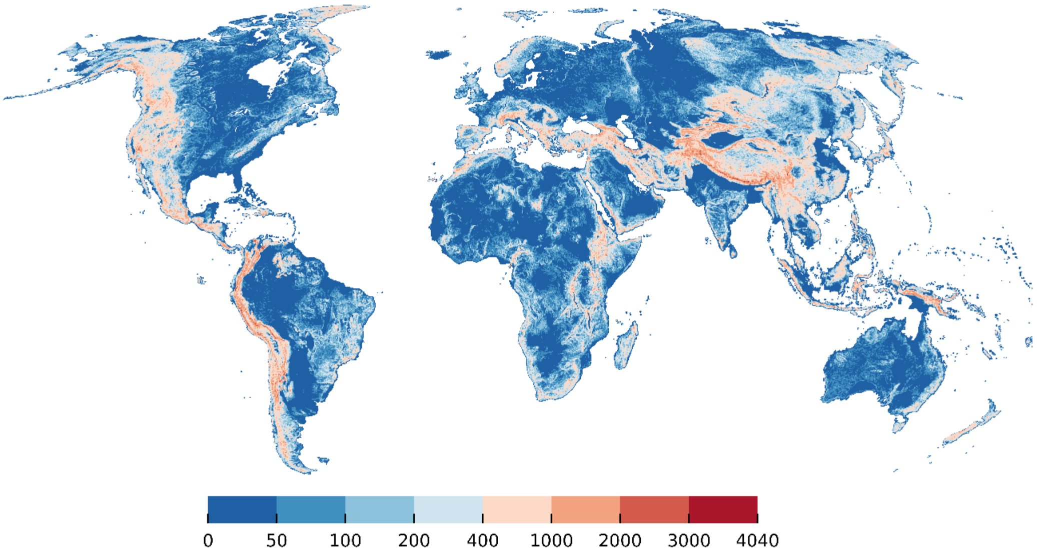

Figure S4.7 Land surface elevation difference between 30" mean land surface elevation in 5' grid cell and mean elevation of neighboring 5' cells [**m**].

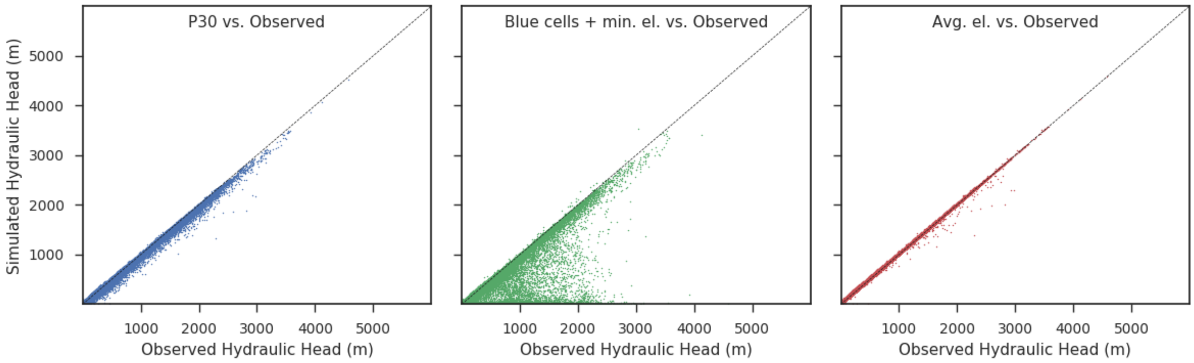

Figure S4.8 Comparison between three alternatives for setting $\boldsymbol{h_{swb}}$. Left to right: Fit of simulated hydraulic heads observations if $\boldsymbol{h_{swb}}$ is set (1) to the 30th percentile of the 30" land surface elevations (standard model) , (2) alternatively to the average elevation of all "blue" cells of the 30" water table results of Fan et al. (2013) or (3) is set to the average of the 30" land surface elevations. A blue cell has a WTD of less than 0.25 m and indicates GW discharge to the surface. If no "blue" cell exists in the 5' cell, the minimum elevation of the 30" land surface elevation values within the cell was used.

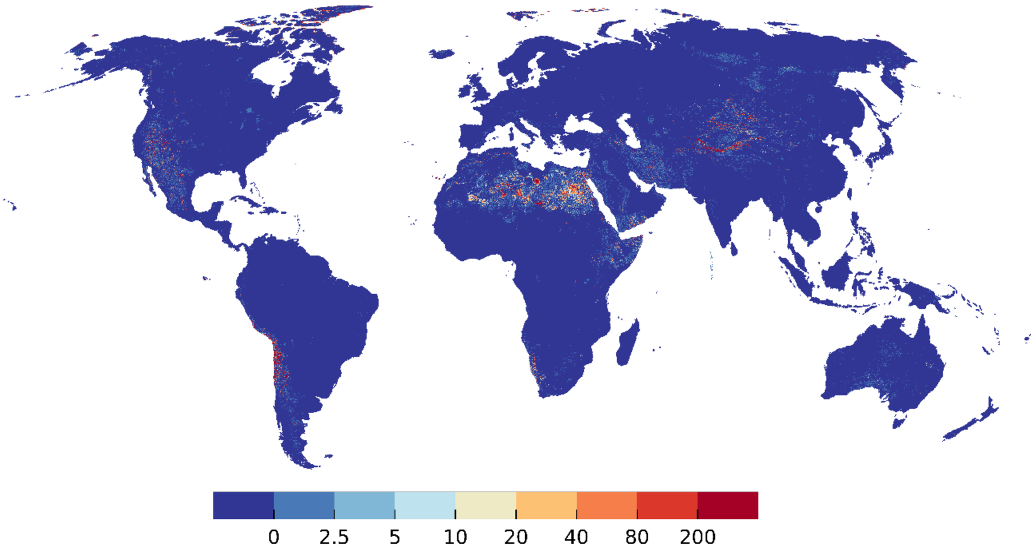

Fig. S4.9 Depth to groundwater [$\boldsymbol{m}$] for SW body elevation $\boldsymbol{h_{swb}}$ at average of 30" land surface elevations.

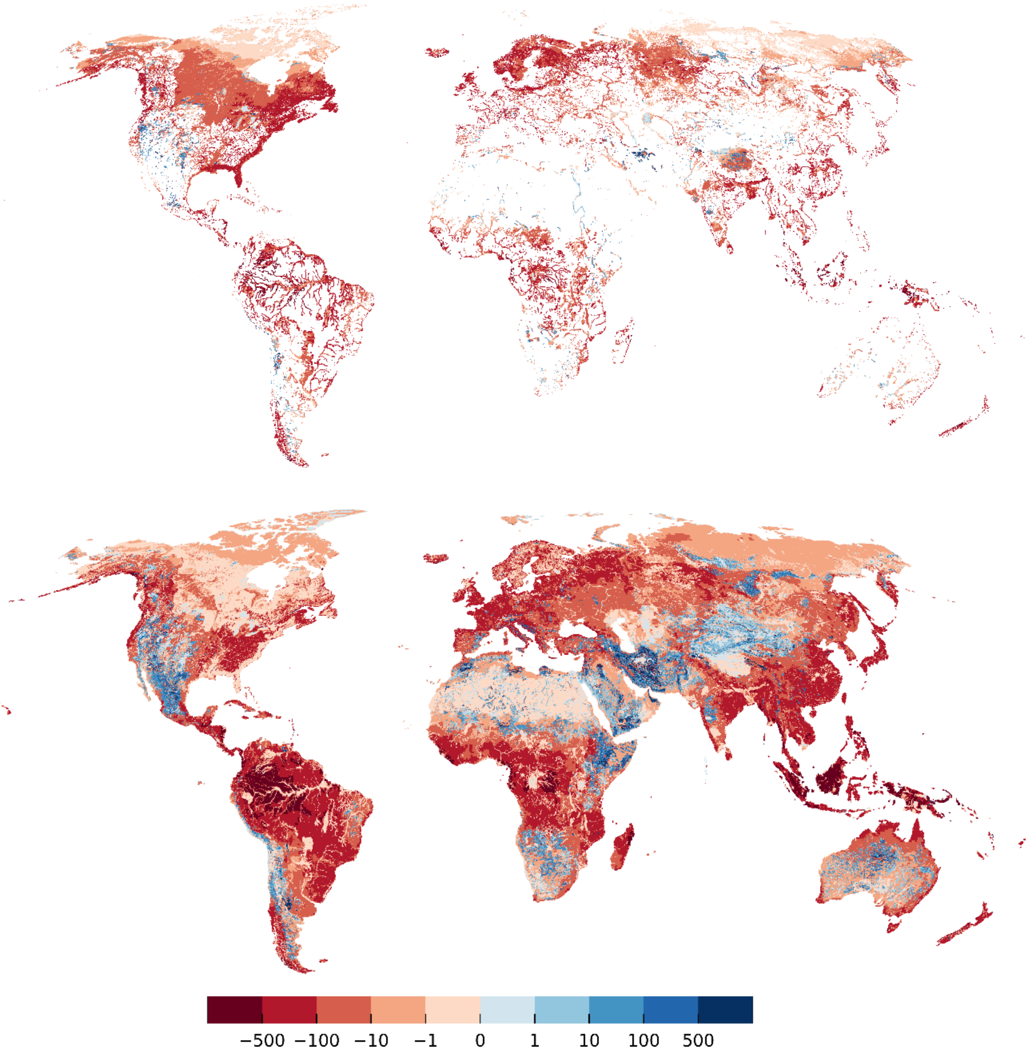

Figure S4.10 Gaining and losing rivers (lower panel) and wetlands and lakes (upper panel) as flow into/out the GW [$\boldsymbol{mm\ year^{-1}}$] if $\boldsymbol{h_{swb}}$ is set to average elevation of all “blue” cells of the 30" water table results of Fan et al. (2013) (right). A blue cell is defined as a depth to groundwater of less than 0.25 m. If no “blue” cell exist in the 5' cell, the minimum elevation of the 30" land surface elevation values is used. Red denotes gaining SW bodies.

References

Alcamo, J., Döll, P., Henrichs, T., Kaspar, F., Lehner, B., Rösch, T., and Siebert, S.: Development and testing of the WaterGAP 2 global model of water use and availability, Hydrological Sciences Journal, 48, 317–337, doi:10.1623/hysj.48.3.317.45290, 2003.

Döll, P. and Fiedler, K.: Global-scale modeling of groundwater recharge, Hydrol. Earth Syst. Sci., 12, 863–885, doi:10.5194/hess-12-863-2008, 2008.

Döll, P., Hoffmann-Dobrev, H., Portmann, F. T., Siebert, S., Eicker, A., Rodell, M., Strassberg, G., and Scanlon, B.R.: Impact of water withdrawals from groundwater and surface water on continental water storage variations, Journal of Geodynamics, 59-60, 143–156, doi:10.1016/j.jog.2011.05.001, 2012.

Döll, P., Kaspar, F., and Lehner, B.: A global hydrological model for deriving water availability indicators: model tuning and validation, Journal of Hydrology, 270, 105–134, doi:10.1016/S0022-1694(02)00283-4, 2003.

Döll, P., Müller Schmied, H., Schuh, C., Portmann, F. T., and Eicker, A.: Global-scale assessment of groundwater depletion and related groundwater abstractions: Combining hydrological modeling with information from well observations and GRACE satellites, Water Resour. Res., 50, 5698–5720, doi:10.1002/2014WR015595, 2014.

Fan, Y., Li, H., and Miguez-Macho, G.: Global patterns of groundwater table depth, Science (New York, N.Y.), 339, 940–943, doi:10.1126/science.1229881, 2013.

Faunt, C. C. (Ed.): Groundwater Availability of the Central Valley Aquifer, California, U.S. Geological Survey Professional Paper, 1776, 225 pp., 2009.

Faunt, C. C., Sneed, M., Traum, J., and Brandt, J. T.: Water availability and land subsidence in the Central Valley, California, USA, Hydrogeol J, 24, 675–684, doi:10.1007/s10040-015-1339-x, 2016.

Gleeson, T., Moosdorf, N., Hartmann, J., and van Beek, L. P. H.: A glimpse beneath earth's surface: GLobal HYdrogeology MaPS (GLHYMPS) of permeability and porosity, Geophys. Res. Lett., 41, 3891–3898, doi:10.1002/2014GL059856, 2014.

Müller Schmied, H., Eisner, S., Franz, D., Wattenbach, M., Portmann, F. T., Flörke, M., and Döll, P.: Sensitivity of simulated global-scale freshwater fluxes and storages to input data, hydrological model structure, human water use and calibration, Hydrol. Earth Syst. Sci., 18, 3511–3538, doi:10.5194/hess-18-3511-2014, 2014.

Poeter, E. P., Hill, M. C., Lu, D., Tiedeman, C., and Mehl, S. W.: UCODE 2014, with new capabilities to define parameters unique to predictions, calculate w eights using simulated values, estimate parameters w ith SVD, evaluate uncertainty with MCMC, and more, Integrated Groundwater Modeling Center IGWMC, of the Colorado School of Mines, 2014.

Chapter 4

Spatially distributed sensitivity of simulated global groundwater heads and flows to hydraulic conductivity, groundwater recharge and surface water body parameterization

Hydrol. Earth Syst. Sci., 23, 4561–4582, 2019
https://doi.org/10.5194/hess-23-4561-2019

Hydrology and Earth System Sciences
Open Access
EGU

Spatially distributed sensitivity of simulated global groundwater heads and flows to hydraulic conductivity, groundwater recharge, and surface water body parameterization

Robert Reinecke[1], **Laura Foglia**[3], **Steffen Mehl**[5], **Jonathan D. Herman**[4], **Alexander Wachholz**[1], **Tim Trautmann**[1], **and Petra Döll**[1,2]

[1]Institute of Physical Geography, Goethe University Frankfurt, Frankfurt am Main, Germany
[2]Senckenberg Leibniz Biodiversity and Climate Research Centre Frankfurt (SBiK-F), Frankfurt am Main, Germany
[3]Department of Land, Air and Water Resources, University of California, Davis, USA
[4]Department of Civil & Environmental Engineering, University of California, Davis, USA
[5]Department of Civil Engineering, California State University, Chico, USA

Correspondence: Robert Reinecke (reinecke@em.uni-frankfurt.de)

Received: 7 January 2019 – Discussion started: 18 February 2019
Revised: 13 September 2019 – Accepted: 10 October 2019 – Published: 14 November 2019

Abstract. In global hydrological models, groundwater storages and flows are generally simulated by linear reservoir models. Recently, the first global gradient-based groundwater models were developed in order to improve the representation of groundwater–surface-water interactions, capillary rise, lateral flows, and human water use impacts. However, the reliability of model outputs is limited by a lack of data and by uncertain model assumptions that are necessary due to the coarse spatial resolution. The impact of data quality is presented in this study by showing the sensitivity of a groundwater model to changes in the only available global hydraulic conductivity dataset. To better understand the sensitivity of model output to uncertain spatially distributed parameters, we present the first application of a global sensitivity method for a global-scale groundwater model using nearly 2000 steady-state model runs of the global gradient-based groundwater model G^{3}M. By applying the Morris method in a novel domain decomposition approach that identifies global hydrological response units, spatially distributed parameter sensitivities are determined for a computationally expensive model. Results indicate that globally simulated hydraulic heads are equally sensitive to hydraulic conductivity, groundwater recharge, and surface water body elevation, though parameter sensitivities vary regionally. For large areas of the globe, rivers are simulated to be either losing or gaining, depending on the parameter combination, indicating a high uncertainty in simulating the direction of flow between the two compartments. Mountainous and dry regions show a high variance in simulated head due to numerical instabilities of the model, limiting the reliability of computed sensitivities in these regions. This is likely caused by the uncertainty in surface water body elevation. We conclude that maps of spatially distributed sensitivities can help to understand the complex behavior of models that incorporate data with varying spatial uncertainties. The findings support the selection of possible calibration parameters and help to anticipate challenges for a transient coupling of the model.

1 Introduction

Global groundwater dynamics have been significantly altered by human withdrawals and are projected to be further modified under climate change (Taylor et al., 2013). Groundwater withdrawals have led to lowered water tables, decreased base flows, and groundwater depletion around the globe (Konikow, 2011; Scanlon et al., 2012; Wada et al., 2012; Wada, 2016; Döll et al., 2014). To represent groundwater–surface-water body interactions, lateral and vertical flows, and human water use impacts on head dynamics, it is necessary to simulate the depth and temporal variation of the groundwater table. Global-scale hydrological models have

Published by Copernicus Publications on behalf of the European Geosciences Union.

recently moved to include these processes by implementing a gradient-based groundwater model approach (de Graaf et al., 2015; Reinecke et al., 2019). This study is based on G^{3}M (Döll et al., 2009), one of the two global groundwater models capable of calculating hydraulic head and surface water body interaction on a global scale. However, the lack of available input data and the necessary conceptual assumptions due to the coarse spatial resolution limit the reliability of model output. These substantial uncertainties suggest an opportunity for diagnostic methods to prioritize efforts in data collection and parameter estimation.

Sensitivity analysis is a powerful tool to assess how uncertainty in model parameters affects model outcome, and it can provide insights into how the interactions between parameters influence the model results (Saltelli et al., 2008). Sensitivity methods can be separated into two classes: local and global methods. Local methods compute partial derivatives of the output with respect to an input factor at a fixed point in the input space. By contrast, global methods explore the full input space, though at higher computational costs (Pianosi et al., 2016). The large number of model evaluations required can render global methods unfeasible for computationally demanding models, though increased computational resources have facilitated their application, e.g., Herman et al. (2013a), Herman et al. (2013b), and Ghasemizade et al. (2017). Still, existing studies of global models either focus on exploring uncertainties by running their model with a limited set of different inputs for a quasi-local sensitivity analysis (Wada et al., 2014; Müller Schmied et al., 2014, 2016; Koirala et al., 2018) or applying computationally inexpensive methods based on a limited set of model evaluations (Schumacher et al., 2015). For example, de Graaf et al. (2015, 2017) determined the coefficient of variation for head results in a global groundwater model with 1000 model runs evaluating the impact of varying aquifer thickness, saturated conductivity, and groundwater recharge. To the knowledge of the authors, the only other study that applied a global sensitivity analysis to a comparably complex global model is Chaney et al. (2015). An overview of the application of different sensitivity analysis methods for hydrological models can be found in Song et al. (2015) and Pianosi et al. (2016).

G^{3}M uses input from, and it is intended to be coupled with and integrated into, the global hydrological model WaterGAP Global Hydrology Model (WGHM) (Döll et al., 2014). This study investigates the sensitivity of steady-state hydraulic heads and exchange flows between groundwater and surface water to variations in main model parameters (e.g., groundwater recharge, hydraulic conductivity, and riverbed conductance). To this end the method of Morris (Morris, 1991) is applied.

Morris is a global sensitivity method as it provides an aggregated measure of local sensitivity coefficients for each parameter at multiple points across the input space and analyses the distribution properties (Razavi and Gupta, 2015). It requires significantly fewer model runs, compared to other global methods, to provide a meaningful ranking of sensitive parameters enabling the exploration of computationally demanding models (Herman et al., 2013a). The application of a global sensitivity method for a complex worldwide model of groundwater flows is unique, and Morris is currently the best available method to handle the computational constraints.

To reduce the number of necessary model runs when conducting global sensitivity analysis for computationally demanding models we introduce the concept of global hydrological response units (GHRUs) (Sect. 2.2.3) (similar to Hartmann et al., 2015, for example). Using the GHRUs we present an application of the Morris method (Morris, 1991) to the Global Gradient-based Groundwater Model, G^{3}M (Reinecke et al., 2019).

Sensitivities of the model are explored in three steps: (1) to understand the impact of improved input data, in particular hydraulic conductivity, we investigate the changes in simulated hydraulic head that result from changing the hydraulic conductivity data from the GLHYMPS 1.0 dataset (Gleeson et al., 2014) to 2.0 (Huscroft et al., 2018). (2) Based on prior experiments (de Graaf et al., 2015; Reinecke et al., 2019) eight parameters are selected for a Monte Carlo experiment to quantify uncertainty in simulated hydraulic head and groundwater–surface-water interactions. The parameters are sampled with a newly developed global region-based sampling strategy and build the framework for the (3) Morris analysis. Elementary effects (EEs), a metric of sensitivity, are calculated and their means and variances ranked to determine global spatial distributions of parameter sensitivities and interactions. The derived global maps show, for the first time, the sensitivity and parameter interactions of simulated hydraulic head and groundwater–surface-water flows in the simulated steady-state global groundwater system to variations in uncertain parameters. Foremost, these maps help future calibration efforts by identifying the most influential parameters and answer the question if the calibration should focus on different parameters for different regions helping to understand regional deviations from observations. Additionally, they guide the further development of the model, especially in respect to the coupling efforts highlighting which parameters will influence the coupled processes the most. Lastly, they show in which regions global groundwater models might benefit the most from efforts in improving global datasets like global hydraulic conductivity maps.

2 Methodology and data

2.1 The model G^{3}M

G^{3}M (Reinecke et al., 2019) is a global groundwater model intended to be coupled with WaterGAP (Döll et al., 2003, 2012, 2014; Müller Schmied et al., 2014) and is based on the Open Source groundwater modeling framework G^{3}M-f[1] (Reinecke, 2018). It computes lateral and vertical groundwater flows as well as surface water exchanges for all land areas of the globe except Antarctica and Greenland on a resolution of 5 arcmin with two vertical layers with a thickness of 100 m each, representing the aquifer. The groundwater flow between cells is computed as

$$\frac{\partial}{\partial x}\left(K_x\frac{\partial h}{\partial x}\right)+\frac{\partial}{\partial y}\left(K_y\frac{\partial h}{\partial y}\right)+\frac{\partial}{\partial z}\left(K_z\frac{\partial h}{\partial z}\right) + \frac{Q}{\Delta x\Delta y\Delta z}=S_\mathrm{s}\frac{\partial h}{\partial t}, \tag{1}$$

where $K_{x,y,z}$ [L T^{-1}] is the hydraulic conductivity along the x, y, and z axis between the cells with size $\Delta x\Delta y\Delta z$; S_s [L^{-1}] is the specific storage; h [L] is the hydraulic head; and Q [L^3 T^{-1}] denotes the in- and outflows of the cells to or from external sources of groundwater recharge from soil (R) and surface water body flows (Q_swb) (see also Reinecke et al., 2019[Eqs. (1, 2)]). The evaluation presented in this study is based on a steady-state variant of the model representing a quasi-natural equilibrium state, not taking into account human interference (a full description of the steady-state model and indented coupling can be found in Reinecke et al., 2019). The stand-alone steady-state simulations were performed as an initial step to identify the dominant parameters that are also likely to be important for controlling transient groundwater flow.

2.1.1 Groundwater recharge

Groundwater recharge (R) is based on mean annual R computed by WaterGAP 2.2c for the period 1901–2013. Human groundwater abstraction was not taken into account; not because it is not computed by WaterGAP but rather because there is no meaningful way to include it into a steady-state model which represents an equilibrium (abstractions do not equilibrate).

2.1.2 Hydraulic conductivity

Hydraulic conductivity (K) is derived from GLHYMPS 2.0 (Huscroft et al., 2018) (shown in Fig. 2a). The original data were gridded to 5 arcmin by using an area-weighted average and used as K of the upper model layer. For the second layer, K of the first layer is reduced by an e-folding factor f used by Fan et al. (2013) (a calibrated parameter based on terrain slope), assuming that hydraulic conductivity decreases exponentially with depth. Hydraulic conductivity of the lower layer is calculated by multiplying the upper layer value by $\exp(af^{-1})^{-1}$ where $a=-50$ (m) (Fan et al., 2013, Eq. 7).

Currently only two datasets, GLHMYPS 1.0 and 2.0 (Gleeson et al., 2014; Huscroft et al., 2018), are available and are used by a number of continental and global models (de Graaf et al., 2015; Maxwell et al., 2015; Keune et al., 2016; Reinecke et al., 2019). GLHMYPS 1.0 (Gleeson et al., 2014) is compiled based on the global lithology map GLiM (Hartmann and Moosdorf, 2012) and data from 92 regional groundwater models and derives permeabilities (for the first 100 m vertically) based on Gleeson et al. (2011), differentiating the sediments into the categories fine-grained, coarse-grained, mixed, consolidated, and unconsolidated. Permafrost regions are assigned a K value of 10^{-13} m s^{-1} based on Gruber (2012). Areas of deeply weathered laterite soil (mainly in tropical regions) are mapped as unconsolidated sediments as they dominate K (Gleeson et al., 2014).

The global permeability map was further improved with the development of GLHYMPS 2.0 by Huscroft et al. (2018). A two-layer setup was established in GLHYMPS 2.0 with the lower layer matching the original GLHYMPS 1.0. For the upper layer in GLHYMPS 2.0, a global database of unconsolidated sediments (Börker et al., 2018) was integrated into GLHYMPS 2.0, resulting in overall slightly increased K (Fig. 2a). The thickness of the upper layer was deduced from the *depth-to-bedrock* information available from SoilGrid (Hengl et al., 2017). No thickness was assigned to the lower layer.

2.1.3 Surface water body conductance

The in- and outflows Q are described similar to MODFLOW as flows from the cell: a flow from the cell to a surface water body is negative, and the reverse flow is positive. Thus gains and losses from surface water bodies (lakes, wetlands and rivers) are described as

$$Q_\mathrm{swb}=\begin{cases}C_\mathrm{swb}\left(E_\mathrm{swb}-h\right), & h>B_\mathrm{swb},\\ C_\mathrm{swb}\left(E_\mathrm{swb}-B_\mathrm{swb}\right), & h\le B_\mathrm{swb},\end{cases} \tag{2}$$

where h is the simulated hydraulic head, E_swb is the head of the surface water body, and B_swb is the bottom elevation. The conductance C_swb of the surface water body bed is calculated as

$$C_\mathrm{swb}=\frac{KLW}{E_\mathrm{swb}-B_\mathrm{swb}}, \tag{3}$$

where K is the hydraulic conductivity, L the length, and W the width of the surface water body. For lakes (including reservoirs) and wetlands, the conductances C_lak and C_wet are estimated based on K of the aquifer and surface water body area divided by a static thickness of 5 m ($E_\mathrm{swb}-B_\mathrm{swb}=5$ m). For a steady-state simulation the surface water body data show the maximum spatial extent of wetlands, an extent that is seldom reached, in particular in the case of wetlands in dry areas. To account for that we assume for global wetlands ($C_\mathrm{gl.wet}$) that only 80 % of their maximum extent is reached in the steady state (Reinecke et al., 2019).

[1] Available on http://globalgroundwatermodel.org/ (last access: 12 November 2019).

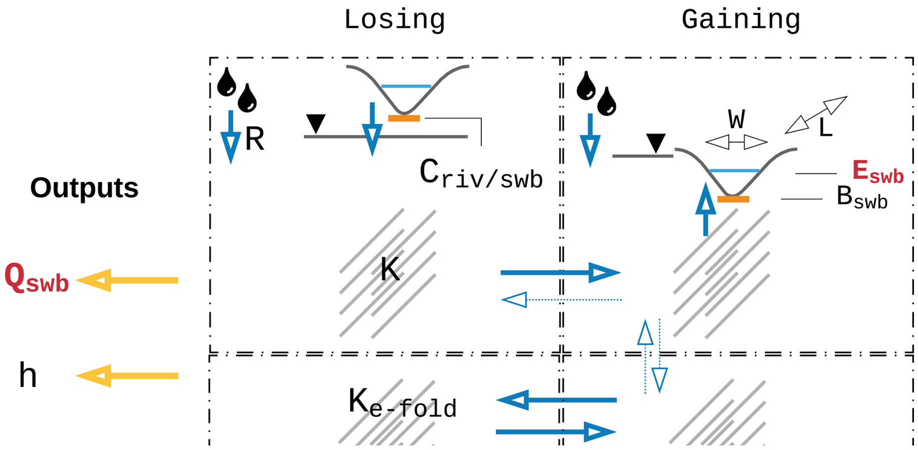

Figure 1. Parameterization and outputs of the G^{3}M model. Q_{swb} is the flow between the aquifer and surface water bodies, h is the simulated hydraulic head, K is the hydraulic conductivity, $K_{\text{e-fold}}$ is K scaled by an e-folding factor (see Sect. 2.1.2), E_{swb} is the surface water body head, B_{swb} is the bottom elevation of the surface water body, C_{swb} is the conductance of the surface water bodies, and R is the groundwater recharge. In red are the outputs and parameters that are of foremost importance for coupling.

Global wetlands are defined as wetlands that are recharged by streamflow coming from an upstream 5 arcmin grid cell in WaterGAP (Döll et al., 2009). For gaining rivers, the conductance is quantified individually for each grid cell following an approach proposed by Miguez-Macho et al. (2007). According to Miguez-Macho et al. (2007), the river conductance C_{riv} in a steady-state groundwater model needs to be set in a way that the river is the sink for all the inflow to the grid cell that is not transported laterally to neighboring cells. This inflow consists of R and inflow from neighboring cells.

$$C_{\mathrm{riv}} = \frac{R + Q_{\mathrm{eq}_{\mathrm{lateral}}}}{h_{\mathrm{eq}} - E_{\mathrm{riv}}}\; h > E_{\mathrm{riv}}, \tag{4}$$

where $Q_{\mathrm{eq}_{\mathrm{lateral}}}$ is the lateral flow based on the equilibrium head h_{eq} of Fan et al. (2013) and E_{riv} is the head of the river ($E_{\mathrm{swb}} = E_{\mathrm{swb,riv}}$ in Table 1). These conductance equations are inherently empirical as they use a one-dimensional flow equation to represent the three-dimensional flow process that occurs between groundwater and surface water. Future efforts will investigate using approaches appropriate for large-scale models, such as those described by Morel-Seytoux et al. (2017). An extensive description on the chosen equations and implications can be found in Reinecke et al. (2019).

2.1.4 Surface water body elevation

The vertical location of surface water bodies has a great impact on model outcome (Reinecke et al., 2019). Their vertical location E_{swb} is set to the 30th percentile of the 30 arcsec land surface elevation values of Fan et al. (2013) per 5 arcmin cell, e.g., the elevation that is exceeded by 70 % of the hundred 30 arcsec elevation values within one 5 arcmin cell. B_{swb} is calculated based on that head elevation with different values for wetlands and lakes (Reinecke et al., 2019, Table 1). For rivers, B_{swb} is equal to $h_{\mathrm{riv}} - 0.349 \times Q_{\mathrm{bankfull}}^{0.341}$ (Allen et al., 1994), where Q_{bankfull} is the bankfull river discharge in the 5 arcmin grid cell (Verzano et al., 2012).

2.1.5 Ocean boundary

The outer boundary condition in the model is described by the ocean and uses an equation similar to MODFLOW's general head boundary condition as flow

$$Q_{\mathrm{ocean}} = C_{\mathrm{oc}}\left(h_{\mathrm{ocean}} - h\right), \tag{5}$$

where h_{ocean} is the elevation of the ocean water table set to 0 m worldwide and C_{oc} is the conductance of the boundary condition set to $10\,\mathrm{m}^2\,\mathrm{d}^{-1}$ based on average K and aquifer thickness.

2.2 Sensitivity analysis

2.2.1 Sensitivity of simulated head to choice of hydraulic conductivity dataset

Parameterization of aquifer properties based on hydrogeological data is an important decision in groundwater modeling. We first investigate the effect of switching to a newly available global permeability dataset to explore the sensitivity of h to the variability in geologic data. The results are then compared to the effects of parameter variability, as quantified by the Monte Carlo experiments.

GLHYMPS 2.0 (Huscroft et al., 2018) provides an update of the only available global permeability map (Gleeson et al., 2014). To quantify how the new hydraulic conductivity estimates change the simulation outcome of the groundwater model we calculate a basic sensitivity index:

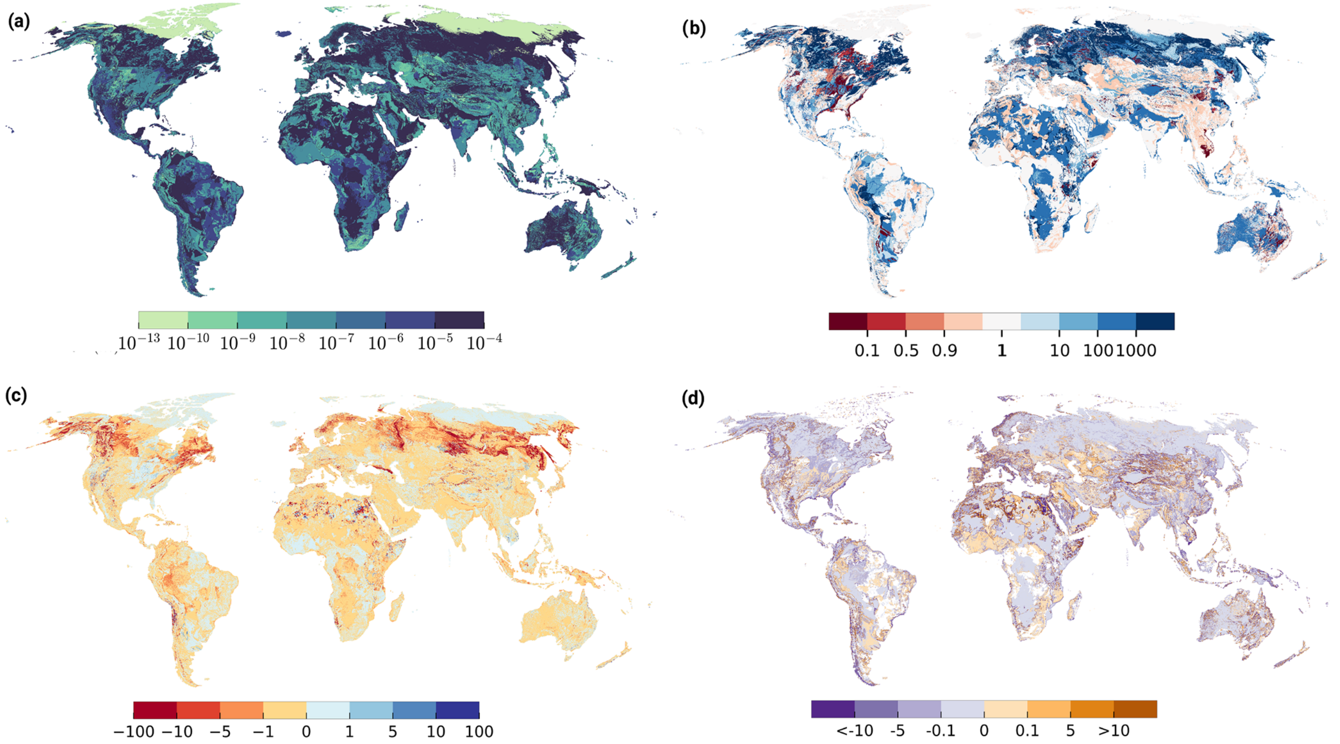

Figure 2. Impact of hydraulic conductivity datasets GLHYMPS 1.0 and GLHYMPS 2.0. **(a)** GLHYMPS 2.0 ($\mathrm{m\,s^{-1}}$), **(b)** K differences, expressed as K(GLHYMPS 2.0)/K(GLHYMPS 1.0). Blue indicates higher values in GLHYMPS 2.0, **(c)** h(GLHYMPS 2.0) minus h(GLHYMPS 1.0) (m), **(d)** the sensitivity of h to change in the GLHYMPS dataset based on Eq. (6) (white indicates that no index could be calculated).

$$S = \frac{\frac{h_2-h_1}{h_1}}{\frac{K_2-K_1}{K_1}}, \tag{6}$$

where the sensitivity S of h to a change in K is calculated based on the change in h (h_1 is the hydraulic head calculated with GLHYMPS 1.0 and h_2 with GLHYMPS 2.0), and the change in K_1 and K_2 (the hydraulic conductivity) is based on GLHYMPS 1.0 and 2.0, respectively.

2.2.2 Sensitivity of head and surface water body flow to choice in parameters

Along with K, additional parameters influence the model outcome. In this study we apply the method of Morris (Morris, 1991) as a screening method to identify which parameters are most important for the two main model outcomes, namely h and groundwater–surface-water interactions (Q_{swb}). The Morris method provides a compromise between accuracy and computational cost in comparison to other Monte Carlo-like methods (Campolongo et al., 2007). Compared to other global methods, like the more robust variance-based methods, e.g., Sobol (1993), Morris has drawbacks as it may provide false conclusions (Razavi and Gupta, 2015). The attribution of what is a direct effect (model response only due to one parameter change) and what is an effect of interaction (response to nonlinear interaction of parameters on model output) is not trivial. Morris is prone to scale issues; that is, that the step size of the analysis can have a significant impact on the conclusions, especially for significantly nonlinear responses (Razavi and Gupta, 2015). In this study we address this by limiting the parameter ranges of the multipliers where we suspect nonlinearity in the model response. In general the choice of the chosen global sensitivity method may yield different results (Dell'Oca et al., 2017). On the other hand, Janetti et al. (2019) showed for a regional-scale groundwater study that different global methods showed similar results for hydraulic conductivity parameterization. Nevertheless, Morris is a well established and recognized method (Razavi and Gupta, 2015) that has the advantage of computational efficiency compared to variance-based methods to screen the most sensitive parameters (Herman et al., 2013a).

Each model execution represents an individually randomized "one-factor-at-a-time" (OAT) experiment (Pianosi et al., 2016), where one parameter is changed per simulation. Parameter samples are based on trajectories. Each trajectory starts at a point in the parameter space and perturbs one parameter at a time. After all parameters are changed, a new trajectory begins from a different point in the parameter space.

Based on the model executions using these parameter perturbations, the Morris method calculates an elementary effect (EE) d for every trajectory of an ith parameter (in this study parameter multipliers).

$$d_i(\boldsymbol{X}) = \left(\frac{y(X_1, \ldots, X_{i-1}, X_i + \Delta, X_{i+1}, \ldots, X_k) - y(\boldsymbol{X})}{\Delta} \right), \quad (7)$$

where Δ is the trajectory step size for the parameter multiplier X_i, $\boldsymbol{X}$ is the vector of model parameters multipliers of size k and $y(\boldsymbol{X})$ the model output (e.g., in the presented model h or Q_{swb}). Each EE is a local sensitivity measure that is finally aggregated to a global measure. This total effect of the ith parameter is computed as the absolute mean of the EEs for all trajectories and is denoted as μ^* (Campolongo et al., 2007). If μ^* is large, it means the parameter is sensitive, on average, throughout the parameter space.

The standard deviation of EEs (σ_i) is an aggregated measure of the intensity of the interactions of the ith parameter with the other parameters, representing the degree of nonlinearity in model response to changes in the ith parameter (Morris, 1991). If σ_i is large, it means that the sensitivity of the parameter varies a lot between different points in the parameter space. For a completely linear model, EEs are the same everywhere (because the local gradients are the same everywhere), and σ_i is zero. Therefore, a higher σ_i entails a more nonlinear model with more interactive components.

The derived metrics μ^* and σ_i are both measures of intensity (higher values are more sensitive/interactive) and do not represent absolute values of sensitivity or interaction. Both can only be interpreted meaningfully in comparison with values derived for other parameters. To achieve that, μ^* and σ_i are used to rank the most sensitive parameters. Values for all parameters are sorted from highest to lowest, and the parameter with the highest value is selected as the most influential parameter with the highest rank (hereafter called rank 1). The parameter with the second highest value (rank 2) is the second most influential parameter and so on. The robustness of the parameter ranking is assessed by calculating confidence intervals as described in detail in Appendix A.

Previous experiments (de Graaf et al., 2015; Reinecke et al., 2019) showed the importance of hydraulic conductivity, groundwater recharge, and surface water body elevation to the simulated hydraulic head. Together with the highly uncertain surface water body and ocean conductance we thus selected eight model parameters for the sensitivity analysis. The analysis was conducted by using randomly sampled multipliers in the ranges presented in Table 1.

Throughout the analysis the following parameters, including the convergence criterion and spatial resolution, stay fixed: global mean sea-level, bottom elevation of surface water bodies, and their width and length. The baseline parameters are assumed to be equal to Reinecke et al. (2019). Hydraulic conductivity is based on a global dataset (Sect. 2.1.2), the conductance is calculated as previously shown (Sect. 2.1.3), and the groundwater recharge baseline is equal to the mean annual values calculated by WaterGAP (Sect. 2.1.1). Parameter ranges were chosen to ensure that a high percentage of model realizations converge numerically. For example, the uncertainty of E_{swb} in the model is higher than the ranges used in this study, but the sampling range was restricted because a larger range led to nonconvergence. Furthermore, the chosen river conductance approach uses R as parameter and includes a nonlinear threshold between losing and gaining surface water bodies, which strongly affects numeric stability. As in any sensitivity analysis, the choice of parameter ranges involves some subjectivity that may influence the ranking of sensitive parameters in the results.

2.2.3 Global hydrological response units

Even though the number of model evaluations are less for OAT experiments than for “all-at-a-time” experiments (Pianosi et al., 2016), varying every parameter independently in every spatial grid cell leads to an unfeasible amount of model runs. On the other hand, the use of global multipliers that vary a parameter uniformly for all computational cells may lead to inconclusive results, as the sensitivity for every cell to this change is spread to the whole computational domain. A possible solution would be to separate the globe into zones with similar geological characteristics based on the GLHYMPS dataset, but this may still result in an infeasible number of required simulations. Each simulation takes about 30 min to 1 h on a commodity computer (more if the parameters hinder a fast convergence).

To overcome these limitations, we introduce the use of a global hydrological response unit (GHRU). Every GHRU represents a region of similar characteristics, regarding three characteristics: E_{swb} (Sect. 2.1.3 and 2.1.4), K (Sect. 2.1.2), and R (Sect. 2.1.1). This does not constitute a zoning approach often used for calibration in traditional regional groundwater modeling, only a separation into parameter multipliers. A uniform random distribution within the ranges given in Table 1 is used to sample the parameter multipliers for all GHRUs. Characteristics for each model cell are normalized to [0, 1] and used to create a 3-D point space (based on the three characteristics for each model cell). We apply a k-means (Lloyd, 1982) clustering algorithm to identify these regions.

K-means clustering partitions n points into k clusters, where each point belongs to the cluster with a minimized pairwise squared distance to the mean in that cluster. Figure 3a shows a map of k-means clustering (six clusters) categories based on a normalized three-dimensional space of E_{swb}, K, and R per grid cell.

The number of clusters was determined based on the feasible number of model evaluations. K-means constitute an unsupervised machine learning approach that builds the required number of clusters automatically; thus it is necessary afterwards to examine what main characteristics these clusters represent (shown in Table 2). Characteristics are encoded

Table 1. Range of parameter multipliers used in the Morris experiments. Each parameter multiplier is sampled in log space ($\log_{10}$(Multiplier)) with sampling based on Campolongo et al. (2007) and optimized with Ruano et al. (2012).

Parameter	Unit	Multiplier range	Description
K	LT^{-1}	0.1–100	Saturated hydraulic conductivity
E_{swb}	L	0.9977–1.0023	SWB elevation
C_{lak}	$\mathrm{L}^2\,\mathrm{T}^{-1}$	0.5–2	Conductance of lakebed
C_{wet}	$\mathrm{L}^2\,\mathrm{T}^{-1}$	0.5–2	Conductance of wetland bed
$C_{\mathrm{gl.wet}}$	$\mathrm{L}^2\,\mathrm{T}^{-1}$	0.5–2	Conductance of global wetland bed
C_{riv}	$\mathrm{L}^2\,\mathrm{T}^{-1}$	0.5–2	Conductance of riverbed
R	$\mathrm{L\,T}^{-1}$	0.5–2	Groundwater recharge
C_{oc}	$\mathrm{L}^2\,\mathrm{T}^{-1}$	0.1–10	Conductance of the ocean boundary

C_{oc} is equal for all ocean cells.

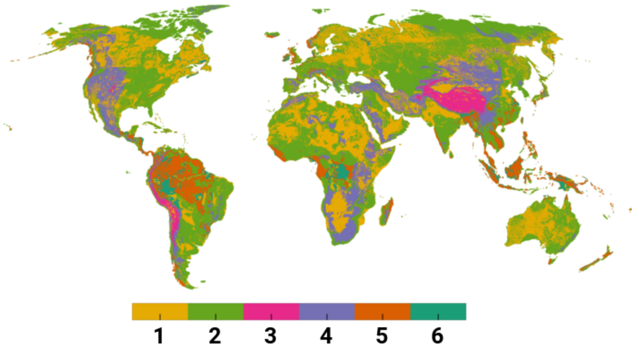

Figure 3. Map of k-means clustering categories, each representing a GHRU. Each color identifies a region where the combination of all three parameters is similar.

as relative values – high (↑), medium (∼), low (↓) – of the three parameter values based on their mean value per cluster. These characteristics are used to connect calculated parameter sensitivities to GHRUs when analyzing the results of the experiment.

2.2.4 Experiment configuration

The total number of necessary simulations N is determined with $N = r(k+1)$ (Campolongo et al., 2007), where r is the number of elementary effects and k is the number of parameters. For 7 parameters (without the ocean boundary) and 6 GHRUs we get a total number of parameters $k = 42 + 1$, where $+1$ stands for the ocean boundary, which is not varied by GHRU, resulting in 1848 simulations. Elementary effects are based on an initial random sampling of 10 000 trajectories using Campolongo et al. (2007) and then reduced by assuming 42 (number of parameters times GHRUs without ocean boundary) so-called optimized trajectories following Ruano et al. (2012). Only random sampling might result in nonoptimal coverage of the input space; thus the initial random trajectories are used to select only those that maximize the dispersion in the input space. This optimal set of trajectories is approximated with a reasonable computational demand using the methodology developed by Ruano et al. (2012).

The experiment resulted in 1848 simulations with an overall runtime of 2 months on a machine with 20 computational cores (enabled hyper-threading) and 188 GB RAM. Each simulation required about 8 GB of RAM and was assigned four computational threads while running the simulations in cohorts of 10 simulations at once. Changes in parameters were stacked over all experiments. Thus, an experiment may have changed R (also affecting C_{riv} for gaining conditions) while containing a C_{riv} multiplier from a previous experiment. Sampling and analysis was implemented with the Python library SALib (Herman and Usher, 2017). For each experiment, the model was run until it reached an equilibrium state (steady-state model). All other parameters and convergence criteria can be found in Reinecke et al. (2019). If a simulation failed (6 of 1848 did not converge) the missing results were substituted randomly from another simulation within the cohort to preserve the required ordering of parameter samples for the used Python implementation of the Morris method. This number is low enough that it does not bias the results in any significant way (Branger et al., 2015).

A converged simulation does not necessarily constitute a valid result for all computed cells. Numeric difficulties based on the model configuration (due to the selected parameter multipliers) may lead to cells with calculated h that are unreasonable – more specifically, a hydraulic head that is far above or below the land surface and/or leads to a large mass budget error. In the presented study these simulations are retained, as a removal would require either a rerun of simulations with a different convergence criterion and inclusion of this in the analysis or a modification of the Morris method to allow the removal of simulations. Confidence intervals (95 %) are derived via bootstrapping using 1000 bootstrap resamples (see Appendix A).

Table 2. Mean values of GHRU characteristics and their summarized description, where ↑ is read as a relatively high value, ∼ as medium, and ↓ as low; e.g., ↑↑ E indicates a cluster with very high and relatively high (↑) average E_{swb}. Additionally, the last two columns show the percentage of cells per GHRU where μ^* of h and Q_{swb} could be reliably determined (described in Sect. 3.2.6).

					% of reliable μ^*	
GHRU	$\mu(E_{\mathrm{swb}})$ (m)	$\mu(K)$ (m s^{-1})	$\mu(R)$ (mm d^{-1})	GHRU description	h	Q_{swb}
1	454	10^{-4}	0.15	$\sim E, \uparrow K, \sim R$	9.54 %	6.58 %
2	286	10^{-6}	0.15	$\downarrow E, \sim K, \sim R$	12.07 %	14.41 %
3	4107	10^{-6}	0.13	$\uparrow\uparrow E, \sim K, \downarrow R$	0.08 %	4.09 %
4	1355	10^{-6}	0.11	$\uparrow E, \sim K, \downarrow R$	3.17 %	17.19 %
5	303	10^{-6}	1.24	$\downarrow E, \sim K, \uparrow R$	31.62 %	26.37 %
6	194	10^{-4}	1.25	$\downarrow E, \uparrow K, \uparrow R$	29.00 %	14.36 %

3 Results

3.1 Sensitivity to updated GLHMYPS dataset

Global-scale hydrogeological data are limited. Figure 2b shows the change in K between GLHYMPS 1.0 (Gleeson et al., 2014) and the upper layer of GLHYMPS 2.0 (Huscroft et al., 2018), where an overall increase can be observed due to the change in unconsolidated sediments. Although unconsolidated sediments cover roughly 50 % of the world's terrestrial surface, their extent was underestimated in previous lithologic maps by half (Börker et al., 2018). The largest increase in K can be found between 50 and 70° N because of glacial sediments that were assigned high K values. Different lithologies, e.g., alluvial terrace sediments and glacial tills, have all been grouped into the hydrolithological category of sand. Areas of decreased hydraulic conductivity are, for example, the Great Lakes, south of Hudson Bay, and parts of Somalia. The area around Hudson Bay was assumed to consist of unconsolidated sediments in GLHYMPS 1.0 (Gleeson et al., 2014) and was changed to consolidated. In Somalia, evaporites, which are known for low K, were incorporated from the Global Unconsolidated Sediments Map Database (GUM) (Börker et al., 2018). Furthermore, GUM provides a detailed mapping of loess and loess-like depositions, which were assigned lower K values. These regions can be observed to be the only regions with reduced K (Fig. 2b). Overall, the increase in unconsolidated sediments is probably the main cause for the increased K.

Due to the change in K, the simulated h changes accordingly (Fig. 2c). In areas where the K decreased h increased, e.g., eastern North America. Overall heads decreased, especially in central Russia by up to 10 to 100 m. A slight increase in head can be observed in areas with no change in K. This can be either due to changes in groundwater flow patterns due to the overall increase in K or due to numerical noise.

Based on these results, a local sensitivity index was calculated using Eq. (6), shown in Fig. 2d. White constitutes areas where either the relative change of K was zero or the head of the GLHYMPS 1.0 simulation was zero. Overall, h and K change in the opposite directions (positive values indicate a change in the same direction). An overall increase in K has led to a overall decrease in h as the higher K values are able to transport more water for a given hydraulic gradient, especially along coastlines and mountainous areas. Increased sensitivity indexes can be observed at boundaries of areas of large spatial extent where the initial K was equal, whereas the h changes inside that area are relatively small (e.g., the Arabian Peninsula). In regions where an increase in K leads to a decrease in head, an increase in h at the boundary to other hydrolithological structures can be observed. Areas with changing indexes next to each other, e.g., in the Sahara, possibly point to a numerically unstable model region with a general sensitivity to parameter changes. GLHYMPS 2.0 represents the best available global data for hydraulic conductivity, and the results of this initial experiment indicate a significant sensitivity to updating the model with this new dataset.

3.2 Monte Carlo experiments

To assess the variability of model outputs we used the Monte Carlo-like OAT experiments to quantify the output uncertainty as given in the 1848 model realizations.

3.2.1 Variability of hydraulic head

The spatial distribution of variability in the main model output h provides insights into model stability and highlights regions which are most sensitive to parameter changes. Observable differences between simulations can be caused by (1) the parameter change of the OAT experiment, (2) the interactive effects due to combinations of parameter changes, (3) numerical noise (slight variations in outcome due to the nature of the numerical algorithm or floating point errors that cannot be attributed to a specific parameter change), and (4) a nonoptimal solution of the groundwater equation (Eq. 1) even if the convergence criterion is met. The latter error (4) can be observed in the model where a strong nonlinear rela-

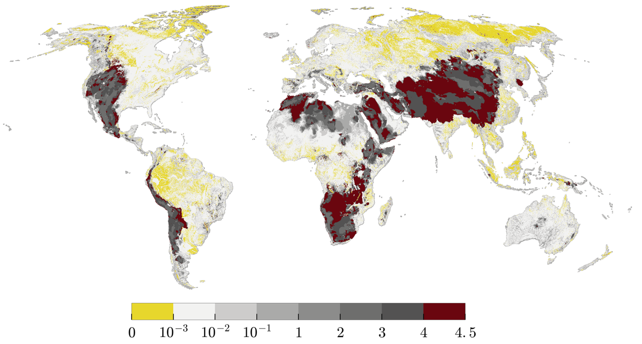

Figure 4. Absolute coefficient of variation $(\sigma(h)\mu(|h|)^{-1})$ (%) of simulated h per cell over all Monte Carlo realizations. Yellow indicates that h results changed very little, white to gray values indicate a growing difference in model results, and red values indicate a very high variation of h over all model realizations.

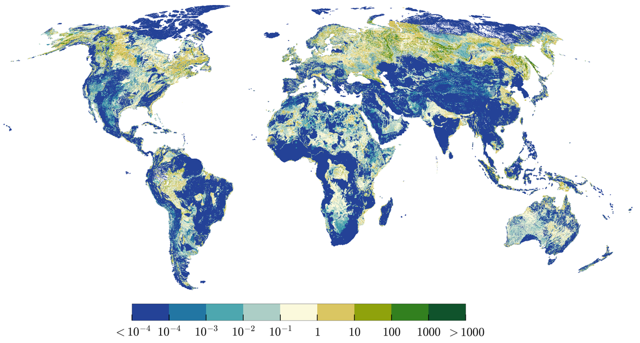

Figure 5. Uncertainty in h caused by variability in hydraulic conductivity data between GLHYMPS 1.0 and 2.0 (dominant in brown to green) in relation to uncertainty in h caused by variability in parameters based on Monte Carlo simulations (dominant in blue to light blue) calculated as $\frac{|h1-h2|}{\mathrm{IQR}(h_{\mathrm{mc}})}$, where $h1/2$ is the simulated head based on GLHMYPS 1.0 and 2.0 and h_{mc} the simulated head of all Monte Carlo experiments.

tion may produce solutions that fit the convergence criterion but should be considered nonvalid, e.g., because of a mass balance that is unacceptably imprecise.

Figure 4 shows the absolute coefficient of variation (ACV) of h per cell over all Monte Carlo experiments. The ACV is used to make a sound comparison of variance taking into account the mean of the h value per cell (because the mean might be negative the absolute value is used). Yellow indicates that h changed little (mostly for regions with shallow groundwater), white to gray values indicate a growing difference in model results, and red values indicate a high variation of h over all model realizations. The latter areas represent either very low R (Sahara, Australia, South Africa) or a high variance in elevations, e.g., Himalaya, Andes, and the Rocky Mountains. These are expected to have a high sensitivity to parameter changes as the multiplier of E_{swb} produces the highest shifts in regions with high elevation. Any changes in E_{swb} might cause a switch from gaining to losing conditions and vice versa (discussed in Sect. 3.2.2). Additionally, a change in R directly influences the conductance term C_{riv} that might also be changed by a multiplier. These combinations may yield conditions that are exceptionally challenging for the numerical solver. Switches between the two conditions constitute a nonlinearity in the equation which might require a smaller temporal step-size to be solved. In a nutshell, if an iteration leads to a gaining condition and the next to a losing condition, the switch renders the approximated heads of the preceding iterations invalid as the equation changed. In the worst case this can lead to an infinite switch between the two conditions without finding the correct solution. Areas with a high variance in hydraulic heads will also produce wide confidence intervals for parameters which are highlighted in Fig. A2.

Figure 5 relates the uncertainty in h, due to a change from GLHYMPS 1.0 to 2.0 to the interquartile range of h of all Monte Carlo realizations, and thus uncertainty in h due to parameter variation. Parameter variation is the dominant cause for h variability in mountainous regions, whereas the change in geologic data has a dominant impact in northern latitudes and the upper Amazon. In Australia, central Africa, and northern India the impact of increasing K is almost as high as the variability caused by the variation of parameters in the Monte Carlo experiments. This suggests that a reduced uncertainty in K in these regions will improve the model results.

3.2.2 Variability of losing/gaining surface water bodies

Surface water bodies that provide focused, indirect groundwater recharge to the aquifer system are an important recharge mechanism to support ecosystems alongside streams (Stonestrom, 2007). They are important for agriculture and industrial development, especially in arid regions.

Losing or gaining surface water bodies are determined by h in relation to E_{swb}. When h drops below E_{swb} water is lost to the aquifer (Eq. 4). Figure 6 shows for each grid cell the percentage of the model runs in which the surface water bodies in the cell lose water to the groundwater. Regions with a higher percentage are in losing conditions for most of the applied parameter values. Areas with the highest deviation in h (Fig. 4), and thus the lowest agreement over all model realizations, are similar to the regions where some parameter combinations lead to losing surface water bodies, while others lead to gaining surface water bodies (Fig. 6). Overall arid and mountainous regions show high percentages of Monte Carlo realizations with losing conditions, with dominantly 20 %–50 % of the realizations resulting in losing surface water bodies. h in these regions falls below E_{swb} either due to low recharge or high gradients. Surface-water–groundwater interaction in these regions should be more closely investigated to improve model performance. The Sahara region stands out with large areas that contain losing surface water

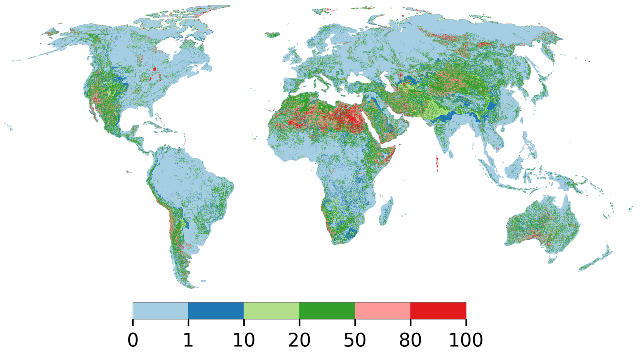

Figure 6. Percentage of all Monte Carlo realizations that resulted in a losing surface water body in a specific cell.

bodies in almost all model realizations. Values close to 100 % are furthermore reached in the Great Lakes, the Colorado Delta, the Andes, the Namib Desert, along the coast of Somalia, the Aral lake, lakes and wetlands in northern Siberia, and partially in Australian wetlands. Wetlands in Australia and the Sahara are likely to be overestimated in size in the context of a steady-state model.

3.2.3 Parameter sensitivities as determined by the method of Morris

The global-scale sensitivity of h and Q_{swb} is summarized in Table 3, which lists the percentage fractions of all cells for which a certain parameter has a certain rank regarding sensitivity and parameter interaction.

Overall, E_{swb} and R are the most important parameters for both model outputs over all ranks, followed by K. Q_{swb} is more sensitive to R than h, whereas h is more sensitive to E_{swb}. C_{riv} appears to be dominant in only the second and third rank for both model outputs. This means that for the majority of cells a change in E_{swb} and R, rather than C_{riv}, dominates changes in Q_{swb} and h. K and R directly influence the calculation of C_{riv} and thus show a higher sensitivity.

The standard deviation of EEs (σ_i) is an aggregated measure of the intensity of the interactions of the ith parameter with the other parameters, representing the degree of nonlinearity in the model response to changes in the ith parameter (Morris, 1991). A high parameter interaction indicates that the total output variance rises due to the interaction of the parameter with other parameters.

E_{swb} shows higher interactions for h than for Q_{swb}. C_{riv} shows a high interaction on the first rank even if it is not the dominant effect. This interaction is likely due to changes and K and R that directly influence the computation of C_{riv}. Both model outputs are sensitive to changes in R but show a relatively low degree of interaction for the first rank. A higher percentage of cells with an increased interaction of R is only visible in the second and third rank.

Table 3. Percentage of cells for which parameters are ranked 1 to 3 based on μ^* and σ. Percentages are shown for each model output, h and Q_{swb}. For example, h is the most sensitive to parameter E_{swb} (rank 1) in 57.2 % of all grid cells, while R is the most important parameter for Q_{swb} in 59.8 % of those cells. Significant values are highlighted in bold.

		% of cells					
		Rank 1		Rank 2		Rank 3	
Parameter	Output	μ^*	σ	μ^*	σ	μ^*	σ
K	h	24.2	18.8	21.7	12.9	7.1	4.3
	Q_{swb}	18.4	15.4	21.1	7.3	8.8	4.7
E_{swb}	h	**57.2**	46.3	14.8	19.9	13.4	18.9
	Q_{swb}	18.5	14.3	11.2	27.7	**36.0**	34.4
C_{lak}	h	1.0	0.5	3.9	2.4	4.3	2.5
	Q_{swb}	0.5	0.6	2.2	0.9	2	0.9
C_{wet}	h	1.4	0.5	3.4	1.4	5.3	4.5
	Q_{swb}	0.5	0.8	3.6	2.1	4.2	2.8
$C_{\mathrm{gl.wet}}$	h	0.9	0.9	1.8	10.2	8.4	8.1
	Q_{swb}	0.4	0.8	2.3	15.2	9.4	7.8
C_{riv}	h	2.0	28.0	**32.8**	29.3	28.7	18.1
	Q_{swb}	1.4	62.6	**47.8**	16.2	28.8	10.0
R	h	13.4	4.1	22.7	23.6	**33.8**	43.2
	Q_{swb}	**59.8**	5.1	11.3	30.5	10.7	39.2
C_{oc}	h	1.3	1.0	0.3	0.2	0.5	0.4
	Q_{swb}	0.5	0.4	0.5	0.2	0.2	0.2

Percentage of cells with nonoverlapping CIs (see Appendix A and Sect. 3.2.6) μ^*: 11.8 % (h) and 13.3 % (Q_{swb}). C_{oc} is rank 1 for h in 23 % of all ocean cells and in 11 % for Q_{swb}.

Lakes and wetlands show low sensitivity and interaction in relation to the total number of cells in Table 3 because they only exist in a certain percentage of cells. Table 4 shows the percentage fractions relative for cells with more than 25 % coverage of a lakes, global wetlands, and/or wetlands. The dominant parameter (by percentage) for all cells with respective surface water body is always E_{swb} for h (in 79.2 % of the lakes and in (79.9 %) 66.3 % of the (global) wetlands) and R (∼ 54 %–77 % of all cells) for Q_{swb}. For the second rank the conductance of the surface water body $C_{\mathrm{lak,wet,gl.wet}}$ dominated h, C_{riv} for Q_{swb}. Thus for lakes and wetlands E_{swb} and R are more relevant to h and Q_{swb} than the conductance of these surface water bodies.

3.2.4 Maps of global sensitivity

To show the spatial distribution of the parameters that affect h and Q_{swb} the most, ranked parameters were plotted for every cell in Fig. 7. The top of Fig. 7 represents the most sensitive parameters in terms of h (left) and Q_{swb} (right). Areas that should be judged with caution due to overlapping CIs are shown in Fig. A2.

For h E_{swb} stands out in mountainous regions with spots of C_{riv} and in regions with low recharge. These regions align with highly variable outputs shown in Fig. 4. K is most im-

Table 4. Percentage fractions of the most frequent parameter for rank 1 (R1) and 2 (R2) of all cells with more than 25 % coverage of a lakes, global wetland, or wetland.

	$\mu^*(h)$		$\mu^*(Q_{\text{swb}})$	
	% R1 = E_{swb}	% R2 = $C_{\text{lak,wet,gl.wet}}$	% R1 = R	% R2 = C_{riv}
Lakes	79.2	64.6	54.2	38.8
Wetlands	66.3	47.3	77.2	46.9
Gl. Wetlands	79.9	56.4	66.3	31.7*

* $C_{\text{riv}} = 31.7\,\%$, $C_{\text{gl.wet}} = 40.6\,\%$. Percentage of second most frequent parameter not shown. Percentage in relation to cells with lakes, global wetland, or wetland > 25 %. Percentage-wise R1($\mu^*(h)$) was always followed by R, except for global wetlands, where the second most frequent R1 was $C_{\text{gl.wet}}$ R1($\mu^*(Q_{\text{swb}})$) was followed percentage-wise by E_{swb} except for local wetlands with K, R2($\mu^*(Q_{\text{swb}})$) by $C_{\text{lak,wet,gl.wet}}$ except for global wetlands with C_{riv}.

portant for h in Australia, the northern Sahara, the Emirates, and across Europe. The second rank (second row in Fig. 7) shows values that are not as important as the top row but dominant over all other parameters. In the regions with large output variations (compare Fig. 4) K and for parts of the Himalaya R are dominant in the second rank (for h). C_{lak} is clearly visible in parts of Nepal and along the Brahmaputra.

For Q_{swb} E_{swb} is dominant in the first rank in, for example, the Rocky Mountains, Andes, Hijaz Mountains in Saudi Arabia, and the Himalaya. R stands out in regions in the Tropical Convergence Zone as well as in northern latitudes. C_{wet} appears as a dominant parameter in areas with large wetlands with a bigger impact on Q_{swb} results than on h. K seems to be equally spatially distributed for h as well as for Q_{swb}. There seems to be no correlation between the initial K spatial distribution and a highly ranked K sensitivity for both model outputs. Areas with a dominant K are possibly influenced by a high interaction with other model components (K shows a high interaction Table 3 that is also reflected spatially in Sect. 3.2.5). For the second rank in the Tropical Convergence Zone C_{riv} and K dominate for Q_{swb}. In general Q_{swb} seems to be more robust to show the effects in the highly variable regions. That is, Q_{swb} is not responding as extremely as h to parameter changes. This further indicates the assumption that E_{swb} is also mainly responsible for the h variations observed in Sect. 3.2.1.

Zooming in on Europe (Fig. 8) for h, as an example, shows, similar to the global picture, that R and K have the highest impact on h along with E_{swb}. E_{swb} is dominant in mountainous regions like the Alps and the Apennines as well as in regions with lots of surface water bodies, e.g., the southern part of Sweden in the area of lakes Vättern and Vänern and in the Finnish Lakeland. R appears dominant in east Italy in the Po Valley, the Netherlands, and the wetlands in southwestern France. Almost invisible in the global picture is C_{oc}, a dominant parameter for most cells that have the ocean as boundary condition (only observable for h). Predominantly C_{riv} follows E_{swb} as the second most important parameter. Only visible in the second rank are the wetlands, e.g., in west Scotland.

3.2.5 Maps of global parameter interaction

Similar to the spatial parameter sensitivities, Fig. 9 shows the parameter interactions for h and Q_{swb}. Parallel to Fig. 7, the first row of Fig. 9 represents the most interactive parameters in terms of h change (left) and Q_{swb} (right). The highest interaction with other parameters can be observed for E_{swb} for regions with high h variability, similar to Fig. 7. This means that for E_{swb} the model is not only sensitive, but also that the sensitivity of the parameter varies a lot between different points throughout the parameter space, suggesting a nonlinear model response. C_{riv} showed no sensitivity on rank 1 in Fig. 7, although it shows a high interaction in regions sensitive to R (compare Figs. 7 and 9) and is more visible for Q_{swb}. This means changes in C_{riv} lead to nonlinear model responses. K regions in the second rank are similar to where K already showed a high sensitivity for h (compare Fig. 7). In the Himalaya R and C_{riv} show a large spatial pattern. For Q_{swb}, $C_{\text{gl.wet}}$ is clearly visible where C_{riv} was most interactive before.

3.2.6 Sensitivity per GHRU

Average sensitivities and parameter interactions for each of the six GHRUs are shown in Fig. 10a. A dominant average per GHRU does not imply a rank 1 in each cell but rather provides an indication of its average importance per GHRU. Each GHRU is described by the notation in Table 2. The average sensitivities and interactions shown are normalized to [0,1] because the calculated μ^* and σ present no absolute measure of sensitivity. Mean values of μ^* and σ that are very close to zero are not shown in Fig. 10.

The values shown in Fig. 10a should be judged with caution as they also include the regions that show possibly unreliable results, i.e., those where any overlap in CIs indicates that the ranking of the parameters cannot be clearly determined (see additional explanation in Fig. A1).

To judge the reliability of the outcomes per GHRU Table 2 shows the percentage of reliable results for h and Q_{swb} for each GHRU, where reliable results exclude over 80 % of all sensitivity values.

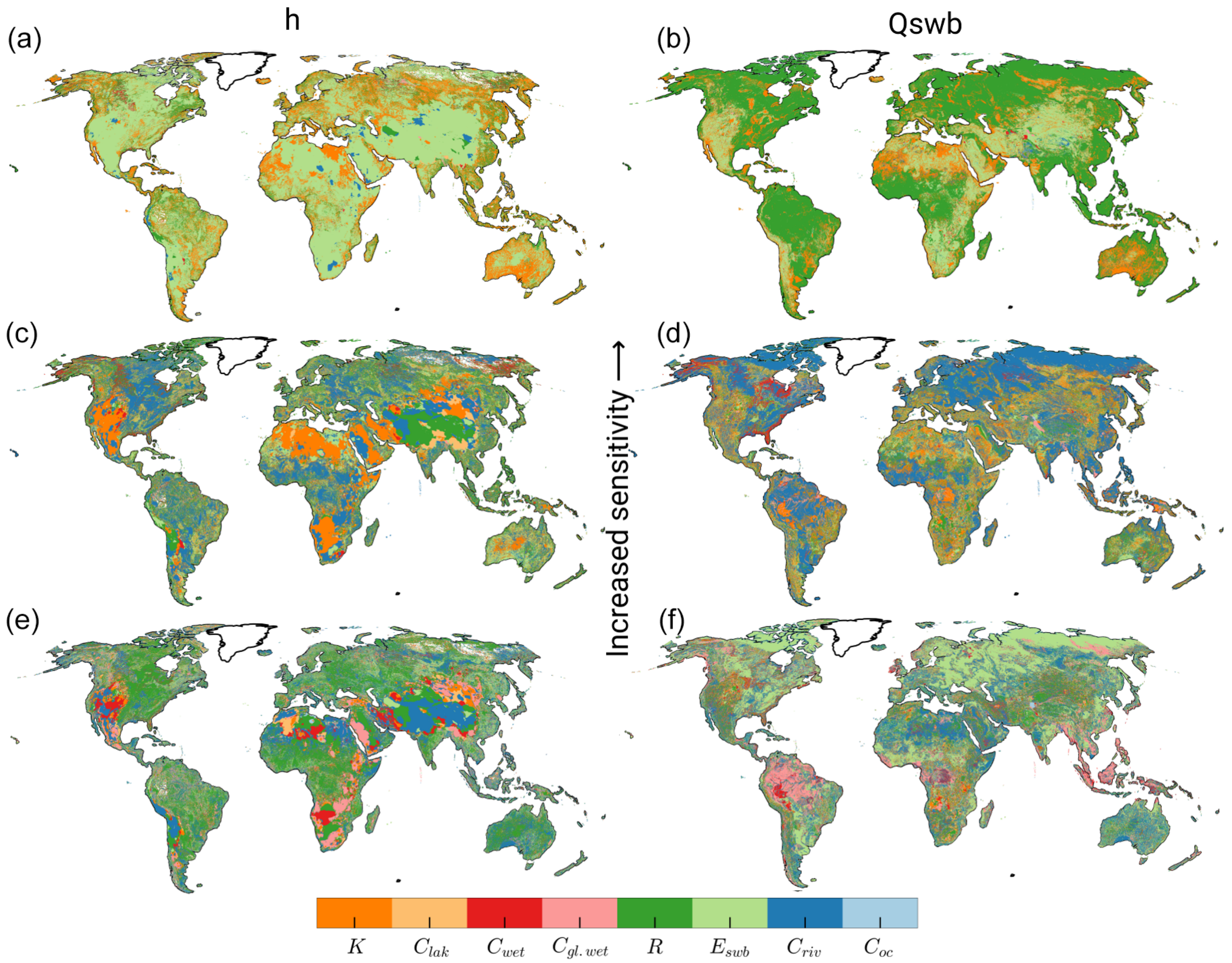

Figure 7. Ranking of μ^* of h **(a, c, e)** and Q_{swb} **(b, d, f)**. Panels **(a, b)** show the first rank, **(c, d)** the second, and **(e, f)** the third rank.

Figure 10b shows only cells with reliable results, based on their confidence intervals, resulting in 11.8 % of all grid cells for h and 13.3 % for Q_{swb}. GHRUs in high and very high elevations show low reliability concerning h results as expected (compare Fig. 4). Q_{swb} appears as more robust in these regions.

Figure 10a shows a similar picture to the two global maps (Figs. 7 and 9). All GHRUs show a linear correlation of sensitivity and degree of interaction. The GHRU with average elevation, average recharge, and high K (GHRU 1) shows a higher average response in Q_{swb} than h. h is most sensitive to C_{riv}, and less sensitive to the other parameters. Q_{swb} is clearly most sensitive to K and $C_{\mathrm{gl.wet}}$ and shows a high interaction in this GHRU. Lower-lying regions with average K and R (GHRU 2) show high sensitivity of h only to E_{swb} with a high interaction, while Q_{swb} is affected in decreasing order by $C_{\mathrm{gl.wet}}$, and K. Results for h sensitivity in GHRU 3, with very high elevations, average K, and low R, should be judged with caution because only a very low fraction is based on results with nonoverlapping CIs (Table 2). Compared to other GHRUs, GHRU 3 shows rather clustered sensitivities and parameter interactions. h is most sensitive to E_{swb} and R and Q_{swb} to C_{lak}, K, and C_{wet}. GHRU 4, which differs from GHRU 3 by its high but not very high land surface elevation, clearly shows E_{swb}, K, and R as the most dominant and interactive parameter for Q_{swb}, followed by C_{wet}. Similarly Q_{swb} is most sensitive to E_{swb} and K. In low-lying and rather flat regions with high groundwater recharge (GHRU 5), sensitivities of h are close to zero, except for K, possibly because changes in h are too small in flat regions (compare Fig. 4) due to small h gradients. Q_{swb} is most sensitive to E_{swb} and $C_{\mathrm{gl.wet}}$. GHRU 6 is relatively small and like GHRU 5 only occurs in the tropical zone (Fig. 3a). In this GHRU, which differs from GHRU 5 only by K being high instead of average, the dominant parameters of Q_{swb} are similar to other GHRUs where E_{swb} is

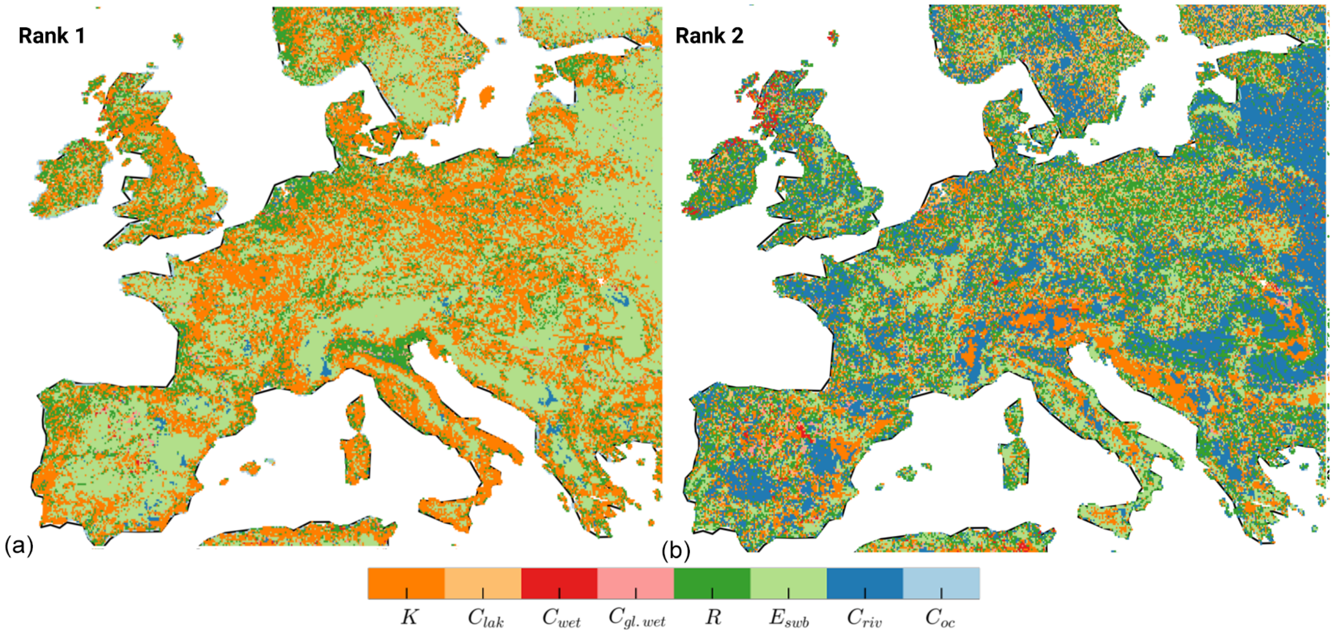

Figure 8. Enlarged view of Europe of Fig. 7. Ranking of μ^* of h (**a**: rank 1, **b**: rank 2).

clearly the most dominant followed by R and K. h shows a response to wetlands but again like in GHRU 5 a very low response to E_{swb}.

Taking into account only the reliable regions changes the perception in Fig. 10b. GHRU 1 shows rather similar sensitivities and parameter interactions as compared to other GHRUs. h is most sensitive to E_{swb}, and only somewhat less sensitive to C_{riv} and C_{wet}. Q_{swb} is clearly most sensitive to C_{riv} and shows a high interaction in this GHRU. GHRU 2 shows high sensitivity of h only to E_{swb} with a high interaction while Q_{swb} is equally affected by K, E_{swb}, and R. Results for h sensitivity in GHRU 3 are not very representative for the whole GHRU as only a very small fraction of cells shows reliable results (Table 2). Like in GHRU 2, Q_{swb} is equally affected by K, E_{swb} and R. GHRU 4 shows E_{swb} as clearly most dominant and interactive parameter for h, followed by K and C_{wet}. For GHRU 5, sensitivities of h could not be determined reliably, possibly because changes in h are too small in flat regions (compare Fig. 4) due to small h gradients. Q_{swb} is most sensitive to R (as rivers are gaining rivers that need to drain groundwater recharge) followed by K. In GHRU 6 the dominant parameters of Q_{swb} are the same as for GHRU 5 (except for E_{swb}) while h is most sensitive to C_{lak}.

4 Discussion

This study presents a novel spatially distributed sensitivity analysis for a high-resolution global gradient-based groundwater model encompassing 4.3 million grid cells. While these maps are challenging to interpret, they yield new ways of understanding model behavior based on spatial differences and help to prepare calibration efforts by identifying parameters that are most influential in specific regions. Furthermore, they guide the future development of the model and the intended coupling efforts of the groundwater model to the hydrological model. In particular, the sensitivity of Q_{swb} and the importance of E_{swb}, which are the two major coupling components, are of interest.

However, the large number of grid cells with either statistically zero sensitivity values (overlapping CI with zero) or unreliable results limit the relevance and applicability of the study results. For most of the statistically zero sensitivity values the CI is very large, and it is therefore very unlikely that the parameter is not influential. The study suggests that the highly nonlinear and conceptual approach to the surface water body conductance (in particular the sudden change of conductance between gaining and losing rivers) needs to be revised as it may affect the stability of transient model results. Additionally the results suggest that elevation of the water table of surface water bodies is a promising calibration parameter alongside with hydraulic conductivity.

The presented results need to be considered against the backdrop of the high h variability of the Monte Carlo experiments (Sect. 3.2.1). Some of these simulations cannot be considered as a valid result for a h distribution, an issue not faced with other simpler traditional bucket-like hydrological models. This is due to multiple model challenges: (1) the evaluated model approximates a differential equation and can show nonlinear behavior for different parameterizations, (2) the equations used for rivers present a nonlinear model component (switch between equations for gain-

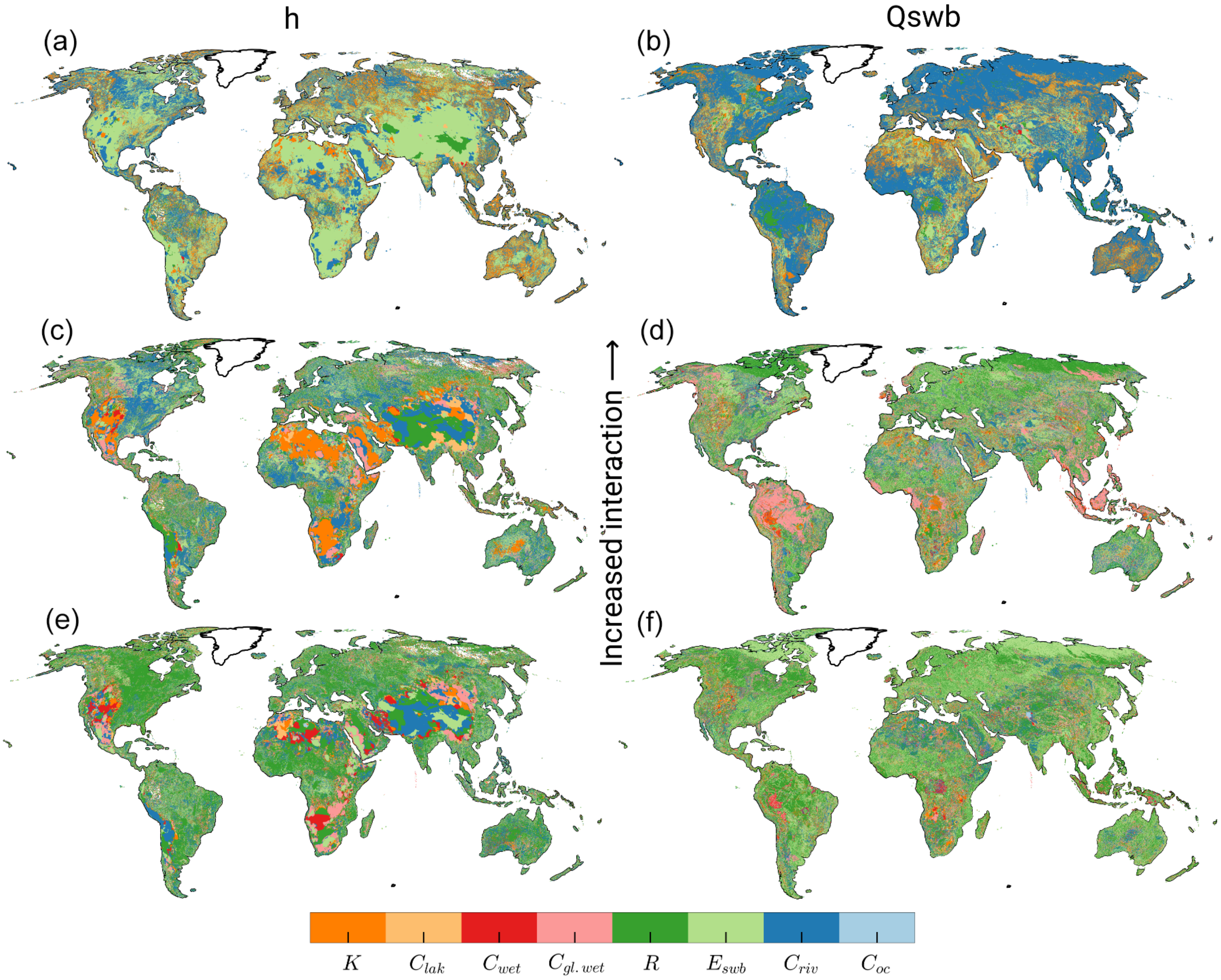

Figure 9. Ranking of σ^* of h **(a, c, e)** and Q_{swb} **(b, d, f)**. Panels **(a, b)** show the first rank, **(c, d)** the second, and **(e, f)** the third rank.

ing and losing conditions as well as relation to K and R), (3) the convergence criterion for the steady-state solution is solely based on a vector norm of residuals (metric of changes of the solution inside the conjugate gradient approach) and maximum h change between iterations and does not contain an automated check for a reasonable mass balance. On the other hand, it is challenging to include a validation mechanism in the presented analysis to alleviate these problems while maintaining a reasonable model runtime (as a stricter convergence criterion will most likely increase the number of necessary iterations) and/or number of necessary model runs. It is questionable whether results based on different convergence criteria can be compared. This would necessitate including the numeric stability in the sensitivity analysis as well.

However, the results help to answer the research questions at hand. While overlapping CIs blur the ranking of the parameters in some regions, they still provide evidence of what parameters the calibration should focus on and how the importance of parameters varies per region. The sensitivity of Q_{swb} to parameters, especially E_{swb}, will help to guide the future model development and coupling to the hydrological model. In general, the analysis helped to identify the elevation of surface water bodies as a focus for future research.

Around 30 % of all μ^* values had a confidence interval that was larger than 10 % of the μ^* value. This suggests that even more model runs are required and that large extents of the model experienced numerically unstable results as the spatial distribution of head variance and large confidence intervals overlap.

The selection of parameter ranges can influence the results of a sensitivity analysis significantly (Pianosi et al., 2016). Even parameters that are suspected of not being sensitive can show highly nonlinear behavior in certain parts of the parameter space that are only activated when one expands the ranges of the parameters. The presented ranges in this

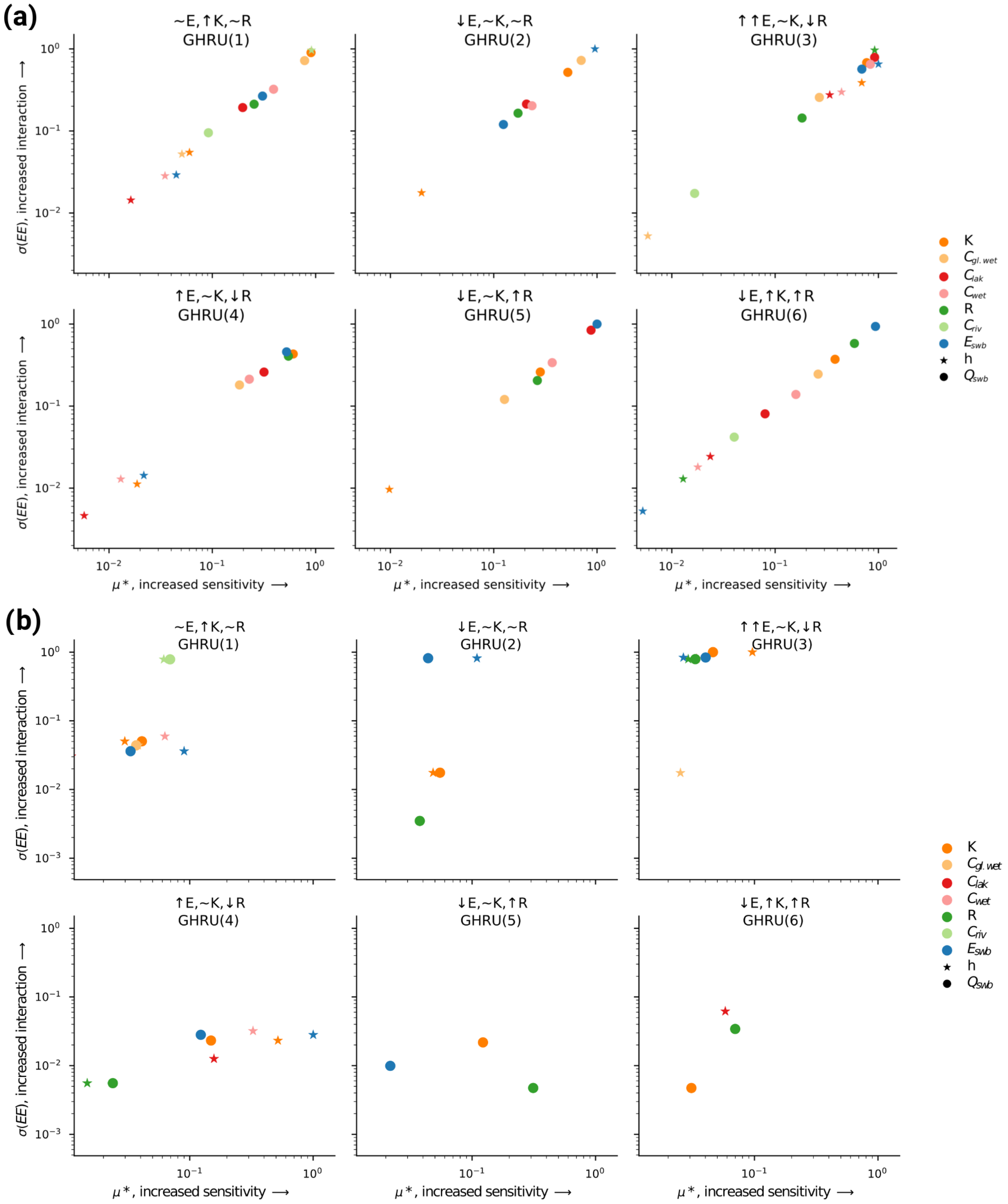

Figure 10. Normalized average sensitivity and parameter interaction per GHRU for h and Q_{swb} **(a)**. If a parameter is not present the mean sensitivity for that GHRU was close to zero (overlapping CI with zero). Does not include ocean parameter sensitivity. Mean characteristics, their symbols for each GHRU, and the reliability of the sensitivity measure (only μ^* not σ) are shown in Table 2. **(b)** Only reliable results (after removing overlapping CI).

study do not explore the full assumed uncertainty range. Specifically, the small range of E_{swb} is likely influencing the outcome of the parameter rankings. The range was chosen to allow a reasonable number of simulations to converge as the range of E_{swb} directly influences the convergence of the model. The presented results, however, do show that the model output is highly sensitive to changes in E_{swb} in most areas of the globe. The response in mountainous regions can be attributed to applying E_{swb} as a multiplier, which has a higher impact in regions where the initial water body elevation is high. On the other hand, this is accounting for the fact that the uncertainty of E_{swb} is largest in regions with highly variable topography per 5 arcmin grid cell.

The only previous sensitivity analysis of a global gradient-based groundwater model to our knowledge was done by de Graaf et al. (2015). Based on varying K, aquifer thickness, and R, the coefficient of variation of the steady-state hydraulic head was computed (de Graaf et al., 2015, Fig. 5). From that analysis it was determined that K has the highest impact and aquifer thickness the lowest. It is not clear how the coefficient of variation determined these outcomes. The relatively low impact of aquifer thickness was also observed by Reinecke et al. (2019). Therefore, this parameter was not included in this study. Both de Graaf et al. (2015) and this study show a high h variance in parts of Australia and the Sahara (de Graaf et al., 2015, Fig. 5), possibly due to the low initial R. Variations in the mountainous regions, on the other hand, are not reflected in de Graaf et al. (2015) as their analysis did not vary E_{swb}.

Besides the large h variance, which is likely the main cause for the low percentage of reliable cells, the confidence intervals of the sensitivity indices in this experiment suggest that additional simulations are necessary to determine more reliable results. Additionally, the small parameter ranges, required for stable model runs, influenced the overall outcome and might be a reason for cells with inconclusive results.

For cells with lakes and wetlands, E_{swb} dominates over the variations in conductance for h (Table 4), confirming the importance in determining the surface water body elevation. For Q_{swb}, on the other hand, R is most influential in these cells even though it does not affect the conductance equation for these surface water bodies. Apparently, available recharge is driving the interaction more than it influences changes in head. In regions with high recharge (GHRU 5) Q_{swb} was more robust to parameter changes than h. This is possibly due to the generally lower response in Q_{swb} to changes in E_{swb}, which can be explained by the constant flow for losing surface water bodies (including rivers) as soon as h drops below E_{swb}. Thus changes is E_{swb} do not affect Q_{swb} afterwards (as long as the surface water body remains in losing conditions). Both model outcomes show a high sensitivity to R while the interaction of R is only visible at the third rank, suggesting that if R changes other parameter changes do not influence the model response further.

Separating the complex global domain into a selected number of GHRUs enables a sensitivity analysis in accordance with computational constraints (e.g., maximum number of core hours). It alleviates the drawbacks of global-scale multipliers while keeping a reasonable number of total simulations. The presented decomposition based on three parameters E_{swb}, K, and R was guided by the high sensitivity of model output to these parameters. Other factors like lithology and surface water body characteristics should be investigated as additional characteristics for GHRUs.

5 Conclusions

For the first time, spatially distributed sensitivities of the global steady-state distribution of hydraulic head and flows between the groundwater and the surface water bodies were calculated and presented. We found the Morris sensitivity analysis method can yield insights for computationally challenging (concerning computation time and numerical difficulties) models with reasonable computational demand. This study applied a novel approach for domain decomposition into GHRUs. Applying parameter multipliers simultaneously to all grid cells within each of the six GHRUs allowed a more meaningful sensitivity calculation than would be possible if the parameters would have varied simultaneously in all grid cells, while maintaining a feasible number of simulations.

Based on only a small fraction of grid cells for which parameters could be ranked reliably according to their importance for simulated model output, steady-state hydraulic heads (h) were found to be comparably affected by hydraulic conductivity (K), groundwater recharge (R), and the elevation of the water table of surface water bodies (E_{swb}). Rankings for individual grid cells vary, but globally none of the three dominates with respect to h. The simulated flows between groundwater and surface water bodies (Q_{swb}) are clearly most sensitive to R. This is due to the model parameterization of river conductance that is computed as a function of R, assuming that under steady-state conditions, groundwater discharge to rivers should tend to increase with increasing R (Eq. 4). The results indicate that changes in R between time steps for a fully coupled transient model could pose a challenge to the model convergence and that the equations might need to be reconsidered for a fully coupled model. In general the uncertainty due to the parameterization of groundwater–surface-water exchange flows (E_{swb} and $C_{\mathrm{riv,gl.wet,wet,lak}}$) needs to be further investigated as they have a high impact on h distribution and Q_{swb}.

In high mountainous regions (Rocky Mountains, Andes, Ethiopian Highlands, Arabian Peninsula, Himalaya) and regions with low recharge (Sahara, southern Africa) the computed h showed an unreasonably high variance due to the numerical instability of the simulations in these areas. In the case of high elevations and thus large variations in E_{swb} or in the case of low groundwater recharge, it is not possible to solve steady-state groundwater flow equations with arbitrary parameter combinations and a constant convergence parameter. Q_{swb} was found to somewhat be more robust than h in these regions. These results suggest that the parameterization of E_{swb} needs to be reconsidered and is a likely parameter for future calibration. In general more robust global sensitivity methods are required that allow the exclusion of certain simulations from the analysis.

The lack of reliable data at the global scale, in particular hydraulic conductivity data with high horizontal and vertical resolution, hinders the development of global groundwater models. A simple sensitivity analysis on the impact of small changes to an existing global hydraulic conductivity dataset (GLHYMPS 1.0 Gleeson et al., 2014 to 2.0 Huscroft et al., 2018) showed that knowledge about the distribution of K is pivotal for the simulation of h, as even slight changes in K may change model results by up to 100 m.

The presented study results refer to the uncoupled steady-state groundwater model G^{3}M. As G^{3}M is currently being integrated into the global hydrological model WaterGAP, future work will extend this sensitivity analysis to fully coupled transient simulations.

Data availability. The data for this study can be provided upon reasonable request. They are not publicly available due to the very large outputs of all 2000 model executions that exceed multiple hundred gigabytes. For the model code see https://doi.org/10.5194/gmd-12-2401-2019 (Reinecke et al., 2019). The sensitivity analysis framework is available at https://doi.org/10.21105/joss.00097 (Herman and Usher, 2017).

Appendix A

Confidence intervals are determined based on 1000 bootstrap resamples following Archer et al. (1997) for all simulation outputs. Bootstrapping is an established statistical method that relies on random sampling with replacement using the original data. This sampling from a set of independent, identically distributed data is equivalent to sampling from the empirical distribution function of the data, allowing confidence intervals to be determined (Archer et al., 1997).

The derived metrics μ^* and σ_i are both measures of intensity (higher values are more sensitive/interactive) and do not represent absolute values of sensitivity. Both can only be interpreted meaningfully in comparison with values derived for other parameters. To achieve that, μ^* and σ_i should be presented in so-called *ranks*. Values for all parameters are sorted from highest to lowest, and the parameter with the highest value is selected as the most influential parameter with the highest rank. The parameter with the second highest value is the second most influential parameter and so on.

Figure A1 shows the conceptual issues that are entailed with this ranking approach. The absolute mean (μ^*) of all EEs of parameter 1 (P1) might be bigger than μ^* of P2, but as their CIs are overlapping a clear ranking is not possible. On the other hand it is evident that P1 and P2 are clearly more sensitive than P3. An overlapping suggests that even if the μ^* values are different a ranking should be considered with care. Two parameters could be equally important or in some regions inside one GRHU their importance could be inverse to what the μ^* values suggest. But even if they overlap, the μ^* provides a valuable measure of the overall importance of the parameters, also in comparison with much less important parameters.

Additionally, not only the overlapping should be considered but also the size of the CI in comparison to the μ^*. It is a useful indicator of whether the sampling of the parameter space was too small and more simulations are required to gain a clearer picture. 15 % is an arbitrary value that we considered an appropriate boundary. Other studies used 10 % (Herman et al., 2013a) or 3.5 % (Vanrolleghem et al., 2015).

Figure A2 shows regions where CIs were smaller than 15 % of the calculated μ^* of the first rank and regions where more simulations, or a more sophisticated approach to ensure numerical stability, are likely required.

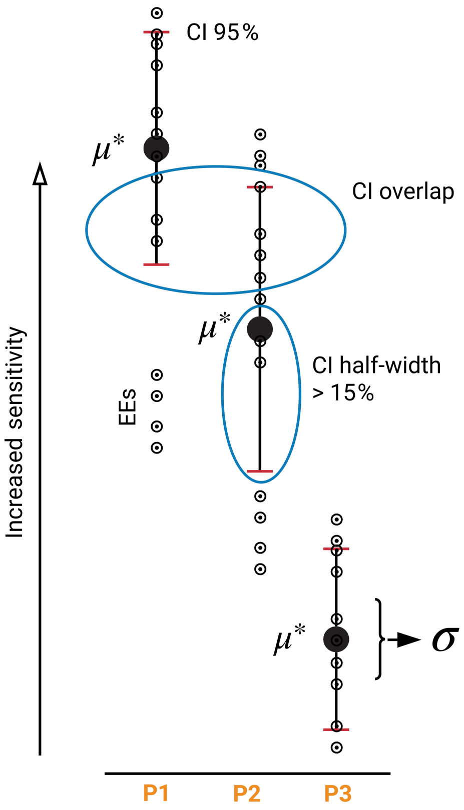

Figure A1. Illustration of derivation of presented metrics. Blue circles show the two criteria used to judge the quality of the results. μ^* is calculated based on the EEs (circles); however, the CI is calculated based on bootstrap resamples of the simulation outputs.

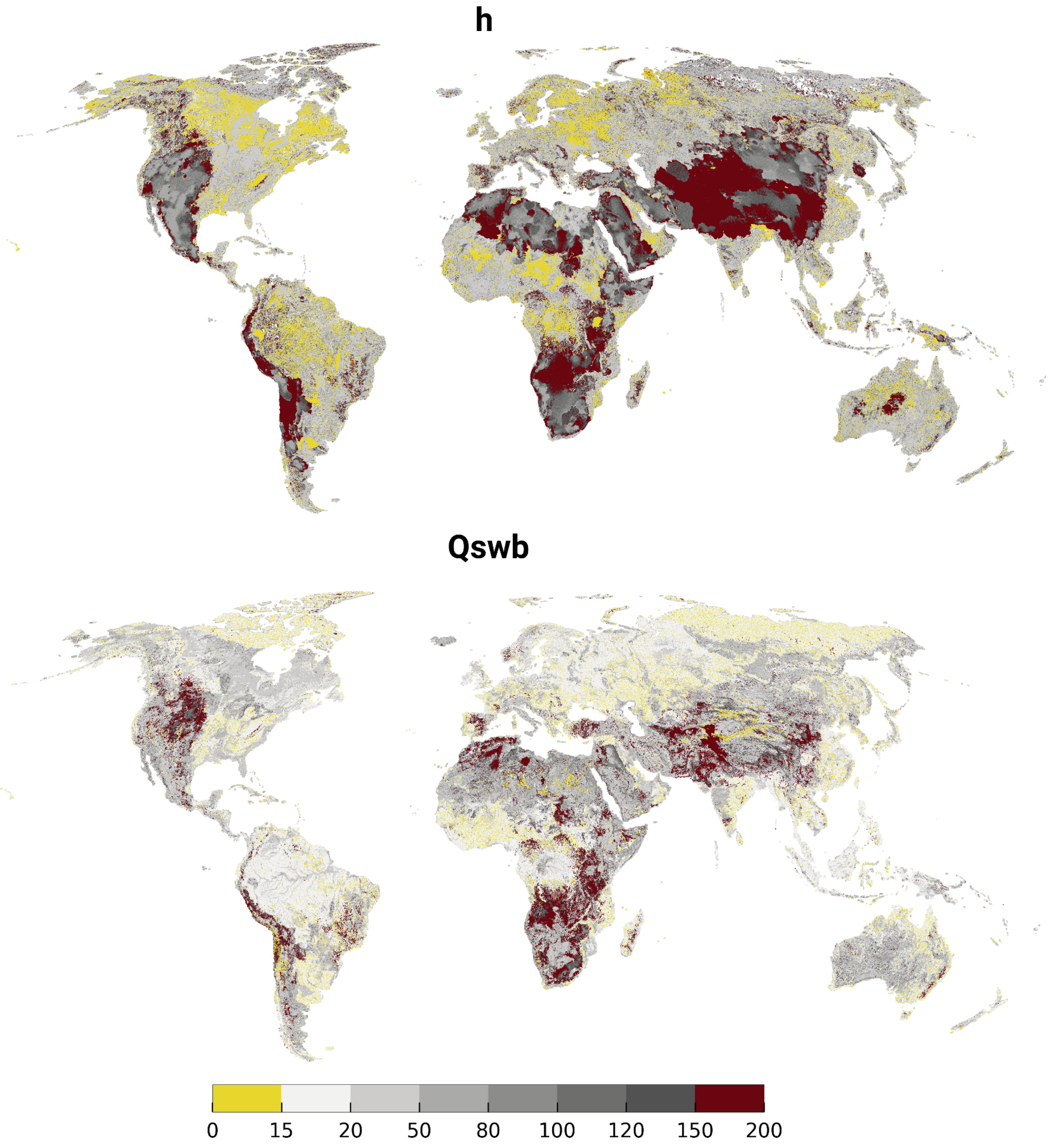

Figure A2. Confidence interval (95) in relation to the μ^* for rank 1 of h and Q_{swb}. Yellow regions indicate a sufficient sampling size.

Author contributions. RR led the conceptualization, formal analysis, methodology, software, visualization, and writing of the original draft. JH, LF, SM, and TT supported review and editing as well as the development of the methodology. AW supported visualization and the writing of original draft of Sect. 3.1. PD supervised the work of RR and made suggestions regarding the analysis, structure, and wording of the text and design of tables and figures.

Competing interests. The authors declare that they have no conflict of interest.

Financial support. This research has been supported by the Friedrich-Ebert Foundation PhD fellowship.

Review statement. This paper was edited by Monica Riva and reviewed by Francesca Pianosi and one anonymous referee.

References

Allen, P. M., Arnold, J. C., and Byars, B. W.: Downstream channel geometry for use in planning-level models, J. Am. Water Resour. Assoc., 30, 663–671, https://doi.org/10.1111/j.1752-1688.1994.tb03321.x, 1994.

Archer, G., Saltelli, A., and Sobol, I.: Sensitivity measures, ANOVA-like techniques and the use of bootstrap, J. Stat. Comput. Simul., 58, 99–120, 1997.

Börker, J., Hartmann, J., Amann, T., and Romero-Mujalli, G.: Global Unconsolidated Sediments Map Database v1.0 (shapefile and gridded to 0.5° spatial resolution), https://doi.org/10.1594/PANGAEA.884822, supplement to: Börker, J., et al. (accepted): Terrestrial Sediments of the Earth: Development of a Global Unconsolidated Sediments Map Database (GUM), Geochem. Geophy. Geosy., https://doi.org/10.1002/2017GC007273, 2018.

Branger, F., Giraudet, L.-G., Guivarch, C., and Quirion, P.: Global sensitivity analysis of an energy–economy model of the residential building sector, Environ. Model. Softw., 70, 45–54, https://doi.org/10.1016/j.envsoft.2015.03.021, 2015.

Campolongo, F., Cariboni, J., and Saltelli, A.: An effective screening design for sensitivity analysis of large models, Environ. Model. Softw., 22, 1509–1518, https://doi.org/10.1016/j.envsoft.2006.10.004, 2007.

Chaney, N., Herman, J., Reed, P., and Wood, E.: Flood and drought hydrologic monitoring: the role of model parameter uncertainty, Hydrol. Earth Syst. Sci., 19, 3239–3251, https://doi.org/10.5194/hess-19-3239-2015, 2015.

de Graaf, I. E., Sutanudjaja, E., Van Beek, L., and Bierkens, M.: A high-resolution global-scale groundwater model, Hydrol. Earth Syst. Sci., 19, 823–837, https://doi.org/10.5194/hess-19-823-2015, 2015.

de Graaf, I. E., van Beek, R. L., Gleeson, T., Moosdorf, N., Schmitz, O., Sutanudjaja, E. H., and Bierkens, M. F.: A global-scale two-layer transient groundwater model: Development and application to groundwater depletion, Adv. Water Resour., 102, 53–67, https://doi.org/10.1016/j.advwatres.2017.01.011, 2017.

Dell'Oca, A., Riva, M., and Guadagnini, A.: Moment-based metrics for global sensitivity analysis of hydrological systems, Hydrol. Earth Syst. Sci., 21, 6219–6234, https://doi.org/10.5194/hess-21-6219-2017, 2017.

Döll, P., Kaspar, F., and Lehner, B.: A global hydrological model for deriving water availability indicators: model tuning and validation, J. Hydrol., 270, 105–134, https://doi.org/10.1016/S0022-1694(02)00283-4, 2003.

Döll, P., Hoffmann-Dobrev, H., Portmann, F. T., Siebert, S., Eicker, A., Rodell, M., Strassberg, G., and Scanlon, B.: Impact of water withdrawals from groundwater and surface water on continental water storage variations, J. Geodynam., 59, 143–156, https://doi.org/10.1016/j.jog.2011.05.001, 2012.

Döll, P., Müller Schmied, H., Schuh, C., Portmann, F. T., and Eicker, A.: Global-scale assessment of groundwater depletion and related groundwater abstractions: Combining hydrological modeling with information from well observations and GRACE satellites, Water Resour. Res., 50, 5698–5720, https://doi.org/10.1002/2014WR015595, 2014.

Döll, P., Fiedler, K., and Zhang, J.: Global-scale analysis of river flow alterations due to water withdrawals and reservoirs, Hydrol. Earth Syst. Sci., 13, 2413–2432, https://doi.org/10.5194/hess-13-2413-2009, 2009.

Fan, Y., Li, H., and Miguez-Macho, G.: Global patterns of groundwater table depth, Science, 339, 940–943, https://doi.org/10.1126/science.1229881, 2013.

Ghasemizade, M., Baroni, G., Abbaspour, K., and Schirmer, M.: Combined analysis of time-varying sensitivity and identifiability indices to diagnose the response of a complex environmental model, Environ. Model. Softw., 88, 22–34, https://doi.org/10.1016/j.envsoft.2016.10.011, 2017.

Gleeson, T., Smith, L., Moosdorf, N., Hartmann, J., Dürr, H. H., Manning, A. H., van Beek, L. P. H., and Jellinek, A. M.: Mapping permeability over the surface of the Earth, Geophys. Res. Lett., 38, L02401, https://doi.org/10.1029/2010GL045565, 2011.

Gleeson, T., Moosdorf, N., Hartmann, J., and Van Beek, L.: A glimpse beneath earth's surface: GLobal HYdrogeology MaPS (GLHYMPS) of permeability and porosity, Geophys. Res. Lett., 41, 3891–3898, https://doi.org/10.1002/2014GL059856, 2014.

Gruber, S.: Derivation and analysis of a high-resolution estimate of global permafrost zonation, The Cryosphere, 6, 221–233, https://doi.org/10.5194/tc-6-221-2012, 2012.

Hartmann, A., Gleeson, T., Rosolem, R., Pianosi, F., Wada, Y., and Wagener, T.: A large-scale simulation model to assess karstic groundwater recharge over Europe and the Mediterranean, Geosci. Model Dev., 8, 1729–1746, https://doi.org/10.5194/gmd-8-1729-2015, 2015.

Hartmann, J. and Moosdorf, N.: Global Lithological Map Database v1.0 (gridded to 0.5° spatial resolution), https://doi.org/10.1594/PANGAEA.788537, 2012.

Hengl, T., Mendes de Jesus, J., Heuvelink, G. B. M., Ruiperez Gonzalez, M., Kilibarda, M., Blagotić, A., Shangguan, W., Wright, M. N., Geng, X., Bauer-Marschallinger, B., Guevara, M. A., Vargas, R., MacMillan, R. A., Batjes, N. H., Leenaars, J. G. B., Ribeiro, E., Wheeler, I., Mantel, S., and Kempen, B.: SoilGrids250m: Global gridded soil information based on machine learning, PLOS ONE, 12, 1–40, https://doi.org/10.1371/journal.pone.0169748, 2017.

Herman, J. D. and Usher, W.: SALib: an open-source Python library for sensitivity analysis, J. Open Source Softw., 2, 97, https://doi.org/10.21105/joss.00097, 2017.

Herman, J. D., Kollat, J., Reed, P., and Wagener, T.: Method of Morris effectively reduces the computational demands of global sensitivity analysis for distributed watershed models, Hydrol. Earth Syst. Sci., 17, 2893–2903, https://doi.org/10.5194/hess-17-2893-2013, 2013a.

Herman, J. D., Reed, P. M., and Wagener, T.: Time-varying sensitivity analysis clarifies the effects of watershed model formulation on model behavior, Water Resour. Res., 49, 1400–1414, https://doi.org/10.1002/wrcr.20124, 2013b.

Huscroft, J., Gleeson, T., Hartmann, J., and Börker, J.: Compiling and mapping global permeability of the unconsolidated and consolidated Earth: GLobal HYdrogeology MaPS 2.0 (GLHYMPS 2.0), Geophys. Res. Lett., 45, 1897–1904, https://doi.org/10.1002/2017GL075860, 2018.

Janetti, E. B., Guadagnini, L., Riva, M., and Guadagnini, A.: Global sensitivity analyses of multiple conceptual models with uncertain parameters driving groundwater flow in a regional-scale sedimentary aquifer, J. Hydrol., 574, 544–556, https://doi.org/10.1016/j.jhydrol.2019.04.035, 2019.

Keune, J., Gasper, F., Goergen, K., Hense, A., Shrestha, P., Sulis, M., and Kollet, S.: Studying the influence of groundwater representations on land surface-atmosphere feedbacks during the European heat wave in 2003, J. Geophys. Res.-Atmos., 121, 13301–13325, https://doi.org/10.1002/2016JD025426, 2016.

Koirala, S., Kim, H., Hirabayashi, Y., Kanae, S., and Oki, T.: Sensitivity of global hydrological simulations to groundwater capillary flux parameterizations, Water Resour. Res., 55, 402–425, https://doi.org/10.1029/2018WR023434, 2018.

Konikow, L. F.: Contribution of global groundwater depletion since 1900 to sea-level rise, Geophys. Res. Lett., 38, L17401, https://doi.org/10.1029/2011GL048604, 2011.

Lloyd, S.: Least squares quantization in PCM, IEEE T. Inform. Theory, 28, 129–137, https://doi.org/10.1109/TIT.1982.1056489, 1982.

Maxwell, R. M., Condon, L. E., and Kollet, S. J.: A high-resolution simulation of groundwater and surface water over most of the continental US with the integrated hydrologic model ParFlow v3, Geosci. Model Dev., 8, 923–937, https://doi.org/10.5194/gmd-8-923-2015, 2015.

Miguez-Macho, G., Fan, Y., Weaver, C. P., Walko, R., and Robock, A.: Incorporating water table dynamics in climate modeling: 2. Formulation, validation, and soil moisture simulation, J. Geophys. Res.-Atmos., 112, D13108, https://doi.org/10.1029/2006JD008112, 2007.

Morel-Seytoux, H. J., Miller, C. D., Miracapillo, C., and Mehl, S.: River seepage conductance in large-scale regional studies, Groundwater, 55, 399–407, https://doi.org/10.1111/gwat.12491, 2017.

Morris, M. D.: Factorial sampling plans for preliminary computational experiments, Technometrics, 33, 161–174, https://doi.org/10.1080/00401706.1991.10484804, 1991.

Müller Schmied, H., Eisner, S., Franz, D., Wattenbach, M., Portmann, F. T., Flörke, M., and Döll, P.: Sensitivity of simulated global-scale freshwater fluxes and storages to input data, hydrological model structure, human water use and calibration, Hydrol. Earth Syst. Sci., 18, 3511–3538, https://doi.org/10.5194/hess-18-3511-2014, 2014.

Müller Schmied, H., Adam, L., Eisner, S., Fink, G., Flörke, M., Kim, H., Oki, T., Portmann, F. T., Reinecke, R., Riedel, C., Song, Q., Zhang, J., and Döll, P.: Variations of global and continental water balance components as impacted by climate forcing uncertainty and human water use, Hydrol. Earth Syst. Sci., 20, 2877–2898, https://doi.org/10.5194/hess-20-2877-2016, 2016.

Pianosi, F., Beven, K., Freer, J., Hall, J. W., Rougier, J., Stephenson, D. B., and Wagener, T.: Sensitivity analysis of environmental models: A systematic review with practical workflow, Environ. Model. Softw., 79, 214–232, https://doi.org/10.1016/j.envsoft.2016.02.008, 2016.

Razavi, S. and Gupta, H. V.: What do we mean by sensitivity analysis? The need for comprehensive characterization of "global" sensitivity in Earth and Environmental systems models, Water Resour. Res., 51, 3070–3092, https://doi.org/10.1002/2014WR016527, 2015.

Reinecke, R.: G^{3}M-f a global gradient-based groundwater modelling framework, J. Open Sour. Soft., 3, 548, https://doi.org/10.21105/joss.00548, 2018.

Reinecke, R., Foglia, L., Mehl, S., Trautmann, T., Cáceres, D., and Döll, P.: Challenges in developing a global gradient-based groundwater model (G^{3}M v1.0) for the integration into a global hydrological model, Geosci. Model Dev., 12, 2401–2418, https://doi.org/10.5194/gmd-12-2401-2019, 2019.

Ruano, M., Ribes, J., Seco, A., and Ferrer, J.: An improved sampling strategy based on trajectory design for application of the Morris method to systems with many input factors, Environ. Model. Softw., 37, 103–109, https://doi.org/10.1016/j.envsoft.2012.03.008, 2012.

Saltelli, A., Ratto, M., Andres, T., Campolongo, F., Cariboni, J., Gatelli, D., Saisana, M., and Tarantola, S.: Global sensitivity analysis: the primer, John Wiley & Sons, New York, USA, 2008.

Scanlon, B. R., Faunt, C. C., Longuevergne, L., Reedy, R. C., Alley, W. M., McGuire, V. L., and McMahon, P. B.: Groundwater depletion and sustainability of irrigation in the US High Plains and Central Valley, P. Natl. Acad. Sci. USA, 109, 9320–9325, https://doi.org/10.1073/pnas.1200311109, 2012.

Schumacher, M., Eicker, A., Kusche, J., Schmied, H. M., and Döll, P.: Covariance Analysis and Sensitivity Studies for GRACE Assimilation into WGHM, in: IAG 150 Years, International Association of Geodesy Symposia, Vol. 143, edited by: Rizos, C. and Willis, P., Springer, Cham, 2015.

Sobol, I. M.: Sensitivity estimates for nonlinear mathematical models, Math. Model. Comput. Exp., 1, 407–414, 1993.

Song, X., Zhang, J., Zhan, C., Xuan, Y., Ye, M., and Xu, C.: Global sensitivity analysis in hydrological modeling: Review of concepts, methods, theoretical framework, and applications, J. Hydrol., 523, 739–757, https://doi.org/10.1016/j.jhydrol.2015.02.013, 2015.

Stonestrom, D. A.: Ground-water recharge in the arid and semiarid southwestern United States, USGS, 1703, available at: http://pubs.usgs.gov/pp/pp1703 (last access: 12 November 2019), 2007.

Taylor, R. G., Scanlon, B., Döll, P., Rodell, M., Van Beek, R., Wada, Y., Longuevergne, L., Leblanc, M., Famiglietti, J. S., Edmunds, M., Konikow, L., Green, T., Chen, J., Taniguchi, M., Bierkens, M. F. P., Macdonald, A., Fan, Y., Maxwell, R., Yechieli, Y., and Treidel, H.: Ground water and climate change, Nat. Clim. Change, 3, 322–329, https://doi.org/10.1038/nclimate1744, 2013.

Vanrolleghem, P. A., Mannina, G., Cosenza, A., and Neumann, M. B.: Global sensitivity analysis for urban water quality modelling: Terminology, convergence and comparison of different methods, J. Hydrol., 522, 339–352, https://doi.org/10.1016/j.jhydrol.2014.12.056, 2015.

Verzano, K., Bärlund, I., Flörke, M., Lehner, B., Kynast, E., Voß, F., and Alcamo, J.: Modeling variable river flow velocity on continental scale: Current situation and climate change impacts in Europe, J. Hydrol., 424, 238–251, https://doi.org/10.1016/j.jhydrol.2012.01.005, 2012.

Wada, Y.: Modeling Groundwater Depletion at Regional and Global Scales: Present State and Future Prospects, Surv. Geophys., 37, 419–451, https://doi.org/10.1007/s10712-015-9347-x, 2016.

Wada, Y., Beek, L. P. H., and Bierkens, M. F. P.: Nonsustainable groundwater sustaining irrigation: A global assessment, Water Resour. Res., 48, W00L06, https://doi.org/10.1029/2011WR010562, 2012.

Wada, Y., Wisser, D., and Bierkens, M. F. P.: Global modeling of withdrawal, allocation and consumptive use of surface water and groundwater resources, Earth Syst. Dynam., 5, 15–40, https://doi.org/10.5194/esd-5-15-2014, 2014.

Chapter 5

Importance of spatial resolution in global groundwater modeling

Research paper\

Importance of spatial resolution in global groundwater modeling

Robert Reinecke
Corresponding author: Institute of Physical Geography, Goethe University Frankfurt, Altenhöferallee 1, 60438 Frankfurt, Germany and International Centre for Water Resources and Global Change (UNESCO), Federal Institute of Hydrology, 56002 Koblenz, Germany; reinecke@em.uni-frankfurt.de

Alexander Wachholz
Institute of Physical Geography, Goethe University Frankfurt and Department of Aquatic Ecosystem Analysis, Helmholtz Centre for Environmental Research, Magdeburg, Germany; alexander.wachholz@ufz.de

Steffen Mehl
Department of Civil Engineering, California State University, Chico, USA; smehl@csuchico.edu

Laura Foglia
Department of Land, Air and Water Resources, University of California, Davis, USA; lfoglia@ucdavis.edu

Christoph Niemann
Institute of Physical Geography, Goethe University Frankfurt, Germany; c.niemann@em.uni-frankfurt.de

Petra Döll
Institute of Physical Geography, Goethe University Frankfurt and Senckenberg Leibniz Biodiversity and Climate Research Centre (SBiK-F), Frankfurt, Germany; p.doell@em.uni-frankfurt.de

Conflict of interest: None.
Keywords: Global groundwater, global hydrology, spatial resolution, New Zealand, Canterbury

Article Impact Statement: Global groundwater models are a new endeavor for hydrologists that face multiple challenges.

Abstract

Global-scale gradient-based groundwater models are a new endeavor for hydrologists who wish to improve global hydrological models (GHMs). In particular, the integration of such groundwater models into GHMs improves the simulation of water flows between surface water and groundwater and of capillary rise and thus evapotranspiration. Currently, these models are not able to simulate water table depth adequately over the entire globe. Unsatisfactory model performance compared to well observations suggests that a higher spatial resolution is required to better represent the high spatial variability of land surface and groundwater elevations. In this study, we use New Zealand as a testbed and analyze the impacts of spatial resolution on the results of global groundwater models. Steady-state hydraulic heads simulated by two versions of the global groundwater model G^{3}M, at spatial resolutions of 5 arc-minutes (9 km) and 30 arc-seconds (900 m), are compared with observations from the Canterbury region. The output of three other groundwater models with different spatial resolutions is analyzed as well. Considering the spatial distribution of residuals, general patterns of unsatisfactory model performance remain at the higher resolutions, suggesting that an increase in model resolution alone does not fix problems such as the systematic overestimation of hydraulic head. We conclude that (1) a new understanding of how low-resolution global groundwater models can be evaluated is required, and (2) merely increasing the spatial resolution of global-scale groundwater models will not improve the simulation of the global freshwater system.

Introduction

Groundwater is the largest source of available freshwater (Gleeson et al., 2016). The assessment of global groundwater resources has been the subject of multiple studies recently, including impacts of groundwater abstractions (Wada et al., 2010) and climate change (Portmann et al., 2013; Cuthbert et al., 2019). Furthermore, global hydrological models (GHMs) started to replace their bucket-like linear groundwater storage models with (hydraulic) head gradient-based models to better represent the interaction between surface water and groundwater as well as lateral and vertical flows, including capillary rise (de Graaf et al., 2015, 2017, 2019; Reinecke et al., 2019a,b). Compared to established regional models, global groundwater models are a new endeavor for groundwater hydrologists that is mostly unexplored. These models use a rather coarse spatial resolution (1) due to a lack of available global data and (2) to handle the computational demand that arises from fully coupling groundwater models to surface hydrology models. In typical GHMs, each cell has a river, in addition to other possible surface water bodies, that can cause changes in the flows to and from the groundwater. These changes represent an enormous challenge for the numerical solution while sustaining reasonable run times that allow for sensitivity analysis and data assimilation. Currently, the available global groundwater models have grid cell sizes that range from 30″ (arc-seconds, $\sim$ 900 m by 900 m at the equator) to 5′ (arc-minutes, $\sim$ 9 km by 9 km at the equator) (Reinecke et al., 2019a). In comparison, the spatial resolution of traditional groundwater models ranges from centimeters for transport models, e.g., García-Gil et al. (2016), over 1 m to 50 m for local models, e.g., Limberg et al. (2010), up to 1 mile for extensive regional models like the Central Valley Model CVHM (Faunt et al., 2016).

Unfortunately, global models show unsatisfying performance for simulated head compared with well observations, often by more than 100 m (Reinecke et al., 2019a; de Graaf et al., 2017). The reasons for these significant over- and underestimates are likely the spatial resolution of the model, improper comparisons to observations, lack of high-resolution data, and assumptions of surface water body location and extent. Higher-resolution models (e.g., 30″), like the global steady-state model of Fan et al. (2013), seem to exceed the performance (much smaller difference to global observations) of the coarse-scale (5′) models (Reinecke et al., 2019a), leading to the assumption that an increase in spatial resolution will improve model performance. In general, the hydrological community has argued that a higher spatial resolution in all earth system models is necessary to represent essential processes better (Wood et al., 2011). The topic of scales in hydrological systems has also been extensively discussed for fractal scaling of river networks, topography and spatial scaling of conductivity (Mark and Aronson, 1984; Rosso et al., 1991; Wörman et al., 2007; Gupta et al., 2007).

One of the primary purposes for integrating gradient-based groundwater models into GHMs is to improve the simulation of the flows between surface water bodies and groundwater. In particular, the dynamic simulation of flows between surface water bodies and groundwater cannot be achieved with the bucket-like linear groundwater reservoir models in current GHMs (Reinecke et al., 2019a). To compute the flow between a surface water body and groundwater, the hydraulic head of the water body is needed. Determination of this head as the elevation of the water surface within a computational grid cell depends on the used Digital Elevation Model (DEM), e.g., HydroSHEDS

(Lehner et al., 2008) and the simulated temporal storage changes in the surface water bodies. For example, if the GHM only contains one river per computation cell (typical for global models), the river elevation accuracy is limited by the spatial resolution of the GHM and the aggregation method used to determine the elevation. GHMs currently use spatial resolutions varying from 2° ($\sim$ 200 km) up to $5'$ ($\sim$ 9 km), whereas most GHMs use a resolution of 0.5° (Sood and Smakhtin, 2015). Contrarily global DEMs are available up to a 12 m resolution (DLR, 2016). Krakauer et al. (2014) suggested a spatial resolution of $6'$ to simulate groundwater flow at continental scales. The two gradient-based groundwater models, coupled to GHMs, use a spatial resolution of $5'$ and $6'$, respectively (Reinecke et al., 2019a; de Graaf et al., 2017).

Due to the coarse spatial resolution used in global-scale groundwater models, one simulated head value represents a large volume of the groundwater system, making a comparison to observations extremely challenging. For example, it is unlikely that wells are equally distributed inside these large cells. So how can one determine an average observed head for a cell from these wells that is an appropriately aggregated representation of reality? An aggregation to an arithmetic average measurement might misrepresent the reality due to not only a nonuniform distribution inside the cell but even more when the wells also differ in their hydrogeologic characteristics (e.g., different aquifer layer). This may result in the undesirable phenomenon that sparsely available observations falsely indicate a better fit than a dense measurement network (Beven, 2000).

Related to this issue is that gradient-based models compute heads, but observations are often available as water table depths (WTDs). Thus, to compare these two values, either (1) the simulated head has to be subtracted from the average land surface elevation (based on an available DEM) for the computation cell or (2) the WTD has to be converted to a hydraulic head. Calculation of the head is achieved by either using a known land surface elevation of the WTD measurement location (which is often not available), a high-resolution DEM, or the land surface elevation assigned to the grid cell of the groundwater model. Either way, both methods include the uncertainty of the DEM combined with the error of averaging observations.

In this paper, we reevaluate the pursuit of higher spatial resolution for global models in the context of global groundwater models. New Zealand (NZ) is used in this study as a small-world representation with a well-defined ocean boundary condition and shorter runtimes compared to the global model. We present uncertainties in well observations and surface elevation from DEMs in the context of coarse model resolution. Results show the sensitivity of a global groundwater model (G^{3}M) (Reinecke et al., 2019a) to changes in only spatial resolution from $5'$ to $30''$ and model outputs compared to available well observations. We focus on the Canterbury region due to the large density of available measurements. By comparing the simulated steady-state WTD of five different global-scale models in this region, we show that model performance is still not acceptable to reliably compute surface water to groundwater interactions on the global-scale, and that our community needs to be clear about the limitations and uncertainties of global groundwater models. Based on previous sensitivity analysis results (Reinecke et al., 2019b), we investigate from where uncertainties in the current model approach originate. Finally, we discuss how the results of macro-scale models should be presented and how the current shortcomings can be addressed.

Methods

The global groundwater model

G^{3}M (Reinecke et al., 2019a) is a global gradient-based groundwater model intended to be coupled with the GHM WaterGAP (Döll et al., 2014; Müller Schmied et al., 2014) and is based on the Open Source groundwater modeling framework G^{3}M-f (available on `globalgroundwatermodel.org`)(Reinecke, 2018). G^{3}M implements the same saturated groundwater flow equations and processes as many established modeling codes, such as MODFLOW (Harbaugh, 2005) (for a detailed discussion see Reinecke et al. (2019a)). It computes lateral and vertical groundwater flows as well as exchanges with surface-water bodies for all land areas of the globe (except Antarctica) with a resolution of $5'$ (ca. 9 km by 9 km at the equator) with two vertical layers with a thickness of each 100 m. The evaluation presented in this study is based on a steady-state variant of the model representing an equilibrium state, without any groundwater pumping (Reinecke et al., 2019a).

Fig. 1 shows the conceptual nature of the model. In each model cell, there is one river and possibly multiple other surface water bodies like lakes and wetlands (not shown in Fig. 1). Groundwater recharge is based on mean annual groundwater recharge (Döll et al., 2014) computed by WaterGAP 2.2c (Müller Schmied et al., 2014) for the period 1901-2013. This simulated recharge is uncertain as components leading to this flow are uncertain (e.g., precipitation, computation of evapotranspiration, and total runoff and its partitioning into fast runoff and groundwater recharge) but the calibration constrains total runoff to streamflow observations. WaterGAP also computes consumptive use as net groundwater and surface water abstractions, which can be taken into account as a correction factor on groundwater recharge.

Hydraulic conductivity (K) is derived from GLHYMPS 2.0 (Huscroft et al., 2018). The original data (polygons of different spatial resolution) were gridded to $5'$ by area-weighted averaging and used as K for the upper model layer. For the second layer, K of the first layer (K_{upper}) is reduced by an e-folding factor f (a calibrated parameter based on terrain slope from Fan et al. (2013)), assuming that K decreases exponentially with depth. K of the lower layer (K_{lower}) is calculated with an equation from Fan et al. (2013, Eq. 7) as

$$K_{\text{lower}} = \frac{K_{\text{upper}}}{\exp\left(-\frac{50}{f}\right)} \tag{1}$$

where 50 is a factor in meters. Application of the e-folding factor reduces the mean K from 10^{-6} m s^{-1} (first layer) to 10^{-11} m s^{-1} for the second layer.

Testbed: New Zealand

NZ, consisting of a total of 4602 $5'$ cells in two layers, is characterized by a simple continuous boundary condition (the ocean) and diverse topography while providing continuous and dense well observations for some regions. It allows for model exploration with much lower runtimes as compared to simulations for the whole globe. Model parameters and input data are the same as in the global version.

To investigate the sensitivity of model performance to spatial resolution, a $30''$ (ca. 900 m by 900 m at the equator) G^{3}M version was set up for NZ, comprising 433,468

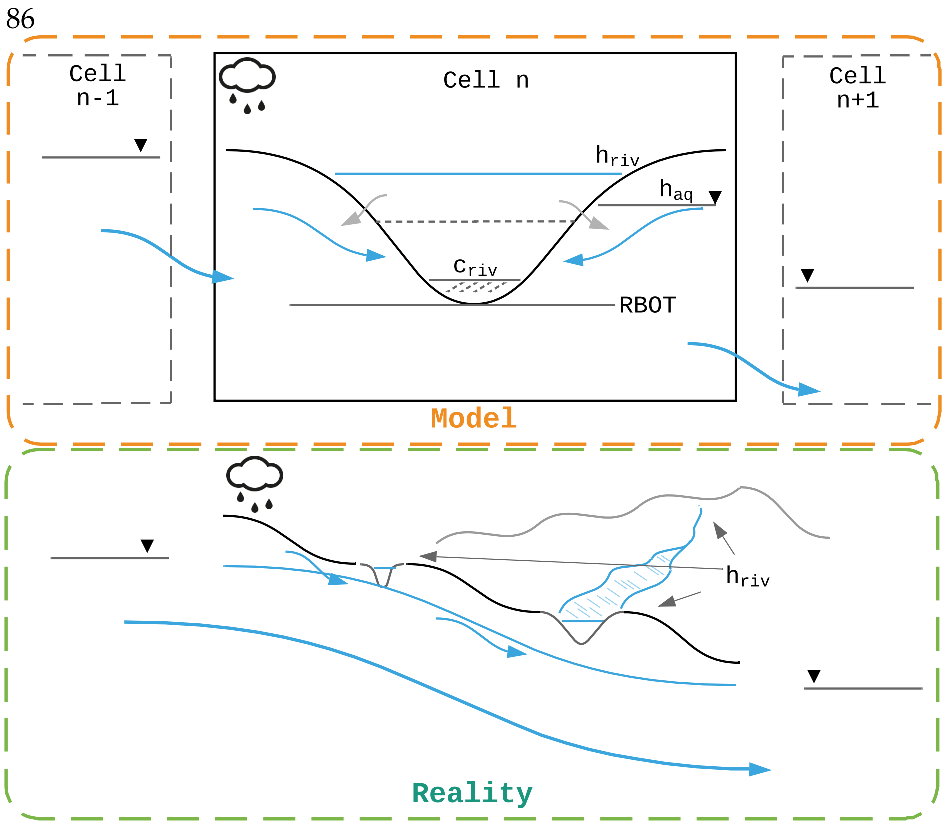

Figure 1: Comparison of the global gradient-based groundwater model approach to equivalent groundwater flow processes. The conceptual groundwater model has only one river in every model grid cell (common in GHMs) and flow between cells is an average over much more complex hydrogeological units and local interactions with surface water. Exchange with the surface water bodies is calculated as a function of the head in the aquifer h_{aq}, the river head h_{riv}, the bottom of the streambed $RBOT$, and a conductance c_{riv} that varies between losing and gaining conditions. Details can be found in Reinecke et al. (2019a)

model cells. The 30″ model uses the same input as the 5′ model except for the land surface elevation and the location of rivers. Total river length and width are equal in both models. Contrary to the 5′ model, which contains a river in each model cell, the 30 ″ model contains the same rivers only in selected cells. These cells are determined using 30″ HydroSHEDS (Lehner et al., 2008) information. From HydroSHEDS we derive the length at 30″ resolution together with information on the drainage relation of the cells expressed as a number of upstream cells. Upstream cells are the number of cells that are assumed to drain into an individual cell. Based on this information Algorithm 1 determines the $30''$cells that contain a river, which are assumed to be those with the largest number of upstream $30''$ cells. While it is assumed that all $5'$ cells contain a river, this is the case only for 14% of the cells in the $30''$ model variant.

```
Result: The $30''$ model contains the same total river length and width as the $5'$
        model. Only selected $30''$ cells contain a river.
foreach $5'$ cell do
    foreach $30''$ cell do
        order by upstream cells;
    end
    total_l_riv ;                      /* The total length of the $5'$ river */
    l_riv ;     /* The current length of all $30''$ rivers in this cell */
    while l_riv < total_l_riv do
        select the next $30''$ cell with the highest upstream number;
        l_hydro = river length for this cell from HydroSHEDS;
        /* l_hydro is the length of the river in the $30''$ cell        */
        /* The width is the same as the $5'$ river                      */
        l_riv += l_hydro;
    end
end
```

Algorithm 1: Determining the $30''$ inside a $5'$ cell which contains a river

All other surface water bodies (lakes and wetlands) are incorporated as a fraction of the total grid cell size. For the $5'$ version, this fraction is based on the area that lakes and wetlands cover in each grid cell, based on the Global Lakes and Wetlands Database GLWD (Lehner and Döll, 2004). The same fraction is assigned to each $30''$ cell contained in the $5'$ cell.

In the $5'$ model, the elevation of the surface water bodies is the 30th percentile (P_{30}) of the $30''$ DEM values within the $5'$ grid cell. This elevation was found to provide the best global fit to observations (Reinecke et al., 2019a). For the $30''$ model, the elevation of the surface water bodies was set to the $30''$ DEM value.

The Canterbury region

Our study focuses on the Canterbury region in NZ due to a large number of available groundwater well observations. It is located on the central-eastern South Island (see also Fig. 4 and 5). The region covers an area of 44,508 km^2 and is home to a population of 624,000 (June 2018) (Aotearoa, 2018). It consists of the Southern Alps in the hinterland and the Canterbury Plains in the coastal area. While the Southern Alps consist mostly of greywacke and schist, the Canterbury Plains are composed of Quaternary gravel, sand, and silt deposited by rivers and meltwater outwash (Westerhoff and White, 2013). In the higher elevations of the Canterbury Plains, aquifers are typically unconfined while in the lower parts, confined conditions occur where marine deposits are interbedded with the terrestrial sediments (Westerhoff and White, 2013). The Canterbury Plains is the region with the most groundwater usage in New Zealand (Westerhoff and White, 2013). Groundwater recharge occurs through rainfall, braided rivers, and artificial recharge (Westerhoff and White, 2013).

Available global groundwater models

Only three global gradient-based groundwater models are currently available (de Graaf et al., 2015; Reinecke et al., 2019a; Fan et al., 2013). This study analyzes steady-state hydraulic heads simulated by these three models as well as by a regional model for NZ (Table 1). The model by Westerhoff et al. (2018) is a refined version for NZ of the model by Fan et al. (2013), with different hydraulic conductivities, groundwater recharge, and land surface elevations. The main difference between G^{3}M and the models of Fan et al. (2013) and Westerhoff et al. (2018) is that no interaction with surface water bodies is simulated in the latter. Groundwater is removed as soon as it reaches the surface. Fan et al. (2013) and Westerhoff et al. (2018) are only able to simulate steady-state conditions, whereas de Graaf et al. (2015) and G^{3}M can also run transient conditions and simulate interaction with surface water bodies. The simulated heads used in this study are from steady-state simulations.

Table 1: Comparison of available global (steady-state) models for NZ. Only Westerhoff et al. (2018) is restricted to NZ - all other models provide world-wide results. Fan et al. (2013) and Westerhoff et al. (2018) have no prescribed river elevation. In both models groundwater is removed as soon as it reaches the land surface elevation.

	Fan et al. (2013)	Westerhoff et al. (2018)	G^{3}M	de Graaf et al. (2015)
Spatial resolution	$30''$ ($\sim$900 m)	$7.5''$ ($\sim$200 m)	$5'$ ($\sim$9 km)	$6'$ ($\sim$10 km)
Surface elevation	$30''$ DEM	avg. of 8 m DEM	avg. of $30''$ DEM	avg. of $30''$ DEM
River elevation	-	-	P$_{30}$ of $30''$ DEM	avg. of $30''$ DEM + calculation based on bankfull flow and naturalized river discharge
Conductivity data	Global lithology (Hartmann and Moosdorf, 2012)	QMAP[1] Rattenbury and Isaac (2012)	GLHYMPS[2] 2.0 (Huscroft et al., 2018)	GLHYMPS[2] 1.0 (Gleeson et al., 2014)
Aquifer thickness	infinite	infinite	200 m	calibrated
Layers	1	1	2	2
Groundwater recharge	mean of multiple GHMs (1961-1990)	simulated recharge (Westerhoff et al., 2018)	WaterGAP mean (1901-2013)	PCR-GLOBWB (Sutanudjaja et al., 2018) mean (1960-2010)
Calibrated	manual	yes	no	manual

[1] QMAP (Quarter-million MAP)

[2] GLHYMPS (GLobal HYdrogeology MaPS)

Observations

The observations used in this study are based on a dataset of piezometric time series from individual groundwater wells by Westerhoff and White (2013) that are temporally aggregated to an average WTD. Time series length is on average 12.4 years, with a median of 7 years. The longest time series is from 1894 - 2013.

Observed head values are calculated using the observed WTD and an 8 m DEM (LINZ, 2012) resulting in 4459 observations. This DEM is the DEM with the highest resolution that is freely available for New Zealand. We assume that it provides the best estimate of the observation elevation we can obtain for the entire model domain. For comparison with simulated values, the observations are aggregated by a geometric mean. The geometric mean was chosen as it is more robust against outliers and because the data is skewed. The number of (aggregated) observations to which the simulated heads can be compared depends on the model resolution (see № in Table 2).

It is unknown whether an observation was made from a confined or an unconfined aquifer. Thus, the following analysis does not treat the observations differently, even though it is likely that some observations are obtained from a confined aquifer. We assume that all observations correspond to simulated heads in the upper layer of the models.

Results

Impact of spatial resolution and aggregation on comparing simulated heads against observations.

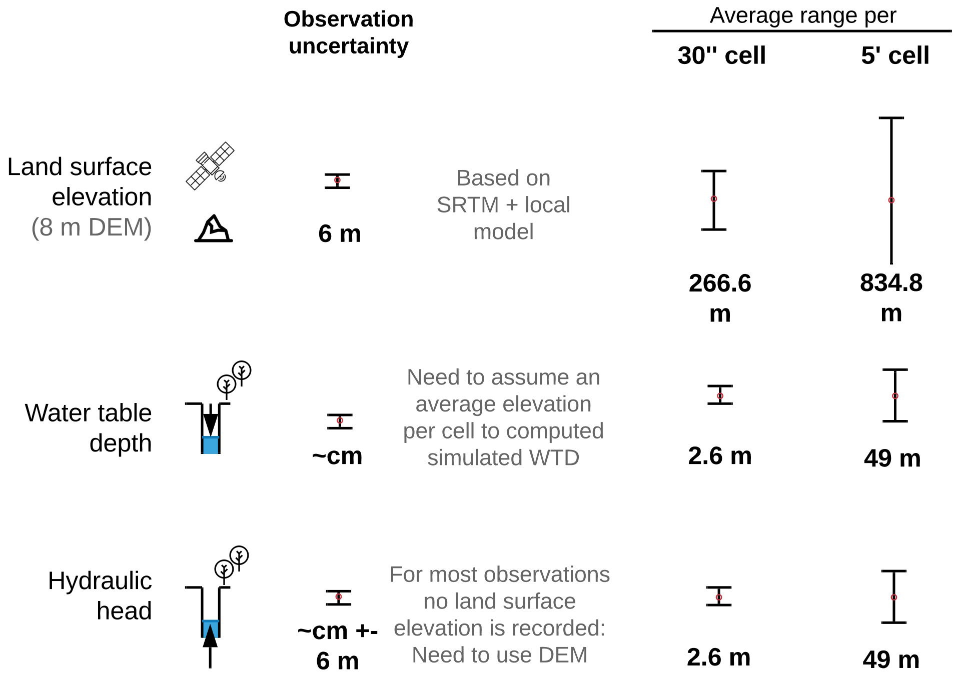
Observation uncertainty
Average range per
30'' cell
5' cell
Land surface elevation
(8 m DEM)
6 m
Based on SRTM + local model
266.6 m
834.8 m
Water table depth
~cm
Need to assume an average elevation per cell to computed simulated WTD
2.6 m
49 m
Hydraulic head
~cm +- 6 m
For most observations no land surface elevation is recorded: Need to use DEM
2.6 m
49 m

Figure 2: Uncertainties of land surface elevation, water table, and head observations and the additional uncertainty due to spatial aggregation of observations to the two grid-cell sizes. The DEM measurement uncertainties are based on Rodriguez et al. (2006) for NZ. Head observations are calculated assuming the land surface elevation of the 8 m DEM. Thus the head uncertainty is the sum of the uncertainties of the WTD observation and the DEM. WTD observations are temporally averaged values from Westerhoff et al. (2018) for the Canterbury region (see Observations). Average ranges of values per grid cell over NZ are shown for both 30″ and 5′ cells.

Depending on the spatial resolution of the model, there is inherent uncertainty in land surface elevation per model grid cell because each cell represents an aggregated characteristic of the reality (Fig. 1), where land surface elevations within the grid cells areas may vary by hundreds of meters. Considering all grid cells in NZ, even in a 30″ cell, the average range of 8 m DEM elevations is 266.6 m, and increases to 834.8 m for the 5″ cell (Fig. 2). These significant variations are important as within each grid cell, there is currently only one value for the elevation of the water table of the surface water bodies, and the simulation results strongly depend on the assumed surface water elevations (Reinecke et al., 2019a).

Moreover, determining a value for the land surface elevation also impacts the model performance evaluation as observations are well measurements of WTD that need to be converted to head observations by using the land elevation to compare them to model results. In other words, the simulated head needs to be converted to simulated WTD, assuming an average cell elevation. For some measurements, land surface elevation is available, but for most measurements, including the only available global data set of observed groundwater heads by Fan et al. (2013), land surface elevation must be based on a DEM. To compare simulated groundwater heads to ”observed” values, de Graaf et al. (2015, 2017); Reinecke et al. (2019a) used a 30″ DEM to calculate observed head values. All head observations in this study were obtained by first subtracting WTD of individual wells from the 8 m DEM. The range of the observed WTD and head per 30″ cell is relatively low, 2.6 m on average, but gets much higher for 5′ cells, with an average variation of 49 m per cell (Fig. 2).

Figure 3 shows the range of observed heads in all 5′ grid cells that contain at least one observation well, together with the aggregated observed value. For most cells, the range of observed heads in the 5′ cell is much larger than the deviation of the simulated head from the aggregated observed value. For lower aggregated observed head values, the range of observed heads decreases likely due to flatter terrain at lower land surface elevations. Aggregated observed heads between 100 m and 400 m have a large variability, with a range of over 200 m. In mountainous areas, the range of observed heads decreases due to the limited number of available head observations existing within the 5′ cell.

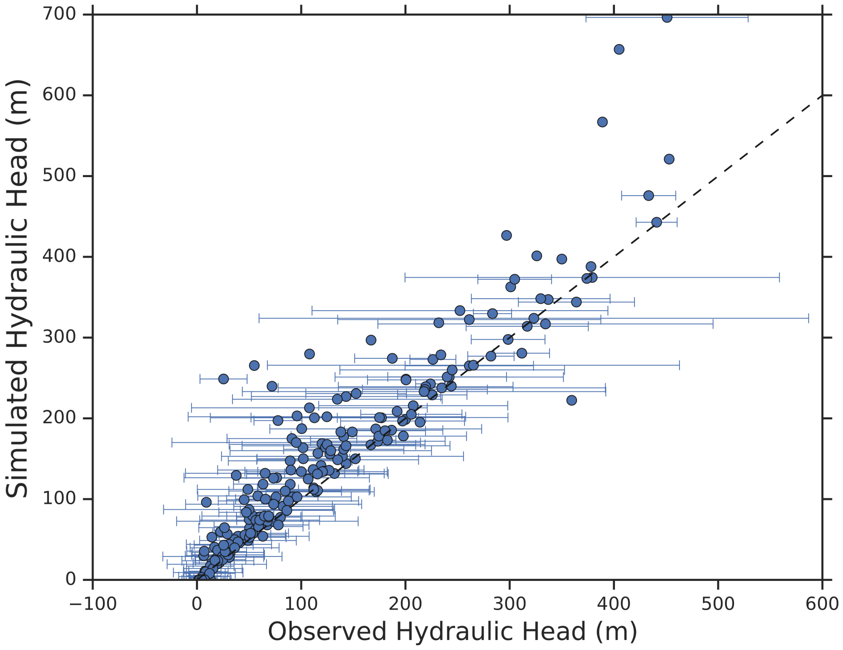

Figure 3: Hydraulic heads simulated by the 5′ G^{3}M as compared to the range of observed head values (8 m DEM - observed WTD) values in the 5′ model cells in the Canterbury region of NZ, including 4459 observations in 163 cells. Dots show geometric means of observed head values (see also Observations).

The relation between land surface elevation and simulated head at different spatial resolutions along a profile in the Canterbury region

To understand the implications of spatial resolution on model performance, Fig. 4 shows a land surface elevation profile through the Canterbury region along with simulated heads. Please note that the profile is not a NS or WE profile; thus, the lengths of the grid cell intersections along the degrees latitude axis vary. The figure shows the cross-section with the most available observations and follows roughly the groundwater flow direction. The majority of observation wells are at lower elevations where groundwater is used for irrigation. This observation bias makes it difficult to assess how the model behaves in challenging mountainous regions.

Averaging the 30″ DEM to 5′ reshapes how the region is represented. For example, near the coast (to the right), the 5′ surface elevation is almost 50 m above the 30″ DEM. This is because most of the 100 30″ cells within this 5′ cell have a higher land surface elevations than the 30″ cells along the profile. Thus, averaging to coarser resolution also

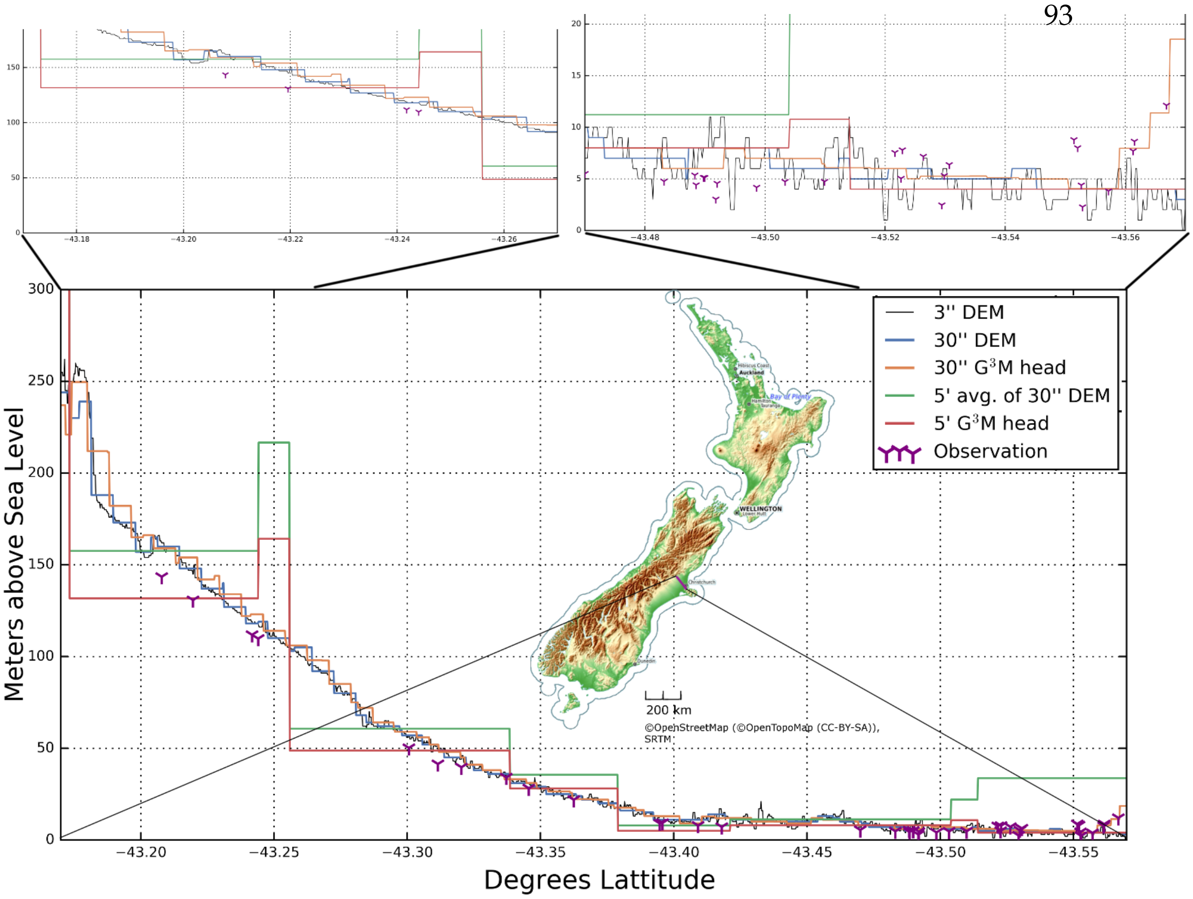

Figure 4: Elevation and simulated head profile at different spatial resolutions through Canterbury. Observed heads are located within a distance of 200 m from the cross section. Observed heads are calculated based on observed WTD and an 8 m DEM.

impacts elevation gradients.

Because the assumed surface water body elevation (P_{30} of 30″ DEM) near the coast is close to the observations, simulated heads are relatively close to the observed heads. However, when using the mean 5′ land surface elevation to derive simulated WTD, a land surface elevation difference to the 8 m DEM of 50 m translates to directly to a difference of 50 m in WTD. Further upslope, this issue gets more severe. Between 43.24° S and 43.27° S, the 5′ average of the surface elevation is almost 100 m away from the 30″ elevation. The simulated head differs by 50 m from the 30″ head at this location. Just due to this scale effect, head and WTD simulated by a 5′ resolution model will be off by a large magnitude from any observed value. The 30″ simulated head, on the other hand, follows the 30″ DEM more closely and thus is also closer to the observations in most cases, but by chance, e.g., at 43.22° S, the 5 ′ simulation result fits much better (further discussed in The sensitivity of simulated head to spatial resolution). Comparing the $30''$ DEM to the high-resolution 8 m DEM shows that the $30''$ DEM is a relatively good approximation of the real topography in most parts, even though it can deviate by $\sim$ 10 m even at low elevations. More significant deviations can be seen in regions with a large slope, e.g., at 43.17° S, where the 8 m DEM is almost 15 m lower.

The sensitivity of simulated head to spatial resolution

Fig. 5 shows the steady-state heads of the two model variants compared to observations. According to the RMSE, the $30''$ model, with a value of 28.54 m, outperforms the $5'$ model with a value of 52.00 m. These numbers can be somewhat misleading regarding the model performance. As the well density is higher at lower land surface elevations where fit is generally better. The number of aggregated observation values increases more strongly at lower land elevations than at higher land surface elevations with less dense observations. Therefore, the lower RMSE of the $30''$ model does not necessarily indicate a better overall model performance. Both scatter plots show a persistent overestimation of heads with a similar magnitude and distribution. The $5'$ model produces fewer underestimates but one with a higher magnitude. The underestimates of the $30''$ model are few compared to the overestimates. Due to the scale, the underestimates are hardly visible on the map. The 60 m underestimate of the $30''$ model is located close to the Waikamari river and the elevation profile. In general, the underestimates of the $5'$ model appear at higher elevations, whereas the $30''$ model shows increased underestimates at lower elevations; this can also be observed on the maps. They also show a better agreement (deviation from the aggregated observed head smaller than 10 m) at lower elevations towards the coast.

The overestimates in the $5'$ model are mainly located where the contours of observed water table bulge at the location of two major rivers - the Ashburton River and the Rakaia River. In 1974, both rivers were found to lose water to the groundwater in their lower parts close to the coast (Mandel, 1974). For the Ashburton River, this agrees with the simulated contours but not with the observed contours that throughout show gaining conditions. For the Rakaia, both the simulations and observations indicate

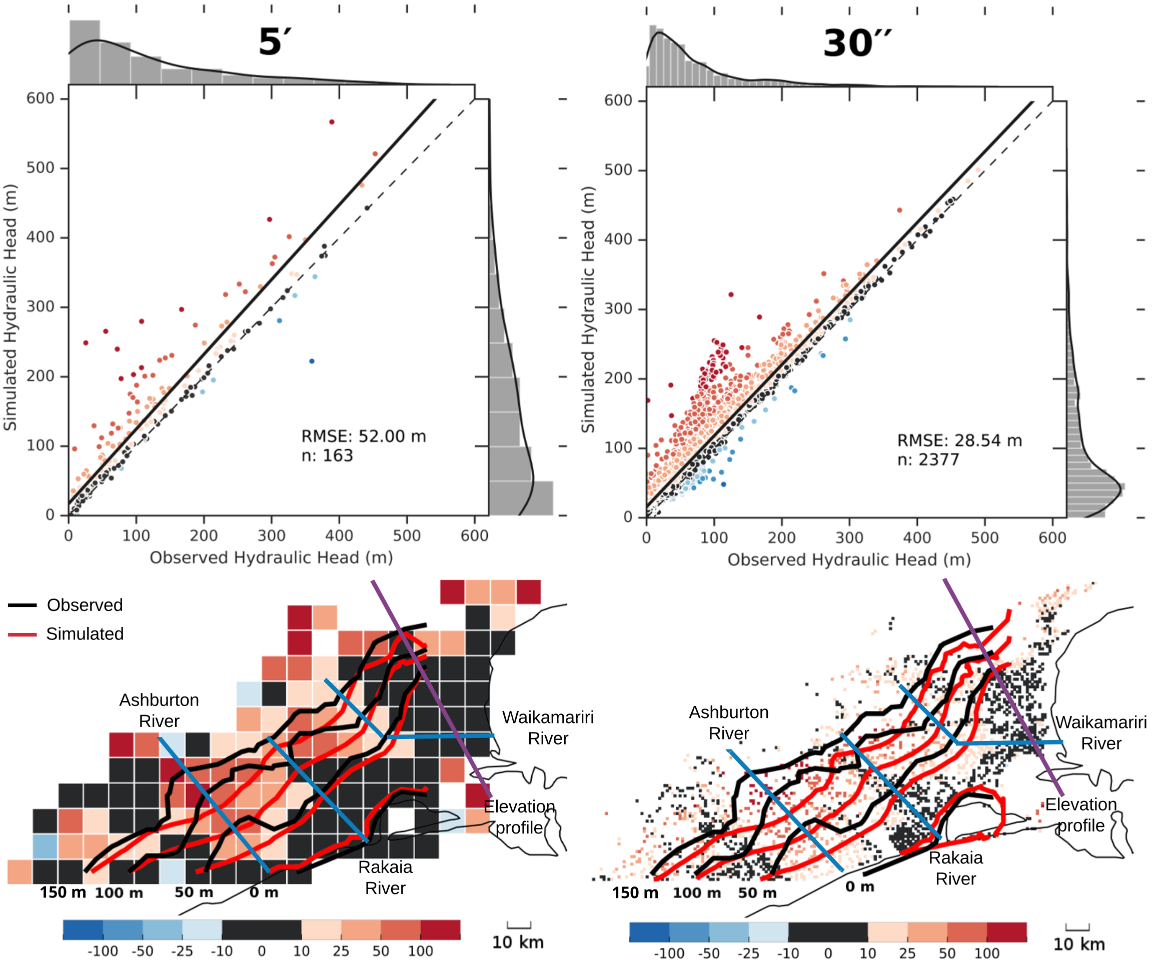

Figure 5: Simulated heads compared with observed heads for two different model resolutions (5′ and 30″) for the Canterbury region. The scatterplot shows the 1:1 line as dashed and the regression as solid line. The normalized histogram indicates the number of the respective values of simulated and observed heads. The colors of the scatter points corresponds to the colors of the grid cells on the maps. The maps show deviations between simulated and (geometric mean) aggregated observed head (simulated minus observed). On the 30″ map the blue cells are hardly visible due to the high resolution and overlaps with the contour lines. Contours for the observed head (black) in both maps are based on the 5′ average as the 30″ resolution led to artifacts in the interpolation method. Contours of simulated head (red) are shown for the corresponding spatial resolution of 5′ and 30″. The purple line shows the cross section of the elevation profile in Fig. 4.

losing conditions close to the coast. Overestimation of observed heads could be due to high levels of groundwater pumping or underestimation of hydraulic conductivities (Westerhoff et al., 2018).

Comparison to other models

The systematic overestimation of heads in the Canterbury region is not unique to the G^{3}M model but persists in the global model of Fan et al. (2013) and the higher resolution and locally refined adapted version of this model by Westerhoff et al. (2018) (Fig. 6, see also Table 1). Again, the higher spatial resolution of the Westerhoff et al. (2018) model has a lower RMSE for the observed heads, but like G^{3}M and the Fan et al. (2013) model tends to overestimate.

Westerhoff (2017, p. 227-240) attributed the overestimation not only to the pumping of groundwater but also to an underestimation of hydraulic conductivity in his model compared to the local estimates of Broadbent and Callander (1991). Glacial outwash gravels are known to occur especially adjacent to the rivers (e.g., Ashburton and Rakaia River) (Mandel, 1974), and vertical vein-like flow through unconfined gravels was reported (Mandel, 1974). Neither are considered by any of the investigated models and could explain the overestimation of the hydraulic head. GLHYMPS 2.0 (Huscroft et al., 2018) (the hydraulic conductivity dataset used in G^{3}M) contains homogeneous K for the study area, and in G^{3}M vertical K is assumed to be 10% of the horizontal K; an assumption which is questionable for unconsolidated sands and gravel deposits.

Simulation of WTD

Gradient-based groundwater models formulate the groundwater flow equations in terms of the hydraulic head relative to a specified datum. However, estimates of WTD are required for comparison with observations (see Observations) as well as for assessing the impact of capillary rise on evapotranspiration in GHMs (Reinecke et al., 2019a). Most GHMs do not implement capillary rise even though the impact of groundwater on the water budget simulated at the land surface-atmosphere interface has been widely studied (Vergnes et al., 2014). WTD is calculated as the surface elevation of the model

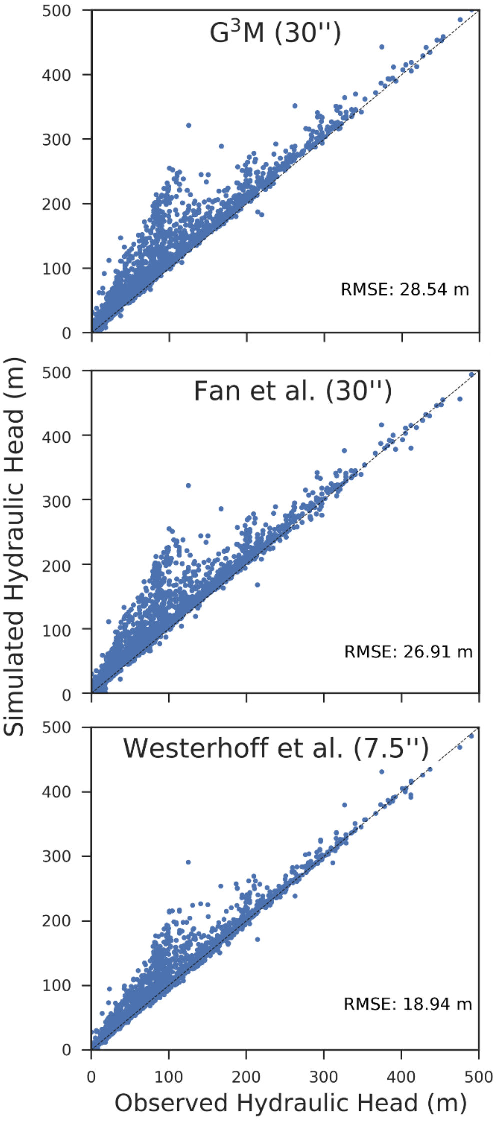

Figure 6: Simulated head (m) of two 30″ (G^{3}M and Fan et al. (2013)) and one 7.5″ (Westerhoff et al. (2018)) groundwater models compared to observations in Canterbury. The observed heads are derived from observed WTD (see Observations) and a 8 m DEM. Multiple observations inside one cell are aggregated with a geometric mean to 30″ and 7.5″ (depending on the model they are compared to).

minus the simulated head. Figure 7 shows that all global models require substantial improvements to represent adequately WTD in the Canterbury region. Only the WTD simulated by the high-resolution model of (Westerhoff et al., 2018) shows a (weak) correlation with observed WTD. All other models tend to deviate by 50 m or more. All high resolution (30″ or higher) models underestimate the WTD, thus simulate a water table that is too shallow, while the coarser-scale models tend to both over- and

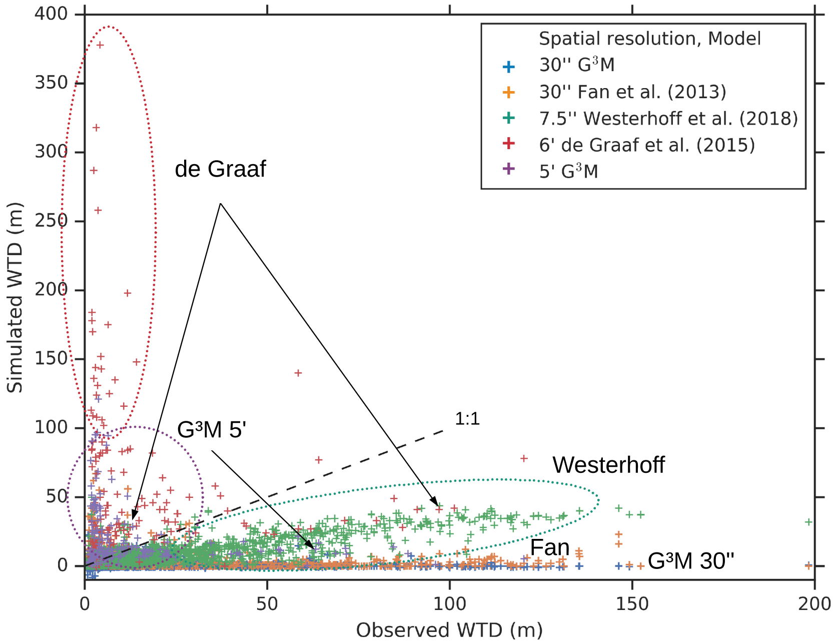

Figure 7: Simulated WTD in Canterbury compared to observed WTD for various steady-state groundwater models: G^{3}M (5′ and 30″), Fan et al. (2013) (30″), de Graaf et al. (2015) (6′), and Westerhoff and White (2013) (7.5″). The 7.5″ values are aggregated to 30″ for better visibility. The aggregation only improves the readability of the plot and does not change the general trend of the results.

underestimate WTD. Both 30″ models, even though they differ regarding the interaction with surface water bodies, simulate low WTD everywhere, no matter if observed WTD is shallow or up to 100 m deep. Only the 30″ G^{3}M model also overestimates WTD (obfuscated in Fig. 7 due to the number of scatter points, also compare Fig. 5). Some of the overestimates in the 30″ G^{3}M are above the land surface. These overestimates are likely caused by the large gradient between the upland and the lowlands. The model of de Graaf et al. (2015) seems to strongly overestimate (by more than 300 m) the WTD in most cases, while the 5′ G^{3}M shows wrong estimates in both directions with slightly less severe overestimates.

Impact of model parameter values on simulated heads

Groundwater abstractions heavily influence the study region. However, groundwater abstractions are not represented in any of the steady-state groundwater models. The impact of groundwater abstractions can be represented by decreasing natural groundwater recharge by net abstractions (abstractions minus return flow to groundwater). A decreased effective groundwater recharge is expected to lead to lower heads, and thus a better representation of heads observed in the Canterbury region. However, when subtracting abstractions simulated by WaterGAP (Müller Schmied et al., 2014) from natural groundwater recharge applied to G^{3}M, we found that they are too small to reduce the overestimation significantly. This is even the case if total water abstractions from surface water and groundwater, as computed by WaterGAP, are assumed to be abstracted from groundwater.

Evaluating 50 experiments with varying hand-tuned parameter sets, we determined by trial-and-error, with the 5′ G^{3}M variant, which variations of the three most influential parameters can significantly reduce the overestimation of heads in the Canterbury region. Using the Method of Morris (Reinecke et al., 2019b), groundwater recharge, hydraulic conductivity, and elevation of surface water bodies were found to be most influential for the simulated 5′ head in New Zealand (Fig. S1 in supporting information). Therefore, the 5′ baseline experiment (same as Fig. 5) with an RMSE of 52 m was compared to experiments where 1) a factor of 10^3 homogeneously reduces groundwater recharge, 2) K is increased by a factor of $10^{4.5}$ in the mountain cells (average elevation $<$ 400 m and average slope $> 5°$) and 100 in the other cells or 3) an alternative subgrid parameterization (SP) for determining the surface water body elevation is used. With SP, surface water body elevation is not determined as the 30th percentile of the 30″ land surface elevations within the 5′ cell but as the mean of the elevations of all existing 15″ rivers within the 5′ cell. These rivers are defined by the 15″ HydroSHEDS river network map (Lehner et al., 2008). Also, combinations of two and all three alternatives are evaluated (Fig. S1).

With the extreme reduction of groundwater recharge to almost zero, the simulated heads show better agreement compared to the aggregated observed heads (RMSE: 39.57 m), but no reduction of overestimation is visible. The extreme increase in K also leads to a smaller RMSE (43.48 m) but adds more underestimates of the observed head. Estimation of the surface water body elevation by using higher-resolution DEM and derived river network data in a physically meaningful way (SP), however, reduces the fit to observations (RMSE: 60.31 m). A combination of SP with an increased *K* (RMSE 43.48 m) shows no differences to only increasing the *K* (RMSE 43.48 m). Combining SP with the groundwater recharge reduction, the RMSE (40.9 m) is similar to the value achieved by recharge reduction alone. A similar pattern results if a reduced recharge is combined with an increased *K*, leading to a higher RMSE of 41.59 m but less visible overestimates than recharge reduction alone, but overall much more severe (300 m) underestimates. The combination of all three changes yields similar results with even more underestimates, an RMSE of 41.45 m, and no overestimates larger than 200 m. Extreme reduction of groundwater recharge produces the lowest RMSE, and the experiments show that there are non-linear relationships between the parameters. A systematic model calibration may lead to a better agreement (e.g., smaller RMSE) with observations.

Discussion

Inclusion of gradient-based instead of bucket-like groundwater models in GHMs can improve the simulation of exchanges with surface water bodies and evapotranspiration as both require simulation of sufficiently accurate groundwater heads. While GHMs compute water flows and storages independent of any absolute elevations (Müller Schmied et al., 2014), gradient-based groundwater models, as well as GHMs coupled to gradient-based groundwater models, require determination of groundwater heads that depend on absolute elevations of the location on which they occur, elevation of the water level in surface water bodies, and the elevation of the land surface. This poses significant challenges that have not been encountered yet in global hydrological modeling.

Representation of spatially strongly variable land surface elevations in coarsely discretized global groundwater models is is inherently incomplete, uncertain, and a function of grid-cell size (Fig. 4). The model input land surface elevation as well as simulated head and WTD for a grid cell are an average representation of, in reality, a distribution of land surface elevation, heads and WTDs that may strongly vary within the cell.

We need to contemplate how global-scale models should be designed so that they can estimate water flows between the groundwater and surface water bodies and between groundwater and the unsaturated zone adequately, at least in a way that fits hydrologists' perceptual model. According to Beven (2012), a perceptual model is a representation of a watershed (in this case, not only a watershed but large scale groundwater processes spanning multiple watersheds) that is based on our understanding of real-world processes and is translated into a numerical model. Importantly, our understanding, especially at these large scales and subsurface systems, might be weak and highly uncertain (Neuman, 2002).

Furthermore, to what extent is a comparison of hydraulic heads computed by macro-scale groundwater models with large grid cells to well observations meaningful for evaluating model performance? Publications on macro- and global-scale scale groundwater models often show scatterplots comparing simulated head values to aggregated observations of the hydraulic head e.g., de Graaf et al. (2015, 2017, 2019); Fan et al. (2013); Maxwell et al. (2015); Reinecke et al. (2019a). Such scatterplots can provide a rough visualization of model biases (Fig. 6) but data points close to the 1:1 line and high values of the coefficient of determination (R^2) or the Nash-Sutcliffe coefficient (modeling efficiency) are not indicative of a high model quality as the variation of the heads is a strong function of the topography in non-arid climates (Toth, 1963; Haitjema and Mitchell-Bruker, 2005). The ability to simulate both flows between surface water and groundwater and capillary rise depends on the ability to simulate WTD rather than hydraulic head. If land surface elevation is the same within the whole model domain, then scatterplots of heads and WTD would look the same. The larger the variation of land surface elevation within the spatial domain, the more the fit of simulated and observed heads shown by scatterplots becomes visually better just because land surface elevations dominate the visualization. Due to an increased variation of the observed head, both the coefficient of determination and the Nash-Sutcliffe coefficient increase, too. This is an issue only in the case of simulating larger spatial domains such as NZ or the globe as these spatial domains contain a much larger range of land surface elevations than the smaller spatial domains for which groundwater modeling is typically done.

Before this paper, no publication on global groundwater models showed a direct comparison of observed and simulated WTD. The comparison of WTD in this study reveals the abysmal performance of all global/macroscale models (Fig. 7). This corresponds to large RMSE values for WTD between 18.9 m and 52.0 m and biases between a mean WTD underestimation of 16.0 m and a WTD overestimation of 42.3 m (Table 2). The model of Westerhoff et al. (2018), in which a global groundwater model algorithm is applied for NZ only, shows the best WTD performance. This might be due to a combination of factors: the calibration of the model, its spatial resolution, and the use of high-resolution conductivity data. For the three high-resolution models, the two performance criteria are almost the same regarding WTD and head, but they are different for the two lower-resolution models, the $5'$ G^{3}M and the $6'$ de Graaf et al. (2015) model. For the $5'$ G^{3}M, performance of head is much better than performance of WTD, while the opposite is true for the de Graaf et al. (2015) model (Table 2). Performance values likely differ a lot between head and WTD for the lower-resolution models due to the much larger number of well observations that are aggregated to one "observed" value within the cell as compared to the high-resolution models (Table 2). Both performance criteria would be equal for WTD and head if the same land surface elevations were used to compute "simulated" WTD or "observed" head but we preferred to calculate best estimates of "observed" head by using the best estimate of land surface elevation to compute "observed" head from actual observed WTD. However, it is not possible to use these spatially varying land surface elevations at the well locations to compute simulated WTD from actual simulated head; instead, the land surface elevation of the grid cell is used. An alternative for determining "simulated" WTD, just for determining model performance, is to calculate "simulated" WTD as the difference between the mean land surface elevations of the observation wells within the model grid cell and the simulated head, but this was not explored.

Suspecting that the opposite performance of the $5'$ G^{3}M and de Graaf et al. (2015) model may be caused by differences in the grid cell extents which encompass different observation wells, we determined RMSE values that would result if random samples of only fractions of all available 4459 observations were used for performance testing. However, the opposite behavior persists for all fractions and the 100 random samples for each fraction class (Figure 8). RMSE values of the two models for WTD and head positively correlate with the absolute values of the biases, but it is unclear why for

Table 2: Bias and RMSE comparison for WTD and head for various steady-state models (Table 1). Simulated WTD is calculated based on the respective model land surface elevation. Observed WTD is the geometric average of all observations in the model grid cells, while observed head was calculated by first computing the hydraulic head at the observations wells by using a high-resolution DEM and then averaging over all observation wells in the model grid cells (see Observations). The bias (b) is calculated as the arithmetic average of the residuals (simulated - observed). Nº is the number of grid cells for which b and RMSE are computed.

Model	Resolution	Nº	b(WTD)	b(head)	RMSE(WTD)	RMSE(head)
Westerhoff et al. (2018)	7.5″	3148	-9.7 m	9.1 m	19.3 m	18.8 m
Fan et al. (2013)	30″	2377	-14.4 m	14.7 m	28.7 m	26.9 m
G^3M	30″	2377	-16.0 m	17.1 m	29.2 m	28.5 m
G^3M	5′	163	2.5 m	25.9 m	35.5 m	52.0 m
de Graaf et al. (2015)	6′	147	42.3 m	-8.1 m	79.9 m	30.1 m

example, the absolute WTD bias of 5′ G^3M is so much smaller than the corresponding value of the de Graaf et al. (2015) model (with the opposite being true for the absolute head bias). This behavior may be related to the different assumptions about the elevation of the surface water bodies (Reinecke et al., 2019a,b).

Figure 8 reveals that values of model performance indicators strongly depend on the available observations. RMSE could vary by more than 10 m or even 30 m for different sets of observation wells. Interestingly, RMSE tends to increase with an increasing number of observations (Figure 8).

Differences between simulated and observed heads and WTDs can depend strongly on which point observation the simulated result is compared to. Unless there is (1) an extensive number of rather homogeneously distributed observation wells within each large model grid cell, (2) with observations that characterize the average groundwater distribution in such a large area, observations cannot be aggregated in a way that is meaningful for a comparison to simulated heads or WTD. In most cases, it is unlikely that both conditions are fulfilled.

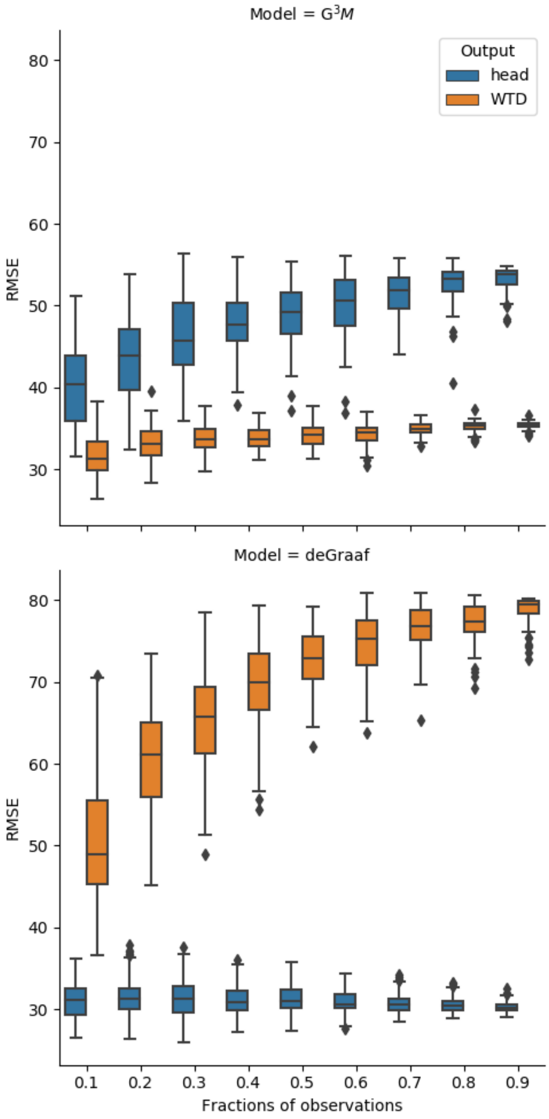

Figure 8: Box plot of RMSE as a function of fractions of observations for head and WTD [m]. Each box is based on 100 repeated random samples (for the according fraction) from all available observations that are then aggregated to the according spatial resolution. Whiskers represent the 1.5 interquartile range.

In conclusion, while we found that increasing spatial resolution of the groundwater model improves the fit to observations (compare the RMSE of five models in Table 2), we suspect that this is partially due to decreased variability of point observation values in the smaller grid cells, and thus a better representation of average conditions within the grid cells by the observed point values. Regardless, the bias, a general overestimation of observed heads, remained in the testbed region.

Based on the results presented, one cannot conclude that an increased spatial resolution is by itself is sufficient for improving the model's ability to simulate heads and flows accurately. Somewhat surprisingly, the 30′′ variant of G^{3}M shows similar performance to the contrasting 30′′ model of Fan et al. It is unclear why this is the case.

Additional research is necessary to investigate which deviations from observations occur in transient simulations and if the fit to temporal variations is better than the fit to WTD. Testing the simulation of temporal variations might be more meaningful for coarse-scale groundwater models than testing steady-state WTD.

A limitation of this study is the steady-state nature of the model output and the comparison to observations in a region that is profoundly impacted by groundwater abstractions. Abstractions are another challenge for the evaluation of global groundwater models as we can expect a high density of observations mostly in regions with intensive use of groundwater. At the same time, we do not have any global data of groundwater pumping and therefore rely on simulation results of GHMs like WaterGAP (Müller Schmied et al., 2014). A possible approach in future studies would be to use known elevations of springs and wetlands to estimate the WTD in regions where no observations are available.

To find an explanation for the overestimated heads, we analyzed an ensemble of model variants with a different combination of the most critical model parameters but the model fit was not substantially improved. While automated calibration could be a solution, Westerhoff (2017) showed that this might lead to implausibly high *K* values. Additionally, other calibration efforts of global models led to non-physical parameters (de Graaf et al., 2017) and automated calibration on the global-scale might not be feasible due to computational limitations. Furthermore, it is questionable whether calibration against spatially aggregated heads is meaningful.

Conclusions

Global-scale simulation of groundwater heads and flows is challenging. This is predominantly due to high spatial variability of the elevations of the land surface and the water table as their variations (or spatial gradients) govern resulting water flows, but cannot be easily represented with the rather large grid cells required in global-scale groundwater modeling. The large grid cells also make a meaningful comparison to point observations of groundwater well difficult.

Due to the coarse resolution, global groundwater models have difficulty representing correctly the flow of water through the subsurface because the range of land surface elevation within one computational cell may be, for example, 1000 m more than the thickness of the aquifers. In addition, due to the lack of high-quality global data, model input is highly uncertain. Both issues strongly differentiate global groundwater modeling from the well-established local or regional basin-scale groundwater modeling.

We need new strategies for evaluating macro-scale groundwater models as we demonstrated in this study that comparison of simulated grid cell values to well observations, that need to be aggregated to the model cell size, is problematic. The number and range of observed values per cell can vary greatly and affects both how observation data relate to a particular model and comparisons of models with different spatial resolutions. A suitable approach to represent the subgrid variability of elevations and hydraulic heads within large grid cells is needed to improve evaluation of macro-scale groundwater models.

Gradient-based groundwater models are required to improve the established GHMs, but the community needs to be open about their shortcomings when advancing them. Increasing the spatial resolution of global groundwater models will not necessarily result in better models - only more copious amounts of output. To accurately assess these complex models, we require not only more high-quality hydraulic head observations but also estimates of (preferably large-scale) exchange flows between groundwater and surface water. International efforts for combining already available local groundwater-related data into global datasets should be intensified.

Acknowledgments

The model framework code can be obtained from `globalgroundwatermodel.org`. We like to thank Rogier Westerhof for providing the steady-state observations for Canterbury New Zealand and additional insights into his model and we like to thank Inge de Graaf, Ying Fan, and Miguez-Macho for providing their model output. Moreover, we like to thank the three anonymous reviewers and Scott James for their insightful comments that improved this manuscript.

Authors' contributions: RR led the conceptualization, formal analysis, methodology, software development, visualization, and writing of the original draft. AW built the 30″ datasets, ran the models, led the initial analysis, and did initial visualizations. AW, LF, SM, CN supported review and editing. PD supervised the work of RR and made suggestions regarding the analysis, structure and wording of the text and design of tables and figures.

Supporting Information

The model framework code can be obtained from globalgroundwatermodel.org. Additional Supporting Information may be found in the online version of this article:

> **Figure S1.** Most sensitive parameters and scatterplots for different model experiments.

Please note: "Supporting Information" is generally not peer reviewed.

References

Aotearoa, S. N. T. (2018). Population numbers. data retrieved from Stats NZ Tatauranga Aotearoa, `https://www.stats.govt.nz/information-releases/subnational-population-estimates-at-30-june-2018-provisional` (last accessed June 2019).

Beven, K. (2012). *Rainfall-Runoff Modelling: The Primer: Second Edition*, volume 15. Wiley.

Beven, K. J. (2000). Uniqueness of place and process representations in hydrological modelling. *Hydrology and Earth System Sciences*, 4(2):203–213.

Broadbent, M. and Callander, P. F. (1991). A resistivity survey near waimakariri river, canterbury plains, to improve understanding of local groundwater flow and of the capabilities of the survey method. *New Zealand Journal of Geology and Geophysics*, 34(4):441–453.

Cuthbert, M., Gleeson, T., Moosdorf, N., Befus, K., Schneider, A., Hartmann, J., and Lehner, B. (2019). Global patterns and dynamics of climate–groundwater interactions. *Nature Climate Change*, 9(2):137–141.

de Graaf, I. E., Gleeson, T., van Beek, L. R., Sutanudjaja, E. H., and Bierkens, M. F. (2019). Environmental flow limits to global groundwater pumping. *Nature*, 574(7776):90–94.

de Graaf, I. E., Sutanudjaja, E., Van Beek, L., and Bierkens, M. (2015). A high-resolution global-scale groundwater model. *Hydrology and Earth System Sciences*, 19(2):823–837.

de Graaf, I. E., van Beek, R. L., Gleeson, T., Moosdorf, N., Schmitz, O., Sutanudjaja, E. H., and Bierkens, M. F. (2017). A global-scale two-layer transient groundwater model: Development and application to groundwater depletion. *Advances in Water Resources*, 102:53–67.

DLR (2016). Tandem-x. `https://tandemx-science.dlr.de` (last accessed June 2019).

Döll, P., Müller Schmied, H., Schuh, C., Portmann, F. T., and Eicker, A. (2014). Global-scale assessment of groundwater depletion and related groundwater abstractions: Combining hydrological modeling with information from well observations and grace satellites. *Water Resources Research*, 50(7):5698–5720.

Fan, Y., Li, H., and Miguez-Macho, G. (2013). Global patterns of groundwater table depth. *Science*, 339(6122):940–943.

Faunt, C. C., Sneed, M., Traum, J., and Brandt, J. T. (2016). Water availability and land subsidence in the central valley, california, usa. *Hydrogeology Journal*, 24(3):675–684.

García-Gil, A., Epting, J., Ayora, C., Garrido, E., Vázquez-Suñé, E., Huggenberger, P., and Gimenez, A. C. (2016). A reactive transport model for the quantification of risks induced by groundwater heat pump systems in urban aquifers. *Journal of Hydrology*, 542:719 – 730.

Gleeson, T., Befus, K. M., Jasechko, S., Luijendijk, E., and Cardenas, M. B. (2016). The global volume and distribution of modern groundwater. *Nature Geoscience*, 9(2):161.

Gleeson, T., Moosdorf, N., Hartmann, J., and Van Beek, L. (2014). A glimpse beneath earth's surface: Global hydrogeology maps (glhymps) of permeability and porosity.

Geophysical Research Letters, 41(11):3891–3898.

Gupta, V. K., Troutman, B. M., and Dawdy, D. R. (2007). Towards a nonlinear geophysical theory of floods in river networks: An overview of 20 years of progress. In *Nonlinear Dynamics in Geosciences*, pages 121–151, New York, NY. Springer New York.

Haitjema, H. M. and Mitchell-Bruker, S. (2005). Are water tables a subdued replica of the topography? *Groundwater*, 43(6):781–786.

Harbaugh, A. W. (2005). *MODFLOW-2005, the US Geological Survey modular ground-water model: the ground-water flow process*. US Department of the Interior, US Geological Survey Reston, VA.

Hartmann, J. and Moosdorf, N. (2012). Global Lithological Map Database v1.0 (gridded to 0.5° spatial resolution).

Huscroft, J., Gleeson, T., Hartmann, J., and Börker, J. (2018). Compiling and mapping global permeability of the unconsolidated and consolidated earth: Global hydrogeology maps 2.0 (glhymps 2.0). *Geophysical Research Letters*, 45(4):1897–1904.

Krakauer, N. Y., Li, H., and Fan, Y. (2014). Groundwater flow across spatial scales: importance for climate modeling. *Environmental Research Letters*, 9(3):034003.

Lehner, B. and Döll, P. (2004). Development and validation of a global database of lakes, reservoirs and wetlands. *Journal of Hydrology*, 296(1):1 – 22.

Lehner, B., Verdin, K., and Jarvis, A. (2008). New global hydrography derived from spaceborne elevation data. *Eos, Transactions American Geophysical Union*, 89(10):93–94.

Limberg, A., Hörmann, U., and Verleger, H. (2010). Modellentwicklung zur berechnung des höchsten grundwasserstandes im land berlin. *Brandenburg. Geowiss. Beitr*, 17(1-2):23–37.

LINZ, d. s. (2012). Land information new zealand 8 m dem. data retrieved from LINZ data service, `https://data.linz.govt.nz/layer/51768-nz-8m-digital-elevation-model-2012` (last accessed June 2019).

Mandel, S. (1974). The groundwater resources of the canterbury plains. Technical report, Lincoln College. New Zealand Agricultural Engineering Institute.

Mark, D. M. and Aronson, P. B. (1984). Scale-dependent fractal dimensions of topographic surfaces: An empirical investigation, with applications in geomorphology and computer mapping. *Journal of the International Association for Mathematical Geology*, 16(7):671–683.

Maxwell, R. M., Condon, L. E., and Kollet, S. J. (2015). A high-resolution simulation of groundwater and surface water over most of the continental us with the integrated hydrologic model parflow v3. *Geoscientific Model Development*, 8(3):923–937.

Müller Schmied, H., Eisner, S., Franz, D., Wattenbach, M., Portmann, F. T., Flörke, M., and Döll, P. (2014). Sensitivity of simulated global-scale freshwater fluxes and storages to input data, hydrological model structure, human water use and calibration. *Hydrology and Earth System Sciences*, 18(9):3511–3538.

Neuman, S. (2002). Accounting for conceptual model uncertainty via maximum likelihood bayesian model averaging. *Acta Universitatis Carolinae - Geologica*, 46(2-3):529–534.

Portmann, F. T., Döll, P., Eisner, S., and Flörke, M. (2013). Impact of climate change on renewable groundwater resources: assessing the benefits of avoided greenhouse gas emissions using selected CMIP5 climate projections. *Environmental Research Letters*, 8(2):024023.

Rattenbury, M. and Isaac, M. (2012). The qmap 1: 250 000 geological map of new zealand project. *New Zealand Journal of Geology and Geophysics*, 55(4):393–405.

Reinecke, R. (2018). G^{3}m-f a global gradient-based groundwater modelling framework. *JOSS*, 3:548.

Reinecke, R., Foglia, L., Mehl, S., Trautmann, T., Cáceres, D., and Döll, P. (2019a). Challenges in developing a global gradient-based groundwater model (g^{3}m v1.0) for the integration into a global hydrological model. *Geoscientific Model Development*, 12(6):2401–2418.

Reinecke, R., Foglia, L., Mehl, S., Herman, J. D., Wachholz, A., Trautmann, T., and Döll, P. (2019b). Spatially distributed sensitivity of simulated global groundwater heads and flows to hydraulic conductivity, groundwater recharge, and surface water body parameterization. *Hydrology and Earth System Sciences*, 23(11):4561–4582.

Rodriguez, E., Morris, C. S., and Belz, J. E. (2006). A global assessment of srtm performance. *Photogrammetric engineering & remote sensing*, 72.

Rosso, R., Bacchi, B., and La Barbera, P. (1991). Fractal relation of mainstream length to catchment area in river networks. *Water Resources Research*, 27(3):381–387.

Sood, A. and Smakhtin, V. (2015). Global hydrological models: a review. *Hydrological Sciences Journal*, 60(4):549–565.

Sutanudjaja, E. H., van Beek, R., Wanders, N., Wada, Y., Bosmans, J. H. C., Drost, N., van der Ent, R. J., de Graaf, I. E. M., Hoch, J. M., de Jong, K., Karssenberg, D., López López, P., Peßenteiner, S., Schmitz, O., Straatsma, M. W., Vannametee, E., Wisser, D., and Bierkens, M. F. P. (2018). Pcr-globwb 2: a 5 arcmin global hydrological and water resources model. *Geoscientific Model Development*, 11(6):2429–2453.

Toth, J. (1963). A theoretical analysis of groundwater flow in small drainage basins. *Journal of geophysical research*, 68(16):4795–4812.

Vergnes, J.-P., Decharme, B., and Habets, F. (2014). Introduction of groundwater capillary rises using subgrid spatial variability of topography into the isba land surface model. *Journal of Geophysical Research: Atmospheres*, 119(19):11,065–11,086.

Wada, Y., van Beek, L. P. H., van Kempen, C. M., Reckman, J. W. T. M., Vasak, S., and Bierkens, M. F. P. (2010). Global depletion of groundwater resources. *Geophysical Research Letters*, 37(20).

Westerhoff, R., White, P., and Miguez-Macho, G. (2018). Application of an improved global-scale groundwater model for water table estimation across new zealand. *Hydrology and Earth System Sciences*, 22(12):6449–6472.

Westerhoff, R. S. (2017). *Satellite remote sensing for improvement of groundwater characterisation*. PhD thesis, University of Waikato.

Westerhoff, R. S. and White, P. A. (2013). Application of equilibrium water table estimates using satellite measurements to the canterbury region, new zealand. *GNS Science Report*, 43:25 p.

Wood, E. F., Roundy, J. K., Troy, T. J., van Beek, L. P. H., Bierkens, M. F. P., Blyth, E., de Roo, A., Döll, P., Ek, M., Famiglietti, J., Gochis, D., van de Giesen, N., Houser, P., Jaffé, P. R., Kollet, S., Lehner, B., Lettenmaier, D. P., Peters-Lidard, C., Sivapalan, M., Sheffield, J., Wade, A., and Whitehead, P. (2011). Hyperresolution global land surface modeling: Meeting a grand challenge for monitoring earth's terrestrial water. *Water*

Resources Research, 47(5).

Wörman, A., Packman, A. I., Marklund, L., Harvey, J. W., and Stone, S. H. (2007). Fractal topography and subsurface water flows from fluvial bedforms to the continental shield. *Geophysical Research Letters*, 34(7).

List of Figures

Supporting Information

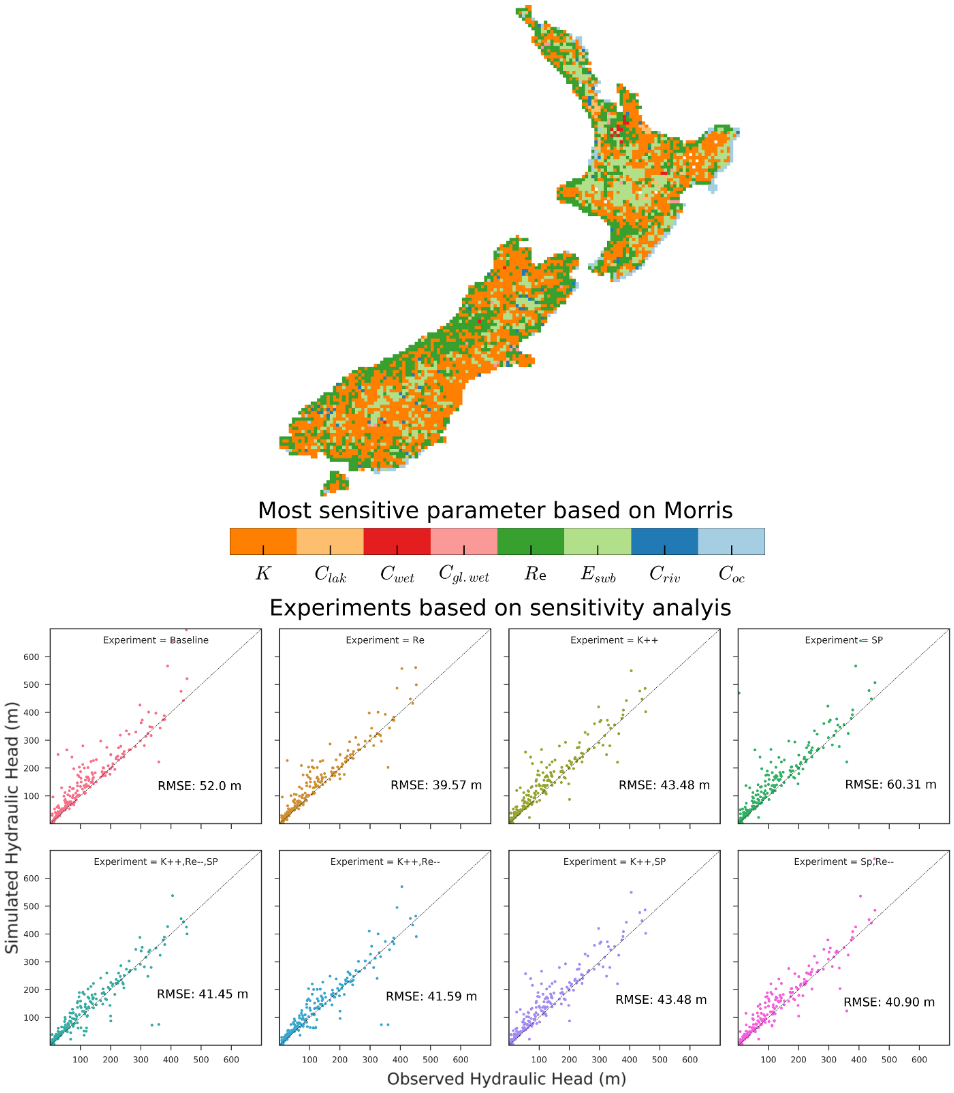

Figure S1: Most sensitive parameters in NZ (top maps) based on a Method of Morris analysis of Reinecke et al. (2019). K is hydraulic conductivity, $C_{lak,wet,gl.wet}$ conductance of the lakes, local wetlands, and global wetlands, respectively. Re is groundwater recharge, E_{swb} elevation of surface water bodies, C_{riv} river conductance and C_{oc} conductance of the ocean boundary (see Reinecke et al. (2019) for an extended explanation of the parameters and the experiment setup). Comparison of simulated head ($5'$) to aggregated observed head (scatterplots) for different model experiments. Each experiment varies one to three parameters equally over NZ, groundwater recharge, K, and the surface water body elevation parameterization (SP) separately and in all combinations.

References

Reinecke, R., Foglia, L., Mehl, S., Herman, J. D., Wachholz, A., Trautmann, T., and Döll, P. (2019). Spatially distributed sensitivity of simulated global groundwater heads and flows to hydraulic conductivity, groundwater recharge, and surface water body parameterization. *Hydrology and Earth System Sciences*, 23(11):4561–4582.

Chapter 6

Simulation of global groundwater storage declines using a global hydrological model with an integrated gradient-based groundwater component

Chapters 3, 4, and 5 show the development and evaluation of the stand-alone steady-state variant of G^{3}M. This was the first step towards the targeted goal of a fully integrated (fully coupled) model with the GHM WaterGAP. This chapter focuses on the coupling concept and its challenges resulting in WaterGAP-G^{3}M. Results of a partially integrated model are presented and compared to established regional scale models. Structured similar to a journal paper draft, this chapter is a basis for a future publication while it leaves out a general motivation for modeling groundwater and an overview of the state of research as this is already discussed in chapter 3.

6.1 Introduction

Global-scale hydrological models have recently moved towards including gradient-based groundwater models for an improved represention of groundwater-surface water interactions, lateral and vertical flows as well as human water use impacts (de Graaf et al., 2015, 2017). G^{3}M (**g**lobal **g**radient-based **g**roundwater **m**odel) (Reinecke et al., 2019a) is a new MODFLOW-like groundwater model that replaces the former linear groundwater reservoir of the GHM WaterGAP (Alcamo et al., 2003; Döll et al., 2003, 2012, 2014; Müller Schmied et al., 2014). The main challenge of integrating the model G^{3}M into the established model WaterGAP is that both models are currently simulating their processes on two different spatial resolutions. G^{3}M is simulating the lateral and vertical groundwater flows and exchanges with surface water bodies on 5′ (ca. 9 km by 9 km at the Equator), whereas WaterGAP simulates surface water flows, storages, and human abstractions on 0.5°. Thus, each WaterGAP cell connects to 36 G^{3}M cells. Flows calculated by G^{3}M and forwarded to WaterGAP need to be aggregated to 0.5° while changes calculated by WaterGAP need to be sampled to the higher resolution of 5′. To complicate matters, the coupling can be achieved on different temporal timescales. For example WaterGAP computes groundwater recharge on daily timesteps but G^{3}M might run on weekly or even monthly timesteps. Updating the recharge then can be achieved at the end of each G^{3}M timestep as an aggregation of the daily recharge, or the stepsize of G^{3}M could be adapted to daily steps which again entails consequences for the runtime of the model and the numeric stability. The goal is to preserve the total water balance of the integrated model and sustain a numerically stable model. A numerically stable model is necessary as instabilities can lead to large over- or underestimates of hydraulic heads and flows. Especially the latter is a challenging task as the changes in the surface water body head from WaterGAP can trigger non-linear changes in G^{3}M.

This chapter (study) demonstrates the integration concept along with first results for an integrated WaterGAP-G^{3}M model with coupled rivers. In addition, an alternative, more physically based, approach for calculating the conductance of surface water bodies is presented together with the now possible implementation of capillary rise. The results of a transient simulation from 1901-2013 are compared to observations from the Central Valley as well as to simulated groundwater storage changes of two established groundwater models of the region: CVHM (Faunt et al., 2016) and C2VSim (Brush et al., 2013).

The following section 2 displays the models WaterGAP and G^{3}M alongside a coupling concept resulting in WaterGAP-G^{3}M, a description of a possible capillary rise implementation, and a physical based river conductance approach. Section 3 displays results of changing the conductance approach for a steady-state simulation together with a transient analysis of the integrated model. The chapter closes with a discussion of current issues and pathways to completing the integration.

6.2 Methods

6.2.1 WaterGAP-G^{3}M

WaterGAP computes human water use in five sectors and the resulting net abstractions from groundwater and surface water for all land areas of the globe excluding Antarctica on a spatial resolution of 0.5° (Alcamo et al., 2003; Döll et al., 2003, 2012, 2014; Müller Schmied et al., 2014). With daily time steps, WGHM simulates flows among the water storage compartments canopy, snow, soil, groundwater, lakes, man-made reservoirs, wetlands and rivers. To this point the groundwater storage was simulated based on a linear groundwater reservoir model (see also Eq. S1 in the supplement of chapter 3). This study is utilizes WaterGAP version 2.2d to replace the linear storage with the model G^{3}M and form the new model WaterGAP-G^{3}M (see Eq. 1 and 2 in chapter 3).

G^{3}M is a global gradient-based groundwater model that computes lateral and vertical groundwater flows as well as flows between the groundwater and surface water bodies for all continents excluding Antarctica on a 5′ spatial resolution. The steady-state version of G^{3}M is described in great detail in chapter 3 and the conductivity input is the same as in chapter 4.

The change in groundwater storage $\frac{dGWS}{dt}$ and the three-dimensional groundwater flow including the boundary conditions are described by a partial differential equation

$$
\begin{aligned}
&\frac{dGWS}{dt} = \\
&\left[\frac{\partial}{\partial x}\left(K_x\frac{\partial h}{\partial x}\right)+\frac{\partial}{\partial y}\left(K_y\frac{\partial h}{\partial y}\right)+\frac{\partial}{\partial z}\left(K_z\frac{\partial h}{\partial z}\right)+\frac{R_g+Q_{swb}-NA_g-Q_{cr}+Q_{ocean}}{\Delta x\Delta y\Delta z}\right] \\
&\times \Delta x\Delta y\Delta z \\
&= S_s\frac{\partial h}{\partial t}\Delta x\Delta y\Delta z \qquad (6.1)
\end{aligned}
$$

where $K_{x,y,z}$ $[LT^{-1}]$ is the hydraulic conductivity along the x, y, and z axes between the cells, S_s $[L^{-1}]$ the volumetric specific storage, $\Delta x\Delta y\Delta z$ $[L^3\ ]$ the volume of the cell, and h $[L]$ the hydraulic head. In- and outflows to the aquifer are accounted for as follows: Q_{swb} $[LT^{-1}]$ is flow between the surface water bodies (rivers, lakes, reservoirs and wetlands) and the groundwater, Q_{cr} $[L^3T^{-1}]$ is capillary rise, i.e. the flow from the groundwater to the soil, and Q_{ocean} $[L^3T^{-1}]$ is the flow between the ocean boundary and the groundwater. Q_{swb} and Q_{ocean} are positive if the flow is into the groundwater and negative if it is out of the cell. R_g $[L^3T^{-1}]$ is diffuse groundwater recharge from soil, NA_g $[L^3T^{-1}]$ is the net-groundwater-abstraction. The equation is solved by using the finite differences method (see chapter 2 and appendix A for details).

Storage

Compared to the steady-state version the storage component (right side of Eq. 6.1) is no longer 0 but computed for the lower model layer as confined and pseudo-unconfined for the upper layer, pseudo-unconfined because the transmissivity of the layer is still calculated as confined as described in chapter 3, but the storage is treated as unconfined. The specific yield S_y [-] is set to 15% for layer 1 and the volumetric specific storage S_s $[L^{-1}]$ to 0.00015 m^{-1} (Table 6.1) as a first global estimate.

Time-steps, numerical control, and spin-up

The groundwater model is simulating hydraulic heads on weekly time steps (Table 6.1) and receives information from WaterGAP on monthly time-steps. As for now it is the best trade-off between a small step-size that assures convergence of the numerical solution and a larger step-size (that requires less steps in total) for minimizing computation time. A daily coupling is possible but results in a simulation time of months. This aspect can be changed in the future to allow an exchange of information on a weekly or fortnightly basis.

The convergence criterions are adapted as well as shown in Table 6.1. A smaller criterion is required as the head changes per step can be relatively small. If the chosen step-size is too large it will influence the accuracy of the head response to flow changes, for example its response to seasonal changes in groundwater recharge.

A spin-up phase is introduced to ensure that the choice of the initial state is not leading to underlying trends in the following transient simulation. Such trends could obfuscate the seasonal trends, or the changing climate, or impacts by human interference leading to wrong results. Figure 6.1 shows this process together with the changing inputs per spin-up stage. The first stage is the steady-state model (see chapter 3) that uses averaged results from Fan et al. (2013) as a starting point. It is forced with the yearly average groundwater recharge of 1901-2013 of WaterGAP. After the steady-state is obtained the groundwater model is coupled to WaterGAP and

TABLE 6.1: Additional or changed parameters in the transient model compared to the steady-state.

Parameter	Symbol	Unit	Value	Description
Specific storage	S_s	m^{-1}	0.00015	Storage coefficient in confined conditions.
Specific yield	S_y	-	0.15	Storage coefficient in unconfined conditions.
Max. head change	-	m	0.5	Convergence criterion for maximum head change in two inner iterations
Residual convergence	-	$m^3 day^{-1}$	10^{-110}	Scaled norm of the conjugate gradient residuals
Max. inner iterations	-	-	15	Maximum number of conjugate gradient iterations per Picard iteration
Time-step	-	T	Weekly	Temporal resolution of the conjugate gradient step

forced with monthly groundwater recharge and net abstractions from groundwater. No surface water bodies are coupled in this phase. This spin-up stage is as long as WaterGAPs five year spin-up. Alternatively, a mechanism is possible that checks if the last spin-up year differs by a given percentage from the current year until a quasi steady-state is reached.

The conductance of the rivers is only scaled by the groundwater recharge (compare chapter 3) in the steady-state step. To reduce non-linearities the calculated conductance in the steady-state (see chapter 3) is kept for the remaining transient run.

Integration of G^{3}M into WaterGAP

The information that is dispatched from WaterGAP to G^{3}M are the changes in surface water body head h_{swb}, changes in groundwater recharge R_G, and changes in net abstraction from groundwater NA_G. In the opposite direction G^{3}M is calculating flows between the groundwater and surface water bodies like rivers, lakes and wetlands Q_{swb} (and in a later development stage capillary rise) that need to be transferred to WaterGAP. In this chapter(study) transfer of h_{swb} and Q_{swb} is only enabled for rivers to reduce the amount of variable processes and understand the coupling for rivers before moving on to other surface water bodies in the future. For this the coupling is already implemented for all surface water bodies but not switched on. Figure 6.2 shows this exchange of information for the temporal and spatial domain. In the current implementation h_{swb} starts at the 30th percentile (P_{30}) of the 30″ DEM

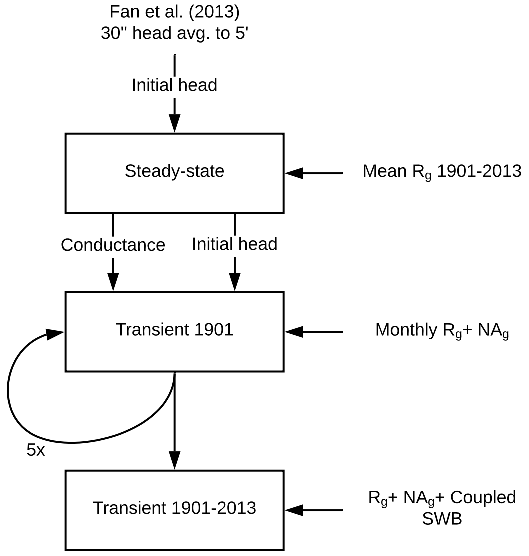

FIGURE 6.1: Spin-up of WaterGAP-G^{3}M.

as described in chapter 3. h_{swb} is then updated as a change in elevation from the second month on. Similar, R_G and NA_G are updated every month even if WaterGAP computes R_G also on a daily resolution. To dampen the sudden changes between the monthly timesteps a future implementation should consider weekly updates as already shown in Fig. 6.2 as gray arrows. Calculated exchanges between the surface water bodies and the groundwater are then transferred to WaterGAP at the end of each month. Again this could also be implemented as weekly update.

On the spatial domain, change in h_{swb} is applied equally to all gridcells within a 0.5° cell. This can be changed into a more sophisticated approach that scales the change by the $5'$ river size and/or calculated exchange flows in the last time-step (further discussed in section 6.4). R_G, and NA_G are distributed equally to each $5'$ gridcell within a 0.5° gridcell.

Due to climate conditions or flows to the groundwater, streams can run dry. This needs to be accounted for in the coupling process as the $5'$ cells then should no longer be allowed to lose any water, even if the river stage is above the simulated hydraulic head of the aquifer. In the current implementation all streams that are calculated to run dry in WaterGAP result in a h_{riv} change in G^{3}M to the bottom elevation of the river $RBOT$ (see chapter 3). The implementation of G^{3}M-f is altered in a way that as soon as $h_{riv} = RBOT$ the calculated flow is 0 and no more water is lost to the groundwater. Should the simulated aquifer head move above $RBOT$ an inflow to the river is calculated. If the now gaining condition results in a rewettening of the river in WaterGAP, and thus rising h_{riv}, this will allow the river in G^{3}M to possibly lose water in the next timestep.

The integrated model is shown in Fig. 6.3 as part of one WaterGAP-G^{3}M cell similar to the previous graphical descriptions of WaterGAP in Müller Schmied et al. (2014), which also features an extensive analysis of the shown processes. The major change compared to WaterGAP 2.2d is the now possible two-way flow between the groundwater and the surface water bodies calculated based on simulated hydraulic heads shown as green and red arrows. The vertical water balance of WaterGAP is only affected when capillary rise is integrated into the model.

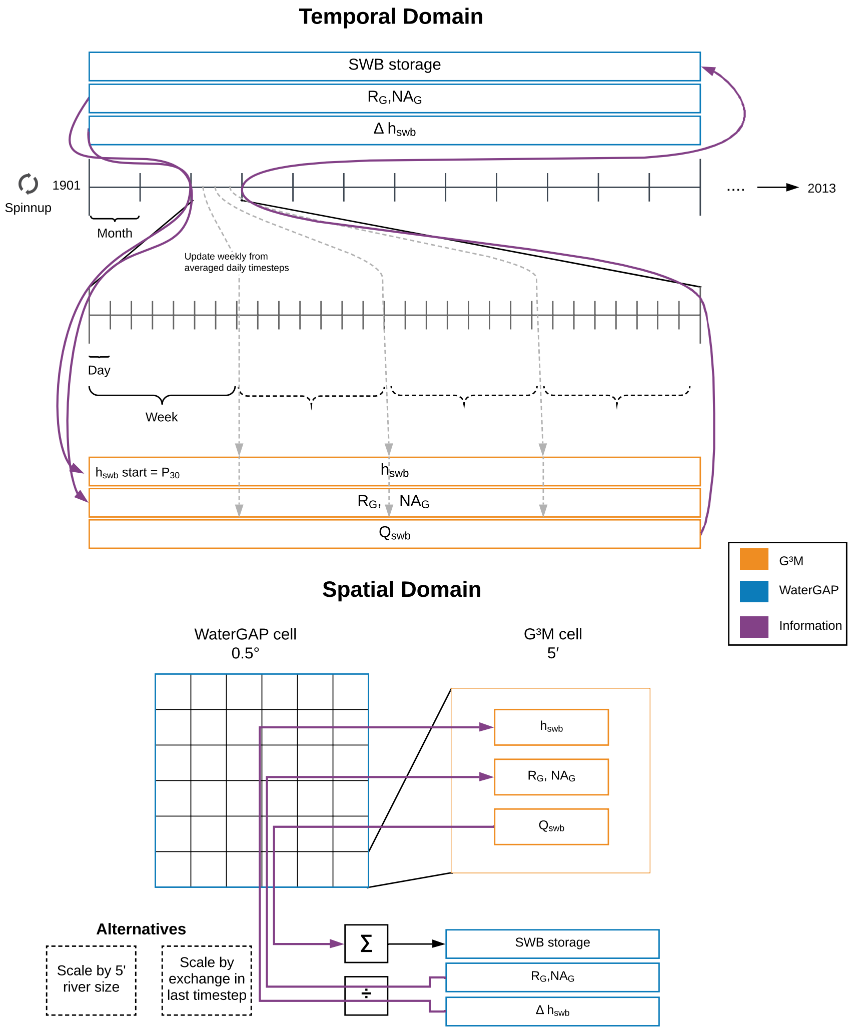

FIGURE 6.2: Coupling of WaterGAP and G^{3}M in the temporal and spatial domain. Weekly updates are not implemented yet (gray dashed arrows). Variables belonging to the two models are colored accordingly (orange for G^{3}M and blue for WaterGAP). The direction of information flow between the two models is depicted as solid purple arrow.

6.2.2 A possible capillary rise implementation

Capillary rise is to be implemented as a flow that improves the evapotranspiration calculated by WaterGAP. This flow is not yet implemented in G^{3}M but can be added as additional external flow component in G^{3}M-f. For future developments a possible implementation is described here based on Haasnoot et al. (2014) with the capillary rise Q_{cr} [LT^{-1}] computed as

$$Q_{cr} = C_{max} \times C_f \times C_{soil} \tag{6.2}$$

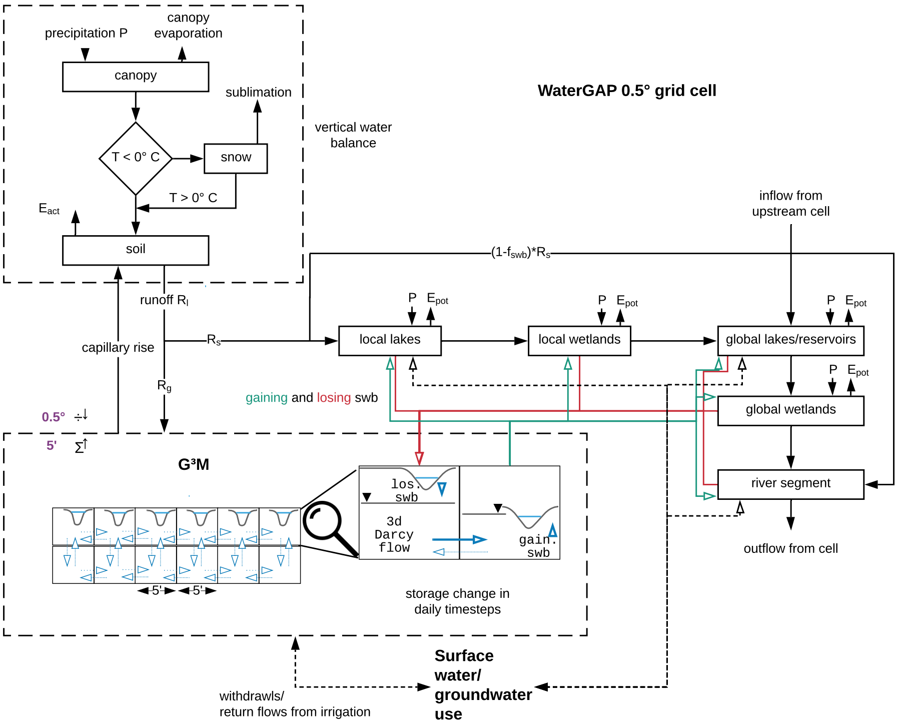

FIGURE 6.3: Fluxes and storages of one 0.5° WaterGAP-G^{3}M cell. Boxes represent water storage compartments (a dashed box the groundwater model), arrows water inflows and outflows. Colored arrows represent the one directional flows of gaining and losing conditions of surface water bodies.

where C_{max} [LT^{-1}] is the maximum capillary rise as a function of soil type and potential evapotranspiration PET, C_f [-] a factor calculated based on the depth to groundwater

$$C_f = \begin{cases} 0 & wtd \geq D_c \\ 1 - \frac{wtd - 0.5 \times D_r}{D_c - 0.5 \times D_r} & \frac{1}{2} D_r < wtd < D_c \\ 1 & wtd \leq \frac{1}{2} Dr \end{cases} \tag{6.3}$$

where D_r [L] is the rootzone depth and D_c [L] the water table depth wtd [L] at which there is no more capillary rise (can be defined e.g. as function of soil type and PET), and Cap_{soil} [-] as

$$C_{soil} = max(0, (1 - \frac{S}{S_{max}})) \tag{6.4}$$

where S is the soil moisture and S_{max} the soil moisture capacity. To implement this an accurate estimate of the global water table depth is necessary.

6.2.3 A physically based conductance approach

An additional possible alteration to G^{3}M is an alternative conductance approach. Currently the conductance of the surface water bodies c_{swb} [L^{2}T^{-1}] is described by the equation (see also chapter 3)

$$c_{swb} = \frac{KLW}{h_{swb} - B_{swb}} \tag{6.5}$$

where K [LT^{-1}] is the conductivity of the aquifer, L [L] the length of the surface water body, W [L] the width, and B_{swb} [L] is the bottom elevation. It is applied to rivers only in losing conditions (see chapter 3). This approach has been criticized by Morel-Seytoux et al. (2017); Morel-Seytoux (2019a,b) as an empirical approach that can only be obtained through calibration. Morel-Seytoux et al. (2017); Morel-Seytoux (2019b) proposes an analytical and physically based estimate of the exchange flow for coarse-scale models based on river and aquifer properties. The following summarizes the approach as one possible implementation for the river conductance c_{riv} (again only for the losing condition) that is already implemented in G^{3}M-f.

$$c_{riv} = 2LK\Gamma \tag{6.6}$$

where L is again the length of the river, K the saturated hydraulic conductivity of the aquifer and Γ a factor

$$\Gamma = R_f \frac{\Gamma_{iso}^{rect}}{\left(1 + Re\Gamma_{iso}^{rect}\frac{\Delta}{D_{aq}}\right)} \tag{6.7}$$

where Re is a reduction factor

$$R_f = 1 - 0.333 \times \xi - 0.294 \times \xi^2 \tag{6.8}$$

where ξ is defined as

$$\xi = (1 - \sqrt{d_p}) \times (1 - \rho) \tag{6.9}$$

where d_p is the degree of penetration defined as

$$d_p = D_{river}/D_{aq} \tag{6.10}$$

where D_{river} is the depth of the river and D_{aq} the average aquifer depth.

$$\Gamma_{iso}^{rect} = \frac{\Gamma^{rect}}{\left(1 + \Gamma^{rect}\frac{\Delta_{std}}{D_{aq}}\right)} \tag{6.11}$$

where δ_{std} is the distance excess over the far distance as

$$\Delta_{std} = \sigma_{fd} - (2 \times D_{aq}) \tag{6.12}$$

where σ_{fd} is defined as

$$\sigma_{fd} = 2 \times \frac{D_{aq}}{\rho} \tag{6.13}$$

and ρ as

$$\rho = \sqrt{ani} \tag{6.14}$$

where ani is the vertical anisotropy in the aquifer as $\frac{K_{vert}}{K_{hoz}}$. Γ^{rect} in Eq. 6.11 is defined as

$$\Gamma^{rect} = \Gamma_{dist}\left(1 + a_1 d_p + a_2 d_p^2\right) \tag{6.15}$$

where a_1 and a_2 are estimated by the Table 6.2. The normalized wetted perimeter used in Table 6.2 is defined as

$$W_p^N = \frac{W}{D_{aq}} \tag{6.16}$$

TABLE 6.2: Parameters for conductance equations.

Condition	a_1	a_2
$W_p^N < 1, d_p < 0.2$	0.89	-2.43
$W_p^N < 1, d_p < 0.5$	0.538	-0.387
$W_p^N < 3, d_p < 0.2$	0.819	-1.34
$W_p^N \geq 3, d_p < 0.2$	0.89	-2.43
else	0.89	-2.43

where W is again the width of the river. Γ_{dist} in Eq. 6.15 is defined as

$$\Gamma_{dist} = \frac{1}{\left(2\frac{1}{\pi log(\frac{2}{1-\sqrt{e^{-\pi W_p^N}}})}\right)} \tag{6.17}$$

Δ in Eq. 6.7 is defined as

$$\Delta = \frac{G}{4} - B - \sigma_{fd} \tag{6.18}$$

where G is the length of the grid cell and B

$$B = \frac{W}{2} \tag{6.19}$$

.

6.3 Results

Results shown in this section are based on a version of WaterGAP-G^{3}M that features coupled rivers, groundwater recharge, and net abstraction from groundwater, without coupling other surface water bodies. This setup reduces the number of coupled processes to gain an understanding on what the coupling entails and what might need to be improved before coupling all surface water bodies.

6.3.1 Comparison of conductance approaches in steady-state conditions

The approach described in section 6.2.3 was applied as river conductance instead of the old Eq. 6.5 while keeping the approach described in chapter 3 that derives conductance based on the groundwater recharge when the aquifer head is above the river head elevation. Figure 6.4 shows the effect for a steady-state simulation. In general the new approach (Fig. 6.4 (b)) shows similar spatial patterns contrarily to the old approach (Fig. 6.4 (a)). Higher global river conductances especially in the humid regions with large wetlands can be observed (Fig. 6.4 (b)). To understand the impact of the new approach and the reasons for the different patterns a more in depth analysis e.g. a comparison of model performance is required.

Figure 6.4 depicts the impacts on the hydraulic heads as head difference between the the two approaches for steady-state simulations. In the Kongo where the conductance is increased the heads increased by more than 10 m. North and south of Africa the heads even decreased whenever the conductance also increased.

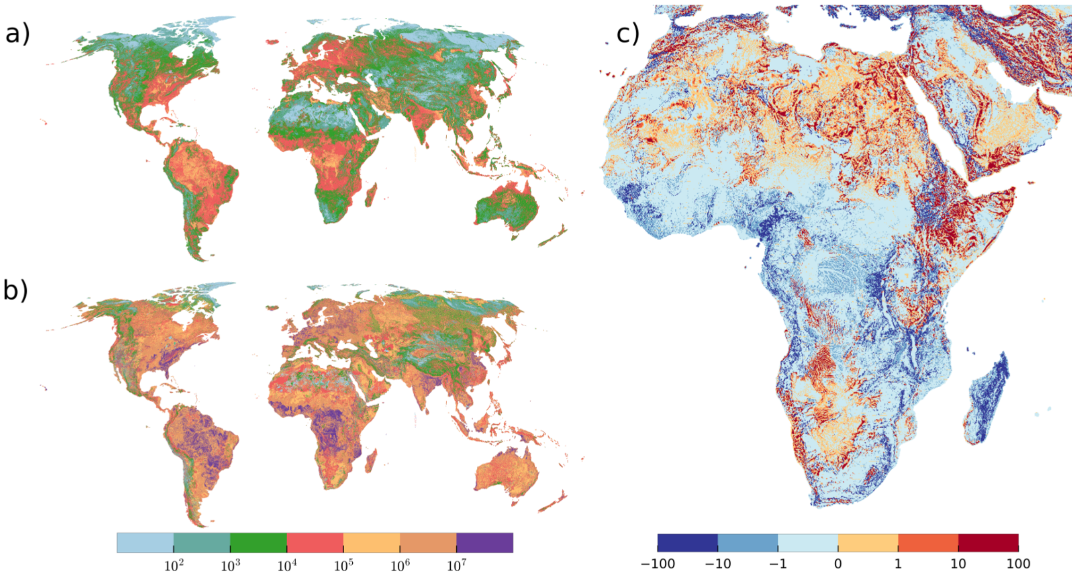

FIGURE 6.4: Comparison of conductance approaches. a) Global river conductance [m^2d^{-1}] of the standard approach and b) the approach proposed by Morel-Seytoux et al. (2017) and c) the steady-state hydraulic head difference [m] (standard minus Morel-Seytoux et al. (2017)) between the approaches for Africa.

6.3.2 Transient budget

In- and outflows were aggregated over all cells and are shown in Fig. 6.5 for the spin-up phase of a two-layer model. Equally to the MODFLOW notation the flows are calculated relatively to the cell. IN means into the cell and OUT out of the cell. A larger storage IN means that water has been removed from pore space and is associated with a decline in head. Similarly, an increase in river IN means that more rivers are losing water to the aquifer and there is more *in*flow to the model cell.

The first step shows the difference between the steady-state and the first spin-up year. Total budget error, a percentage of difference in and outflows as an indicator of numerical goodness (see chapter 3), shows that the numerical solution is close to the analytical solution even though it fluctuates in the beginning but approaches zero with the continuing spin-up. The storage, on the other hand, shows first a closely related pattern to R_g for the outflow of water from storage (IN flow) and a decreasing trend for the inflow into storage (OUT flow). In the middle of the 4th year this changes suddenly. Both flows increase exponentially (y-axis is log-scaled) with the same magnitude. Because the flows cancel each other out an increase is not affecting the total budget error, but most likely leads to inaccurate heads and an inaccurate storage. This is likely caused by an instability in the vertical conductance equation that governs how flow is treated if cells are dry. This is possibly happening in mountainous areas where simulated hydraulic heads are below the cell elevation. An indication is another simulation with only one layer shown in Fig. 6.6.

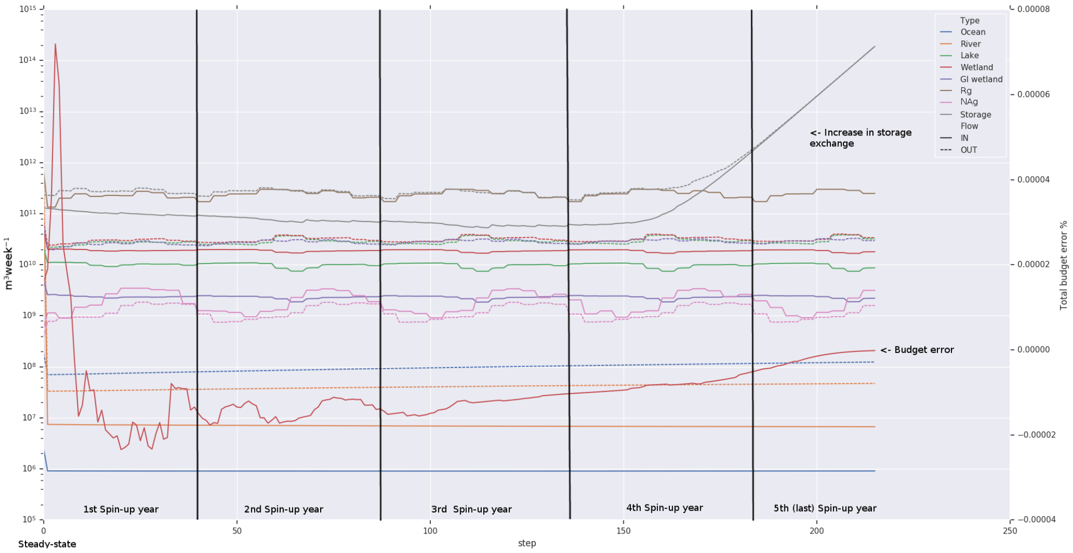

FIGURE 6.5: Global sums of in and outflows to or from the groundwater cells for a two-layer WaterGAP-G^{3}M. The right y-axis additionally shows the total budget error.

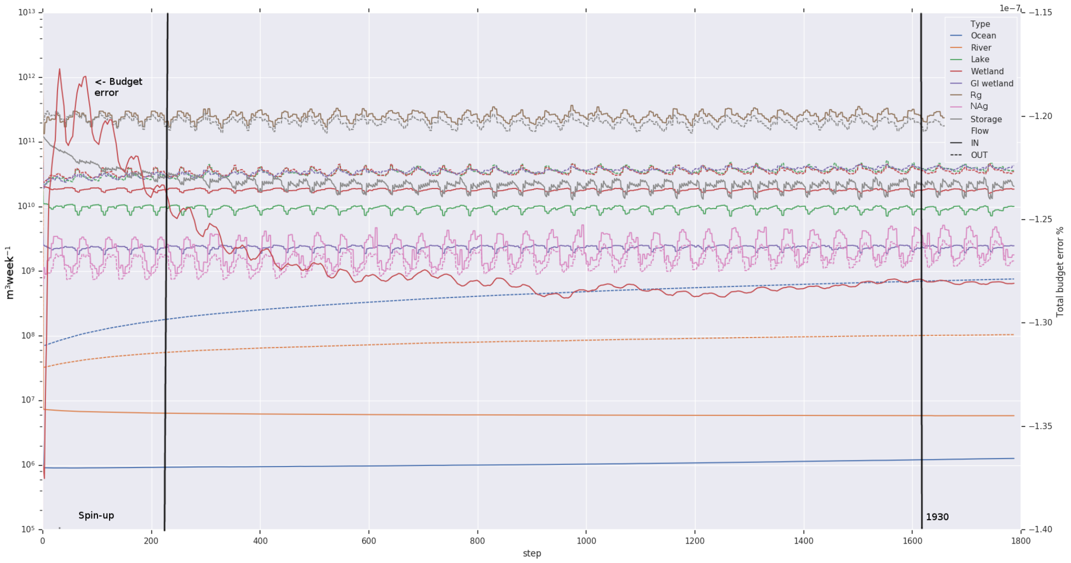

FIGURE 6.6: Global sums of in and outflows to or from the groundwater cells for a one-layer WaterGAP-G^{3}M. The second y-axis additionally shows the total budget error.

Similar to the two-layer model the R_g pattern in Fig. 6.6 is equal for the spin-up period but then changes within the years afterwards. The total budget error is closer to zero than the two-layer model suggesting a larger numeric stability. Compared to the two-layer model it is negative and equilibrates at 1.28×10^{-7}. Due to the larger numeric stability and decreased number of total cells the total runtime is decreased by 10 fold for the one layer model. To show that no sudden storage exchange rate increase is present at a later stage in this model the plot shows the simulation period till 1930. The flow into storage (OUT flow) is closer aligned to R_g in the spin-up phase and gets smaller by volume with each year but still resembles the R_g pattern. Outflow of storage (IN flow) is again showing a decline in volume and then starts to resemble the R_g pattern as well. In general the outflow of storage is globally smaller than the inflow into storage.

Flow from losing rivers drop at the start of the spin-up phase and stay constant. Possibly this has two reasons: Firstly, in regions where rivers are losing the head is not increasing enough to turn them into a gaining state. Secondly, multiple rivers are dry in the beginning of the simulation period, which prohibits them from losing any more water to the groundwater. This then also decreases the heads in these regions further if the groundwater is not recharged by the rivers. It needs to be investigated whether this is a coupling error or a different spin-up strategy is required. The flows into the rivers increase steadily; faster in the spin-up and slower afterwards. An equal pattern with different flow volumes can be observed for the ocean boundary. Heads are generally increasing and thus necessitate the two boundaries to drain more water. Flows into and out of other surface water bodies, lakes, wetlands, and global wetlands, resemble R_g and are in general relatively stable. All of these surface water bodies are not coupled in this version. NA_g is globally smaller by volume than the other flows except rivers and the ocean boundary. The recharge through surface water irrigation can be observed as generally higher than the groundwater abstractions for that simulation period.

6.3.3 Hydraulic head development

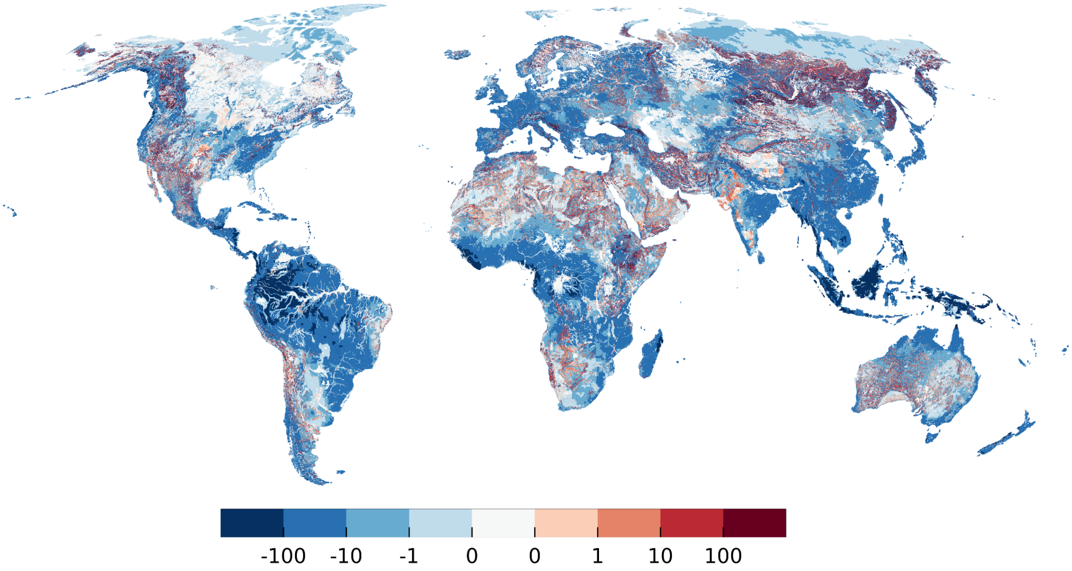

FIGURE 6.7: Difference [m] of steady-state head and head after the transient spin-up. Blue indicates that the heads are higher after the spin-up.

To further investigate how the heads develop during the spin-up Fig. 6.7 shows the difference from the initial steady-state head. Due to the large storage exchange of the two-layer model this analysis and the following outline will focus on the one-layer model. In general the spin-up leads to much higher heads in the tropical convergence zone, Europe, and the Eastern USA. It is likely that this increase is overestimating heads and is due to the river coupling that is not able to drain enough of the incoming recharge. What stands out is the unchanged hydraulic head in the Amazon and the Kongo. This is likely to the unchanged drainage of the global wetlands (they are not coupled yet) in these areas, which already showed a large influence in the steady-state model. Other areas that did not experience much change in head are large parts of Canada, Sweden, Finland, and Tibet. Again this is likely through the unchanged major drainage components; lakes and wetlands are dominant in these regions according to the sensitivity analysis presented in chapter 4. Decreases in heads are scattered but can mainly be observed in mountainous and arid regions e.g. the Andes and Sahara. Large decreases in head occur often together with large increases in neighbouring cells e.g. at the border of Russia and Mongolia. These decreases in heads are likely a result of now dry rivers, which lost enough water to keep the head level in the steady-state.

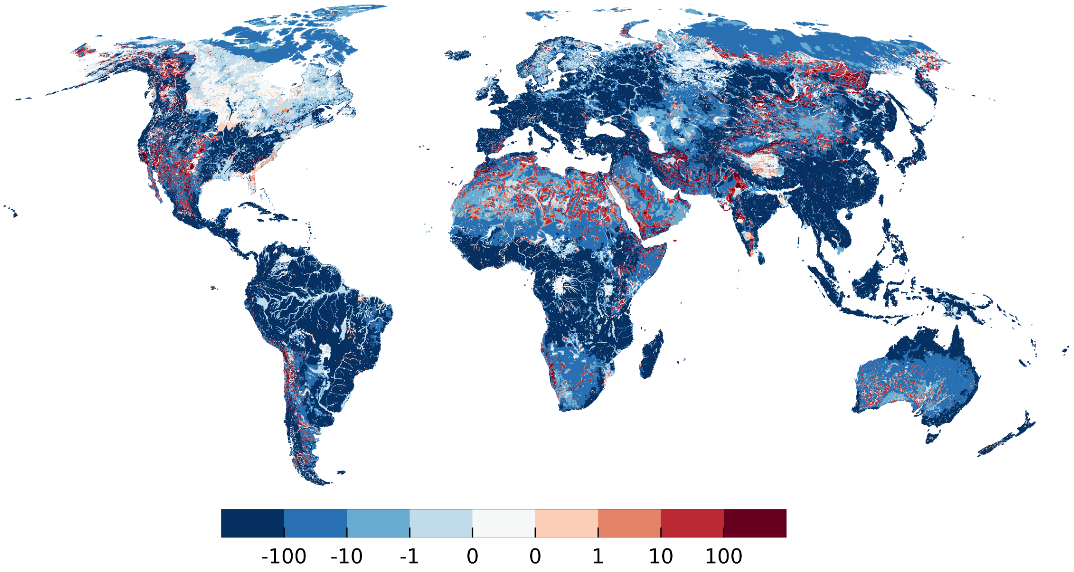

FIGURE 6.8: Difference [m] of simulated head in January 1901 and simulated head in January 2013. Blue indicates that the heads are higher in 2013.

Complementary to the spin-up phase a simulation till 2013 shows an increase in simulated head (Fig. 6.8). Again an increase stands out in the tropical convergence zone and in Europe. Areas with large wetlands and lakes like in Canada, the Amazon, and Sweden show little difference over the simulation period because of the uncoupled surface water bodies. A large decrease in head can be observed in the Central Valley, the High Plaines Aquifer, the Northern Mississippi, Namibia, Saudi Arabia, Iran, and the Three-state region in West India all of which are areas that are known to be affected by groundwater depletion and are similar to the areas shown in Döll et al. (2014, Fig. 3).

Multiple areas show a mixed decrease and increase of hydraulic heads like the Sahara, Australia, and the Andes. This is likely caused by the large gradients and the insufficient drainage by the coupled rivers.

6.3.4 Simulated heads compared to observations

Figure 6.9 shows a comparison of the relative head change (relative to the beginning of the time series) measured by USGS (United States Geological Survey) wells in the Central Valley and the relative simulated head change by WaterGAP-G^{3}M. Alternative representations like head anomaly or mean seasonal cycle (not shown here) showed that heads in parts of the valley steadily, and unrealistically, increase or decrease depending on the region. Most of the observation wells of the USGS are available in the North of the Central Valley. Only simulated cells that contain at least one

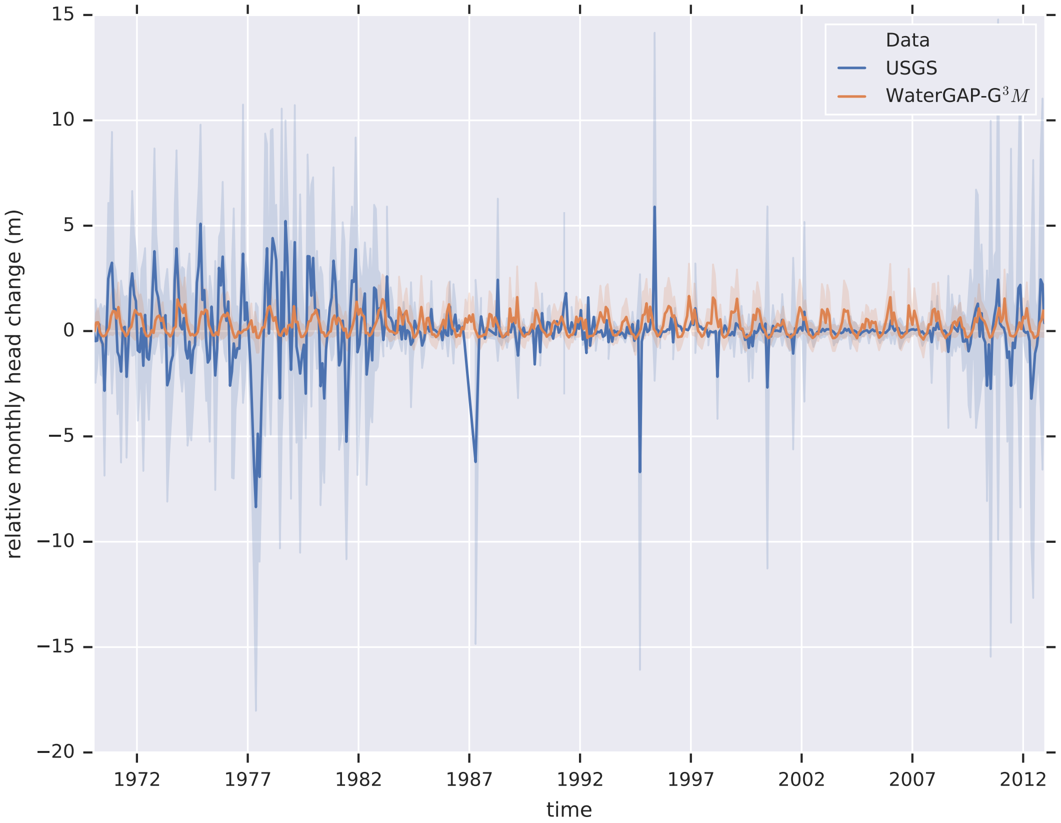

FIGURE 6.9: Relative head change to start of time series in the Central Valley based on 2902 USGS well observations in 74 WaterGAP-G^{3}M cells. The solid line shows the mean, the opaque the standard deviation.

observation well are compared. Multiple observations per cell are not aggregated to show the full variability. It is evident that the relative head changes are not as big in the model as the observed for the 70s and the beginning of 2008. Aligned with the alternative representations (not shown) the majority of head changes is positive suggesting again a hidden trend in the model. Because most cells are in the North of the valley were depletion is not that severe yet that aligns with the global picture of head overestimations. Nevertheless, the response to seasonal variability is clearly visible and roughly aligns with the observations. It is likely that this response can be improved by choosing different storage coefficients and improving the coupling scheme which is likely responsible for the inherent trend.

6.3.5 Comparison to two Central Valley models

CVHM (Faunt et al., 2016) and C2VSim (Brush et al., 2013) are two established hydrological models of the Central Valley in California. CVHM (Central Valley Hydrologic Model) is a detailed three-dimensional model of the Central Valley that simulates water demand and supply as well as surface water and groundwater flows on monthly timesteps with the modeling software MODFLOW. It consists of 10 layers to a depth of about 550 m and is divided into 1 mile by 1 mile cells. C2VSim (California Central Valley Groundwater-Surface Water Simulation Model) simulates groundwater and surface flows using the Integrated Water Flow Model (IWFM) on a finite element grid of 1392 elements and 3 layers. In comparison CVHM is a more

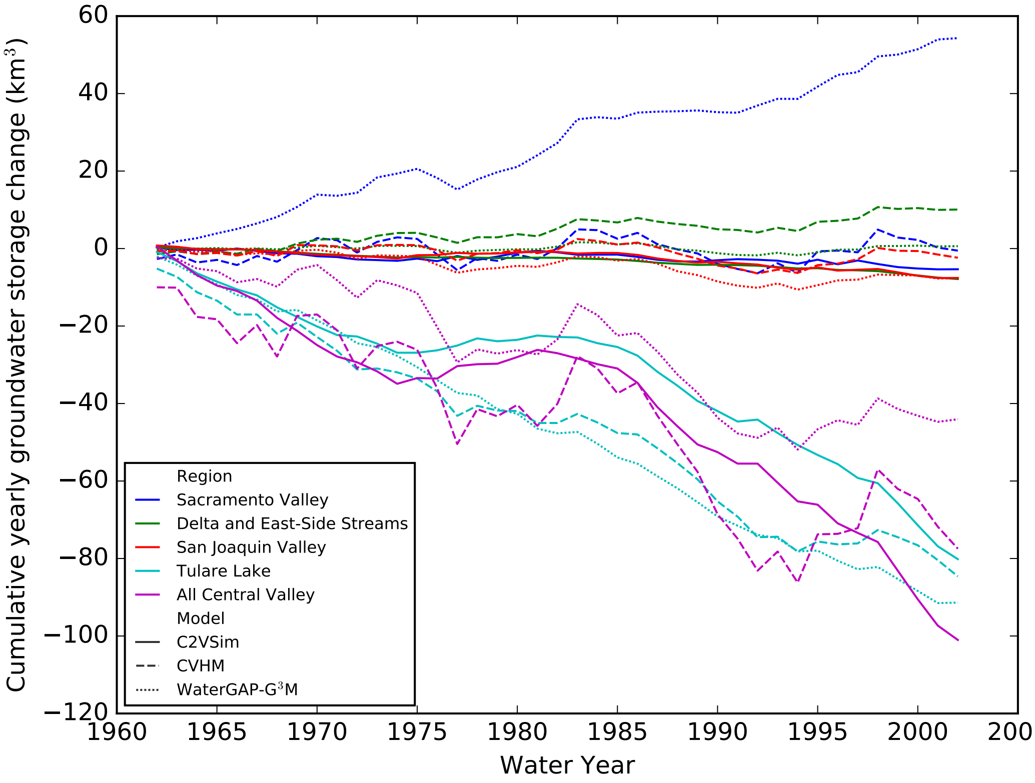

FIGURE 6.10: Simulated cumulative storage change in the Central Valley of two established regional models (CVHM and C2VSim) compared to the one-layer WaterGAP-G^{3}M (1791 model cells of G^{3}M in the Central Valley).

traditional groundwater model and C2VSim a hydrological model that e.g. also contains routed surface water flow.

Figure 6.10 shows how the one-layer WaterGAP-G^{3}M compares to these two models based on cumulative calculated storage change from 1962 until 2003. The change in storage is compared for the whole Central Valley as well as to four subregions as defined by Brush et al. (2013). These regions are defined by the major hydrologic characteristics of the four cardinal points relative to Sacramento. *Sacramento Valley* is north of the Sacramento–San Joaquin River Delta and is drained by the Sacramento River. *Delta and East-side Streams* define San Francisco bay and the streams leading to that delta, mainly the Sacramento and San Joaquin River. *The San Joaquin Valley* lies south of the Sacramento–San Joaquin River Delta and is as well drained by the San Joaquin River. *Tulare Lake* is a dry lake in the southern San Joaquin Valley. The lake dried up after its tributary rivers were diverted for agricultural irrigation and municipal water uses.

Over the whole Central Valley WaterGAP-G^{3}M performs very similar to CVHM even if the storage decline is not as severe. C2VSim computes a less diverse decline with a continues trend from 1980 until 2003, whereas CVHM and WaterGAP-G^{3}M show a recovery-period in e.g. the beginning of 2000. In the south (Tulare Lake) this is reversed as CVHM and WaterGAP-G^{3}M simulate a very similar steep decline in storage and C2VSim a recovery in the 80s. While CVHM and C2VSim compute only little changes for the Sacramento Valley WaterGAP-G^{3}M simulates a continuous increase in storage. While the trend disagrees with the two established models the peaks are again similar to the CVHM model. This trend aligns with the increase in head seen in the previous section for parts of the Central Valley. Likely this is again connected to the decreased drainage capabilities of the large rivers in that regions, but could also be caused by losing wetlands that are not coupled yet. For the other regions, west and north of Sacramento, WaterGAP-G^{3}M simulates a similar smaller change in storage compared to the whole Central Valley. The overall difference in the decline for the complete Central Valley is likely to be explained by the increased trend in the Sacramento Valley.

6.4 Discussion

This chapter (study) presented a partially coupled WaterGAP-G^{3}M that is already able to reproduce the storage decline in the Central Valley similarly to established regional models. Still, the integration of G^{3}M into WaterGAP is not complete and requires additional investigation on the temporal and spatial coupling. de Graaf et al. (2017) coupled their model on fortnightly timesteps as best trade-off for efficiency and impact on streamflow performance (personal communication Marc Bierkens, 2019). It needs yet to be investigated what impact the integrated model has on the simulated streamflow of WaterGAP-G^{3}M and how it differs from previous versions without an integrated gradient-based groundwater model. WaterGAP computes groundwater recharge on daily timesteps, thus moving from a monthly coupling to a weekly or fortnightly coupling is feasible and should be tested next. On the spatial domain this chapter hinted two alternatives to the equal distribution of river head changes: (1) a distribution scaled by $5'$ river size or (2) a distribution scaled by the exchange flow in the last timestep. The latter assumes that the river with the most exchange in the last timestep is likely the main river simulated in WaterGAP and thus should receive the most change in head. It is to be investigated if that assumption holds and how the approaches differ from each other concerning model performance. In general, the river coupling needs to be investigated more closely as the current coupling leads to a significantly decreased influence as a drainage component in the groundwater model. Of course, it is furthermore necessary to complete the coupling of other surface water bodies like lakes and wetlands. The code for this coupling is already implemented but has not been tested yet.

The alternative approach for river conductance results in generally higher global conductances. It is currently not clear if it supports a better performance of the groundwater model. Additionally, the approach is very complex and it is questionable if the more physically based approach is currently the correct choice for a rather conceptual global model.

WaterGAP-G^{3}M is intended to simulate groundwater on two different layers where the lower layer represents slow groundwater flows that are not directly influenced by the coupled surface water bodies. First transient simulations of a two-layer WaterGAP-G^{3}M showed that the vertical flows between the two layers are currently inducing storage instabilities that hint that a technical or conceptual error is still present in the model. The center of the issue might be the correction that is applied if a partially saturated cell still receives vertical flow from a fully saturated upper cell. The calculation that adjusts the equation is complex and possibly not fitted for the present model configuration (see also Harbaugh (2005, chapter 5.7) and appendix A). In general the vertical flow correction, as simulated hydraulic heads cross between layer boundaries, has received a lot of criticism in the MODFLOW community (personal communication Steffen Mehl, 2019) and should be examined closely for future model development.

With one layer the model shows a stable numerical behavior and a reasonable response to seasonally changing groundwater recharge and net abstractions from groundwater. Unfortunately, the current coupling of rivers seems to reduce their function of major drainage and water supply component in the global budget. This can also be seen in the simulated head differences between the start and end of the simulation period showing relatively stable results in the regions where other uncoupled surface water bodies, like lakes and wetlands, exist. As a result of the reduced drainage capabilities an unreasonable increase in head is observable for other regions with no large non-river surface water bodies. This aligns with the head changes shown for the Central Valley. An improved river coupling is likely able to remove that persistent head increase. Additionally, an improved storage coefficient based on the geology using GLHYMPS (Huscroft et al., 2018) or through calibration would further improve the results. de Graaf et al. (2017) used a very high specific yield over 30% after calibration. It needs to be investigated if such a value is necessary for a global scale conceptual model to fit the amplitude of local well observations.

Even considering the mentioned issues the uncalibrated one-layer model is already able to show a very promising performance of simulating the groundwater storage decline in the Central Valley compared to two established regional models. This comparison should be continued to gain more insights into how WaterGAP-G^{3}M performs in a region largely affected by groundwater depletion that offers a lot of data and expert knowledge about the interaction of groundwater, surface water and human water use. Eventually, this will result in a global model that is able to provide simulation results in regions where no local or regional models are available.

Chapter 7

Synthesis and Conclusions

Groundwater is an essential source of freshwater and an important component of the global hydrological cycle. Until recently it was not well represented in GHMs. In this thesis a new groundwater modeling framework is presented and used to build a global groundwater model that is coupled to a state-of-the-art GHM.

Based on the previous chapters and the presented scientific results the research questions stated in section 1.3 are discussed and the scientific advances summarized. The synthesis is separated into the four main research questions and discussed along the sub-questions. The chapter closes with an outlook on future research.

RQ 1: Which kind of software architecture is necessary for a complex scientific model intended to simulate groundwater on a global scale as efficiently as possible providing the capability to be coupled to an existing GHM?

RQ 1.1: What is a possible software architecture that enables to build global groundwater models that can efficiently be coupled to GHMs?

The proposed architecture in chapter 2 shows how an implementation can be modular while being computationally efficient. It allows for a flexible implementation of new process and enables running the simulation on different temporal and spatial scales. For an efficient coupling to another model the logical separation between writing outputs to files and the calculation of processes is key. A separated system allows to calculate results based on available in memory information of the model it is coupled to without writing the data to disk first. If it is necessary to write files to a disk and then read them into another model, which is the case when coupling a model with MODFLOW, two issues arise: (1) The two models need to communicate when the correct information is available and decide on a common data format. Leading to avoidable synchronization issues and adding complexity. (2) Write and read operations will result in idle computation time that is wasted, so the goal needs to be to access the information directly in memory. However, this is possible with the presented model framework G^{3}M-f.

RQ 1.2: What means are necessary to ensure high quality in a complex scientific software?

A robust scientific software is required to produce reproducible results and enable model inter-comparison (Hutton et al., 2016). In this thesis three methods are proposed and implemented to ensure a high software quality. (1) First, the architecture needs to be designed to anticipate the fast changing nature of research software. It needs to be extensible (see appendix B) and allow continuous changes to adapt to new requirements. An established software engineering practice is to enforce a high degree of separation of concerns and use modern versioning software to accompany the development process. (2) The model computes physical processes that rely on the correctness of equations. What is self-evident in every science, to check the consistency of the units used in the equations, needs to be part of robust research software as well. Without it we cannot ensure the correctness of the solution and maintainability of the software. (3) And lastly, automated testing of the application can not only detect mistakes during the development process but also ensure the correctness of the scientific software.

RQ 1.3: What kind of equations and approaches are best for this spatial scale?
The PCR (Preconditioned Conjugate Gradient) solver, a commonly used solver for groundwater models, proved to produce stable and fast steady-state conditions (chapter 3). On the other hand it struggles with non-linearities especially in the fully coupled model (chapter 6). It is likely that a multi-grid solver can improve the speed of the solution process as a result of the size of the matrix problem. Additionally, a parallel preconditioner could furthermore speed up the solution.

The equations traditionally used in established models like MODFLOW were successfully applied to simulate groundwater on a global scale. The parameterization of these equations however is challenging. Choosing a conductance for surface water bodies on the global scale is difficult because the parameters cannot be observed directly and are almost always a calibration parameter in regional groundwater models (Morel-Seytoux, 2019a). To simulate surface water to groundwater flows the equations presented in this thesis rely on a combination of an approach by Miguez-Macho et al. (2007) and a traditional approach often used in MODFLOW which was also heavily criticized lately (Morel-Seytoux, 2019a,b) and is discussed in detail in chapter 6. Because surface water body conductance cannot be observed directly it is currently not possible to tell which approach is better. It is worth to invest more time in improving the estimation of this parameter as the sensitivity study in chapter 4 showed that the heads are highly sensitive to changes in the surface water body parameterization.

RQ 2: Is it possible to simulate groundwater on a global scale with a gradient-based approach and what do global groundwater processes look like?

RQ 2.1: How big are lateral and vertical fluxes of groundwater and how do they compare to other flows?
Based on the steady-state results presented in chapter 3 the percentage of recharge that is transported through lateral flow to neighboring cells depends on five interdependent factors: (1) the hydraulic conductivity between the cells (2) groundwater recharge applied to the cells (3) the flows from and to surface water bodies, (4) their conductance, and (5) the hydraulic head gradients between the cells. In large areas of the globe, where groundwater discharges to surface water bodies, the lateral flow percentage is less than 0.5 % of the total groundwater recharge to the grid cell. Most of the groundwater recharge in a grid cell is then simulated to leave the grid cell by discharge to surface water bodies. In regions where surface water bodies recharge the groundwater, lateral flows exceed groundwater recharge and increasingly when there is no outflow possible other than through lateral flow (over 100 % of groundwater recharge).

RQ 2.2: Which surface water bodies lose water, which gain water, in what amounts, and how are they distributed?
In the steady-state model G^3M 93 % of all grid cells contain gaining rivers, and only 7% losing rivers. Gaining lakes and wetlands are found in 12 % and 11 % of the cells, respectively, whereas only 0.2 % contain a losing lake or wetland. Rivers with riparian wetlands such as the Amazon River or areas dominated by wetlands and lakes receive comparably small amounts of baseflow as most of the groundwater is drained by the wetland. Gaining rivers, lakes and wetlands with large baseflows can be found in the Congo Basin as well as in Bangladesh and Indonesia, where groundwater recharge is high. Low values occur in dry and in permafrost areas where groundwater recharge is small.

Losing surface water bodies are caused by a combination of low groundwater recharge and steep mountainous terrain. While the steep Himalayas receive enough groundwater recharge to have gaining surface water bodies, this is not the case for the much dryer mountain ranges around the Taklamakan desert in Central Asia, or mountainous Iran where surface water bodies are losing. Rivers lose more than 100 mm year^{-1} in Ethiopia and Somalia, West Asia, Northern Russia, the Rocky Mountains and the Andes. The Nile is correctly simulated to be a losing river as well as the the man-made Lake Nasser. On the other hand, no losing stretches are simulated along the Niger and its wetlands and almost none in the North-eastern Brazil even though that losing conditions are known to occur there. This might be linked to the surface water body elevation and an inadequate representation of the local geology.

RQ 2.3: How should we treat groundwater in mountainous regions?
Groundwater movement below mountains has only been investigated through tracer studies e.g. Manning and Caine (2007) and is not well understood yet. Studies exists on very local aquifers e.g. Tague and Grant (2009) but it is still unclear how deep and how fast groundwater infiltrates through fractures in bedrock and how it moves laterally. Modelling the groundwater in mountainous regions has two major challenges. Firstly, representing the complex geology in mountainous with the existing datasets. And secondly, verifying the simulated average depth to groundwater. In the near future it will not be possible to observe how much water is stored below mountains and thus the average simulated hydraulic head is impossible to verify. On the other hand observations from perched aquifers suggest a much shallower groundwater than the one simulated by the model. Additional research is necessary to better represent these local aquifer systems in the global model. Results of the steady-state model show heads that drop far below the model bottom as there is no impermeable layer that would forbid that as implemented in other models e.g. Parflow (Maxwell et al., 2015). This leads to the issue that the transmissivities in these areas cannot be computed based on the saturation of the cell as the head is already below the prescribed bottom elevation. Either this then leads to no-flow boundaries practically excluding areas with very low heads or a large increase in the model layer size is necessary. In the presented model the transmissivity is calculated based on the assumption of a fully saturated layer. Disregarding mountainous areas altogether also is not a solution as this would exclude very large portions of the world where no simulation of losing or gaining conditions could be simulated for the GHM.

RQ 2.4: How much groundwater leaves through the ocean boundary?
In the steady-state model 1.3*10^7 m^3day^{-1} of water flow from the groundwater to the ocean. This is less than 0.1% of the total groundwater recharge (Reinecke et al., 2019a, Fig. 3). In the transient model this flow into the ocean is increasing possibly due to the globally overestimated heads.

RQ 2.5: How well does the developed groundwater model represent world-wide observations in steady-state conditions?
The steady-state G^3M performs reasonably well in flat areas compared to mountainous regions. It is evident that model performance deteriorates with increasing land surface elevation and positively correlates with variations of land surface elevation within each grid cell. The comparison of aggregated observed head is distorting the performance of the model. Each model cell is as large as 9 by 9 km at the Equator and can contain very diverse measurements. Currently, no method is available to reliably judge whether the average simulated groundwater head is representative for the observed point measurements.

RQ 3: What uncertainties are inherent to global groundwater modeling and can we quantify them?

RQ 3.1: What parameters have the most impact on the model results and how are uncertainties distributed?
Globally simulated steady-state hydraulic heads are equally sensitive to hydraulic conductivity, groundwater recharge and surface water body elevation, although parameter sensitivities vary regionally. Maps of regional sensitivity distribution were created and published in Reinecke et al. (2019b). The surface water body elevation is most important in mountainous regions and regions with low recharge for the head distribution and dominant for the flow between groundwater and surface water in the Rocky Mountains, Andes, Hijaz Mountains in Saudi Arabia and the Himalaya. Groundwater recharge is most influential in the Tropical Convergence Zone and in the northern latitudes. Hydraulic conductivity is most important for the simulation of the hydraulic head in Australia, the northern Sahara, the Emirates, and across Europe.

RQ 3.2: How does the spatial resolution of the model affect the results?
Increasing the spatial resolution of the model is improving the fit to observations according to metrics like the RMSE although it is not removing systematic over- or underestimates of hydraulic head. Rather a better fit to observations is due to the improved representation of the heterogeneity of the topography. Based on the results presented in chapter 5 one cannot conclude that an increased spatial resolution is an elixir for improving the model performance.

RQ 4: How can a global gradient-based groundwater model be integrated within an existing GHM?

RQ 4.1: How can the newly developed model be integrated into the existing model WaterGAP? How can the different spatial and temporal resolutions be integrated?
The main challenge of integrating a global gradient-based groundwater model into a GHM is the numerical convergence and coupling on different spatial and temporal

scales. Keeping runtimes as low as possible is therefore the overall goal. Hence, it is necessary to chose as large temporal steps in the groundwater model as possible but still consider convergence issues as a large step size means a rather large change in parameters like recharge in between steps.

RQ 4.2: How does the complexity of the integrated model affect the model runtime?
With G^{3}M a steady-state solution can be obtained within half an hour on a commodity PC. However, the transient fully coupled model runtime is harder to estimate and heavily depends on how the processes are coupled. At a daily coupling the runtime for one year takes about one week of computation time with 40 parallel processes. In comparison, with weekly timesteps and a monthly coupling computation takes about two weeks for a complete simulation from 1901 to 2013. Techniques like domain decomposition can improve this even further. Currently, all continents are simulated together in one matrix. Because most of them share no, or only a small, boundary it is possible to simulate them in parallel.

RQ 4.3: Does the non-linearity, introduced through the coupling, affect the numerical stability of the groundwater model? What temporal resolution is necessary to provide stable results?
The non-linearity of the coupled model is affecting the numerical stability of the solver. Non-linearity is introduced through the large seasonal global changes in groundwater recharge and changes of surface water body elevation, causing switches from gaining to losing conditions. With the setup presented in chapter 6 it is not possible to obtain stable converging results with a monthly stepsize; only daily to weekly steps have been successfully applied.

RQ 4.4: Is the fully coupled groundwater model able to represent groundwater seasonality compared to observations and other large scale groundwater models? How is groundwater affected by global seasonal changes?
Compared to observations from the Central Valley normalized simulated hydraulic head changes resemble roughly the seasonal pattern of the observed. Overall the head increases are much larger than the observed likely due to an incomplete coupling of rivers. Simulated heads of other large scale groundwater models were not compared to the integrated model yet.

RQ 4.5: How much has the groundwater storage changed in the last century?
In the Central Valley groundwater storage declines were simulated similar to established regional models except for the trend in the Sacramento Valley where WaterGAP-G^{3}M simulated an increase in storage. This difference is possibly due to current coupling issues. A global change in groundwater storage has not been investigated yet but global head trends suggest that storage overall increased except in regions where depletion is to be expected. A decline in head is visible in WaterGAP-G^{3}M e.g. for the High Planes Aquifer and West India similar to Döll et al. (2014, Fig.3).

RQ 4.6: How do gaining and losing conditions of surface water bodies change over time in a fully coupled groundwater model?
The current implemented model WaterGAP-G^{3}M only contains fully coupled rivers that seem to underestimate the drainage capabilities of rivers due to an unknown error. Currently, the distribution of gaining and losing conditions does not change

throughout the simulation period. All other surface water bodies are not fully coupled and thus behave similar to the steady-state model.

RQ 4.7: How do the outputs of WaterGAP differ from the integrated groundwater model compared to the former model with a linear storage model?
Answering this question is up to speculation at this point as the fully coupled model is not yet producing satisfying results. Especially the main outputs like streamflow of the GHM need to be reevaluated and compared to the former results to determine the impact of the coupled model. This comparison is especially interesting for periods of drought were the former version of WaterGAP was not able to correctly simulate the continuing water loss from surface water bodies as they get disconnected from the groundwater. It needs to be proven if the effort of such a complex model is necessary to improve a GHM and if it is possible that similar results can be obtained by using a approximation of the processes through a proxy model.

7.1 Outlook

This thesis presents the modeling framework G^{3}M-f and the global groundwater model G^{3}M which is used to simulate a global natural equilibrium water table and analyze the resulting flows. Compared to observations the global equilibrium model showed persistent underestimates of simulated hydraulic heads even though less than a previously presented model. Following this the equilibrium model was then used to analyze the uncertainties of the model using a global sensitivity method. Further, G^{3}M is integrated into the GHM WaterGAP and first transient results show a good agreement with existing models in the Central Valley.

However, results in this thesis show that multiple improvements are required to advance global groundwater modeling. Firstly, global datasets on hydrogeology need to be improved to properly parameterize the model which could be achieved by integrating already available local data. Results presented in this thesis show that the current available data is globally underestimating the hydraulic conductivity and that it is highly influencing the outcome of the simulated heads. Furthermore, it is necessary to investigate into how spatially heterogeneous topography can be represented in the coarse model cells allowing then a valid comparison to observations and to further improve the model to use estimates of water table depth to simulate capillary rise on a global scale. In general, the impact of a spatial resolution on the results of global groundwater modeling needs to be investigated further.

The presented model, even with an efficient software implementation, requires long computation times that limit the assessment of uncertainties e.g. through sensitivity analysis. It is to be investigated if the complex groundwater model can be replaced by a so called proxy-model that for example takes the simulated steady-state groundwater table as baseline and computes changes in groundwater level and exchanges with surface water bodies based on simpler analytical functions without solving the time consuming partial differential equations. This would introduce additional possibilities to investigate the large uncertainties of the groundwater model and the GHM and how they are connected in even greater detail.

With the transient coupling concept this thesis provided first results of a WaterGAP-G^{3}M model that is already able to simulate storage declines compared to established models reasonably well. As soon as the coupling is completed the model provides the stage to answer new research questions like:

- How did the groundwater level change over the last century?

- How does groundwater interact with other components of the water cycle on a global scale?
- Can the model contribute to better understand man-made groundwater depletion?
- In particular, how do groundwater changes affect ecologically important flow regimes of rivers?
- Does the groundwater model improve the performance in terms of discharge compared to measured discharge?
- What effect has climate change on groundwater and how can we use this information for future water management?

Eventually, this can lead to a model that can be used in regions where no local model is available to still provide a first estimation of groundwater storage behaviour and enable climate and human impact studies of regional groundwater resources.

GOETHE-UNIVERSITÄT FRANKFURT

Zusammenfassung

Von linearen Speichermodellen zu gradientenbasierter Grundwassermodellierung: Die Entwicklung eines globalen Grundwassermodells und seine Integration in ein globales hydrologisches Modell

von Robert REINECKE M.Sc.

Wasser ist Ursprung und die Voraussetzung des Lebens; für den Menschen nimmt es eine zentrale Rolle in der Landwirtschaft, als Trinkwasser und nicht zuletzt in verschiedenen industriellen Prozessen ein. Durch den Klimawandel und andere menschliche Eingriffe in die Natur werden Wasserressourcen und damit auch die Wasserverfügbarkeit für Menschen und andere Biota verändert (Taylor et al., 2013). Globale hydrologische Modelle sind in der Lage, die komplexen, weltweiten Prozesse des Wasserkreislaufs auf und unterhalb der Landoberfläche, die nur sehr eingeschränkt messbar sind, in vereinfachter Form abzubilden und erlauben somit Rückschlüsse auf menschliche und klimatische Einflüsse auf das Frischwassersystem.

Grundwasser spielt als größter von Menschen nutzbarer Süßwasserspeicher eine zentrale Rolle für die Wasserversorgung. Das Volumen wird dabei auf 22,6 Millionen km^3 in den oberen 2 km der Erdkruste geschätzt im Vergleich zu den 100 Tausend km^3 in Oberflächengewässern (Gleeson et al., 2016). Durch langfristige Eingriffe, z. B. durch Entnahme von Grundwasser für die Bewässerung, hat der Mensch tiefgreifende Veränderungen im Ökosystem hervorgerufen. Grundwasser ist die Quelle für geschätzt 40% aller menschlichen Wasserentnahmen weltweit (Döll et al., 2014). Dauerhafte Grundwasserentnahmen, die die natürliche Grundwasserneubildung übersteigen, können zu Grundwasserversiegen führen (Wada et al., 2010; Taylor et al., 2013). Eine Erschöpfung des Grundwassers kann dabei nicht nur (1) versiegende Brunnen bedingen, sondern auch (2) zum Austrocknen von Flüssen und Seen beitragen, die durch Grundwasser gespeist wurden, (3) zu einer Verschlechterung der Wasserqualität führen, (4) Pumpkosten erhöhen und (5) sogar zu Landabsenkungen führen. Global hat die anhaltende Nutzung von Grundwasser zur Bewässerung schon zu weitreichend abgesenkten Grundwasserspiegeln beigetragen (Scanlon et al., 2012; Gleeson et al., 2012; Döll et al., 2014) sowie, Modellberechnungen zufolge, auch signifikat zum Anstieg des Meeresspiegels (Wada et al., 2010; Konikow, 2011; Wang et al., 2018).

Globale hydrologische Modelle können dabei helfen, den globalen Wasserkreislauf und seine Beeinflussung durch den Menschen besser zu verstehen. Dabei simulieren globale hydrologische Modelle den kontinentalen Wasserkreislauf, indem sie Abläufe zwischen Wasserspeichern wie beispielsweise Kronendach, Schnee, und Bodenzone zusammen mit dem Durchfluss von Flüssen berechnen. Bislang wird in globale hydrologische Modellen Grundwasser mit Hilfe eines linearen Speichermodells vereinfacht dargestellt. Jedoch erlaubt dies nicht, die Höhe des Grundwasserspiegels, den lateralen Fluss zwischen Modellzellen, den kapillaren Aufstieg in die

wasserungesättigte Bodenzone, noch den Wasseraustausch zwischen Oberflächengewässern und Grundwasser zu simulieren.

Die besondere Herausforderung bei der Entwicklung eines globalen gradientenbasierten Modells liegt in der schwachen globalen Datengrundlage und den hohen Anforderungen an die Rechenzeit. Bisher gibt es nur ein einziges globales hydrologisches Modell, welches ein gekoppeltes gradientenbasiertes Grundwassermodell enthält (de Graaf et al., 2015, 2017). Allerdings werden bei diesem Modell die simulierten Standrohrspiegelhöhen verglichen mit globalen Beobachtungen weit unterschätzt. Das Grundwassermodell wurde mit Hilfe der etablierten Modellierungssoftware MODFLOW (Harbaugh, 2005) entwickelt, welches sich jedoch nur begrenzt für die Entwicklung eines gekoppelten Modells eignet.

Die vorliegende Arbeit hat zum Ziel, das etablierte globale hydrologische Modell *WaterGAP* hinsichtlich der Grundwasserberechnung durch ein gradientenbasiertes Grundwassermodell zu erweitern. WaterGAP berechnet Frischwasserflüsse und Speicher auf allen Kontinenten außer in der Antarktis. Dabei bezieht WaterGAP menschliche Einflüsse wie Bewässerung und den Bau von Staudämmen mit ein. Im Folgenden werden die vier Hauptforschungsfragen dieser Arbeit erläutert und Ergebnisse des neu entwickleten Modells G^{3}M (**G**lobales **g**radienten-basiertes **G**rundwasser**M**odell) vorgestellt.

Forschungsfrage 1: Welche Software-Architektur wird benötigt, um ein komplexes wissenschaftliches Modell zu entwickeln, das Grundwasser auf einer globalen Skala simuliert, dabei sowohl effizient ist als auch eine Kopplung mit einem existierenden hydrologischen Modell ermöglicht?

Für die Implementierung des Grundwassermodells wurde eine eigene Modellierungsumgebung entwickelt (G^{3}M-f), die eine möglichst effiziente Kopplung mit dem bestehenden Modell ermöglicht, aber auch als Grundlage für andere Grundwassermodelle genutzt werden kann. Ein Hauptaugenmerk in der Entwicklung wurde dabei auf die effiziente Kopplung mit anderen Modellen gelegt. So ist z. B. der Datenaustausch zwischen den Modellen im Rechenspeicher möglich, da G^{3}M-f direkt als Laufzeitbibliothek in das zu koppelnde Modell einzubinden ist. Weiterhin wurde die Architektur so gestaltet, dass häufige Änderungen an der Software ohne großen Zeitaufwand möglich sind und eine nachhaltige Nutzung in der Forschung gewährleistet ist. Die Software umfasst über 70.000 Zeilen C++ Code für das gesamte globale Modell. Das Design der Softwarearchitektur, ihre Implementierung, Validierung sowie numerische Herausforderungen werden in dieser Arbeit vorgestellt. Dabei wird mit dem Verfahren der konjugierten Gradienten die Grundwasserströmungsgleichung

$$\frac{\partial}{\partial x}\left(K_x\frac{\partial h}{\partial x}\right)+\frac{\partial}{\partial y}\left(K_y\frac{\partial h}{\partial y}\right)+\frac{\partial}{\partial z}\left(K_z\frac{\partial h}{\partial z}\right)+\frac{Q}{\Delta x\Delta y\Delta z}=S_s\frac{\partial h}{\partial t}$$

gelöst. $K_{x,y,z}$ $[LT^{-1}]$ bezeichnet dabei die hydraulische Leitfähigkeit entlang der x, y und z Achse der Berechnungszellen, welche eine Größe von $\Delta x\Delta y\Delta z$ hat. S_s $[L^{-1}]$ ist die spezifische Speicherkapazität des Gesteins, h $[L]$ die Standrohrspiegelhöhe und Q $[L^3T^{-1}]$ der Fluss in oder aus der Zelle hinaus z. B. lateral oder durch Oberflächengewässer.

Der Code wurde der Öffentlichkeit als OpenSource Software zur Verfügung gestellt[1].

Forschungsfrage 2: Ist es möglich, Grundwasser auf einer globalen Skala zu simulieren? Und falls ja, wie sehen die globalen Grundwasserprozesse aus?

Zunächst wurde ein globales Grundwassermodell mit dem Namen G^3M auf Basis von G^3M-f erstellt, welches ein globales natürliches Gleichgewicht repräsentiert, dass sich nach einer unendlich langen Zeit mit gleichen Bedingungen einstellen würde (Reinecke et al., 2019a). Ein solches Modell berechnet keine Grundwasserspeicheränderungen. Es hilft aber, das modellierte System besser zu verstehen und Trends zu entdecken, die im zeitlichen Verlauf eines Modells (z. B. bei einer Simulation der Wasserstände der letzten 100 Jahre) Prozesse langfristig beeinflussen können. Weiterhin kann es als Anfangsbedingung für eine solche transiente Simulation dienen.

Die Ergebnisse dieses neuen Modells zeigen bessere Übereinstimmungen mit Beobachtungsdaten als bereits existierende Modelle. Eine Karte des globalen Grundwasserspiegels basierend auf diesem Modell ist in Abbildung 7.1 zu sehen. Im natürlichen Equilibrium fließen dabei $1{,}3{*}10^7 m^3 Tag^{-1}$ Wasser vom Grundwasser in die Ozeane. Das sind 0.1% der globalen Grundwasserneubildung. Da es sich um ein Gleichgewichtsmodell handelt, sind alle Oberflächengewässer in ihrer Größe und in ihrem Wasserstand unveränderlich, das heißt, dass z. B. die globalen Feuchtgebiete in ihrer Größe sehr wahrscheinlich überschätzt werden. Die Datengrundlage für die Feuchtgebiete weist die jemals erreichte maximale Ausbreitung aus; das globale Gleichgewichtsmodell nimmt 80% dieser Ausbreitung als Fläche an. Sehr wahrscheinlich ist damit in ariden Gebieten, in denen Feuchtgebiete nur sehr selten ihre maximale Größe erreichen, der berechnete Grundwasserspiegel überschätzt. In Gebirgen ist die Höhe des durchschnittlichen Grundwasserspiegels schwer einzuschätzen, da kaum Messungen vorliegen. Weitere Ergebnisse dieses Modells sind erste Karten der weltweiten Verteilung der Interaktionen zwischen Oberflächengewässern und dem Grundwasser. Der Basisabfluss in Flüsse ist dabei ein dominanter Prozess.

Forschungsfrage 3: Welche Unsicherheitsfaktoren beeinflussen die Simulationen von globalem Grundwasser und wie können wir sie quantifizieren?

Um die Unsicherheiten in den Modellergebnissen genauer zu beleuchten, wurde eine Sensitivitätsstudie durchgeführt (**?**). Dafür wurde erstmals ein globales Grundwassermodell mit einer globalen Sensitvtätsmethode untersucht. Globale Sensitvitätsmethoden stellen hohe Anforderungen an die Anzahl an Modellevaluierungen, aber ermöglichen im Gegensatz zu lokalen Methoden die Erkundung des gesamten Parameterraumes (Pianosi et al., 2016). Dabei kann untersucht werden, welche Unsicherheiten in den Modellparametern sich bis in die Modellergebnisse fortsetzen und an welchen Stellen es sich daher lohnt, Unsicherheiten zu reduzieren. Weiterhin lässt sich untersuchen, wie robust die Modellergebnisse sind und inwiefern andere Annahmen zu veränderten Ergebnissen führen.

Die vorliegende Arbeit präsentiert einen neuen Ansatz, um auch rechenintensive Modelle mit globalen Sensitivitätsmethoden zu untersuchen. Die Ergebnisse zeigen, dass berechnete Standrohrspiegelhöhen gleich sensitiv gegenüber Veränderungen

[1] `globalgroundwatermodel.org`

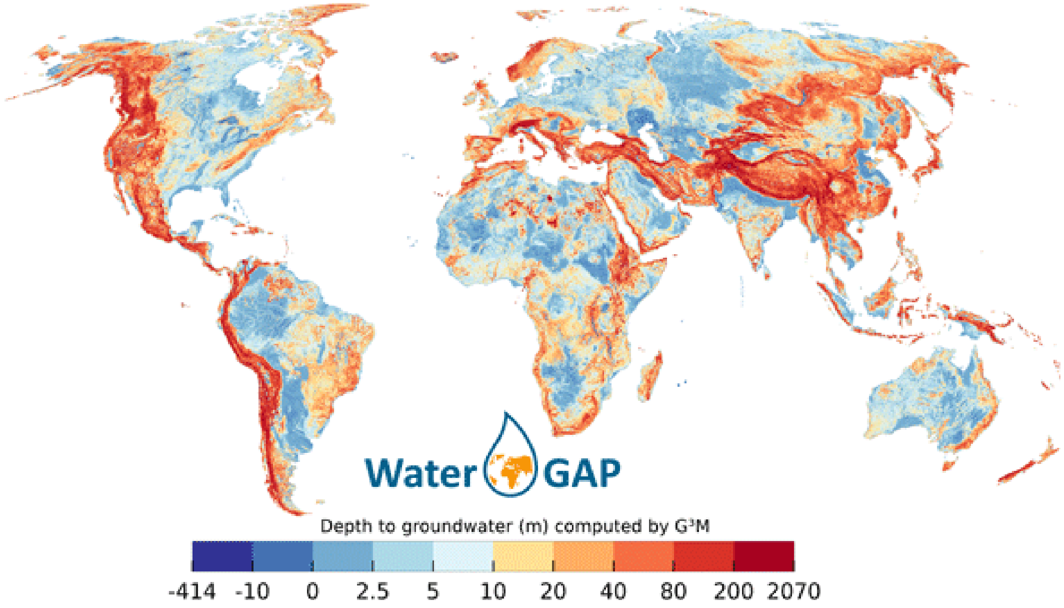

ABBILDUNG 7.1: Grundwasserspiegel in Meter basierend auf einem natürlichen Gleichgewichtsmodell.

in der hydraulischen Leitfähigkeit, Grundwasserneubildung und der Lagehöhe der Oberflächengewässer sind. Dabei sind die Einflüsse der Parameter regional sehr verschieden.

Die gezeigte Relevanz der Lagehöhe der Oberflächengewässer ist eng verknüpft mit der groben räumlichen Auflösung des Modells. Da jede Berechnungszelle im Modell ca. 9 km mal 9 km (am Äquator, zu den Polen kleiner werdend) groß ist, muss für die Oberflächengewässer eine durchschnittliche Lagehöhe angenommen werden. Diese kann ganz maßgeblich (mehrere hundert Meter) pro Zelle von der Realität innerhalb jener Zelle abweichen. Um diese Unsicherheiten durch die räumliche Auflösung weiter zu untersuchen präsentiert diese Arbeit weiterhin Ergebnisse eines Grundwassermodells von Neuseeland. Der Inselstaat wurde wegen seines klaren Randwerteproblems (Ozean) und der gleichzeitig anspruchsvollen Topographie sowie guten Datenlage ausgewählt. Eine hochauflösende Modellvariante auf ca. 900 m mal 900 m Auflösung zeigt, dass eine Erhöhung der räumlichen Auflösung zwar zunächst die Performanz verbessert, allerdings bleiben systematische Über- oder Unterschätzungen der Standrohrspiegelhöhen in bestimmten Regionen bestehen. Daher ist weitere Forschung notwendig, um die globale Parametrisierung weiter zu verbessern. Anhand des hochauflösenden Modells zeigt sich zudem, dass lokale Punkt-Beobachtungen sich nicht ohne weiteres mit durchschnittlich berechneten Standrohrspiegelhöhen vergleichen lassen. Eine Möglichkeit wäre, die durchschnittlich simulierte Höhe anhand hochauflösender Höhenmodelle hoch zu skalieren.

Forschungsfrage 4: Wie lässt sich ein globales Grundwassermodell mit einem existierenden Hydrologischen Modell koppeln?

Bei der Kopplung mit dem etablierten globalen hydrologischen Modell WaterGAP zeigen sich hauptsächlich die unterschiedlichen räumlichen Auflösungen und die numerische Stabilität des Grundwassermodells als Herausforderung. Das Grundwassermodell besitzt eine 36-mal feinere räumliche Auflösung als das hydrologische Modell. Nichtsdestotrotz müssen die berechneten Interaktionen zwischen Oberflächengewässern und dem Grundwasser auf die gröbere Auflösung des hydrologischen Modells aggregiert werden. Genauso müssen berechnete Änderungen z. B. des Wasserspiegels in den Gewässern des hydrologischen Modells auf die feinere Auflösung des Grundwassermodells skaliert werden. Veränderungen im Grundwassermodell durch neue Berechnungen im hydrologischen Modell z. B. eine größere/kleinere Grundwasserneubildung oder einen veränderter Wasserstand stellen eine numerische Herausforderung dar. Die Grundwasserneubildung kann sich beispielsweise von Monat zu Monat (weltweit) stark ändern und so das Grundwassermodell zwingen, einen neuen dazu passenden Zustand zu berechnen. Die Kernherausforderung ist hierbei, entweder an Berechnungsgeschwindigkeit durch kleinere Schrittweiten oder an Genauigkeit durch zu große Schrittweiten zu verlieren.

Erste Resultate zeigen, dass das gekoppelte Modell saisonale Änderungen im Vergleich zu Beobachtungen annähernd nachbilden kann. Auch die berechneten Grundwasserspeicheränderungen im Central Valley in Kalifornien können, im Vergleich zu zwei etablierten regionalen Modellen, gut abgebildet werden und zeigen die zu erwartende Absenkung des Grundwasserspeichers seit den 60er Jahren.

Die in dieser Arbeit vorgestellten Ergebnisse zeigen, dass weitere Forschung notwendig ist, um die Modellergebnisse noch weiter zu verbessern. Für wichtige Datensätze besteht dringender Verbesserungsbedarf z. B. der globalen hydraulischen Leitfähigkeit. Weiterhin ist es notwendig zu untersuchen, welche Dichte von Grundwasserspiegelbeobachtungen notwendig ist, um diese sinnvoll mit den Modellergebnissen zu vergleichen und wie die Topographie innerhalb der Berechnungszellen mit einbezogen werden kann. Dies ist beispielweise für die Berechnung des Kapillaraufstiegs auf der globalen Skala notwendig, da dieser eine sehr genaue Simulation der Wasserspiegelhöhe voraussetzt. Weiterhin sollte die Verbesserung des transienten Modells im Vordergrund stehen. Mit zuverlässigeren Ergebnissen wäre die Beantwortung der folgenden Forschungsfragen möglich:

- Wie haben sich die Grundwasserstände in den letzten hundert Jahren weltweit entwickelt?
- Wie groß sind die zeitlichen Einflüsse des Klimas auf das Grundwasser?
- Wie werden sich die Grundwasserstände in Zukunft entwickeln und wie können wir diese Informationen für zukünftiges Wassermanagement nutzen?
- Wie groß ist der Einfluss von Kapillaraufstieg auf die Evapotranspiration weltweit?
- Wie sehr beeinflussen Änderungen im Grundwasser die Flussregime?

Appendix A

Groundwater Equations

The following equations are mainly based on the MODFLOW 2005 documentation (Harbaugh, 2005) and are provided for completeness.

A.1 Finite-difference equation

The following derives the finite-difference equation from a continuity equation that states that all flows into and out of the cell must be equal to the rate in storage change within the cell (Harbaugh, 2005)

$$\sum Q_i = S\frac{\Delta h}{\Delta t}\Delta V \tag{A.1}$$

where Q is the flow rate into cell $[L^3T^{-1}]$, S the specific storage as volume unit of water that can be released or injected per unit volume of aquifer material per unit in head change $[L^{-1}]$, V the volume of the cell $[L^3]$, and Δh $[L]$ the hydraulic head change over a time interval Δt.

Cells are connected as shown in Fig. A.1 where the center cell is i,j,k. The flow between two cells centers is shown in Fig. A.2. The flow q $[L^3T^{-1}]$ from cell i,j-1,k into the cell i,j,k based on Darcy's law is given as

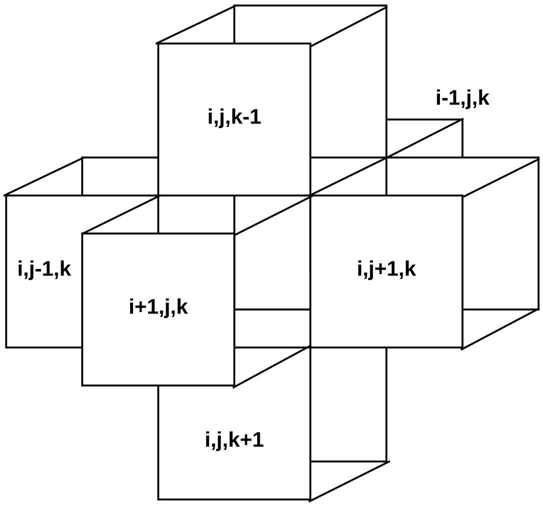

FIGURE A.1: Adjacent cells of center cell i,j,k (modified from (Harbaugh, 2005)).

$$q_{i,j-\frac{1}{2},k} = K_{i,j-\frac{1}{2},k}\Delta c_i \Delta v_k \frac{h_{i,j-1,k} - h_{i,j,k}}{r_{j-\frac{1}{2}}} \tag{A.2}$$

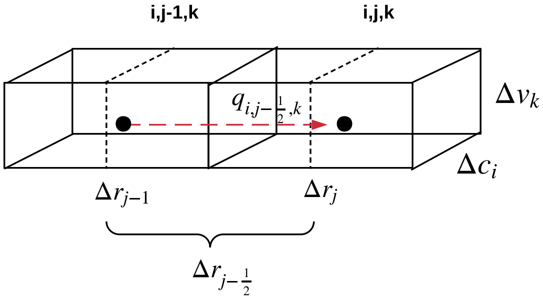

FIGURE A.2: Flow q between the centers of two adjacent cells (modified from Harbaugh (2005)).

where K $[LT^{-1}]$ is the hydraulic conductivity along the row between the two cells from center to center ($\frac{1}{2}$ the distance to the edge), $\Delta c_i \Delta v_k$ $[L^2]$ the area of the cell face normal to the row direction, h $[L]$ the hydraulic head of the cell, and r $[L]$ the distance between the cell centers. The equation is similar for all other directions except for the indices. K between the cells is calculated as harmonic mean.

From Eq. A.2 we can derive a conductance term for each neighbouring cell in row i and layer k as

$$CR_{i,j-\frac{1}{2},k} = \frac{K_{i,j-\frac{1}{2},k} \Delta c_i \Delta v_k}{\Delta r_{j-\frac{1}{2}}} \tag{A.3}$$

where CR is the conductance $[L^2T^{-1}]$. CR stands for conductance row; again the equation is similar for all other surfaces (CV and CC).

A.1.1 Vertical conductance

As mentioned in the previous section CV (Fig. A.3) is as well calculated based on the harmonic mean. Because it is possible to use different weighting algorithms and the equation needs to be modified if in later versions confining layers between nodes need to be included the following depicts the harmonic mean equation for the vertical conductance as

$$CV_{i,j,k+\frac{1}{2}} = \frac{\Delta r_j \Delta c_i}{\frac{\frac{1}{2}\Delta v_{i,j,k}}{K^v_{i,j,k}} + \frac{\frac{1}{2}\Delta v_{i,j,k+1}}{K^v_{i,j,k+1}}} \tag{A.4}$$

.

A.1.2 Dewatered conditions

In rare cases e.g. under perched conditions or through pumping it is possible that a cell is only partially saturated while the cell above is fully saturated as shown in Fig. A.4. In this case the flow between the two nodes no longer depends on the water level in the bottom cell. It would be possible to modify the flow equation to use the elevation of the lower cell $E_{i,j,k+1}$ instead of the head to calculate the vertical flow, however this would lead to an asymmetric matrix which is undesirable for the solution process (Harbaugh, 2005). Harbaugh (2005) proposes a correction term that is applied to the two nodes. While the cell that is above the dewatered condition is using

$$q_c = CV_{i,j,k+\frac{1}{2}}(h^{n-1}_{i,j,k+1} - E_{i,j,k+1}) \tag{A.5}$$

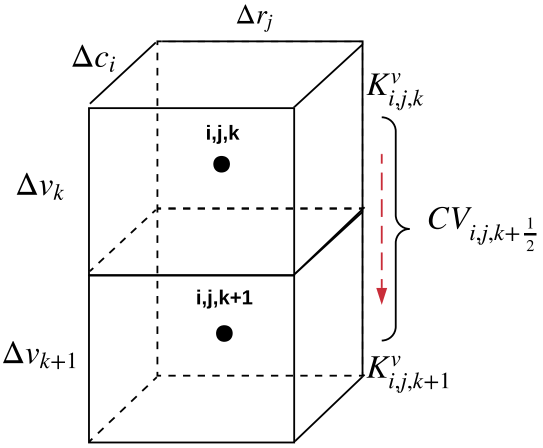

FIGURE A.3: Vertical conductance between two nodes (modified from Harbaugh (2005)).

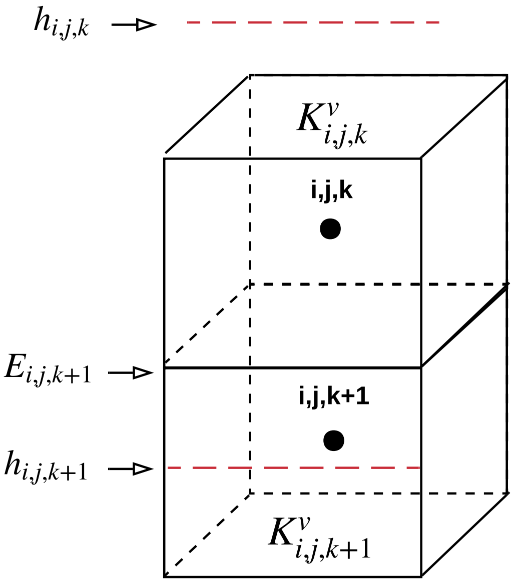

FIGURE A.4: Dewatered condition in lower cell. A correction is applied to limit the downward flow. (modified from Harbaugh (2005)).

the cell that is in the dewatered condition is using

$$q_c = CV_{i,j,k+-\frac{1}{2}}(E_{i,j,k+1} - h^{n-1}_{i,j,k}) \tag{A.6}$$

where in both equations the head from the previous timestep h^{n-1} is used to avoid matrix asymmetry.

A.1.3 External flows

External flows like rivers presented in chapter 3 can be be expressed as

$$a_{i,j,k,n} = p_{i,j,k,n}h_{i,j,k,n} + q_{i,j,k,n} \tag{A.7}$$

where a $[L^3T^{-1}]$ is flow from the nth external source to cell i,j,k, p $[L^2T^{-1}]$ and q $[L^3T^{-1}]$ are constants. $P_{i,j,k}$ and $Q_{i,j,k}$ in the following represent the sum of p and q

respectively.

A.1.4 Backward-difference approximation of h

The time derivative of the hydraulic head is expressed as as backward-difference

$$\frac{\Delta h}{\Delta t} \cong \frac{\Delta h^m - \Delta h^{m-1}}{t^m - t^{m-1}} \tag{A.8}$$

where m is the time at which the flow terms are evaluated. To derive a form like $\boldsymbol{A} \times \boldsymbol{x} = \boldsymbol{b}$ as discussed in section 2.3 where x is a vector of heads to be estimated for the timestep n. Eq. A.9 describes the coefficients for matrix A as

$$\begin{aligned} & CV_{i,j,k-\frac{1}{2}} h_{i,j,k-1} + \\ & CC_{i-\frac{1}{2},j,k} h_{i-1,j,k} + \\ & CR_{i,j-\frac{1}{2},k} h_{i,j-1,k} + \\ & CV_{i,j,k+\frac{1}{2}} h_{i,j,k+1} + \\ & CC_{i+\frac{1}{2},j,k} h_{i+1,j,k} + \\ & CR_{i,j+\frac{1}{2},k} h_{i,j+1,k} + \\ (-CV_{i,j,k-\frac{1}{2}} - CV_{i,j,k+\frac{1}{2}} - CC_{i-\frac{1}{2},j,k} - & CC_{i+\frac{1}{2},j,k} \\ -CR_{i,j-\frac{1}{2},k} - CR_{i,j+\frac{1}{2},k} + HCOF_{i,j,k}) & h_{i,j,k} \\ & \qquad = RHS_{i,j,k} \end{aligned} \tag{A.9}$$

where C(V,C,R) is the conductance from Eq. A.3, RHS the right hand side of the equation also expressed as $\boldsymbol{b}$ above

$$RHS_{i,j,k} = -Q_{i,j,k} - S_{i,j,k} \Delta r_j \Delta c_i \Delta v_k \frac{h_{i,j,k}^{m-1}}{t - t^{m-1}} \tag{A.10}$$

where Q summarises the q parts in Eq. A.7 that are not head dependant and the p part is summarised in the head coefficients $HCOF$

$$HCOF_{i,j,k} = P_{i,j,k} - \frac{S_{i,j,k} \Delta r_j \Delta c_i \Delta v_k}{t - t^{m-1}} \tag{A.11}$$

.

A.2 Dampening algorithm

The dampening algorithm can be useful for non-linear problems that affect the convergence of the solution. Algorithm 2 is adapted from Niswonger et al. (2011). The dampening is used between outer iteration steps reducing the head change that is applied in each outer iteration which affects switches between gaining and losing conditions.

Algorithm 2 Dampening algorithm modified from Niswonger et al. (2011)

```
procedure APPLY_DAMPENING
    $\psi \leftarrow 0.01$
    $\theta_j \leftarrow$ Dampening factor for iteration $j$
    $\theta_l \leftarrow$ Min damp
    $\theta_u \leftarrow$ Max damp
    $cnt \leftarrow 0$ Counter for damping application
    $n_j \leftarrow \sqrt{residuals_j^T \times residuals \times \Delta^T * \Delta}$
    $H_j \leftarrow$ Head change
    $H_{lim} \leftarrow$ Max head change
    $\rho_n \leftarrow n_j / n_{j-1}$
    $\rho_h \leftarrow H_j / H_{j-1}$
    if $\rho_n < 1$ and $\rho_h < 1$ then
        $\lambda \leftarrow \log_{10} \rho_n / \log_{10} \psi$
        if $\lambda < 1$ then
            $\Phi \leftarrow \theta_{j-1} + \lambda * (\theta_u - \theta_{j-1})$
        else
            $\Phi \leftarrow \theta_u$
        cnt $\leftarrow 0$
    if $\rho_n > 1$ then
        $\Phi \leftarrow \theta_{j-1} / \rho_n$
    if $\rho_h > 1$ then
        $\Phi \leftarrow \theta_{j-1} / \rho_h$
    $\theta \leftarrow \sqrt{\theta_{j-1} * \Phi}$
    if $|H_j| > H_{lim}$ and $\theta_j > H_{lim} / |H_j|$ then
        $\theta_j \leftarrow H_{lim} / |H_j|$
    if $\theta_j < \theta_l$ then
        $\theta_j \leftarrow \theta_l$
        $cnt = cnt + 1$
        if $cnt > 10$ then
            $\theta_j \leftarrow \sqrt[3]{\theta_l^2 \theta_u}$
```

Appendix B

Design patterns and design principles

This chapter provides an overview on the key software engineering terms used in this thesis. The terms and principles have been discussed in many books and other publications that are out of scope of this work. Because the presented software is developed in a research field that might not be familiar with many concept this section is intended to provide an overview of important terms.

B.1 Requirements

Requirements are 'a condition or capability needed by a user to solve a problem or achieve an objective' (IEEE, 1990) or 'A condition or capability that must be met or possessed by a system or system component to satisfy a contract, standard, specification, or other formally imposed document' (IEEE, 1990) or a combination of both. Requirements engineering on the other hand refers to the process of defining, documenting and maintaining these requirements. In most projects requirements can be separated into functional and non-functional requirements. Roughly they can be translated into: what should the software do and how should it be done. Functional requirements define a expected relation between input and output. For scientific software a functional requirement might be that a specific flow of a liquid is calculated based on a certain equation. Non-functional requirements define the circumstances of a certain action and mostly refer to the software architecture (Chen et al., 2013) e.g. that it needs to be testable, maintainable or OpenSource.

Extensibility is a design principle that is to support future growth of the software. The internal structure should be affected in a minimal amount by modifications to the functionality or the addition of functionality. Especially when the software is long lived and many new extensions will be expected to the core functionality it is worth it to guide the design by separating the elements of the software in comprehensible units. Change needs to be embraced as part of the design process, and it needs to be accepted that not every future change can be anticipated.

Testability is to which degree a software supports testing in a specific context (Rodríguez et al., 2014). The goal is to design the system in a way that it allows to specify its expected output for a given input. It is only an extrinsic properties of the software but that depends on the quality of the designed software and other non-functional requirements.

Adaptability is the ability of a system to react to new circumstances. For example the presented software is adaptable in the sense that it is capable of running on different spatial resolutions and on different platforms.

Maintainability refers to the ability of an application to be maintained in order to correct known mistakes or adapt to new environments or requirements. It can be summarized in the goal that it should not be cheaper to rewrite the software than to change the code.

B.2 Design patterns

The term design or software patterns has been characterized by Gamma et al. (1995) describing established principles in object-oriented software that solve generic problems. Design patterns are not software or language specific but rather represent an software engineering idiom for problems that have been encountered frequently when trying to write flexible and reusable software. Most non-functional requirements cannot be tested but they can be supported by applying established design principles. Metrics that measure non-functional requirements are not discussed here. The following describes three main patterns out of multiple patterns that have been applied in building this software: (1) Abstract factory, (2) Iterator, and (3) Decorator. In order to avoid the explanation of graphical languages, e.g. UML, key principles are mentioned and how they refer to the software presented in this thesis. For details the reader is referred to the very comprehensive work of Gamma et al. (1995).

Abstract factory is used to create a family of objects that share properties and are intended to be used together. The system creating the objects shall be independent from how the objects are created specifically. In the used software the nodes are an example of the abstract factory pattern. Nodes come in different forms e.g. no-flow boundaries and standard nodes. The process of creating them is decoupled from how the nodes behave and how they are constructed. This way they can be connected and created at various places throughout the simulation without knowing the specific implementation. This reduces code overhead and makes it more flexible to add specific nodes later in the development process without changing the code where they are created.

Iterators provide a way to access elements of an object container in a sequential way without exposing how they are actually organised. The used code has multiple examples of this. One prominent example is how G^{3}M solves consecutive timesteps. The *Stepper* is an Iterator that hides how the internal system is informed about the temporal resolution and the number of steps. It just allows the user to solve the equation for sequential timesteps.

The decorator attaches additional functionality dynamically to an object. In the case of G^{3}M this can be observed in data write-out class. The implemented classes provide the functionality to write out multiple properties of the simulation and its nodes in a flexible way and can be *decorated* with different data formats e.g. CSV or NetCDF to be written out.

Appendix C

Model documentation

G^{3}M - Global Gradient Groundwater Model Documentation

Release 1.0

Robert Reinecke

Jan 20, 2020

CONTENTS:

CHAPTER

ONE

QUICKSTART: THE MODEL FRAMEWORK

The global gradient-based groundwater model framework G^{3}M-f is an extensible model framework. Its main purpose is to be used as a main building block for the global groundwater model G^{3}M. G^{3}M is a newly developed gradient-based groundwater model which adapts MODFLOW [@harbaugh2005modflow] principles for the global scale. It is written in C++ and intended to be coupled to the global hydrological model WaterGAP (http://watergap.de), but can also be used for regional groundwater models and coupling to other hydrological models. While it is intended to be used as a in memory coupled model it is also capable of running a standard standalone groundwater model.

1.1 Getting Started

These instructions will get you a copy of the project up and running on your local machine for development and testing purposes.

1.1.1 Prerequisites

```
clang >= 3.8 with openMP (currently gcc is not supported)
libboost >= 1.56
libGMP
libGtest
```

1.1.2 Build

```
mkdir build
cd build
cmake ../
make
```

1.1.3 How to use

Center building stone for the framework is the GW_interface connecting any model with the groundwater code. Implement this interface if you want to couple your model to G^{3}M-f or build a custom standalone application.

```
class GW_Interface {
    public:
        virtual ~GW_Interface() {}

        virtual void
        loadSettings() = 0;

        virtual void
```

(continues on next page)

(continued from previous page)

```
        setupSimulation() = 0;

        virtual void
        writeData() = 0;

        virtual void
        simulate() = 0;
};
```

1.2 Write out data

Writeout of data is specified by a JSON file called out.json. If you want to add custom fields you can do so in src/DataProcessing/DataOutput.

```
{
  "output": {
    "StaticResult": [
      {
        "name": "wtd",
        "type": "csv",
        "field": "DepthToWaterTable",
        "ID": "false",
        "position": "true"
      }
    ],
    "InnerIteration": {
    },
    "OuterIteration": {
    }
  }
}
```

1.3 Config model

In order to configure the model variables you can simply change the .json file. Thus allows you to change the convergence criteria and the location for your input files.

```
{
  "config": {
    "model_config": {
      "nodes": "grid_simple.csv",
      "row_cols": "true",
      "stadystate": "true",
      "numberofnodes": 100,
      "threads": 1,
      "layers": 2,
      "confinement": [
        "false",
        "true"
      ],
      "cache": "false",
      "adaptivestepsize": "false",
      "boundarycondition": "SeaLevel",
      "sensitivity": "false"
    },
    "numerics": {
```

(continues on next page)

(continued from previous page)

```
      "solver": "PCG",
      "iterations": 500,
      "inner_itter": 10,
      "closingcrit": 1e-8,
      "headchange": 0.0001,
      "damping": "false",
      "min_damp": 0.01,
      "max_damp": 0.5,
      "stepsize": "daily"
    },
  "input": {
    "data_config": {
      "k_from_lith": "true",
      "k_ocean_from_file": "false",
      "specificstorage_from_file": "false",
      "specificyield_from_file": "false",
      "k_river_from_file": "true",
      "aquifer_depth_from_file": "false",
      "initial_head_from_file": "true",
      "data_as_array": "false"
    },
    "default_data": {
      "initial_head": 5,
      "K": 0.008,
      "oceanK": 800,
      "aquifer_thickness": [
        10,
        10
      ],
      "anisotropy": 10,
      "specificyield": 0.15,
      "specificstorage": 0.000015
    },
    "data": {
      "recharge": "recharge_simple.csv",
      "elevation": "elevation_simple.csv",
      "rivers": "rivers_simple.csv",
      "lithologie": "lithology_simple.csv",
      "river_conductance": "rivers_simple.csv",
      "initial_head": "heads_simple.csv"
    }
  }
  }
}
```

1.4 Building a simple model

The following shows the code for a simple model loop running a steady-state model with daily timesteps.

```
void StandaloneRunner::simulate() {
    Simulation::Stepper stepper = Simulation::Stepper(_eq, Simulation::DAY, 1);
    for (Simulation::step step : stepper) {
        LOG(userinfo) << "Running a steady state step";
        step.first->toogleSteadyState();
        step.first->solve();
        sim.printMassBalances();
    }
    DataProcessing::DataOutput::OutputManager("data/out_simple.json", sim).write();
```

(continues on next page)

(continued from previous page)

```
    //sim.save();
}
```

1.5 Deployment in other models

Just implement the GW_interface and provide a DataReader.

1.6 Running the tests

Automated tests consits of gunit test which are compiled automatically with the attached cmake file. You can run them by executing the test executable.

```
runUnitTests
```

1.6.1 Running a simple model

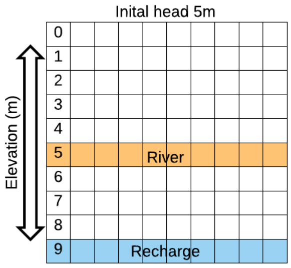

The following picture shows the conceptual example model:

After compilation run:

```
simple_model
```

It will yield a depth to water table CSV file called wtd.csv for a simple model. Results should be similar to Fig. 2.5 in section 2.4 of the dissertation.

1.7 Built With

- Eigen3 - Doing the math magic
- GTest - Test framework
- libboost - C++ magic
- OpenMP - Accelerator und Multi-Core support
- GMP - Large numbers

1.8 Contributing

Please read CONTRIBUTING.md for details on our code of conduct, and the process for submitting pull requests to us.

1.9 Versioning

We use SemVer for versioning. For the versions available, see the tags on this repository.

1.10 Authors and Contributors

- **Robert Reinecke** - *Initial work*

1.11 License

This project is licensed under the GNU General Public License - see the LICENSE file for details. Please note that the code contains a modified version of the Eigen3 library which is published under the MPL 2.0.

1.12 Acknowledgments

- Modflow 2005 for their great documentation
- Eigen3 for their awesome framework

167

CHAPTER

TWO

G^{3}M FRAMEWORK

The following describes the classes and modules that G^{3}M provides for building a groundwater model. The framework is separated into 6 packages:

- DataProcessing
- Logging
- Misc
- Model
- Simulation
- Solver

In order to implement any model the following interface has to be implemented:

template <class *T*>
class *GlobalFlow*::**GW_Interface**

Main interface to the groundwater model.

Interface to the groundwater simulation Implement me!

Subclassed by *GlobalFlow::GlobalStandaloneRunner*, GlobalFlow::StandaloneRunner

Public Functions

virtual *GlobalFlow*::*GW_Interface*~**GW_Interface**()

virtual void *GlobalFlow*::*GW_Interface***loadSettings**() = 0

Read general simulation settings e.g. Options

virtual void *GlobalFlow*::*GW_Interface***setupSimulation**() = 0

Do additional work required for a running simulation

virtual void *GlobalFlow*::*GW_Interface***writeData**(std::string) = 0

Write data for specific year or month

virtual void *GlobalFlow*::*GW_Interface***simulate**() = 0

Simulate/Run the model

void *GlobalFlow*::*GW_Interface***initInterface**(CouplingInterface<T> **intf_ptr*)

CouplingInterface<T> **GlobalFlow*::*GW_Interface***getInterface**()

void *GlobalFlow*::*GW_Interface***deleteInterface**()

2.1 DataProcessing

Data processing is mainly concerned with providing utilities for reading in data (*DataReader*) or writing out data. New types of outputs can be implemented in the *OutputFactory*.

class *GlobalFlow*::**DataReader**

Interface that needs to be implemented for reading in required data for the model.

Subclassed by *GlobalFlow::DataProcessing::GlobalDataReader*, GlobalFlow::DataProcessing::SimpleDataReader

Public Functions

virtual *GlobalFlow*::*DataReader*~**DataReader**()

Virt destructor -> interface

void *GlobalFlow*::*DataReader***initNodes**(NodeVector *nodes*)

Initialize internal ref to node vetor.

Parameters

- `nodes`: The vector of nodes

virtual void *GlobalFlow*::*DataReader***readData**(Simulation::*Options* *op*) = 0

Entry point for reading simulation data.

Attention This method needs to be implemented!

Note *readData()* is called by simulation at startup

Parameters

- `op`: Options object

template <class Fun>
void *GlobalFlow*::*DataReader***loopFiles**(std::string *path*, std::vector<std::string> *files*, Fun *fun*)

Generic method for looping through files inside a directory and applying a generic function.

Parameters

- `path`: the directory
- `files`: a vector of files
- `fun`: a function that is applied e.g. reading the data

int *GlobalFlow*::*DataReader***check**(int *globid*)

Check weather id exists in the simulation.

Return i the position in the node vector

Parameters

- `globid`: Global identifier, can be different from position in node vector

template <class ProcessDataFunction>
void *GlobalFlow*::*DataReader***readTwoColumns**(std::string *path*, ProcessDataFunction *processData*)

Read data from a two-column csv file and apply function to data.

Parameters

- `path`: to the csv file

170

- `processData`: A processing function e.g. upscaling of data

void *GlobalFlow*::*DataReader*`readZeroPointFiveToFiveMin`(std::string *path*)
Creates a mapping of 0.5° ArcIDs to a list of contained 5' GlobIDs.

Parameters

- `path`: to file

const std::unordered_map<int, std::vector<int>> &*GlobalFlow*::*DataReader*`getArcIDMapping`()
provides acccess to mapping of different resolutions

Return <ARCID(0.5°), vector<GlobalID(5')>>

const std::unordered_map<int, int> &*GlobalFlow*::*DataReader*`getGlobIDMapping`()
provides access to mapping of data ids to position in node vector

Return <GlobalID, ID>

std::string *GlobalFlow*::*DataReader*`buildDir`(std::string *path*)
Builds a corect path from the base dir.

Return A path based on the base dir

Parameters

- `path`: The relative path from the config

2.1.1 DataOutput

FieldCollector

enum *GlobalFlow*::DataProcessing::DataOutput::**FieldType**
What kind of data is collected Internal data fields that can be written out.

Values:

GlobalFlow::DataProcessing::DataOutput**ID**
Internal position

GlobalFlow::DataProcessing::DataOutput**ARCID**
Data ID

GlobalFlow::DataProcessing::DataOutput**AREA**
Area of the node

GlobalFlow::DataProcessing::DataOutput**CONDUCT**
Hydraulic conductivity of the node

GlobalFlow::DataProcessing::DataOutput**ELEVATION**
Elevation of the node

GlobalFlow::DataProcessing::DataOutput**SLOPE**
Slope in the node

GlobalFlow::DataProcessing::DataOutput**X**

GlobalFlow::DataProcessing::DataOutput**Y**
Postion of the node in X and Y

GlobalFlow::DataProcessing::DataOutput**HEAD**
Hydraulic head

GlobalFlow::DataProcessing::DataOutput**EQ_HEAD**
The equilibrium head -> inital head

GlobalFlow::DataProcessing::DataOutput**IN**

GlobalFlow::DataProcessing::DataOutput**OUT**
All in and outflows

GlobalFlow::DataProcessing::DataOutput**EQ_FLOW**
Lateral flows based on the equilibrium head

GlobalFlow::DataProcessing::DataOutput**LATERAL_FLOW**
Sum of all lateral flows of node

GlobalFlow::DataProcessing::DataOutput**LATERAL_OUT_FLOW**
Only lateral out flows

GlobalFlow::DataProcessing::DataOutput**WETLANDS**
Is there a wetland?

GlobalFlow::DataProcessing::DataOutput**LAKES**
Is there a lake?

GlobalFlow::DataProcessing::DataOutput**FLOW_HEAD**
Surface water body head

GlobalFlow::DataProcessing::DataOutput**RECHARGE**
GW recharge rate

GlobalFlow::DataProcessing::DataOutput**DYN_RIVER**
Is there a dynamic river?

GlobalFlow::DataProcessing::DataOutput**NODE_VELOCITY**
Velocity of lateral gw flow

GlobalFlow::DataProcessing::DataOutput**RIVER_OUT**
Outflow to river

GlobalFlow::DataProcessing::DataOutput**RIVER_IN**
Inflow from river

GlobalFlow::DataProcessing::DataOutput**WTD**
Depth to groundwater table based on elevation

GlobalFlow::DataProcessing::DataOutput**RIVER_CONDUCT**
Conductance of riverbed

GlobalFlow::DataProcessing::DataOutput**DRAIN_CONDUCT**
Conductance of drainbed

GlobalFlow::DataProcessing::DataOutput**WETLAND_CONDUCT**
Conductance of wetland

GlobalFlow::DataProcessing::DataOutput**GL_WETLAND_CONDUCT**
Conductance of global wetland

GlobalFlow::DataProcessing::DataOutput**LAKE_CONDUCT**
Conductance of lake

GlobalFlow::DataProcessing::DataOutput**OCEAN_OUT**
Boundary condition outflow

GlobalFlow::DataProcessing::DataOutput**GL_WETLAND_OUT**
Global wetland outflow

GlobalFlow::DataProcessing::DataOutput**WETLAND_OUT**
Wetland outflow

GlobalFlow::DataProcessing::DataOutput**LAKE_OUT**
Lake outflow

172

GlobalFlow::DataProcessing::DataOutput**GL_WETLAND_IN**
Global wetland inflow

GlobalFlow::DataProcessing::DataOutput**WETLAND_IN**
Wetland inflow

GlobalFlow::DataProcessing::DataOutput**LAKE_IN**
Lake inflow

GlobalFlow::DataProcessing::DataOutput**NON_VALID**

class *GlobalFlow*::DataProcessing::DataOutput**::FieldCollector**
Iterates over internal fields and searches for data to be written out This is currently relatively inefficient

Public Types

using *GlobalFlow*::DataProcessing::DataOutput::*FieldCollector***pos_v** = std::vector<std::pair<double, double>>

Public Functions

GlobalFlow::DataProcessing::DataOutput::*FieldCollector***FieldCollector** (*FieldType enumField*)

The constructor

Parameters

- `enumField`: What data should be collected

GlobalFlow::DataProcessing::DataOutput::*FieldCollector***FieldCollector** ()

Note Should not be used

pos_v *GlobalFlow*::DataProcessing::DataOutput::*FieldCollector***getPositions** (Simulation::*Simulation &simulation*)

get the positions of the nodes

Return A vector of positions

Parameters

- `simulation`: The simulation

std::vector<large_num> *GlobalFlow*::DataProcessing::DataOutput::*FieldCollector***getIds** (Simulation::*Simulation &simulation*)

Get the data ids of the nodes.

Return A vector of IDs

Parameters

- `simulation`: The simulation

template <**typename** T>
data_vector<T> *GlobalFlow*::DataProcessing::DataOutput::*FieldCollector***get** (Simulation::*Simulation &simulation*)

Collects the data from simulation nodes

Note Relatively inefficient currently

Return The collected data

Parameters

- `simulation`: The simulation

OutputFactory

template <typename T>
class *GlobalFlow*::DataProcessing::DataOutput::**OutputInterface**

Writes data to a file

Subclassed by *GlobalFlow::DataProcessing::DataOutput::CSVOutput< T >*, *GlobalFlow::DataProcessing::DataOutput::GFS_JSONOutput< T >*, *GlobalFlow::DataProcessing::DataOutput::NETCDFOutput< T >*

Public Functions

virtual *GlobalFlow*::DataProcessing::DataOutput::*OutputInterface*~**OutputInterface**()

virtual void *GlobalFlow*::DataProcessing::DataOutput::*OutputInterface***write**(path *filePath*, bool *printID*, bool *printXY*, std::vector<T> *data*, pos_v *p*, a_vector *ids*) = 0

Needs to be implemented

Parameters

- `filePath`:
- `printID`: Bool
- `printXY`: Bool
- `data`: Data vector
- `p`: *Position* vector

template <typename T>
class *GlobalFlow*::DataProcessing::DataOutput::**CSVOutput**

Writes data to a CSV file

Inherits from *GlobalFlow::DataProcessing::DataOutput::OutputInterface< T >*

Public Functions

void *GlobalFlow*::DataProcessing::DataOutput::*CSVOutput***write**(path *filePath*, bool *printID*, bool *printXY*, std::vector<std::pair<double, double>> *data*, pos_v *p*, a_vector *ids*)

void *GlobalFlow*::DataProcessing::DataOutput::*CSVOutput***write**(path *filePath*, bool *printID*, bool *printXY*, std::vector<bool> *data*, pos_v *p*, a_vector *ids*)

void *GlobalFlow*::DataProcessing::DataOutput::*CSVOutput***write**(path *filePath*, bool *printID*, bool *printXY*, std::vector<double> *data*, pos_v *p*, a_vector *ids*)

void *GlobalFlow*::DataProcessing::DataOutput::*CSVOutput***write**(path *filePath*, bool *printID*, bool *printXY*, std::vector<std::string> *data*, pos_v *p*, a_vector *ids*)

template <typename T>
class *GlobalFlow*::DataProcessing::DataOutput::**NETCDFOutput**

Writes data to a NETCDF file

Inherits from *GlobalFlow::DataProcessing::DataOutput::OutputInterface< T >*

174

Public Functions

void *GlobalFlow*::DataProcessing::DataOutput::*NETCDFOutput***write** (path *filePath*, bool *printID*, bool *printXY*, std::vector<std::pair<double, double>> *data*, pos_v *p*, a_vector *ids*)

void *GlobalFlow*::DataProcessing::DataOutput::*NETCDFOutput***write** (path *filePath*, bool *printID*, bool *printXY*, std::vector<bool> *data*, pos_v *p*, a_vector *ids*)

void *GlobalFlow*::DataProcessing::DataOutput::*NETCDFOutput***write** (path *filePath*, bool *printID*, bool *printXY*, std::vector<std::string> *data*, pos_v *p*, a_vector *ids*)

void *GlobalFlow*::DataProcessing::DataOutput::*NETCDFOutput***write** (path *filePath*, bool *printID*, bool *printXY*, std::vector<double> *geo_data*, pos_v *p*, a_vector *ids*)

template <typename T>
class *GlobalFlow*::DataProcessing::DataOutput**::GFS_JSONOutput**

Inherits from *GlobalFlow::DataProcessing::DataOutput::OutputInterface< T >*

Public Functions

void *GlobalFlow*::DataProcessing::DataOutput::*GFS_JSONOutput***write** (path *filePath*, bool *printID*, bool *printXY*, std::vector<T> *data*, pos_v *p*, a_vector *ids*)

Needs to be implemented

Parameters

- `filePath`:
- `printID`: Bool
- `printXY`: Bool
- `data`: Data vector
- `p`: *Position* vector

template <typename T>
class *GlobalFlow*::DataProcessing::DataOutput**::OutputFactory**

Public Static Functions

static *OutputInterface*<T> **GlobalFlow*::DataProcessing::DataOutput::*OutputFactory***getOutput** (OutputType *type*)

OutputManager

class *GlobalFlow*::DataProcessing::DataOutput**::OutputManager**

Public Functions

GlobalFlow::DataProcessing::DataOutput::*OutputManager***OutputManager** (path *output_spec_path*, Simulation::*Simulation* &*sim*, **const** std::string *date* = std::string(""))

void *GlobalFlow*::DataProcessing::DataOutput::*OutputManager***write** ()

Visits all registered output options and triggers write.

void *GlobalFlow*::DataProcessing::DataOutput::*OutputManager***write_p** ()

parallel version of write

2.2 Logging

Provides readable logging facilities

Defines

LOG (level)

NUM_SEVERITY_LEVELS

namespace GlobalFlow

Converter Functions intended to be used internaly only Currently only needed to allow compilation of different internal types There should be a more beautiful solution to this

Enums

enum *GlobalFlow***custom_severity_level**

Values:

*GlobalFlow***debug** = 0

*GlobalFlow***userinfo**

*GlobalFlow***stateinfo**

*GlobalFlow***numerics**

*GlobalFlow***error**

*GlobalFlow***critical**

Functions

template <**typename** CharT, **typename** TraitsT>
std::basic_ostream<CharT, TraitsT> &*GlobalFlow***operator<<** (std::basic_ostream<CharT, TraitsT> &*strm*, *custom_severity_level* *lvl*)

namespace *GlobalFlow***Logging**

Typedefs

typedef boost::log::sources::severity_channel_logger_mt<*custom_severity_level*, std::string> *GlobalFlow*::*Logg*

176

Functions

GlobalFlow::Logging::BOOST_LOG_ATTRIBUTE_KEYWORD(severity, "Severity", custom_se

void *GlobalFlow*::*Logging***initLogFile**()

void *GlobalFlow*::*Logging***initCoutLog**()

GlobalFlow::*Logging***BOOST_LOG_INLINE_GLOBAL_LOGGER_INIT**(global_logger, *global_logger_type*)

2.3 Misc

Contains some deprecated helpers for iterating different grid solutions not documented here.

Defines

X_DEFINE_ENUM_WITH_STRING_CONVERSIONS_TOSTRING_CASE(r, data, elem)

DEFINE_ENUM_WITH_STRING_CONVERSIONS(name, enumerators)

Functions

void **NANChecker**(**const** double &*value*, std::string *message*)

double **roundValue**(double *valueToRound*)
template <class T>
Is<T> **is**(T *d*)

Variables

T **const pi** = std::acos(-T(1))

class NANInSolutionException
Inherits from exception

Private Functions

virtual const char **NANInSolutionException***what**() **const**

class InfInSolutionException
Inherits from exception

Private Functions

virtual const char **InfInSolutionException***what**() **const**
template <class T>
struct Is
#include <Helpers.hpp> http://stackoverflow.com/questions/15181579

Public Functions

bool *Is*`in` (T *a*)

`template <class` Arg, class… *Args*>
bool *Is*`in` (Arg *a*, Args... *args*)

Public Members

T *Is*`d_`

`class Position`

Public Functions

Position`Position` (double *lat*, double *lon*)

Public Members

`const` double *Position*`lat` = {0}

`const` double *Position*`lon` = {0}

`template <typename` C>
`class Singleton`

Public Functions

`virtual` *Singleton*`~Singleton` ()

Public Static Functions

`static` C **Singleton*`instance` ()

Protected Functions

Singleton`Singleton` ()

Private Static Attributes

C **Singleton*`_instance` = 0

2.4 Model

ExternalFlow

`class` *GlobalFlow*::Model`::ExternalFlow`
TODO add flow equation here

178

Public Functions

GlobalFlow::Model::*ExternalFlow***ExternalFlow**(int *id*, FlowType *type*, t_meter *flowHead*, t_s_meter_t *cond*, t_meter *bottom*)

GlobalFlow::Model::*ExternalFlow***ExternalFlow**(int *id*, t_vol_t *recharge*, FlowType *type*)

Only for RECHARGE FAST_SURFACE_RUNOFF

GlobalFlow::Model::*ExternalFlow***ExternalFlow**(int *id*, t_meter *flowHead*, t_meter *bottom*, t_vol_t *evapotrans*)

Constructor for Evapotranspiration.

Return

Parameters

- `id`:
- `flowHead`:
- `bottom`:
- `evapotrans`:

bool *GlobalFlow*::Model::*ExternalFlow***flowIsHeadDependant**(t_meter *head*) **const**

Check if flow can be calculated on the right hand side

Return Bool

Parameters

- `head`: The current hydraulic head

t_s_meter_t *GlobalFlow*::Model::*ExternalFlow***getP**(t_meter *head*, t_meter *eq_head*, t_vol_t *recharge*, t_dim *slope*, t_vol_t *eqFlow*) **const**

The head dependant part of the external flow equation

Return

Parameters

- `head`: The current hydraulic head
- `eq_head`: The equilibrium head
- `recharge`: The current recharge
- `slope`:
- `eqFlow`:

t_vol_t *GlobalFlow*::Model::*ExternalFlow***getQ**(t_meter *head*, t_meter *eq_head*, t_vol_t *recharge*, t_dim *slope*, t_vol_t *eqFlow*) **const**

The head independant part of the external flow equation

Return

Parameters

- `head`:
- `eq_head`:
- `recharge`:
- `slope`:
- `eqFlow`:

FlowType *GlobalFlow*::Model::*ExternalFlow***getType**() **const** t_meter *GlobalFlow*::Model::*ExternalFlow***getBottom**() **const**

t_vol_t *GlobalFlow*::Model::*ExternalFlow***getRecharge**() **const**

t_meter *GlobalFlow*::Model::*ExternalFlow***getFlowHead**() **const**

t_s_meter_t *GlobalFlow*::Model::*ExternalFlow***getDyn**(t_vol_t *current_recharge*, t_meter *eq_head*, t_meter *head*, t_vol_t *eq_flow*) **const**

t_meter *GlobalFlow*::Model::*ExternalFlow***getRiverDiff**(t_meter *eqHead*) **const**

t_s_meter_t *GlobalFlow*::Model::*ExternalFlow***getConductance**() **const**

int *GlobalFlow*::Model::*ExternalFlow***getID**() **const**

void *GlobalFlow*::Model::*ExternalFlow***setMult**(double *mult*)

void *GlobalFlow*::Model::*ExternalFlow***setLock**()

bool *GlobalFlow*::Model::*ExternalFlow***getLock**()

void *GlobalFlow*::Model::*ExternalFlow***setLockRecharge**(t_vol_t *re*)

t_vol_t *GlobalFlow*::Model::*ExternalFlow***getLockRecharge**()

void *GlobalFlow*::Model::*ExternalFlow***setLockConduct**(t_s_meter_t *c*)

t_s_meter_t *GlobalFlow*::Model::*ExternalFlow***getLockConduct**()

void *GlobalFlow*::Model::*ExternalFlow***getERC**(t_vol_t *current_recharge*, t_meter *eq_head*, t_meter *current_head*, t_vol_t *eq_flow*)

FluidMechanics

class *GlobalFlow*::Model::**FluidMechanics**

Provides helper functions for conductance calulcations

Public Functions

GlobalFlow::Model::*FluidMechanics***FluidMechanics**()

t_meter *GlobalFlow*::Model::*FluidMechanics***calcDeltaV**(t_meter *head*, t_meter *elevation*, t_meter *depth*)

Used to calculate if a cell is dry

quantity<MeterSquaredPerTime> *GlobalFlow*::Model::*FluidMechanics***calculateEFoldingConductance**(FlowI *flow*, t_mete *folding_se* t_mete *folding_ne*

quantity<MeterSquaredPerTime> *GlobalFlow*::Model::*FluidMechanics***calculateHarmonicMeanConductance**(

Calculates the horizontal flow between two nodes.

Return A weighted conductance value for the flow between two nodes Calculates the harmonic mean conductance between two nodes. $C = 2 EdgeLenght_1 { (TR_1 TR_2)}{(TR_1 EdgeLenght_1 + TR_2 EdgeLenght_2)}$

Parameters

180

- `flow`: a touple of inputs about the aquifer

double *GlobalFlow*::Model::*FluidMechanics***`smoothFunction__NWT`** (t_meter *elevation*, t_meter *verticalSize*, t_meter *head*)

Simple smoother function to buffer iteration steps in NWT approach

Return smoothed head

Parameters

- `elevation`:
- `verticalSize`:
- `head`:

quantity<MeterSquaredPerTime> *GlobalFlow*::Model::*FluidMechanics***`getHCOF`** (bool *steadyState*, quantity<Dimensionless> *stepModifier*, t_s_meter *storageCapacity*, t_s_meter_t *P*)

Get the coeffiecients for storage and P components

Return HCOF

Parameters

- `steadyState`:
- `stepModifier`:
- `storageCapacity`:
- `P`:

quantity<MeterSquaredPerTime> *GlobalFlow*::Model::*FluidMechanics***`calculateVerticalConductance`** (FlowInpu *flow*)

Calculates the vertical flow between two nodes

Return the vertical conductance

Parameters

- `flow`: a touple of inputs about the aquifer

double *GlobalFlow*::Model::*FluidMechanics***`getDerivate__NWT`** (t_meter *elevation*, t_meter *verticalSize*, t_meter *head*)

Calculate derivates for NWT approach

Return

Parameters

- `elevation`:
- `verticalSize`:
- `head`:

t_s_meter_t *GlobalFlow*::Model::*FluidMechanics***`estimateConductance`** (t_vel *K*, t_meter *length*, t_meter *width*, t_meter *Daq*, t_meter *G*, t_meter *depth*)

Criv = Krb/e*L*W Krb/e = 2*Kh/W*(gamma/(1-G*gamma/Daq) gamma = 1/(2*(1+1/pi*ln(2/(1-sqrt(e^(-pi*WpN)))))) where WpN is a normalized wetted perimeter which is W/Daq

Krb - hydraulic conductivity of the river bed (we will just use that of the aquifer in that cell) e - thickness of the river bed (this is totally unknown, but this falls out in the approximation that we will use) L - the length of the river in the cell (intersect length. . . not sure you have this or not?) W - width of the river in the cell Kh - horizontal hydraulic conductivity of the aquifer (can use the same as Krb above as a start) G - is the side length of the finite difference cell Daq - is the average depth (thickness) of the aquifer in the cell (layer thickness)

NodeInterface

class *GlobalFlow*::Model::**NodeInterface**

Interface defining required fields for a node. A node is the central comutational and spatial unit. A simulated area is seperated into a discrete raster of cells or nodes (seperate computational units which stay in contact to ech other). *Is* equal to 'cell'.

Nodes can be of different physical property e.g. different size.

Subclassed by GlobalFlow::Model::StandardNode, GlobalFlow::Model::StaticHeadNode

Public Functions

template <**class** Archive>
void *GlobalFlow*::Model::*NodeInterface***serialize** (Archive &*ar*, **const** unsigned int *version*)

GlobalFlow::Model::*NodeInterface***NodeInterface** (NodeVector *nodes*, double *lat*, double *lon*, t_s_meter *area*, large_num *ArcID*, large_num *ID*, t_vel *K*, int *stepModifier*, double *aquiferDepth*, double *anisotropy*, double *specificYield*, double *specificStorage*, bool *confined*)

Constructor of abstract class *NodeInterface*.

Parameters

- `nodes`: Vector of all other existing nodes
- `lat`: The latitude
- `lon`: The Longitude
- `area`: Area in m^2
- `ArcID`: Unique ARC-ID specified by Kassel
- `ID`: Internal ID = *Position* in vector
- `K`: Hydraulic conductivity in meter/day (default)
- `stepModifier`: Modfies default step size of day (default=1)
- `aquiferDepth`: Vertical size of the cell
- `anisotropy`: Modifier for vertical conductivity based on horizontal
- `specificYield`: Yield of storage for dewatered conditions
- `specificStorage`: Specific storage - currently for confined and unconfined
- `confined`: *Is* node in a confined layer

virtual *GlobalFlow*::Model::*NodeInterface***~NodeInterface** ()

large_num *GlobalFlow*::Model::*NodeInterface***getID** ()

void *GlobalFlow*::Model::*NodeInterface***setElevation** (t_meter *elevation*)

Set elevation on top layer and propagate to lower layers.

Parameters

182

- `elevation`: The top elevation (e.g. from DEM)

void *GlobalFlow*::Model::*NodeInterface***`setSlope`**(double *slope_percent*)

Set slope from data on all layers Slope input is in % but is required as absolut thus: slope = sloper_percent / 100.

Parameters

- `slope`:

void *GlobalFlow*::Model::*NodeInterface***`setEfold`**(double *efold*)

Set e-folding factor from data on all layers.

Parameters

- `e-fold`:

void *GlobalFlow*::Model::*NodeInterface***`setEqHead`**(t_meter *wtd*)

Calculated equilibrium groundwater-head from eq_wtd Assumes that if initialhead = false that the eq_head is also used as initial head.

Parameters

- `head`:

`template <class` HeadType>
FlowInputHor *GlobalFlow*::Model::*NodeInterface***`createDataTuple`**(map_itter *got*)

FlowInputVert *GlobalFlow*::Model::*NodeInterface***`createDataTuple`**(map_itter *got*)

`template <class` HeadType>
t_vol_t *GlobalFlow*::Model::*NodeInterface***`calcLateralFlows`**(bool *onlyOut*)

Calculate the lateral groundwater flow to the neighbouring nodes Generic function used for calulating equlibrium and current step flow

Return

t_vol_t *GlobalFlow*::Model::*NodeInterface***`getEqFlow`**()

Calculate the equlibrium lateral flows

Return eq lateral flow

t_vol_t *GlobalFlow*::Model::*NodeInterface***`getLateralFlows`**()

Get the current lateral flow

Return

t_vol_t *GlobalFlow*::Model::*NodeInterface***`getLateralOutFlows`**()

Get the current lateral out flows

Return

bool *GlobalFlow*::Model::*NodeInterface***`resetFloodingHead`**()

Cuts off all heads above surface elevation.

Warning Should only be used in spinn up phase!

Return Bool if node was reset

void *GlobalFlow*::Model::*NodeInterface***`scaleRiverConduct`**()

Scales river conduct by 50%.

Warning Should only be used in spinn up phase void *GlobalFlow*::Model::*NodeInterface***updateHeadChange**()

Update the current head change (in comparison to last time step)

Note Should only be caled at end of timestep

void *GlobalFlow*::Model::*NodeInterface***initHead_t0**()

void *GlobalFlow*::Model::*NodeInterface***setHead_direct**(double *head*)

t_vel *GlobalFlow*::Model::*NodeInterface***getK__pure**()

void *GlobalFlow*::Model::*NodeInterface***setSimpleK**()

t_vel *GlobalFlow*::Model::*NodeInterface***getK**()

Get hydraulic conductivity.

Return hydraulic conductivity (scaled by e-folding)

t_vel *GlobalFlow*::Model::*NodeInterface***getK_vertical**()

Get hydraulic vertical conductivity.

Return hydraulic conductivity scaled by anisotropy (scaled by e-folding)

void *GlobalFlow*::Model::*NodeInterface***setK**(t_vel *conduct*)

Modify hydraulic conductivity (applied to all layers below)

Parameters

- `New`: conductivity (if e-folding enabled scaled on layers)

void *GlobalFlow*::Model::*NodeInterface***setK_direct**(t_vel *conduct*)

Modify hydraulic conductivity (no e-folding, no layers)

Parameters

- `New`: conductivity

t_c_meter *GlobalFlow*::Model::*NodeInterface***getOUT**()

Get all outflow since simulation start.

t_c_meter *GlobalFlow*::Model::*NodeInterface***getIN**()

Get all inflow since simulation start.

void *GlobalFlow*::Model::*NodeInterface***toogleStadyState**(bool *onOFF*)

Toogle steady state simulation.

Parameters

- `onOFF`: true=on Turns all storage equations to zero with no timesteps

void *GlobalFlow*::Model::*NodeInterface***updateStepSize**(double *mod*)

t_s_meter *GlobalFlow*::Model::*NodeInterface***getStorageCapacity**()

Storage capacity based on yield or specific storage.

Return Potential flow budget when multiplied by head change Uses an 0.001m epsilon to determine if a water-table condition is present. If the layer is confined or not in water-table condition returns primary capacity.

184

ExternalFlow &*GlobalFlow*::Model::*NodeInterface***getExternalFlowByName** (FlowType *type*)

Get and external flow by its FlowType.

Return Ref to external flow

Parameters

- `type`: The flow type

Exceptions

- `OutOfRangeException`:

t_vol_t *GlobalFlow*::Model::*NodeInterface***getExternalFlowVolumeByName** (FlowType *type*)

Get and external flow volume by its FlowType.

Return Flow volume

Parameters

- `type`: The flow type

t_vol_t *GlobalFlow*::Model::*NodeInterface***getTotalStorageFlow** ()

Get flow budget based on head change.

Return Flow volume Note: Water entering storage is treated as an outflow (-), that is a loss of water from the flow system while water released from storage is treated as inflow (+), that is a source of water to the flow system

t_vol_t *GlobalFlow*::Model::*NodeInterface***calculateExternalFlowVolume** (**const** *ExternalFlow* *&flow*)

Get flow budget of a specific external flows.

Return Flow volume Note: Water entering storage is treated as an outflow (-), that is a loss of water from the flow system while water released from storage is treated as inflow (+), that is a source of water to the flow system

Parameters

- `&flow`: A external flow

t_vol_t *GlobalFlow*::Model::*NodeInterface***calculateDewateredFlow** ()

Caluclate dewatered flow.

Return Flow volume per time If a cell is dewatered but below a saturated or partly saturated cell: this calculates the needed additional exchange volume

t_vol_t *GlobalFlow*::Model::*NodeInterface***getCurrentIN** ()

Get all current IN flow.

Return Flow volume

t_vol_t *GlobalFlow*::Model::*NodeInterface***getCurrentOUT** ()

Get all current OUT flow.

Return Flow volume

void *GlobalFlow*::Model::*NodeInterface***saveMassBalance** ()

Tell cell to save its flow budget.

void *GlobalFlow*::Model::*NodeInterface***setNeighbour**(large_num *ID*, NeighbourPosition *neighbour*)

Add a neighbour.

Parameters

- `ID`: The internal ID and position in vector
- `neighbour`: The position relative to the cell

int *GlobalFlow*::Model::*NodeInterface***getNumofNeighbours**()

NodeInterface **GlobalFlow*::Model::*NodeInterface***getNeighbour**(NeighbourPosition *neighbour*)

Get a neighbour by position.

Return Pointer to cell object

Parameters

- `neighbour`: The position relative to the cell

int *GlobalFlow*::Model::*NodeInterface***addExternalFlow**(FlowType *type*, t_meter *flowHead*, double *cond*, t_meter *bottom*)

At an external flow to the cell.

Return Number assigned by cell to flow

Parameters

- `type`: The flow type
- `flowHead`: The flow head
- `cond`: The conductance
- `bottom`: The bottom of the flow (e.g river bottom)

void *GlobalFlow*::Model::*NodeInterface***removeExternalFlow**(FlowType *type*)

Remove an external flow to the cell by id.

Parameters

- `ID`: The flow id

int *GlobalFlow*::Model::*NodeInterface***getNumOfExternalFlows**()

The number of external flows.

bool *GlobalFlow*::Model::*NodeInterface***hasTypeOfExternalFlow**(FlowType *type*)

Check for an external flow by type.

Return bool

Parameters

- `type`: The flow type

void *GlobalFlow*::Model::*NodeInterface***updateUniqueFlow**(double *amount*, FlowType *flow* = RECHARGE, bool *lock* = true)

Updates GW recharge Curently assumes only one recharge as external flow!

Parameters

- `amount`: The new flow amount

186

- `Should`: the recharge in the dynamic rivers be locked or updated by this change?

void *GlobalFlow*::Model::*NodeInterface*`scaleDynamicRivers`(double *mult*)

Scale dyn rivers for sensitivity

Parameters

- `mult`:

void *GlobalFlow*::Model::*NodeInterface*`updateExternalFlowConduct`(double *amount*, FlowType *type*)

Update wetlands, lakes.

Parameters

- `amount`:
- `type`:

void *GlobalFlow*::Model::*NodeInterface*`updateExternalFlowFlowHead`(double *amount*, FlowType *type*)

Multiplies flow head for Sensitivity An. wetlands, lakes, rivers.

Parameters

- `amount`:
- `type`:

void *GlobalFlow*::Model::*NodeInterface*`setExternalFlowFlowHead`(double *amount*, FlowType *type*)

Sets flowHead An. wetlands, lakes, rivers.

Parameters

- `amount`:
- `type`:

void *GlobalFlow*::Model::*NodeInterface*`addExternalFlowFlowHead`(double *amount*, FlowType *type*)

adds delta to flowHead An. wetlands, lakes, rivers

Note Also checks for locked recharge

Parameters

- `amount`:
- `type`:

void *GlobalFlow*::Model::*NodeInterface*`updateLakeBottoms`(double *amount*)

Update lake bottoms Used for sensitivity.

Parameters

- `amount`:

bool *GlobalFlow*::Model::*NodeInterface*`hasRiver`()

Check for type river.

Return bool

bool *GlobalFlow*::Model::*NodeInterface***hasOcean**()

Check for type ocean.

Return bool

t_vol_t *GlobalFlow*::Model::*NodeInterface***getQ**()

Get Q part of flow equations.

Return volume over time

t_s_meter_t *GlobalFlow*::Model::*NodeInterface***getP**()

Get P part of flow equations.

Return volume over time

t_vol_t *GlobalFlow*::Model::*NodeInterface***calculateNotHeadDependandFlows**()

Get flow which is not groundwater head dependent.

Return volume over time Flow can be added to constant flows on right side of the equations If head is above river bottom for example

std::unordered_map<large_num, t_s_meter_t> *GlobalFlow*::Model::*NodeInterface***getJacobian**()

The jacobian entry for the cell (NWT approach)

Return map <CellID,Conductance>

std::unordered_map<large_num, t_s_meter_t> *GlobalFlow*::Model::*NodeInterface***getConductance**()

The matrix entry for the cell.

Return map <CellID,Conductance> The left hand side of the equation

t_vol_t *GlobalFlow*::Model::*NodeInterface***getRHS**()

The right hand side of the equation.

Return volume per time

double *GlobalFlow*::Model::*NodeInterface***getRHS__NWT**()

The right hand side of the equation (NWT)

Return volume per time

void *GlobalFlow*::Model::*NodeInterface***setHead**(t_meter *head*)

t_meter *GlobalFlow*::Model::*NodeInterface***calcInitialHead**(t_meter *initialParam*)

bool *GlobalFlow*::Model::*NodeInterface***isStaticNode**()

PhysicalProperties &*GlobalFlow*::Model::*NodeInterface***getProperties**()

void *GlobalFlow*::Model::*NodeInterface***enableNWT**()

template <**typename** CompareFunction>
t_vol_t *GlobalFlow*::Model::*NodeInterface***getNonStorageFlow**(CompareFunction *compare*)

Caluclate non storage related in and out flow.

Return Flow volume

188

quantity<Velocity> *GlobalFlow*::Model::*NodeInterface***getVelocity**(map_itter *pos*)

Calculate the lateral flow velocity

Return

Parameters

- pos:

std::pair<double, double> *GlobalFlow*::Model::*NodeInterface***getVelocityVector**()

Calculate flow velocity for flow tracking Vx and Vy represent the flow velocity in x and y direction. A negative value represents a flow in the oposite direction.

Return Velocity vector (x,y)

Public Members

bool *GlobalFlow*::Model::*NodeInterface***cached** = {false}

Calculated equilibrium flow to neighbouring cells Static thus calculated only once.

Depends on: K in cell and eq_head in all 6 neighbours

t_vol_t *GlobalFlow*::Model::*NodeInterface***eq_flow** = {0 * si::cubic_meter / day}

Friends

friend GlobalFlow::Model::NodeInterface::boost::serialization::access

class *GlobalFlow*::Model::*NodeInterface***NodeNotFoundException**

Inherits from exception

2.5 Simulation

Options

class *GlobalFlow*::Simulation::**Options**

Reads simulation options from a JSON file Defines getters and setters for options

Public Types

enum *GlobalFlow*::Simulation::*Options***BoundaryCondition**

Values:

GlobalFlow::Simulation::*Options***CONSTANT_HEAD_SEA_LEVEL**

GlobalFlow::Simulation::*Options***CONSTANT_HEAD_NEIGHBOUR**

GlobalFlow::Simulation::*Options***STATIC_HEAD_SEA_LEVEL**

Public Functions

void *GlobalFlow*::Simulation::*Options***setClosingCrit**(double *crit*)

void *GlobalFlow*::Simulation::*Options***setDamping**(bool *set*)

bool *GlobalFlow*::Simulation::*Options***isDampingEnabled**()

double *GlobalFlow*::Simulation::*Options***getMinDamp**()

double *GlobalFlow*::Simulation::*Options***getMaxDamp**()

double *GlobalFlow*::Simulation::*Options***getMaxHeadChange**()

bool *GlobalFlow*::Simulation::*Options***isConfined**(int *layer*)

bool *GlobalFlow*::Simulation::*Options***isOneLayerApproach**()

vector<bool> *GlobalFlow*::Simulation::*Options***getConfinements**()

BoundaryCondition *GlobalFlow*::Simulation::*Options***getBoundaryCondition**()

bool *GlobalFlow*::Simulation::*Options***isSensitivity**()

bool *GlobalFlow*::Simulation::*Options***isKFromLith**()

bool *GlobalFlow*::Simulation::*Options***isKOceanFile**()

bool *GlobalFlow*::Simulation::*Options***isSpecificStorageFile**()

bool *GlobalFlow*::Simulation::*Options***isSpecificYieldFile**()

bool *GlobalFlow*::Simulation::*Options***isKRiverFile**()

bool *GlobalFlow*::Simulation::*Options***isAquiferDepthDile**()

string *GlobalFlow*::Simulation::*Options***getKDir**()

string *GlobalFlow*::Simulation::*Options***getKRiverDir**()

string *GlobalFlow*::Simulation::*Options***getKOceanDir**()

string *GlobalFlow*::Simulation::*Options***getSSDir**()

string *GlobalFlow*::Simulation::*Options***getSYDir**()

string *GlobalFlow*::Simulation::*Options***getAQDepthDir**()

bool *GlobalFlow*::Simulation::*Options***isRowCol**()

int *GlobalFlow*::Simulation::*Options***getInnerItter**()

long *GlobalFlow*::Simulation::*Options***getNumberOfNodes**()

int *GlobalFlow*::Simulation::*Options***getNumberOfLayers**()

int *GlobalFlow*::Simulation::*Options***getMaxIterations**()

double *GlobalFlow*::Simulation::*Options***getConverganceCriteria**()

string *GlobalFlow*::Simulation::*Options***getSolverName**()

bool *GlobalFlow*::Simulation::*Options***disableDryCells**()

string *GlobalFlow*::Simulation::*Options***getNodesDir**()

string *GlobalFlow*::Simulation::*Options***getElevation**()

string *GlobalFlow*::Simulation::*Options***getEfolding**()

string *GlobalFlow*::Simulation::*Options***getEqWTD**()

string *GlobalFlow*::Simulation::*Options***getSlope**()

string *GlobalFlow*::Simulation::*Options***getBlue**()

vector<string> *GlobalFlow*::Simulation::*Options***getElevation_A**()

vector<string> *GlobalFlow*::Simulation::*Options***getEfolding_a**()

vector<string> *GlobalFlow*::Simulation::*Options***getEqWTD_a**()

vector<string> *GlobalFlow*::Simulation::*Options***getSlope_a**()

vector<string> *GlobalFlow*::Simulation::*Options***getBlue_a**()

string *GlobalFlow*::Simulation::*Options***getRecharge**()

string *GlobalFlow*::Simulation::*Options***getLithology**()

string *GlobalFlow*::Simulation::*Options***getRivers**()

string *GlobalFlow*::Simulation::*Options***getGlobalLakes**()

string *GlobalFlow*::Simulation::*Options***getGlobalWetlands**()

string *GlobalFlow*::Simulation::*Options***getLocalLakes**()

string *GlobalFlow*::Simulation::*Options***getLocalWetlands**()

string *GlobalFlow*::Simulation::*Options***getMapping**()

int *GlobalFlow*::Simulation::*Options***getThreads**()

const bool *GlobalFlow*::Simulation::*Options***adaptiveStepsizeEnabled**()

const int *GlobalFlow*::Simulation::*Options***getStepsizeModifier**()

bool *GlobalFlow*::Simulation::*Options***cacheEnabled**()

int *GlobalFlow*::Simulation::*Options***getInitialHead**()

double *GlobalFlow*::Simulation::*Options***getInitialK**()

double *GlobalFlow*::Simulation::*Options***getOceanConduct**()

vector<int> *GlobalFlow*::Simulation::*Options***getAquiferDepth**()

double *GlobalFlow*::Simulation::*Options***getAnisotropy**()

double *GlobalFlow*::Simulation::*Options***getSpecificYield**()

double *GlobalFlow*::Simulation::*Options***getSpecificStorage**()

void *GlobalFlow*::Simulation::*Options***load**(**const** std::string &*filename*)

void *GlobalFlow*::Simulation::*Options***save**(**const** std::string &*filename*)

Simulation

class *GlobalFlow*::Simulation::**Simulation**

The simulation class which holds the equation, options and data instance Further contains methods for calulating the mass balance and sensitivity methods

Public Types

enum *GlobalFlow*::Simulation::*Simulation***Flows**

Values:

GlobalFlow::Simulation::*Simulation***RIVERS** = 1

GlobalFlow::Simulation::*Simulation***DRAINS**

GlobalFlow::Simulation::*Simulation***RIVER_MM**

GlobalFlow::Simulation::*Simulation***LAKES**

GlobalFlow::Simulation::*Simulation***WETLANDS**

GlobalFlow::Simulation::*Simulation***GLOBAL_WETLANDS**

GlobalFlow::Simulation::*Simulation***RECHARGE**

GlobalFlow::Simulation::*Simulation***FASTSURFACE**

GlobalFlow::Simulation::*Simulation***NAG**

GlobalFlow::Simulation::*Simulation***STORAGE**

GlobalFlow::Simulation::*Simulation***GENERAL_HEAD_BOUNDARY**

Public Functions

GlobalFlow::Simulation::*Simulation***Simulation**()

GlobalFlow::Simulation::*Simulation***Simulation**(*Options op*, *DataReader *reader*)

Solver::*Equation* **GlobalFlow*::Simulation::*Simulation***getEquation**()

void *GlobalFlow*::Simulation::*Simulation***save**()

Serialize current node state

void *GlobalFlow*::Simulation::*Simulation***restore**()

std::string *GlobalFlow*::Simulation::*Simulation***NodeInfosByID**(unsigned long *nodeID*)

Get basic node information by its id

Return A string of information

Parameters

- `nodeID`:

template <int *FieldNum*>
std::string *GlobalFlow*::Simulation::*Simulation***getFlowSumByIDs**(std::array<int, FieldNum> *ids*)

Get budget per node

Return

Parameters

- `ids`:

std::string *GlobalFlow*::Simulation::*Simulation***NodeFlowsByID**(unsigned long *nodeID*)

Return all external flows seperatly

template <**class** FunOut, **class** FunIn>
MassError *GlobalFlow*::Simulation::*Simulation***getError**(FunOut *fun1*, FunIn *fun2*)

Calulate the mass error

Return

Parameters

- `fun1`: Function to get OutFlow
- `fun2`: Function to get InFlow

MassError *GlobalFlow*::Simulation::*Simulation***getMassError**()

Get the total mass balance

Return

MassError *GlobalFlow*::Simulation::*Simulation***getCurrentMassError**()

Get the mass balance for the current step

Return

double *GlobalFlow*::Simulation::*Simulation***getLossToRivers**()

Get the flow lost to external flows

Return

template <**class** Fun>
MassError *GlobalFlow*::Simulation::*Simulation***getError**(Fun *fun*)

Decide if its an In or Outflow

Return

Parameters

- `fun`:

string *GlobalFlow*::Simulation::*Simulation***getFlowByName**(*Flows* *flow*)

Helper function for printing the mass balance for each flow

Return

Parameters

- `flow`:

void *GlobalFlow*::Simulation::*Simulation***printMassBalances**(*custom_severity_level* *level*)

Prints all mass balances

DataReader **GlobalFlow*::Simulation::*Simulation***getDataReader**()

NodeVector **const** &*GlobalFlow*::Simulation::*Simulation***getNodes**()

void *GlobalFlow*::Simulation::*Simulation***writeResiduals**(string *path*)

Get the residuals of the current iteration

Parameters

- `path`:

bool *GlobalFlow*::Simulation::*Simulation***isRestored**()

Stepper

class *GlobalFlow*::Simulation::**Stepper**

holding the simulation iterator

Inherits from GlobalFlow::Simulation::AbstractStepper

Public Functions

GlobalFlow::Simulation::*Stepper***Stepper**(Solver::*Equation* **eq*, **const** TimeFrame *time*, **const** size_t *steps*, bool *dynStep* = false)

virtual Solver::*Equation* **GlobalFlow*::Simulation::*Stepper***get**(int *col*) **const**

Iterator *GlobalFlow*::Simulation::*Stepper***begin**() **const**

Iterator *GlobalFlow*::Simulation::*Stepper***end**() **const**

const TimeFrame *GlobalFlow*::Simulation::*Stepper***getStepSize**()

2.6 Solver

Equation

class *GlobalFlow*::Solver::**Equation**

finite difference equation Should only be accessed through the stepper

Public Types

typedef Eigen::Matrix<pr_t, -1, 1, 0, -1, 1>::Scalar *GlobalFlow*::Solver::*Equation***Scalar**

typedef Matrix<*Scalar*, Dynamic, 1> *GlobalFlow*::Solver::*Equation***VectorType**

Public Functions

GlobalFlow::Solver::*Equation***Equation**(large_num *numberOfNodes*, NodeVector *nodes*, Simulation::*Options* *options*)

GlobalFlow::Solver::*Equation***~Equation**()

void *GlobalFlow*::Solver::*Equation***solve**()

Solve the current iteration step

Solve *Equation*

int *GlobalFlow*::Solver::*Equation***getItter**()

Return The number of iterations

double *GlobalFlow*::Solver::*Equation***getError**()

Return The current residual error

GlobalFlow::Solver::*Equation***Equation**(**const** *Equation*&)

Equation &*GlobalFlow*::Solver::*Equation***operator=**(**const** *Equation*&)

long_vector *GlobalFlow*::Solver::*Equation***getResults**()

bool *GlobalFlow*::Solver::*Equation***toogleSteadyState**()

Toogle the steady-state in all nodes

Return

void *GlobalFlow*::Solver::*Equation***updateStepSize**(double *mod*)

Set the correct stepsize (default is DAY)

Parameters

- `mod`:

VectorType &*GlobalFlow*::Solver::*Equation***getResiduals**()

void *GlobalFlow*::Solver::*Equation***updateClosingCrit**(pr_t *crit*)

void *GlobalFlow*::Solver::*Equation***updateMaxHeadChange**(double *head*)

void *GlobalFlow*::Solver::*Equation***updateMaxItter**(int *itter*)

void *GlobalFlow*::Solver::*Equation***enableDamping**()

Note resests dampening object and counters

194

Friends

std::ostream &**operator<<**(std::ostream &*os*, Equation &*eq*)

Helper to write out current residuals

Return

Parameters

- `os`:
- `eq`:

AdaptiveDamping .. doxygenclass:: GlobalFlow::Solver::AdaptiveDamping

2.7 Tests

Unit Tests The unit tests can be found in the tests folder under Unit. A header file exists for every main model component including the according unit tests.

195

CHAPTER

THREE

G^{3}M STEADY-STATE MODEL

The implementation of the steady state-model along with the input data e.g. yearly average recharge, consists of two classes:

1. The main class which implements the *Groundwater Interface*
2. A data reader implementing the *Data Reader Interface*, which specifies how to read in the data

Main

`class` *GlobalFlow*`::GlobalStandaloneRunner`

A standalone global steady-state groundwater model.

Inherits from *GlobalFlow::GW_Interface< T >*

Public Functions

GlobalFlow::*GlobalStandaloneRunner***GlobalStandaloneRunner**()

Default constructor.

void *GlobalFlow*::*GlobalStandaloneRunner***loadSettings**()

Read general simulation settings e.g. Options

void *GlobalFlow*::*GlobalStandaloneRunner***setupSimulation**()

Do additional work required for a running simulation

void *GlobalFlow*::*GlobalStandaloneRunner***simulate**()

Simulate/Run the model

void *GlobalFlow*::*GlobalStandaloneRunner***writeData**()

Private Functions

set<int> *GlobalFlow*::*GlobalStandaloneRunner***getMapping**()

Helper function for arcID mappings.

Return a set of arcIDs

Private Members

Solver::*Equation* **GlobalFlow*::*GlobalStandaloneRunner*_**eq**

Simulation::*Options* *GlobalFlow*::*GlobalStandaloneRunner***op**

Simulation::*Simulation* *GlobalFlow*::*GlobalStandaloneRunner***sim**

DataProcessing::*GlobalDataReader* **GlobalFlow*::*GlobalStandaloneRunner***reader**

Global Data Reader

class *GlobalFlow*::DataProcessing::**GlobalDataReader**

This class provides methods for loading large input data The paths are specified in the json file in in the data folder.

Inherits from *GlobalFlow::DataReader*

Public Types

using *GlobalFlow*::DataProcessing::*GlobalDataReader***Matrix** = std::vector<std::vector<T>>

Public Functions

GlobalFlow::DataProcessing::*GlobalDataReader***GlobalDataReader**(int *step*)

Constructor.

Parameters

- `step`: Daily, Monthly, . . .

void *GlobalFlow*::DataProcessing::*GlobalDataReader***readData**(Simulation::*Options* *op*)

Entry point for reading simulation data.

Attention This method needs to be implemented!

Note *readData()* is called by simulation at startup

Parameters

- `op`: Options object

Matrix<int> *GlobalFlow*::DataProcessing::*GlobalDataReader***readGrid**(NodeVector *nodes*, std::string *path*, int *numberOfNodes*, double *defaultK*, double *aquiferDepth*, double *anisotropy*, double *specificYield*, double *specificStorage*, bool *confined*)

Method for already gridded defintions - that is structered in row and column.

Note Structured in row, col

Return A Matrix of computational nodes

Parameters

- `nodes`: Vector of nodes
- `path`: Path to read definitions from
- `numberOfNodes`: The number of expected computation nodes
- `defaultK`: The default conductivity
- `aquiferDepth`: The default depth per cell
- `anisotropy`: The default relation of vertical and horizontal conductivity
- `specificYield`: The default specific yield
- `specificStorage`: The default specific storage

- `confined`: If node is part of a confined layer?

int *GlobalFlow*::DataProcessing::*GlobalDataReader*`readLandMask` (NodeVector *nodes*, std::string *path*, int *numberOfNodes*, double *defaultK*, double *aquiferDepth*, double *anisotropy*, double *specificYield*, double *specificStorage*, bool *confined*)

Initial readin of node definitions - without col and row.

Note Without col and row Reads a csv file with x and y coordinates for predefined grid of cells

Return

Parameters

- `nodes`: Vector of nodes
- `path`: Path to read definitions from
- `numberOfNodes`: The number of expected computation nodes
- `defaultK`: The default conductivity
- `aquiferDepth`: The default depth per cell
- `anisotropy`: The default relation of vertical and horizontal conductivity
- `specificYield`: The default specific yield
- `specificStorage`: The default specific storage
- `confined`: If node is part of a confined layer?

void *GlobalFlow*::DataProcessing::*GlobalDataReader*`readOceanData` (std::string *path*)

Read in a custom defintion for the ocean boundary Reads in conductivity and elevation data.

Parameters

- `path`: Where to read from

void *GlobalFlow*::DataProcessing::*GlobalDataReader*`readRiver` (std::string *path*)

Read in a custom river defintion file Structured as: global_ID, Head, Bottom, Conduct.

Parameters

- `path`: Where to read the file from

void *GlobalFlow*::DataProcessing::*GlobalDataReader*`readElevation` (std::string *path*, std::vector<std::string> *files*)

Read elevation data from a specified path Used for multiple files.

Note !Uses setElevation() function. Should only be called after all layers are build as it affects layers below

Parameters

- `path`: Where to read the file from
- `files`: If different files for different regions are given

void *GlobalFlow*::DataProcessing::*GlobalDataReader***readElevation**(std::string *path*)

Read elevation data from a specified path.

Note !Uses setElevation() function. Should only be called after all layers are build as it affects layers below

Parameters

- `path`: Where to read the file from

void *GlobalFlow*::DataProcessing::*GlobalDataReader***readSlope**(std::string *path*, std::vector<std::string> *files*)

Read slope data from a specified path.

Parameters

- `path`: Where to read the file from
- `files`: If different files for different regions are given

void *GlobalFlow*::DataProcessing::*GlobalDataReader***readEfold**(std::string *path*, std::vector<std::string> *files*)

Read e-folding data from a specified path.

Parameters

- `path`: Where to read the file from
- `files`: If different files for different regions are given

void *GlobalFlow*::DataProcessing::*GlobalDataReader***readEqWTD**(std::string *path*)

Read equilibrium water-table information used for the dynamic river computation.

Parameters

- `path`: Where to read the file from

void *GlobalFlow*::DataProcessing::*GlobalDataReader***readGWRecharge**(std::string *path*)

Read difuse gw-recharge.

Parameters

- `path`: Where to read the file from

void *GlobalFlow*::DataProcessing::*GlobalDataReader***readConduct**(std::string *path*)

Read cell conductance defintion.

Note currently does check if val > 10 m/day

Parameters

- `path`: Where to read the file from

template <**typename** ConversionFunction>
void *GlobalFlow*::DataProcessing::*GlobalDataReader***readGWRechargeMapping**(std::string *path*, ConversionFunction *convertToRate*)

Read difuse groundwater recharge from a file and map the value using a conversion function.

Template Parameters

200

- `ConversionFunction`: Allows the dynamic recalcualtion of recharge base don cell area

Parameters

- `path`: Where to read the file from
- `convertToRate`: The conversion function

std::unordered_map<int, std::array<double, 3>> *GlobalFlow*::DataProcessing::*GlobalDataReader*`calulateRiverStage`

Helper function for.

See *readBlueCells*

Return a map of bankfull depth, stream width, and lenght

Parameters

- `path`: Where to read the file from

void *GlobalFlow*::DataProcessing::*GlobalDataReader*`readBlueCells`(std::string *file*, std::unordered_map<int, std::array<double, 3>> *bankfull_depth*)

Reads in river defintions based on a specific elevation data-set.

See *calulateRiverStage*

Parameters

- `file`: to read from
- `bankfull_depth`: A map with addition information

void *GlobalFlow*::DataProcessing::*GlobalDataReader*`readLakesandWetlands`(std::string *pathGlobalLakes*, std::string *pathGlobalWetlands*, std::string *pathLokalLakes*, std::string *pathLokalWetlands*)

Reads in lakes and wetlands defintions based on Lehner and Döll.

Parameters

- `pathGlobalLakes`:
- `pathGlobalWetlands`:
- `pathLokalLakes`:
- `pathLokalWetlands`:

void *GlobalFlow*::DataProcessing::*GlobalDataReader*`addEvapo`()

Adds an evapotraspiration module to cells.

void *GlobalFlow*::DataProcessing::*GlobalDataReader*`addDrainageHack`()

A drainage component similar to de Graaf 2014.

201

CHAPTER

FOUR

G^3M FULLY-COUPLED TRANSIENT MODEL

The fully model coupling to WaterGAP is implemented in two files: watergap.hpp, which implements the gorundwater interface and GroundwaterCoupling.hpp which defines the transfer containers between the two models. The groundwater coupling object defined in watergap.hpp is then called in the main loop in the watergap model.

Model Setup

template <**class** DataArray>
class GroundwaterRunner

Inherits from *GlobalFlow::GW_Interface< DataArray >*

Public Functions

GroundwaterRunner`~GroundwaterRunner`()

void *GroundwaterRunner*`updateGWRechargeFromWaterGAP` (DataArray *field*, short *month*, int *numberOfGridCells*)

void *GroundwaterRunner*`updateNaGFromWaterGAP` (DataArray *field*, short *month*, int *numberOfGridCells*)

void *GroundwaterRunner*`updateSWBFromWaterGAP` (DataArray *rivers*, DataArray *global_wetlands*, DataArray *local_wetlands*, DataArray *global_lakes*, DataArray *local_lakes*, short *month*, int *numberOfGridCells*)

void *GroundwaterRunner*`setRiverStorageinWaterGAP` (DataArray *field*, short *month*, int *numberOfGridCells*)

void *GroundwaterRunner*`setGLWetlandStorageinWaterGAP` (DataArray *field*, short *month*, int *numberOfGridCells*)

void *GroundwaterRunner*`setLcWetlandStorageinWaterGAP` (DataArray *field*, short *month*, int *numberOfGridCells*)

void *GroundwaterRunner*`setGlobalLakeStorageinWaterGAP` (DataArray *field*, short *month*, int *numberOfGridCells*)

void *GroundwaterRunner*`setLocalLakeStorageinWaterGAP` (DataArray *field*, short *month*, int *numberOfGridCells*)

void *GroundwaterRunner*`setGWStorageinWaterGAP` (DataArray *field*, short *month*, int *numberOfGridCells*)

void *GroundwaterRunner*`loadSettings`()

Read general simulation settings e.g. Options

void *GroundwaterRunner*`setupSimulation`()

Do additional work required for a running simulation

void *GroundwaterRunner***spinnup**()
Spinnup for steady-state solution (no GW storage)

void *GroundwaterRunner***spinnup2**()
Spinnup for transient steady-state with 1901 GW abstractions

set<int> *GroundwaterRunner***getMapping**()

void *GroundwaterRunner***adjustConductance**()

void *GroundwaterRunner***adjust_convergence**()

void *GroundwaterRunner***simulate**()
Simulate/Run the model

void *GroundwaterRunner***getResults**()

void *GroundwaterRunner***printMassBalance**()

void *GroundwaterRunner***writeData**(std::string)
Write data for specific year or month

Private Functions

void *GroundwaterRunner***__up_month**()

Private Members

GlobalFlow::Solver::*Equation* **GroundwaterRunner***_eq**

GlobalFlow::Simulation::*Options GroundwaterRunner***op**

GlobalFlow::Simulation::*Simulation GroundwaterRunner***sim**

GlobalFlow::DataProcessing::*GlobalDataReader* **GroundwaterRunner***reader**

int *GroundwaterRunner***current_month** = {0}

std::array<int, 12> *GroundwaterRunner***days_in_month** = {31, 28, 31, 30, 31, 30, 31, 31, 30, 31, 30, 31}

Coupling Component
template <class Container>
class *GlobalFlow*::**WaterGAPCoupling**
Inherits from GlobalFlow::CouplingInterface< Container >

Public Functions

GlobalFlow::*WaterGAPCoupling***WaterGAPCoupling**(NodeVector *nodeVector*, *DataReader* **reader*)

const double *GlobalFlow*::*WaterGAPCoupling***scaleMMperMonthToVolPerDay**(**const** double *data*, **const** double *&area*)

Return data in m^3/day (internal unit is always day even if stepsize is different) FIXME use real moth lenght instead of 30 { 31, 28, 31, 30, 31, 30, 31, 31, 30, 31, 30, 31 };

Parameters

204

- `data`: in mm/month

const double *GlobalFlow*::*WaterGAPCoupling***scaleMMperDayToCubicMeter** (**const** double *data*, **const** double *&area*)

const double *GlobalFlow*::*WaterGAPCoupling***scaleCubicKMtoMeter** (**const** double *data*)

void *GlobalFlow*::*WaterGAPCoupling***updateRechargeInGW** (Container *data*, short *month*, int *numberOfGridCells*)

Updates groundwater recharge.

Note Under development

Parameters

- `field`: in mm/day
- `month`:
- `numberOfGridCells`:

void *GlobalFlow*::*WaterGAPCoupling***updateNetAbstractionInGW** (Container *data*, short *month*, int *numberOfGridCells*)

Update Netabstraction from groundwater.

Note Under development

Parameters

- `field`: in km^3/day
- `month`:
- `numberOfGridCells`:

void *GlobalFlow*::*WaterGAPCoupling***updateRiversInGW** (Container *data*, short *month*, int *numberOfGridCells*)

Update surfacewater head from groundwater.

Parameters

- `data`: River depth in m
- `month`:
- `numberOfGridCells`:

void *GlobalFlow*::*WaterGAPCoupling***updateGlobalWetlandsInGW** (Container *data*, short *month*, int *numberOfGridCells*)

Parameters

- `data`: current storage in km3
- `month`:
- `numberOfGridCells`:

void *GlobalFlow*::*WaterGAPCoupling***updateLocalWetlandsInGW** (Container *data*, short *month*, int *numberOfGridCells*)

void *GlobalFlow*::*WaterGAPCoupling***updateLakesInGW** (Container *data1*, Container *data2*, short *month*, int *numberOfGridCells*) void *GlobalFlow*::*WaterGAPCoupling***writeRiver** (Container *data*, short *month*, int *numberOfGridCells*)

Parameters

- `field`: in km^3
- `month`:
- `numberOfGridCells`:

void *GlobalFlow*::*WaterGAPCoupling***writeGlobalWetlands** (Container *data*, short *month*, int *numberOfGridCells*)

void *GlobalFlow*::*WaterGAPCoupling***writeLocalWetlands** (Container *data*, short *month*, int *numberOfGridCells*)

void *GlobalFlow*::*WaterGAPCoupling***writeLakes** (Container *data*, short *month*, int *numberOfGridCells*)

void *GlobalFlow*::*WaterGAPCoupling***writeStorage** (Container *data*, short *month*, int *numberOfGridCells*)

Note ! ugly cast because of array inconsitency

Parameters

- `field`: in km^3

Parameters

- `month`:
- `numberOfGridCells`:

Private Types

template<>
using *GlobalFlow*::WaterGAPCoupling<Container>**cache_v** = std::unordered_map<int, std::vector<int>>

Private Functions

cache_v *GlobalFlow*::*WaterGAPCoupling***getMap** (int *num*)

Private Members

std::unordered_map<int, double> *GlobalFlow*::*WaterGAPCoupling***RiverHeads_tn**

std::unordered_map<int, double> *GlobalFlow*::*WaterGAPCoupling***GlWetlandStorage_tn**

std::unordered_map<int, double> *GlobalFlow*::*WaterGAPCoupling***WetlandStorage_tn**

std::unordered_map<int, double> *GlobalFlow*::*WaterGAPCoupling***LakeStorage_tn**

bool *GlobalFlow*::*WaterGAPCoupling***prev_r** = {false}

bool *GlobalFlow*::*WaterGAPCoupling***recharge_lock** = {true}

cache_v *GlobalFlow*::*WaterGAPCoupling***cached_ids**

bool *GlobalFlow*::*WaterGAPCoupling***cached** = {false}

CHAPTER FIVE

GNU GENERAL PUBLIC LICENSE

Version 3, 29 June 2007

5.1 Preamble

The GNU General Public License is a free, copyleft license for software and other kinds of works.

The licenses for most software and other practical works are designed to take away your freedom to share and change the works. By contrast, the GNU General Public License is intended to guarantee your freedom to share and change all versions of a program–to make sure it remains free software for all its users. We, the Free Software Foundation, use the GNU General Public License for most of our software; it applies also to any other work released this way by its authors. You can apply it to your programs, too.

When we speak of free software, we are referring to freedom, not price. Our General Public Licenses are designed to make sure that you have the freedom to distribute copies of free software (and charge for them if you wish), that you receive source code or can get it if you want it, that you can change the software or use pieces of it in new free programs, and that you know you can do these things.

To protect your rights, we need to prevent others from denying you these rights or asking you to surrender the rights. Therefore, you have certain responsibilities if you distribute copies of the software, or if you modify it: responsibilities to respect the freedom of others.

For example, if you distribute copies of such a program, whether gratis or for a fee, you must pass on to the recipients the same freedoms that you received. You must make sure that they, too, receive or can get the source code. And you must show them these terms so they know their rights.

Developers that use the GNU GPL protect your rights with two steps: (1) assert copyright on the software, and (2) offer you this License giving you legal permission to copy, distribute and/or modify it.

For the developers' and authors' protection, the GPL clearly explains that there is no warranty for this free software. For both users' and authors' sake, the GPL requires that modified versions be marked as changed, so that their problems will not be attributed erroneously to authors of previous versions.

Some devices are designed to deny users access to install or run modified versions of the software inside them, although the manufacturer can do so. This is fundamentally incompatible with the aim of protecting users' freedom to change the software. The systematic pattern of such abuse occurs in the area of products for individuals to use, which is precisely where it is most unacceptable. Therefore, we have designed this version of the GPL to prohibit the practice for those products. If such problems arise substantially in other domains, we stand ready to extend this provision to those domains in future versions of the GPL, as needed to protect the freedom of users.

Finally, every program is threatened constantly by software patents. States should not allow patents to restrict development and use of software on general-purpose computers, but in those that do, we wish to avoid the special danger that patents applied to a free program could make it effectively proprietary. To prevent this, the GPL assures that patents cannot be used to render the program non-free.

The precise terms and conditions for copying, distribution and modification follow.

5.2 TERMS AND CONDITIONS

0. Definitions.

"This License" refers to version 3 of the GNU General Public License.

"Copyright" also means copyright-like laws that apply to other kinds of works, such as semiconductor masks.

"The Program" refers to any copyrightable work licensed under this License. Each licensee is addressed as "you". "Licensees" and "recipients" may be individuals or organizations.

To "modify" a work means to copy from or adapt all or part of the work in a fashion requiring copyright permission, other than the making of an exact copy. The resulting work is called a "modified version" of the earlier work or a work "based on" the earlier work.

A "covered work" means either the unmodified Program or a work based on the Program.

To "propagate" a work means to do anything with it that, without permission, would make you directly or secondarily liable for infringement under applicable copyright law, except executing it on a computer or modifying a private copy. Propagation includes copying, distribution (with or without modification), making available to the public, and in some countries other activities as well.

To "convey" a work means any kind of propagation that enables other parties to make or receive copies. Mere interaction with a user through a computer network, with no transfer of a copy, is not conveying.

An interactive user interface displays "Appropriate Legal Notices" to the extent that it includes a convenient and prominently visible feature that (1) displays an appropriate copyright notice, and (2) tells the user that there is no warranty for the work (except to the extent that warranties are provided), that licensees may convey the work under this License, and how to view a copy of this License. If the interface presents a list of user commands or options, such as a menu, a prominent item in the list meets this criterion.

1. Source Code.

The "source code" for a work means the preferred form of the work for making modifications to it. "Object code" means any non-source form of a work.

A "Standard Interface" means an interface that either is an official standard defined by a recognized standards body, or, in the case of interfaces specified for a particular programming language, one that is widely used among developers working in that language.

The "System Libraries" of an executable work include anything, other than the work as a whole, that (a) is included in the normal form of packaging a Major Component, but which is not part of that Major Component, and (b) serves only to enable use of the work with that Major Component, or to implement a Standard Interface for which an implementation is available to the public in source code form. A "Major Component", in this context, means a major essential component (kernel, window system, and so on) of the specific operating system (if any) on which the executable work runs, or a compiler used to produce the work, or an object code interpreter used to run it.

The "Corresponding Source" for a work in object code form means all the source code needed to generate, install, and (for an executable work) run the object code and to modify the work, including scripts to control those activities. However, it does not include the work's System Libraries, or general-purpose tools or generally available free programs which are used unmodified in performing those activities but which are not part of the work. For example, Corresponding Source includes interface definition files associated with source files for the work, and the source code for shared libraries and dynamically linked subprograms that the work is specifically designed to require, such as by intimate data communication or control flow between those subprograms and other parts of the work.

The Corresponding Source need not include anything that users can regenerate automatically from other parts of the Corresponding Source.

The Corresponding Source for a work in source code form is that same work.

2. Basic Permissions.

All rights granted under this License are granted for the term of copyright on the Program, and are irrevocable provided the stated conditions are met. This License explicitly affirms your unlimited permission to run the unmodified Program. The output from running a covered work is covered by this License only if the output, given its content, constitutes a covered work. This License acknowledges your rights of fair use or other equivalent, as provided by copyright law.

You may make, run and propagate covered works that you do not convey, without conditions so long as your license otherwise remains in force. You may convey covered works to others for the sole purpose of having them make modifications exclusively for you, or provide you with facilities for running those works, provided that you comply with the terms of this License in conveying all material for which you do not control copyright. Those thus making or running the covered works for you must do so exclusively on your behalf, under your direction and control, on terms that prohibit them from making any copies of your copyrighted material outside their relationship with you.

Conveying under any other circumstances is permitted solely under the conditions stated below. Sublicensing is not allowed; section 10 makes it unnecessary.

3. Protecting Users' Legal Rights From Anti-Circumvention Law.

No covered work shall be deemed part of an effective technological measure under any applicable law fulfilling obligations under article 11 of the WIPO copyright treaty adopted on 20 December 1996, or similar laws prohibiting or restricting circumvention of such measures.

When you convey a covered work, you waive any legal power to forbid circumvention of technological measures to the extent such circumvention is effected by exercising rights under this License with respect to the covered work, and you disclaim any intention to limit operation or modification of the work as a means of enforcing, against the work's users, your or third parties' legal rights to forbid circumvention of technological measures.

4. Conveying Verbatim Copies.

You may convey verbatim copies of the Program's source code as you receive it, in any medium, provided that you conspicuously and appropriately publish on each copy an appropriate copyright notice; keep intact all notices stating that this License and any non-permissive terms added in accord with section 7 apply to the code; keep intact all notices of the absence of any warranty; and give all recipients a copy of this License along with the Program.

You may charge any price or no price for each copy that you convey, and you may offer support or warranty protection for a fee.

5. Conveying Modified Source Versions.

You may convey a work based on the Program, or the modifications to produce it from the Program, in the form of source code under the terms of section 4, provided that you also meet all of these conditions:

> a) The work must carry prominent notices stating that you modified it, and giving a relevant date.
>
> b) The work must carry prominent notices stating that it is released under this License and any conditions added under section 7. This requirement modifies the requirement in section 4 to "keep intact all notices".
>
> c) You must license the entire work, as a whole, under this License to anyone who comes into possession of a copy. This License will therefore apply, along with any applicable section 7 additional terms, to the whole of the work, and all its parts, regardless of how they are packaged. This License gives no permission to license the work in any other way, but it does not invalidate such permission if you have separately received it.
>
> d) If the work has interactive user interfaces, each must display Appropriate Legal Notices; however, if the Program has interactive interfaces that do not display Appropriate Legal Notices, your work need not make them do so.

A compilation of a covered work with other separate and independent works, which are not by their nature extensions of the covered work, and which are not combined with it such as to form a larger program, in or on a volume of a storage or distribution medium, is called an "aggregate" if the compilation and its resulting copyright are not used to limit the access or legal rights of the compilation's users beyond what the individual works permit. Inclusion of a covered work in an aggregate does not cause this License to apply to the other parts of the aggregate.

6. Conveying Non-Source Forms.

You may convey a covered work in object code form under the terms of sections 4 and 5, provided that you also convey the machine-readable Corresponding Source under the terms of this License, in one of these ways:

> a) Convey the object code in, or embodied in, a physical product (including a physical distribution medium), accompanied by the Corresponding Source fixed on a durable physical medium customarily used for software interchange.
>
> b) Convey the object code in, or embodied in, a physical product (including a physical distribution medium), accompanied by a written offer, valid for at least three years and valid for as long as you offer spare parts or customer support for that product model, to give anyone who possesses the object code either (1) a copy of the Corresponding Source for all the software in the product that is covered by this License, on a durable physical medium customarily used for software interchange, for a price no more than your reasonable cost of physically performing this conveying of source, or (2) access to copy the Corresponding Source from a network server at no charge.
>
> c) Convey individual copies of the object code with a copy of the written offer to provide the Corresponding Source. This alternative is allowed only occasionally and noncommercially, and only if you received the object code with such an offer, in accord with subsection 6b.
>
> d) Convey the object code by offering access from a designated place (gratis or for a charge), and offer equivalent access to the Corresponding Source in the same way through the same place at no further charge. You need not require recipients to copy the Corresponding Source along with the object code. If the place to copy the object code is a network server, the Corresponding Source may be on a different server (operated by you or a third party) that supports equivalent copying facilities, provided you maintain clear directions next to the object code saying where to find the Corresponding Source. Regardless of what server hosts the Corresponding Source, you remain obligated to ensure that it is available for as long as needed to satisfy these requirements.
>
> e) Convey the object code using peer-to-peer transmission, provided you inform other peers where the object code and Corresponding Source of the work are being offered to the general public at no charge under subsection 6d.

A separable portion of the object code, whose source code is excluded from the Corresponding Source as a System Library, need not be included in conveying the object code work.

A “User Product” is either (1) a “consumer product”, which means any tangible personal property which is normally used for personal, family, or household purposes, or (2) anything designed or sold for incorporation into a dwelling. In determining whether a product is a consumer product, doubtful cases shall be resolved in favor of coverage. For a particular product received by a particular user, “normally used” refers to a typical or common use of that class of product, regardless of the status of the particular user or of the way in which the particular user actually uses, or expects or is expected to use, the product. A product is a consumer product regardless of whether the product has substantial commercial, industrial or non-consumer uses, unless such uses represent the only significant mode of use of the product.

“Installation Information” for a User Product means any methods, procedures, authorization keys, or other information required to install and execute modified versions of a covered work in that User Product from a modified version of its Corresponding Source. The information must suffice to ensure that the continued functioning of the modified object code is in no case prevented or interfered with solely because modification has been made.

If you convey an object code work under this section in, or with, or specifically for use in, a User Product, and the conveying occurs as part of a transaction in which the right of possession and use of the User Product is transferred to the recipient in perpetuity or for a fixed term (regardless of how the transaction is characterized), the Corresponding Source conveyed under this section must be accompanied by the Installation Information. But this requirement does not apply if neither you nor any third party retains the ability to install modified object code on the User Product (for example, the work has been installed in ROM).

The requirement to provide Installation Information does not include a requirement to continue to provide support service, warranty, or updates for a work that has been modified or installed by the recipient, or for the User Product in which it has been modified or installed. Access to a network may be denied when the modification itself materially and adversely affects the operation of the network or violates the rules and protocols for communication across the network.

Corresponding Source conveyed, and Installation Information provided, in accord with this section must be in a format that is publicly documented (and with an implementation available to the public in source code form), and must require no special password or key for unpacking, reading or copying.

7. Additional Terms.

"Additional permissions" are terms that supplement the terms of this License by making exceptions from one or more of its conditions. Additional permissions that are applicable to the entire Program shall be treated as though they were included in this License, to the extent that they are valid under applicable law. If additional permissions apply only to part of the Program, that part may be used separately under those permissions, but the entire Program remains governed by this License without regard to the additional permissions.

When you convey a copy of a covered work, you may at your option remove any additional permissions from that copy, or from any part of it. (Additional permissions may be written to require their own removal in certain cases when you modify the work.) You may place additional permissions on material, added by you to a covered work, for which you have or can give appropriate copyright permission.

Notwithstanding any other provision of this License, for material you add to a covered work, you may (if authorized by the copyright holders of that material) supplement the terms of this License with terms:

> a) Disclaiming warranty or limiting liability differently from the terms of sections 15 and 16 of this License; or
>
> b) Requiring preservation of specified reasonable legal notices or author attributions in that material or in the Appropriate Legal Notices displayed by works containing it; or
>
> c) Prohibiting misrepresentation of the origin of that material, or requiring that modified versions of such material be marked in reasonable ways as different from the original version; or
>
> d) Limiting the use for publicity purposes of names of licensors or authors of the material; or
>
> e) Declining to grant rights under trademark law for use of some trade names, trademarks, or service marks; or
>
> f) Requiring indemnification of licensors and authors of that material by anyone who conveys the material (or modified versions of it) with contractual assumptions of liability to the recipient, for any liability that these contractual assumptions directly impose on those licensors and authors.

All other non-permissive additional terms are considered "further restrictions" within the meaning of section 10. If the Program as you received it, or any part of it, contains a notice stating that it is governed by this License along with a term that is a further restriction, you may remove that term. If a license document contains a further restriction but permits relicensing or conveying under this License, you may add to a covered work material governed by the terms of that license document, provided that the further restriction does not survive such relicensing or conveying.

If you add terms to a covered work in accord with this section, you must place, in the relevant source files, a statement of the additional terms that apply to those files, or a notice indicating where to find the applicable terms.

Additional terms, permissive or non-permissive, may be stated in the form of a separately written license, or stated as exceptions; the above requirements apply either way.

8. Termination.

You may not propagate or modify a covered work except as expressly provided under this License. Any attempt otherwise to propagate or modify it is void, and will automatically terminate your rights under this License (including any patent licenses granted under the third paragraph of section 11).

However, if you cease all violation of this License, then your license from a particular copyright holder is reinstated (a) provisionally, unless and until the copyright holder explicitly and finally terminates your license, and (b) permanently, if the copyright holder fails to notify you of the violation by some reasonable means prior to 60 days after the cessation.

Moreover, your license from a particular copyright holder is reinstated permanently if the copyright holder notifies you of the violation by some reasonable means, this is the first time you have received notice of violation of this License (for any work) from that copyright holder, and you cure the violation prior to 30 days after your receipt of the notice.

Termination of your rights under this section does not terminate the licenses of parties who have received copies or rights from you under this License. If your rights have been terminated and not permanently reinstated, you do not qualify to receive new licenses for the same material under section 10.

9. Acceptance Not Required for Having Copies.

You are not required to accept this License in order to receive or run a copy of the Program. Ancillary propagation of a covered work occurring solely as a consequence of using peer-to-peer transmission to receive a copy likewise does not require acceptance. However, nothing other than this License grants you permission to propagate or modify any covered work. These actions infringe copyright if you do not accept this License. Therefore, by modifying or propagating a covered work, you indicate your acceptance of this License to do so.

10. Automatic Licensing of Downstream Recipients.

Each time you convey a covered work, the recipient automatically receives a license from the original licensors, to run, modify and propagate that work, subject to this License. You are not responsible for enforcing compliance by third parties with this License.

An “entity transaction” is a transaction transferring control of an organization, or substantially all assets of one, or subdividing an organization, or merging organizations. If propagation of a covered work results from an entity transaction, each party to that transaction who receives a copy of the work also receives whatever licenses to the work the party’s predecessor in interest had or could give under the previous paragraph, plus a right to possession of the Corresponding Source of the work from the predecessor in interest, if the predecessor has it or can get it with reasonable efforts.

You may not impose any further restrictions on the exercise of the rights granted or affirmed under this License. For example, you may not impose a license fee, royalty, or other charge for exercise of rights granted under this License, and you may not initiate litigation (including a cross-claim or counterclaim in a lawsuit) alleging that any patent claim is infringed by making, using, selling, offering for sale, or importing the Program or any portion of it.

11. Patents.

A “contributor” is a copyright holder who authorizes use under this License of the Program or a work on which the Program is based. The work thus licensed is called the contributor’s “contributor version”.

A contributor’s “essential patent claims” are all patent claims owned or controlled by the contributor, whether already acquired or hereafter acquired, that would be infringed by some manner, permitted by this License, of making, using, or selling its contributor version, but do not include claims that would be infringed only as a consequence of further modification of the contributor version. For purposes of this definition, “control” includes the right to grant patent sublicenses in a manner consistent with the requirements of this License.

Each contributor grants you a non-exclusive, worldwide, royalty-free patent license under the contributor’s essential patent claims, to make, use, sell, offer for sale, import and otherwise run, modify and propagate the contents of its contributor version.

In the following three paragraphs, a “patent license” is any express agreement or commitment, however denominated, not to enforce a patent (such as an express permission to practice a patent or covenant not to sue for patent infringement). To “grant” such a patent license to a party means to make such an agreement or commitment not to enforce a patent against the party.

If you convey a covered work, knowingly relying on a patent license, and the Corresponding Source of the work is not available for anyone to copy, free of charge and under the terms of this License, through a publicly available network server or other readily accessible means, then you must either (1) cause the Corresponding Source to be so available, or (2) arrange to deprive yourself of the benefit of the patent license for this particular work, or (3) arrange, in a manner consistent with the requirements of this License, to extend the patent license to downstream recipients. “Knowingly relying” means you have actual knowledge that, but for the patent license, your conveying the covered work in a country, or your recipient’s use of the covered work in a country, would infringe one or more identifiable patents in that country that you have reason to believe are valid.

If, pursuant to or in connection with a single transaction or arrangement, you convey, or propagate by procuring conveyance of, a covered work, and grant a patent license to some of the parties receiving the covered work authorizing them to use, propagate, modify or convey a specific copy of the covered work, then the patent license you grant is automatically extended to all recipients of the covered work and works based on it.

A patent license is “discriminatory” if it does not include within the scope of its coverage, prohibits the exercise of, or is conditioned on the non-exercise of one or more of the rights that are specifically granted under this License. You may not convey a covered work if you are a party to an arrangement with a third party that is in the business of distributing software, under which you make payment to the third party based on the extent of your activity of conveying the work, and under which the third party grants, to any of the parties who would receive the covered work from you, a discriminatory patent license (a) in connection with copies of the covered work conveyed by you (or copies made from those copies), or (b) primarily for and in connection with specific products or compilations that contain the covered work, unless you entered into that arrangement, or that patent license was granted, prior to 28 March 2007.

Nothing in this License shall be construed as excluding or limiting any implied license or other defenses to infringement that may otherwise be available to you under applicable patent law.

12. No Surrender of Others’ Freedom.

If conditions are imposed on you (whether by court order, agreement or otherwise) that contradict the conditions of this License, they do not excuse you from the conditions of this License. If you cannot convey a covered work so as to satisfy simultaneously your obligations under this License and any other pertinent obligations, then as a consequence you may not convey it at all. For example, if you agree to terms that obligate you to collect a royalty for further conveying from those to whom you convey the Program, the only way you could satisfy both those terms and this License would be to refrain entirely from conveying the Program.

13. Use with the GNU Affero General Public License.

Notwithstanding any other provision of this License, you have permission to link or combine any covered work with a work licensed under version 3 of the GNU Affero General Public License into a single combined work, and to convey the resulting work. The terms of this License will continue to apply to the part which is the covered work, but the special requirements of the GNU Affero General Public License, section 13, concerning interaction through a network will apply to the combination as such.

14. Revised Versions of this License.

The Free Software Foundation may publish revised and/or new versions of the GNU General Public License from time to time. Such new versions will be similar in spirit to the present version, but may differ in detail to address new problems or concerns.

Each version is given a distinguishing version number. If the Program specifies that a certain numbered version of the GNU General Public License “or any later version” applies to it, you have the option of following the terms and conditions either of that numbered version or of any later version published by the Free Software Foundation. If the Program does not specify a version number of the GNU General Public License, you may choose any version ever published by the Free Software Foundation.

If the Program specifies that a proxy can decide which future versions of the GNU General Public License can be used, that proxy’s public statement of acceptance of a version permanently authorizes you to choose that version for the Program.

Later license versions may give you additional or different permissions. However, no additional obligations are imposed on any author or copyright holder as a result of your choosing to follow a later version.

15. Disclaimer of Warranty.

THERE IS NO WARRANTY FOR THE PROGRAM, TO THE EXTENT PERMITTED BY APPLICABLE LAW. EXCEPT WHEN OTHERWISE STATED IN WRITING THE COPYRIGHT HOLDERS AND/OR OTHER PARTIES PROVIDE THE PROGRAM “AS IS” WITHOUT WARRANTY OF ANY KIND, EITHER EXPRESSED OR IMPLIED, INCLUDING, BUT NOT LIMITED TO, THE IMPLIED WARRANTIES OF MERCHANTABILITY AND FITNESS FOR A PARTICULAR PURPOSE. THE ENTIRE RISK AS TO THE QUALITY AND PERFORMANCE OF THE PROGRAM IS WITH YOU. SHOULD THE PROGRAM PROVE DEFECTIVE, YOU ASSUME THE COST OF ALL NECESSARY SERVICING, REPAIR OR CORRECTION.

16. Limitation of Liability.

IN NO EVENT UNLESS REQUIRED BY APPLICABLE LAW OR AGREED TO IN WRITING WILL ANY COPYRIGHT HOLDER, OR ANY OTHER PARTY WHO MODIFIES AND/OR CONVEYS THE PROGRAM AS PERMITTED ABOVE, BE LIABLE TO YOU FOR DAMAGES, INCLUDING ANY GENERAL, SPECIAL, INCIDENTAL OR CONSEQUENTIAL DAMAGES ARISING OUT OF THE USE OR INABILITY TO USE

THE PROGRAM (INCLUDING BUT NOT LIMITED TO LOSS OF DATA OR DATA BEING RENDERED INACCURATE OR LOSSES SUSTAINED BY YOU OR THIRD PARTIES OR A FAILURE OF THE PROGRAM TO OPERATE WITH ANY OTHER PROGRAMS), EVEN IF SUCH HOLDER OR OTHER PARTY HAS BEEN ADVISED OF THE POSSIBILITY OF SUCH DAMAGES.

17. Interpretation of Sections 15 and 16.

If the disclaimer of warranty and limitation of liability provided above cannot be given local legal effect according to their terms, reviewing courts shall apply local law that most closely approximates an absolute waiver of all civil liability in connection with the Program, unless a warranty or assumption of liability accompanies a copy of the Program in return for a fee.

END OF TERMS AND CONDITIONS

5.3 How to Apply These Terms to Your New Programs

If you develop a new program, and you want it to be of the greatest possible use to the public, the best way to achieve this is to make it free software which everyone can redistribute and change under these terms.

To do so, attach the following notices to the program. It is safest to attach them to the start of each source file to most effectively state the exclusion of warranty; and each file should have at least the "copyright" line and a pointer to where the full notice is found.

> <one line to give the program's name and a brief idea of what it does.> Copyright (C) <year> <name of author>
>
> This program is free software: you can redistribute it and/or modify it under the terms of the GNU General Public License as published by the Free Software Foundation, either version 3 of the License, or (at your option) any later version.
>
> This program is distributed in the hope that it will be useful, but WITHOUT ANY WARRANTY; without even the implied warranty of MERCHANTABILITY or FITNESS FOR A PARTICULAR PURPOSE. See the GNU General Public License for more details.
>
> You should have received a copy of the GNU General Public License along with this program. If not, see <http://www.gnu.org/licenses/>.

Also add information on how to contact you by electronic and paper mail.

If the program does terminal interaction, make it output a short notice like this when it starts in an interactive mode:

> <program> Copyright (C) <year> <name of author> This program comes with ABSOLUTELY NO WARRANTY; for details type `show w`. This is free software, and you are welcome to redistribute it under certain conditions; type `show c` for details.

The hypothetical commands `show w` and `show c` should show the appropriate parts of the General Public License. Of course, your program's commands might be different; for a GUI interface, you would use an "about box".

You should also get your employer (if you work as a programmer) or school, if any, to sign a "copyright disclaimer" for the program, if necessary. For more information on this, and how to apply and follow the GNU GPL, see http://www.gnu.org/licenses/.

The GNU General Public License does not permit incorporating your program into proprietary programs. If your program is a subroutine library, you may consider it more useful to permit linking proprietary applications with the library. If this is what you want to do, use the GNU Lesser General Public License instead of this License. But

214

first, please read http://www.gnu.org/philosophy/why-not-lgpl.html.

INDEX

References

Alcamo, J., Döll, P., Henrichs, T., Kaspar, F., Lehner, B., Rösch, T., and Siebert, S.: Development and testing of the WaterGAP 2 global model of water use and availability, Hydrological Sciences Journal, 48, 317–337, https://doi.org/10.1623/hysj.48.3.317.45290, 2003.

Beven, K.: Rainfall-Runoff Modelling: The Primer: Second Edition, vol. 15, Wiley, https://doi.org/10.1002/9781119951001, 2012.

Bierkens, M. F. P., Bell, V. A., Burek, P., Chaney, N., Condon, L. E., David, C. H., de Roo, A., Döll, P., Drost, N., Famiglietti, J. S., Flörke, M., Gochis, D. J., Houser, P., Hut, R., Keune, J., Kollet, S., Maxwell, R. M., Reager, J. T., Samaniego, L., Sudicky, E., Sutanudjaja, E. H., van de Giesen, N., Winsemius, H., and Wood, E. F.: Hyper-resolution global hydrological modelling: what is next?, Hydrological Processes, 29, 310–320, https://doi.org/10.1002/hyp.10391, 2015.

Brush, C. F., Dogrul, E. C., and Kadir, T. N.: Development and calibration of the California Central Valley Groundwater-Surface Water Simulation Model (C2VSim), version 3.02-CG, Bay-Delta Office, California Department of Water Resources, 2013.

Chen, L., Ali Babar, M., and Nuseibeh, B.: Characterizing Architecturally Significant Requirements, IEEE Software, 30, 38–45, https://doi.org/10.1109/MS.2012.174, 2013.

Cuthbert, M., Gleeson, T., Moosdorf, N., Befus, K., Schneider, A., Hartmann, J., and Lehner, B.: Global patterns and dynamics of climate–groundwater interactions, Nature Climate Change, 9, 137, https://doi.org/10.1038/s41558-018-0386-4, 2019.

de Graaf, I. E., Sutanudjaja, E., Van Beek, L., Bierkens, M., et al.: A high-resolution global-scale groundwater model, Hydrology and Earth System Sciences, 19, 823–837, https://doi.org/10.5194/hess-19-823-2015, 2015.

de Graaf, I. E., van Beek, R. L., Gleeson, T., Moosdorf, N., Schmitz, O., Sutanudjaja, E. H., and Bierkens, M. F.: A global-scale two-layer transient groundwater model: Development and application to groundwater depletion, Advances in water Resources, 102, 53–67, https://doi.org/10.1016/j.advwatres.2017.01.011, 2017.

Debye, P.: Näherungsformeln für die Zylinderfunktionen für große Werte des Arguments und unbeschränkt veränderliche Werte des Index, Mathematische Annalen, 67, 535–558, https://doi.org/10.1007/BF01450097, 1909.

Döll, P., Kaspar, F., and Lehner, B.: A global hydrological model for deriving water availability indicators: model tuning and validation, Journal of Hydrology, 270, 105–134, https://doi.org/10.1016/S0022-1694(02)00283-4, 2003.

Döll, P., Hoffmann-Dobrev, H., Portmann, F. T., Siebert, S., Eicker, A., Rodell, M., Strassberg, G., and Scanlon, B.: Impact of water withdrawals from groundwater and surface water on continental water storage variations, Journal of Geodynamics, 59, 143–156, https://doi.org/10.1016/j.jog.2011.05.001, 2012.

Döll, P., Mueller Schmied, H., Schuh, C., Portmann, F. T., and Eicker, A.: Global-scale assessment of groundwater depletion and related groundwater abstractions: Combining hydrological modeling with information from well observations and GRACE satellites, Water Resources Research, 50, 5698–5720, https://doi.org/10.1002/2014WR015595, 2014.

Fan, Y., Miguez-Macho, G., Weaver, C. P., Walko, R., and Robock, A.: Incorporating water table dynamics in climate modeling: 1. Water table observations and equilibrium water table simulations, Journal of Geophysical Research: Atmospheres, 112, D10 125, https://doi.org/10.1029/2006JD008111, 2007.

Fan, Y., Li, H., and Miguez-Macho, G.: Global Patterns of Groundwater Table Depth, Science, 339, 940–943, https://doi.org/10.1126/science.1229881, 2013.

Fan, Y., Clark, M., Lawrence, D. M., Swenson, S., Band, L. E., Brantley, S. L., Brooks, P. D., Dietrich, W. E., Flores, A., Grant, G., Kirchner, J. W., Mackay, D. S., McDonnell, J. J., Milly, P. C. D., Sullivan, P. L., Tague, C., Ajami, H., Chaney, N., Hartmann, A., Hazenberg, P., McNamara, J., Pelletier, J., Perket, J., Rouholahnejad-Freund, E., Wagener, T., Zeng, X., Beighley, E., Buzan, J., Huang, M., Livneh, B., Mohanty, B. P., Nijssen, B., Safeeq, M., Shen, C., van Verseveld, W., Volk, J., and Yamazaki, D.: Hillslope Hydrology in Global Change Research and Earth System Modeling, Water Resources Research, 55, 1737–1772, https://doi.org/10.1029/2018WR023903, 2019.

Fang, H. and O'Leary, D. P.: Modified Cholesky algorithms: a catalog with new approaches, Mathematical Programming, 115, 319–349, https://doi.org/10.1007/s10107-007-0177-6, 2008.

Faunt, C., Sneed, M., Traum, J., and Brandt, J. T.: Water availability and land subsidence in the Central Valley, California, USA, Hydrogeology Journal, 24, 675–684, https://doi.org/10.1007/s10040-015-1339-x, 2016.

Gamma, E., Helm, R., Johnson, R., and Vlissides, J.: Design Patterns: Elements of Reusable Object-Oriented Software, Addison-Wesley, 1995.

Garousi, V.: Applying Peer Reviews in Software Engineering Education: An Experiment and Lessons Learned, IEEE Transactions on Education, 53, 182–193, https://doi.org/10.1109/TE.2008.2010994, 2010.

Gauckler, P.: Etudes Théoriques et Pratiques sur l'Ecoulement et le Mouvement des Eaux, Comptes Rendues de l'Académie des Sciences, 64, 818–822, 1867.

Gleeson, T., Wada, Y., Bierkens, M. F., and van Beek, L. P.: Water balance of global aquifers revealed by groundwater footprint, Nature, 488, 197, https://doi.org/10.1038/nature11295, 2012.

Gleeson, T., Befus, K. M., Jasechko, S., Luijendijk, E., and Cardenas, M. B.: The global volume and distribution of modern groundwater, Nature Geoscience, 9, 161, https://doi.org/10.1038/ngeo2590, 2016.

Global Risk Network: World economic forum global risk report 2018, in: World Economic Forum, Geneva, 2018.

Goode, D. J.: Direct Simulation of Groundwater Age, Water Resources Research, 32, 289–296, https://doi.org/10.1029/95WR03401, 1996.

Haasnoot, M., van Deursen, W., Guillaume, J., Kwakkel, J., van Beek, E., and Middelkoop, H.: Fit for purpose? Building and evaluating a fast, integrated model for exploring water policy pathways, Environmental Modelling & Software, 60, 99 – 120, https://doi.org/10.1016/j.envsoft.2014.05.020, 2014.

Harbaugh, A. W.: MODFLOW-2005, the US Geological Survey modular groundwater model: the ground-water flow process, US Department of the Interior, US Geological Survey Reston, VA, 2005.

Hood, J. L., Roy, J. W., and Hayashi, M.: Importance of groundwater in the water balance of an alpine headwater lake, Geophysical Research Letters, 33, https://doi.org/10.1029/2006GL026611, 2006.

Huscroft, J., Gleeson, T., Hartmann, J., and Börker, J.: Compiling and mapping global permeability of the unconsolidated and consolidated Earth: GLobal HYdrogeology MaPS 2.0 (GLHYMPS 2.0), Geophysical Research Letters, 45, 1897–1904, https://doi.org/10.1002/2017GL075860, 2018.

Hutton, C., Wagener, T., Freer, J., Han, D., Duffy, C., and Arheimer, B.: Most computational hydrology is not reproducible, so is it really science?, Water Resources Research, 52, 7548–7555, https://doi.org/10.1002/2016WR019285, 2016.

IEEE: IEEE Standard Glossary of Software Engineering Terminology, IEEE Std 610.12-1990, pp. 1–84, https://doi.org/10.1109/IEEESTD.1990.101064, 1990.

Kang, K. C., Kim, S., Lee, J., and Lee, K.: Feature-oriented engineering of PBX software for adaptability and reuseability, Software: Practice and Experience, 29, 875–896, 1999.

Kearns, F., Parker, D., et al.: Supporting sustainable groundwater management, California Agriculture, 72, 6–7, https://doi.org/10.3733/ca.2018a0007, 2018.

Keune, J., Gasper, F., Goergen, K., Hense, A., Shrestha, P., Sulis, M., and Kollet, S.: Studying the influence of groundwater representations on land surface-atmosphere feedbacks during the European heat wave in 2003, Journal of Geophysical Research: Atmospheres, 121, 13,301–13,325, https://doi.org/10.1002/2016JD025426, 2016.

Konikow, L. F.: Contribution of global groundwater depletion since 1900 to sea-level rise, Geophysical Research Letters, 38, L17 401, https://doi.org/10.1029/2011GL048604, 2011.

Konikow, L. F.: Groundwater depletion in the United States (1900-2008), vol. 63, U.S. Geological Survey Scientific Investigations Report, URL `http://pubs.usgs.gov/sir/2013/5079`, 2013.

Manning, A. H. and Caine, J. S.: Groundwater noble gas, age, and temperature signatures in an Alpine watershed: Valuable tools in conceptual model development, Water Resources Research, 43, W04 404, https://doi.org/10.1029/2006WR005349, 2007.

Masson-Delmotte, V., Zhai, P., Pörtner, H., Roberts, D., Skea, J., Shukla, P., Pirani, A., Moufouma-Okia, W., Péan, C., Pidcock, R., et al.: IPCC, 2018: Summary for Policymakers, Global warming of 1.5°C, p. 32, 2018.

Maxwell, R. M., Condon, L. E., and Kollet, S. J.: A high-resolution simulation of groundwater and surface water over most of the continental US with the integrated hydrologic model ParFlow v3, Geoscientific Model Development, 8, 923–937, https://doi.org/10.5194/gmd-8-923-2015, 2015.

Meyer, B.: Object-oriented software construction, vol. 2, Prentice hall New York, 1988.

Miguez-Macho, G., Fan, Y., Weaver, C. P., Walko, R., and Robock, A.: Incorporating water table dynamics in climate modeling: 2. Formulation, validation, and soil moisture simulation, Journal of Geophysical Research: Atmospheres, 112, D13 108, https://doi.org/10.1029/2006JD008112, 2007.

Morel-Seytoux, H. J.: MODFLOW's River Package: Part 1: A Critique, Physical Science International Journal, 22, 1–9, https://doi.org/10.9734/psij/2019/v22i230129, 2019a.

Morel-Seytoux, H. J.: MODFLOW's River Package: Part 2: Correction, Combining Analytical and Numerical Approaches, Physical Science International Journal, 22, 1–23, https://doi.org/10.9734/psij/2019/v22i330131, 2019b.

Morel-Seytoux, H. J., Miller, C. D., Miracapillo, C., and Mehl, S.: River Seepage Conductance in Large-Scale Regional Studies, Groundwater, 55, 399–407, https://doi.org/10.1111/gwat.12491, 2017.

Müller Schmied, H., Eisner, S., Franz, D., Wattenbach, M., Portmann, F. T., Flörke, M., and Döll, P.: Sensitivity of simulated global-scale freshwater fluxes and storages to input data, hydrological model structure, human water use and calibration, Hydrology and Earth System Sciences, 18, 3511–3538, https://doi.org/10.5194/hess-18-3511-2014, 2014.

Niswonger, R. G., Panday, S., and Ibaraki, M.: MODFLOW-NWT, a Newton formulation for MODFLOW-2005, US Geological Survey Techniques and Methods, 6, 44, 2011.

Padhy, N., Satapathy, S., and Singh, R. P.: State-of-the-Art Object-Oriented Metrics and Its Reusability: A Decade Review, in: Smart Computing and Informatics, pp. 431–441, Springer Singapore, Singapore, 2018.

Pianosi, F., Beven, K., Freer, J., Hall, J. W., Rougier, J., Stephenson, D. B., and Wagener, T.: Sensitivity analysis of environmental models: A systematic review with practical workflow, Environmental Modelling & Software, 79, 214–232, https://doi.org/10.1016/j.envsoft.2016.02.008, 2016.

Reinecke, R., Foglia, L., Mehl, S., Trautmann, T., Cáceres, D., and Döll, P.: Challenges in developing a global gradient-based groundwater model (G^3M v1.0) for the integration into a global hydrological model, Geoscientific Model Development, 12, 2401–2418, https://doi.org/10.5194/gmd-12-2401-2019, 2019a.

Reinecke, R., Foglia, L., Mehl, S., Herman, J. D., Wachholz, A., Trautmann, T., and Döll, P.: Spatially distributed sensitivity of simulated global groundwater heads and flows to hydraulic conductivity, groundwater recharge, and surface water body parameterization, Hydrology and Earth System Sciences, 23, 4561–4582, https://doi.org/10.5194/hess-23-4561-2019, 2019b.

Rodríguez, I., Llana, L., and Rabanal, P.: A General Testability Theory: Classes, Properties, Complexity, and Testing Reductions, IEEE Transactions on Software Engineering, 40, 862–894, https://doi.org/10.1109/TSE.2014.2331690, 2014.

Saad, Y.: ILUT: A dual threshold incomplete LU factorization, Numerical Linear Algebra with Applications, 1, 387–402, https://doi.org/10.1002/nla.1680010405, 1994.

Scanlon, B. R., Faunt, C. C., Longuevergne, L., Reedy, R. C., Alley, W. M., McGuire, V. L., and McMahon, P. B.: Groundwater depletion and sustainability of irrigation in the US High Plains and Central Valley, Proceedings of the national academy of sciences, 109, 9320–9325, https://doi.org/10.1073/pnas.1200311109, 2012.

Shewchuk, J. R. et al.: An introduction to the conjugate gradient method without the agonizing pain, URL ftp://ftp.unicauca.edu.co/Facultades/.FIET_serepiteencuentasyocupaespacio/DEIC/docs/Materias/computacion%20inteligente/parte%20II/semana12/gradient/painless-conjugate-gradient.pdf, 1994.

Sood, A. and Smakhtin, V.: Global hydrological models: a review, Hydrological Sciences Journal, 60, 549–565, https://doi.org/10.1080/02626667.2014.950580, 2015.

Stonestrom, D. A. and Harrill, J. R.: Ground-water recharge in the arid and semiarid southwestern United States-Climatic and geologic framework: Chapter A in Ground-water recharge in the arid and semiarid southwestern United States (Professional Paper 1703), Tech. rep., US Geological Survey, 2007.

Tague, C. and Grant, G. E.: Groundwater dynamics mediate low-flow response to global warming in snow-dominated alpine regions, Water Resources Research, 45, W07 421, https://doi.org/10.1029/2008WR007179, 2009.

Taylor, R. G., Scanlon, B., Döll, P., Rodell, M., Van Beek, R., Wada, Y., Longuevergne, L., Leblanc, M., Famiglietti, J. S., Edmunds, M., et al.: Ground water and climate change, Nature Climate Change, 3, 322, https://doi.org/10.1038/nclimate1744, 2013.

van Beek, L. P. H., Wada, Y., and Bierkens, M. F. P.: Global monthly water stress: 1. Water balance and water availability, Water Resources Research, 47, W07 517, https://doi.org/10.1029/2010WR009791, 2011.

Wada, Y., van Beek, L. P. H., van Kempen, C. M., Reckman, J. W. T. M., Vasak, S., and Bierkens, M. F. P.: Global depletion of groundwater resources, Geophysical Research Letters, 37, L20 402, https://doi.org/10.1029/2010GL044571, 2010.

Wada, Y., Bierkens, M. F. P., de Roo, A., Dirmeyer, P. A., Famiglietti, J. S., Hanasaki, N., Konar, M., Liu, J., Müller Schmied, H., Oki, T., Pokhrel, Y., Sivapalan, M., Troy, T. J., van Dijk, A. I. J. M., van Emmerik, T., Van Huijgevoort, M. H. J., Van Lanen, H. A. J., Vörösmarty, C. J., Wanders, N., and Wheater, H.: Human–water interface in hydrological modelling: current status and future directions, Hydrology and Earth System Sciences, 21, 4169–4193, https://doi.org/10.5194/hess-21-4169-2017, 2017.

Wang, J., Song, C., Reager, J. T., Yao, F., Famiglietti, J. S., Sheng, Y., MacDonald, G. M., Brun, F., Schmied, H. M., Marston, R. A., et al.: Recent global decline in endorheic basin water storages, Nature geoscience, 11, 926, https://doi.org/10.1038/s41561-018-0265-7, 2018.